Synthesis and Electrochemical Studies of Nanostructured Electrodes for High Energy Density Lithium-Sulfur Battery and High Power Density Supercapacitor

Thesis

Submitted in Partial Fulfilment of the Requirements

for the Award of the Degree of

Doctor of Philosophy

In Chemistry

by

E. Hari Mohan

(Roll No. 701379)

Under the Supervision of

Prof. B.V. Appa Rao (NITW)

Dr. Tata Narasinga Rao (ARCI)

Department of Chemistry

National Institute of Technology Warangal

Warangal-506004, Telangana, India

February, 2019

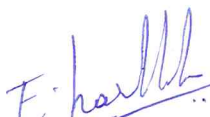*Dedicated to My Beloved Parents and Teachers*

DECLARATION

This is to declare that the work presented in the thesis entitled *"Synthesis and Electrochemical Studies of Nanostructured Electrodes for High Energy Density Lithium-Sulfur Battery and High Power Density Supercapacitor"*, submitted in partial fulfilment of the requirements for the award of **Doctor of Philosophy** in the Department of Chemistry, NIT Warangal is a bonafide work done by me under the supervision of **Prof. B. V. Appa Rao**, Professor of Chemistry (Retd.), Department of Chemistry, NIT Warangal and **Dr. Tata Narasinga Rao**, Associate Director, ARCI, Hyderabad. I declare that this work is original and was not submitted elsewhere for the award of any degree.

I declare that this written submission represents my ideas in my own words and where others' ideas or words have been included, I have adequately cited and referenced the original sources. I also declare that I have adhered to all the principles of academic honesty and integrity and have not misrepresented or fabricated or falsified any idea/data/fact/ source in my submission. I understand that any violation of the above will be a cause for disciplinary action by the Institute and can also evoke penal action from the sources which have thus not been properly cited or from whom proper permission has not been taken when needed.

Date:

Place: **NIT Warangal**

(E. Hari Mohan)

Roll Number: **701379**

Prof. B. V. APPA RAO   Dr. TATA NARASINGA RAO

Professor of Chemistry (Retd.)   Associate Director

Department of Chemistry   ARCI Hyderabad

NIT Warangal   Hyderabad - 500005

Warangal - 506 004

<u>CERTIFICATE</u>

This is to certify that the work presented in the thesis entitled *"Synthesis and Electrochemical Studies of Nanostructured Electrodes for High Energy Density Lithium-Sulfur Battery and High Power Density Supercapacitor"*, is a bonafide work carried out by Mr. E. Hari Mohan under our supervision and was not submitted elsewhere for the award of any degree.

Tata Narasinga Rao   **B.V. Appa Rao**

(Research Supervisor   **(Research Supervisor**

External)   **Internal)**

Date:

Place: **NIT Warangal**

ACKNOWLEDGMENTS

Date:

E. Hari Mohan

Table of Contents

Chapter 1

Chapter 2

Chapter 6

List of Figures

with in-set of FFT patterns (g-i)

the cell fabrication process

List of Tables

List of Symbols and Abbreviations Used in This Thesis

LIBs	Lithium-ion Batteries
Li-S	Lithium-Sulfur
SC	Supercapacitor
LCP	Long Chain Polysulfides
SCP	Short Chain Polysulfides
Li_2S	Lithium Sulfide
ACs	Activated Carbons
LITFSI	Lithium bis(trifluoromethanesulfonyl)imide
DOL	1,3-Dioxalane
DME	Dimethoxyethane
PVDE	Polyvinylidene difluoride
PTFE	Polytetrafluoroethylene
NMP	N-methyl-2-pyrrolidone
SEM	Scanning Electron Microscopy
TEM	Transmission Electron Microscopy
BET	Brunauer Emmett Teller
EDS	Energy Dispersive X-ray spectroscopy
TG	Thermogravimetry
XPS	X-ray Photoelectron Spectroscopy
XRD	X-ray Diffraction
CV	Cyclic Voltammetry
CD	Charge/Discharge
CY	Cycle Performance
ED	Energy Density
$mAh\ g^{-1}$	Milliampere Hour Per Gram
V	Volt
C_s	Specific Capacitance
$A\ g^{-1}$	Ampere Per Gram
$mV\ s^{-1}$	Millivolt per Second
EIS	Electrochemical Impedance Spectroscopy
EDLC	Electrical double layer capacitor

CPE	Constant Phase Element
Cdl	Double layer capacitance
eV	Electron Volt
Z'	Real Impedance
Z"	Imaginary Impedance
W	Warburg Impedance
R_{ct}	Charge Transfer Resistance
R_s	Solution Resistance
Ω	Ohm
ºC	Degree Celsius
NLMC	Neem Leaves- Micro and Mesoporous Carbon
p-GCS	Porous-Graphitic Carbon Sheets
MGC	Micro and Mesoporous Graphitic Carbon
Sn-G	Tin-Graphene
Si/G	Silicon/Graphite

Abstract

The present study is focused on the synthesis of micro and mesoporous carbon materials from neem leaves, tissue paper and jute stalks by KOH activation process and the synthesized carbon materials are labelled as NLMC, p-GCS and MGC respectively. The porous carbon/sulfur composites were prepared by a simple melt-diffusion process. The sulfur infused micro and mesoporous carbon materials act as polysulfide inhibitors for dissolved polysulfide species and inhibit their migration towards the anode surface. Thus, the resulting electrodes namely NLMC-4/S, p-GCS-2/S and MGC/S-2 delivered higher discharge capacities of 784 mAh g^{-1}, 992 mAh g^{-1}, 1016 mAh g^{-1} even after 50 charge/discharge cycles at 0.2 C rate. The effect of modified separators on the electrochemical performance of sulfur cathode was also explored in the present study. The electrode with modified separator exhibits superior electrochemical performance. It acts as a barrier film for the dissolved polysulfide species and reduces their migration to the anode surface. Moreover, it also acts as an upper current collector that increases the electrical conductivity and enhances the reutilization of active material during the redox process.

The high capacity anodes such as tin/graphene and silicon/graphite composites were also developed in the present study. The tin/graphene and silicon/graphite composites have been synthesized by electrodeposition and ball milling process respectively. The Sn/graphene and Si/graphite electrodes delivered high discharge capacities of 587 mAh g^{-1} and 1494 mAh g^{-1} respectively even after 40 cycles at 0.2 C rate. Furthermore, the Li-S battery in full cell configuration has also been fabricated by using the low-cost and best performed cathode and anode materials developed in the present study. The lithiated Si-S cell with optimised weight ratio of cathode, anode and lithium delivered a high discharge capacity of 824 mAh g^{-1} even after 50 cycles at 0.2 C rate. The energy density calculated on the basis of mass of the combined carbon and sulfur on the electrode is 948 Wh kg^{-1}, which is twice that of the conventional Li-ion battery ($LiFePO_4$/graphite cell; calculated on the basis of mass of $LiFePO_4$ cathode with its theoretical capacity; ~544 Wh kg^{-1}). Moreover, the lithiated Si-S pouch cells fabricated in the present study have been tested for powering small electronic components such as 40 LEDs connected in parallel and small toy fan.

The as-prepared NLMC and p-GCS were also explored in supercapacitor application due to their high surface area, large pore volume and good graphitic carbon structures. The NLMC and p-GCS electrodes in symmetric configuration exhibited superior electrochemical

performance of 138 F g^{-1} and 129 F g^{-1} at a current density of 1 A g^{-1}. These electrodes also show good rate capability and long-term cycle stability of 82% and 90% capacitance retention even after 10000 cycles at a current density of 1 A g^{-1}.

New Electrode Materials Developed in the Present Study

The new electrode materials developed in the present study are listed below.

1. Neem leaves-derived micro and mesoporous carbon as an efficient polysulfide inhibitor for sulfur cathode (1M LITFSI as electrolyte) and an electrode for supercapacitor (6M KOH as electrolyte).

2. Tissue paper-derived micro and mesoporous carbon as an efficient polysulfide inhibitor for sulfur cathode and an electrode for supercapacitor.

3. Jute stalks-leaves derived micro and mesoporous carbon as an efficient polysulfide inhibitor for sulfur cathode.

4. Graphene-modified electrodeposited dendritic tin structures as binder free anode for Li-S battery.

5. Nanostructured Silicon/graphite composite as an anode material for Li-S battery.

Layout of the Thesis

This thesis is divided into six chapters. Chapter 1 consists of general introduction on the need for the development of the high energy Li-S battery and high power supercapacitor devices for advanced portable electronics and electric vehicle (EV) applications. This chapter also comprises literature survey on various types of conductive matrix to inhibit the dissolution of polysulfide species into the electrolyte and also for ion adsorption such as porous carbon, graphene, CNTs, conductive polymers, metal oxides and electrolytes used. This chapter also includes the need, objectives and scope of the present study.

Chapter 2 deals with the materials and methods used in the present study. Techniques used for characterization of electrode materials are FE-SEM, TEM, N$_2$ adsorption/desorption studies, energy dispersive X-ray spectroscopy, thermogravimetric analysis, X-ray diffraction analysis, Raman spectroscopy, X-ray photoelectron spectroscopy and the techniques used for electrochemical studies namely cyclic voltammetry, charge-discharge profiles, cycle performance and impedance studies are included in this chapter.

Chapter 3 comprises the synthesis and electrochemical studies of the sulfur infused activated carbon cathode materials. This chapter is sub-divided into four sections. The synthesis and electrochemical studies of micro and mesoporous carbon from fallen neem

leaves are presented in the section 3.1. The synthesis and electrochemical studies of micro and mesoporous carbon synthesized from tissue paper and the synthesis and electrochemical studies of micro and mesoporous carbon synthesized from jute stalks and their application as host for sulfur cathode in a Li-S battery are included in sections 3.2 and 3.3 respectively. Section 3.4 presents a comparison of the micro and mesoporous carbon/sulfur composites developed in the present study with those reported in the literature.

Chapter 4 deals with the synthesis and electrochemical studies of the high capacity anodes and fabrication of lithiated Si-S full cell. This chapter is further divided into four sections, which involve the experimental details, results and discussion of electrodeposited dendritic porous Sn/graphene composite (section 4.1), and Si/Graphite prepared by ball milling process (section 4.2). The electrochemical performance of the individual electrode systems in half cell configuration gives a scope for the development of Li-S battery in full cell configuration. Section 4.3 presents the fabrication of lithiated Si-S full cell and its practical application in powering the small electronic components. A comparison of the electrochemical performance of lithiated Si-S cell developed in the present study with those reported in the literature is included in the section 4.4.

Chapter 5 deals with the electrochemical studies of the porous carbon materials for application in supercapacitors. This chapter is further divided into three sections, which comprise the results and discussion (electrochemical studies) of micro and mesoporous carbon derived from fallen neem leaves (section 5.1) and micro and mesoporous carbon derived from tissue paper (section 5.2) as electrodes for supercapacitor application. Section 5.3 presents the comparison of the micro and mesoporous carbon materials developed in the present study with those reported in the literature. Figure 1 presents the new nanostructured electrode materials developed for Li-S battery and supercapacitor in the form of a schematic diagram.

Chapter 6 deals with the summary and conclusions of the present research study.

Keywords: Nanostructured electrodes, Electrochemical studies, Li-S battery, Supercapacitor, KOH activation, Melt-diffusion, Micro and mesoporous carbon, Polysulfide inhibitor, Micro and mesoporous carbon/sulfur, Tin/graphene, Silicon/graphite, Si-S full cell.

I. New Nanostructured Electrodes Developed for Li-S Battery

Cathode Materials Developed

- NLMC/sulfur (Half-cell configuration)
- p-GCS/sulfur (Half-cell configuration)
- MGC/sulfur (Half-cell configuration)

Low cost and high performing cathode (MGC/S)

Lithiated Si-S Battery (Full-cell configuration)

Lithiated Si-S Battery (Pouch cells)

Anode Materials Developed

- Si/Graphite (Half-cell configuration)
- Sn/Graphene (Half-cell configuration)

Low cost and high performing anode (Si/Graphite)

Application of lithiated Si-S pouch cells for small electronic components

II. Nanostructured Electrodes for Supercapacitor

Porous Carbon Materials Developed

- Symmetric NLMC supercapacitor
- Symmetric p-GCS supercapacitor

Figure 1 Materials developed in the present study for Li-S battery and supercapacitor applications.

Chapter 1

Introduction
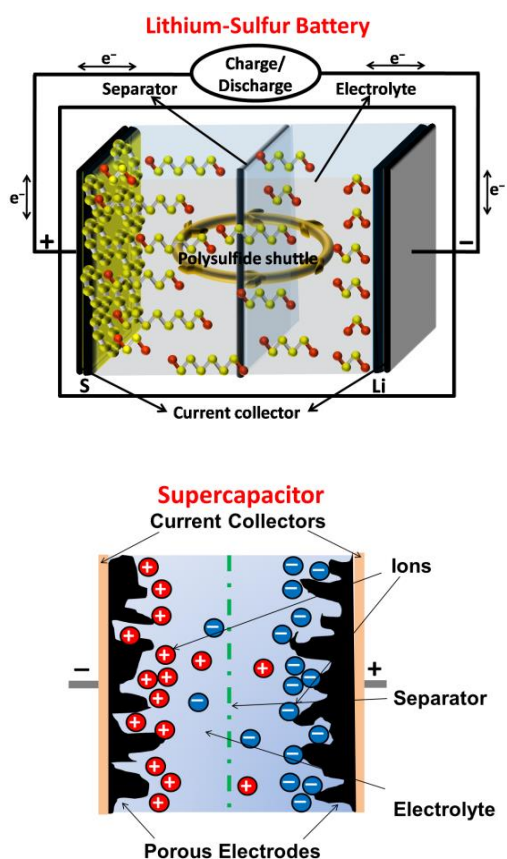
Contents

Introduction

Over the past few decades, energy usage at global level shifted from conventional fossil fuels towards the use of energy generated from the renewable energy sources, which need more economical, efficient and reliable electrochemical energy storage devices. In particular, the development of advanced portable electronic devices and smart grids calls for the electrochemical energy storage devices with much higher power density and energy density. Sony made one such breakthrough in the year 1991 [1], by releasing its first commercial lithium ion battery that has revolutionised the electronics market. The important factor for the successful emerging of the lithium-ion battery (LIB) is its high energy density

and long cycle life, when compared to the other commercially available rechargeable batteries. Considering the widespread impact of lithium-ion battery on consumer electronic devices, it has drawn much attention in large-scale grid storage and electric vehicle applications [2,3]. The companies like Nissan leaf, Tesla, Mahindra have explored the LIBs for application in electric vehicles. The energy density of the LIB being used currently is based on the intercalation chemistry and it has reached its maximum due to the limited charge storage capacity. The conventional LIBs use transition metal phosphate (LiMPO$_4$; M= Fe, Mn, Ni) or oxide (LiMO$_2$; M= Fe, Mn, Ni) as cathode and graphite as anode materials that can deliver maximum discharge capacities of ~170 mAh g^{-1} and ~370 mAh g^{-1} respectively. Moreover, the synthesis and fabrication of these electrode materials involve the use of expensive and toxic chemicals that make the battery highly expensive. Therefore, the use of LIBs for electric vehicles is not satisfactory due to the high fabrication cost and limited driving range distance, despite its high rate of charging. This has led to the search for alternative energy storage systems that have high charge storage capacity as well as high energy density associated with long cycle life, which eventually decrease the cost and weight of the battery pack and also increase the driving range of the electric vehicles (EVs) [4].

Lithium-sulfur battery based on the conversion chemistry is considered to be the next generation electrochemical energy storage system that offers high charge storage capacity and high energy density. In addition to these, the power capability of the device is also an important factor for application in trains, EVs, truck lifts and so on. The supercapacitors can charge/discharge in quick time, which enhances the power density of the device. The combination of high energy density Li-S battery and high power density supercapacitor with suitable battery management system can be one of the best models for these applications. The concept behind is the high power demand during the initial start-up of the EVs and energy recovery during breaking, which decrease the energy of the battery. Therefore, the application of supercapacitors can significantly smoothen the energy demands of the battery and the initial power is drawn from the supercapacitors. As a result, the batteries last for longer time with low discharge and steady energy output.

In Li-S battery, the elemental sulfur cathode has a theoretical specific capacity of 1672 mAh g^{-1} based on the total conversion of S^0 to S^{2-} with lithium. During the charge/discharge process, the Li-S battery operates at 2.1 V with respect to lithium that resulted in high energy density of 2600 Wk kg^{-1}, which is almost 3-5 times higher than that of

the conventionally used energy storage systems (lead-acid, Ni-MH, lithium-ion battery) [5]. Also, the elemental sulfur is naturally abundant, inexpensive and environmentally friendly. In supercapacitors, the porous carbon materials with high surface area use the electrode/electrolyte interface for charge storage. Thus, the high energy density Li-S batteries and high power density supercapacitors are more attractive to advanced portable electronic devices, smart gird storage systems and most importantly for application in EVs, trains and truck lifts. Figure 1.1 shows the comparison of energy and power densities of various energy storage systems for EV applications.
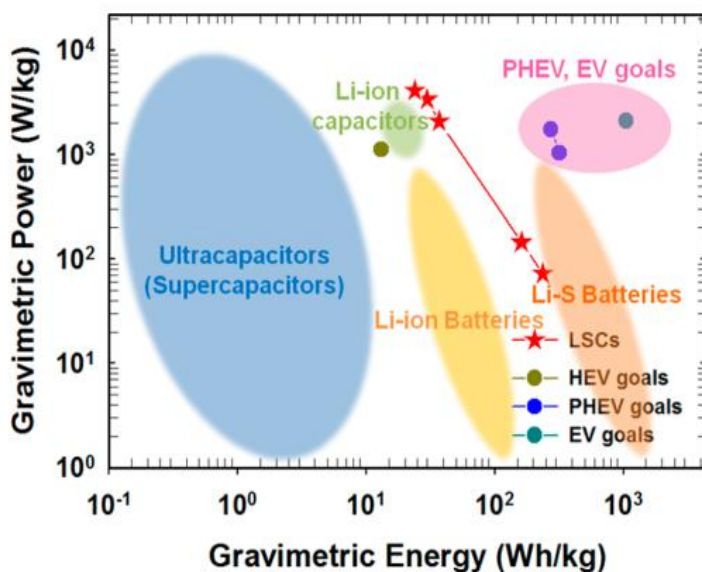
Figure 1.1 Ragone plot: comparison of gravimetric energy and power densities of various energy storage systems. LSCs- Li-S capacitor, HEV- Hybrid Electric Vehicles, PHEV- Plug-in Hybrid Electric Vehicles and EV- Electric Vehicles (adapted from ref [6]).

1.1 Li-S Battery

Principle of Li-S Battery

The typical Li-S cell contains elemental sulfur as a cathode, lithium metal as an anode and both the electrode materials are separated by a polymeric membrane filled with the electrolyte solution. During the charging/discharging process, the reversible electrochemical reaction between lithium and elemental sulfur delivers a high theoretical specific capacity of 1672 mAh g^{-1}. The theoretical capacity of lithium is 3860 mAh g^{-1}, whereas in Li-S battery the capacity is calculated based on the sulfur cathode only (theoretical capacity of Li-S is 1672 mAh g^{-1}) and the lithium metal is used as reference electrode.

The overall electrochemical reaction of the Li-S cell is given in the equation 1.1.

$$16Li + S_8 \leftrightarrow 8Li_2S \qquad (1.1)$$

However, the reduction of elemental sulfur is not a single step process. It involves a series of electron transfer reactions (multi-electron transfer). During the cell discharge, the lithium metal undergoes oxidation to produce an electron and lithium ion. The lithium ions internally migrate through the separator and the electrons flow through the external circuit. The reaction between lithium ions, sulfur atoms and electrons, occurs at the cathode to form soluble long-chain polysulfides (LCP). Subsequently, the long chain polysulfides get further reduced to precipitate shorter chain polysulfides (SCP) as end discharge product [7]. The redox chemistry of sulfur in Li-S cell is given in the equations 1.2 to 1.6.

$$S_8 + 2Li^+ + 2e^- \leftrightarrow Li_2S_8 \qquad (1.2)$$

$$3Li_2S_8 + 2Li^+ + 2e^- \leftrightarrow 4Li_2S_6 \qquad (1.3)$$

$$2Li_2S_6 + 2Li^+ + 2e^- \leftrightarrow 3Li_2S_4 \qquad (1.4)$$

$$Li_2S_4 + 2Li^+ + 2e^- \leftrightarrow 2Li_2S_2 \qquad (1.5)$$

$$2Li_2S_2 + 4Li^+ + 4e^- \leftrightarrow 4Li_2S \qquad (1.6)$$
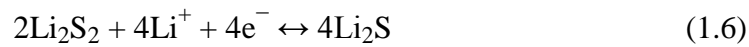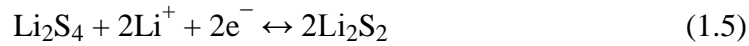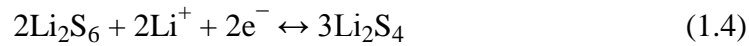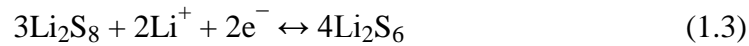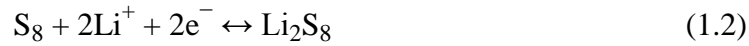
During charging of the cell, the lithium ions are stripped back from the cathode through the electrolyte to the anode and get reduced to metallic lithium at the anode. Whereas, the shorter chain polysulfides are converted entirely to elemental sulfur via. long chain polysulfide intermediates at the cathode.

The discharge curve of Li-S cell represents two plateaus at the potentials of 2.3 V and 2.1 V with three-step reduction process in ether-based electrolyte solution as shown in figure 1.2. The upper plateau at ~ 2.3 V corresponds to the initial reduction reaction of octa-sulfur and lithium ions to form long chain polysulfides (LCP, Li_2S_x, x = 6≥8). The LCP are highly soluble in the electrolyte solution. The lithium ion transport is decreased due to an increase in the viscosity of the internal electrolyte medium during the electrochemical process. As a result of concentration polarisation and high charge transfer resistance, the voltage of the cell drops from 2.3 V to 2.1 V. The sloping region represents a further reduction of high order lithium polysulfide to Li_2S_4 intermediate and the lower plateau at 2.1 V represents the region where the LCP are finally converted to short chain polysulfides (Li_2S, SCP) as end discharge product. The initial two steps are considered to be solid-liquid phase reactions with fast

reaction kinetics, whereas the final step is considered to be the rate-determining step with slow reaction kinetics due to liquid-solid phase reaction [8].
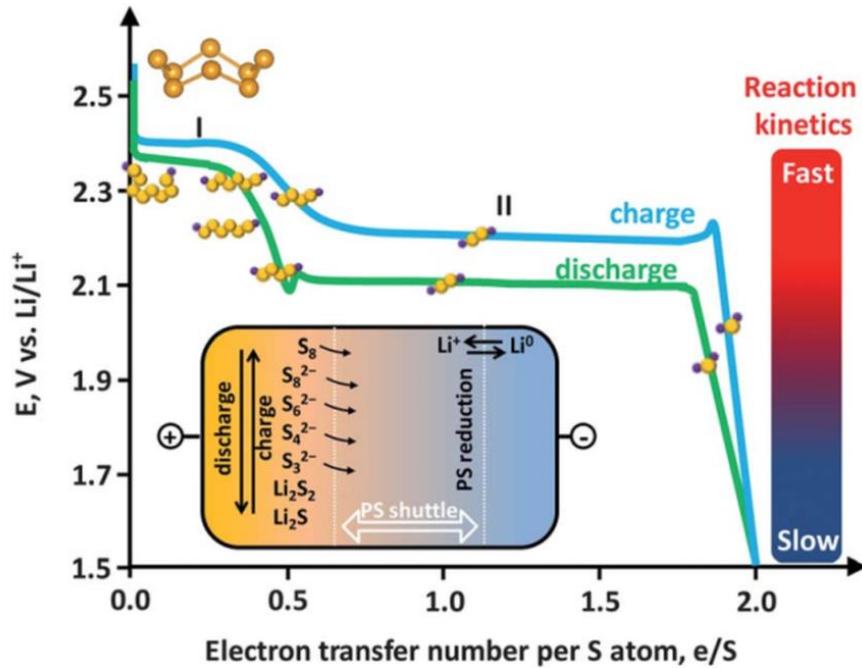
Figure 1.2 Charge/discharge profile and polysulfide shuttle mechanism of Li-S cell (adapted from ref [8]).

The charging curve of Li-S cell also shows a two-step oxidation process of sulfur in the potential region of 2.4 V to 2.6 V. During this process, the precipitated SCP is reversibly converted to elemental sulfur via. LCP intermediate species. Figure 1.2 shows the schematic representation of the charge/discharge profile and polysulfide shuttle mechanism of Li-S cell.

Challenges of Li-S Battery

Even though electrochemistry of the Li-S battery is well known for the past a few decades, commercialization of this system is significantly hampered due to several scientific and technological challenges (figure 1.3). Firstly, the elemental sulfur has low electrical conductivity of 5×10^{-30} S cm^{-1}. Moreover, the end discharge products such as Li_2S and Li_2S_2 are also highly insulating in nature. The non-conducting behaviour of sulfur cathode reduces the utilization of active material during the electrochemical process and therefore, the resulting cell delivers very low specific capacity. Secondly, for a better improvement in the electrochemical performance of Li-S cells, the reduction of cyclo-sulfur to lithium polysulfides occurs via solid-liquid transition. These polysulfides are highly soluble into the electrolyte solution, which directly enhances the utilization of active material. However, the polysulfide dissolution behaviour leads to various limitations in practical use of Li-S cells.

During the discharge process, the formed long chain polysulfides (LCP) diffuse form the cathode side, penetrate through polypropylene separator and react with the lithium anode. In the subsequent charging process, the short chain polysulfides (SCP) diffuse back to cathode to form sulfur via. LCP intermediates. The repeated redox reactions of sulfur cathode involve in "shuttle effect", which leads to irreversible loss of the active material from the cathode. Hence, the cell displays poor cycle performance and low coulombic efficiency. The Li-S cell also suffers from self-discharge with increasing the resting period that causes dynamic instability in the cell. When the sulfur cathode comes into contact with the electrolyte solution, it reacts with lithium ions in the electrolyte to produce soluble polysulfides. Due to concentration gradient in the cell, these polysulfides migrate to the anode surface to form Li_2S precipitate, which decreases the open circuit voltage (OCV) of the cell. Thirdly, the shuttling of polysulfides between the electrodes also leads to the formation of a passivating layer on the anode surface that blocks the ion and electron movement to the electrode [5,9]. Fourthly, the chemical conversion reaction of the sulfur cathode experiences huge volume expansion of 80%, which may pulverize the electrode and mechanically disintegrate it from the current collector. Therefore, the structural and morphological changes occur in the sulfur cathode, resulting in severe capacity fading within a few cycles.
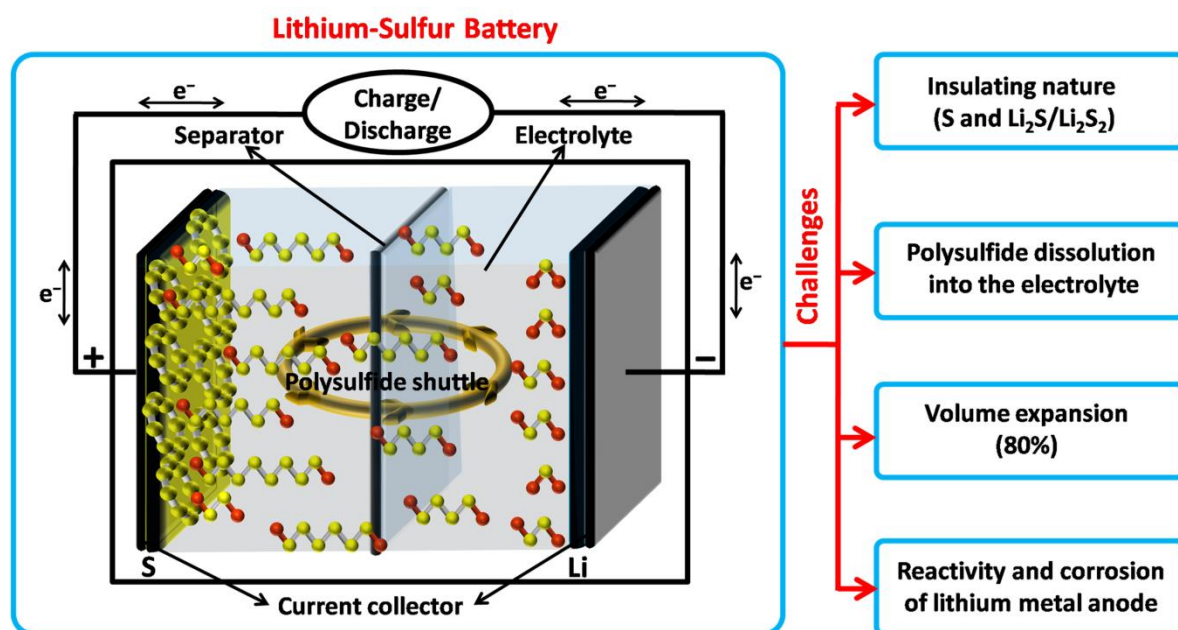
Figure 1.3 Schematic illustration of Li-S battery and their major challenges.

1.1.1 Literature Survey on Li-S Battery

The high energy density Li-S battery with sulfur cathode is considered to be one of the most important energy storage systems in transportation sector. However, the sulfur cathode

prepared by the conventional process using the active material, conductive carbon and binder, involves several technological challenges. Sulfur forms agglomerate clusters on the surface of the electrode during the process of electrode preparation. As a result, the utilization of active material is reduced and the cell shows poor electrochemical performance. Moreover, the redox reaction of the sulfur cathode involves conversion chemistry, unlike the conventional lithium-ion battery, which involves the intercalation reaction. The design of novel cell configuration during the fabrication of sulfur cathode or cell fabrication can overcome the dissolution of polysulfides. Therefore, the research has been directed towards various approaches on developing modified cathode structures, anodes and electrolytes. Figure 1.4 shows the increasing number of research articles every year since the past one decade because of the opportunities provided by modern science and technology [10].
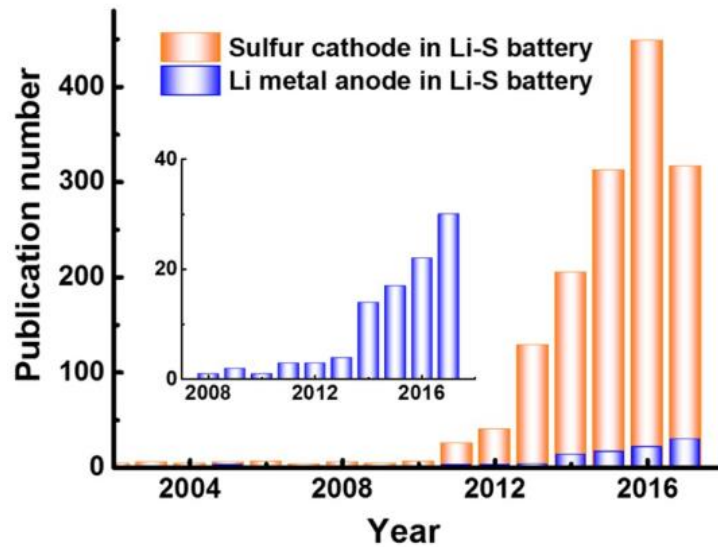
Figure 1.4 Research progress in terms of publications per year on sulfur cathode and lithium metal anode for Li-S battery (adapted from ref [10]).

1.1.1.1 Designing of Cathode Materials

Modification of the cathode structure is the preliminary step in order to improve the electrochemical performance of the Li-S battery. However, the practical energy density of the cell is mainly dependent on the amount of active material loading on the cathode. In addition, the designed cathode should be capable of trapping the dissolved polysulfides and also must have high electronic and ionic conductivities. In order to satisfy these requirements of the cathode, several methods have been developed to synthesize micro/mesoporous carbon materials [11,12], CNTs, graphene/graphene oxide [13,14], conductive polymers [15,16], etc., to infuse sulfur into the conducting medium. The high surface area and the excellent conductivity of

carbon materials can improve the conductivity, play an important role in inhibition of polysulfide dissolution and accommodate large volume expansion during the redox process. Porous carbon current collectors and sandwich-type structures have also shown similar behaviour, which enhances the electrochemical performance of the sulfur cathode. Moreover, the application of surface functionalised composite materials and metal oxides can further trap the dissolved polysulfides by facilitating chemical interaction between the functional groups and polysulfide species during redox process [17]. Hence, these sulfur based composites exhibited good electrochemical stability for longer cycles.

The sulfur composite materials were prepared by two different approaches (a) melt diffusion and (b) chemical process. The initial breakthrough was made by L. F. Nazar's group which gave the scope for the development of sulfur based composites for Li-S rechargeable battery as shown in the figure 1.5 [17]. In the melt-diffusion process, the sulfur and conducting medium (mesoporous carbon) were heat treated upto 155 ºC in an inert atmosphere. At this temperature, the low viscous liquid sulfur penetrates into these porous carbon structures due to capillary forces and gets distributed homogenously throughout the carbon matrix. In addition to the above process, the research has been developed further to infuse sulfur into porous carbon via. vaporization of sulfur, chemical deposition/sulfur melting and two-step heating process (melt-diffusion followed by vaporization of sulfur) [18,19,20]. These processes resulted in molecular level interaction of sulfur with the conducting matrix, which reduces the polysulfide dissolution to achieve high capacity with excellent cycle stability.
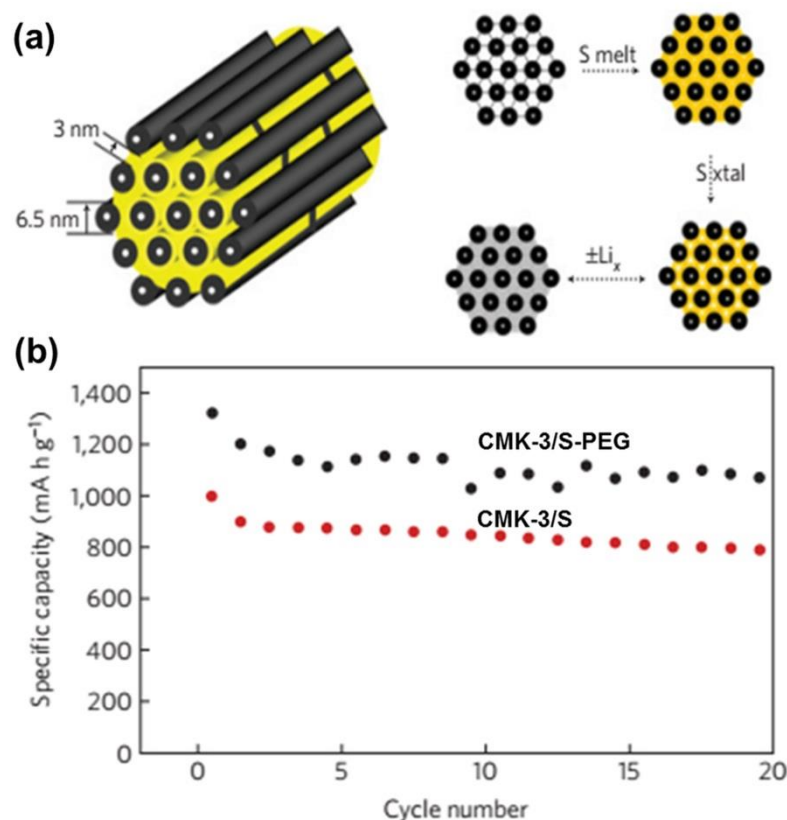
Figure 1.5 (a) Schematic representation and (b) cycle performance of mesoporous carbon/sulfur composite material (adapted from ref [17]).

In the chemical process, the precipitation of sulfur involves strong binding/absorption within porous carbon matrix. Aqueous sodium polysulfide (Na_2S_x) and non-aqueous carbon disulfide (CS_2) systems have been developed for infusion of sulfur into the porous carbon materials. When 2M HCl solution is added to a solution of Na_2S_x in which porous carbon is dispersed, the sulfur particles get infused into the pores of carbon [14]. The strong interaction and well dispersed small sulfur particles with conductive matrix can overcome the insulating nature of sulfur. In non-aqueous system, the CS_2 is used as solvent for the dissolution of sulfur. The soaking of porous carbon materials in CS_2 solution resulted in complete penetration of sulfur that decreased the polysulfide dissolution during redox reaction [21]. Furthermore, these composites were also subjected to heat treatment process in order to improve the impregnation of the elemental sulfur into the conducting medium [18,22]. The electrode materials prepared from the solution-based methods have drawn much attention due to improved electrochemical performance. These processes have an advantage that the sulfur can be easily infiltered into the conductive matrix that improves the active material utilization

and also the ionic and electronic conductivities of the electrode during the charge/discharge process.

1.1.1.1.1 Sulfur-Carbon Based Materials

The electrode prepared from the traditional process contains conductive carbon which can minimize the insulating nature of sulfur. However, the polysulfide dissolution of sulfur cathode during the redox process leads to poor electrical contact between the active material and carbon cluster. As a result, the cell displays degraded capacity in the first few cycles, associated with low coulombic efficiency. The recent progress in the development of micro/mesoporous carbon based materials can effectively satisfy the critical requirements of the sulfur cathode.

Sulfur-Micro/Mesoporous Carbon

Porous carbon materials have unique properties such as high surface area, high pore volume and high electrical conductivity due to interconnected network. The sulfur infused into micro to macro porous carbon cathodes has been widely applicable in Li-S battery due to its high conductivity and excellent polysulfide inhibition property. The porous carbon materials are categorised into three types based on the pore diameter such as microporous, mesoporous and macroporous carbons. Micropores having a diameter of less than 2 nm had an advantage of trapping dissolved polysulfides in them and also accommodating large volume expansion. B. Zhang et al.[23] prepared the microporous carbon/sulfur composite by infiltration of sublimed sulfur into the narrow microporous carbon spheres. During the electrochemical reaction, the sulfur and the formed long chain polysulfides (LCP) are constrained into the narrow micropores, resulting in high discharge capacity with good coulombic efficiency for longer cycles. Despite its considerable advantages, the microporous carbon has limited pore volume that decreases the amount of active material infusion into it. The mesoporous carbon materials have a pore diameter in the range of 2 nm to 50 nm. With the mesoporous carbon, a high amount of active material loading can be achieved. These also enhance the lithium ion and electron mobilities during the charge/discharge process [24]. H. Sohn et al.[25] reported that the mesoporous carbon spheres with high pore size of about 5 nm render high mass transport in the cathode for LCP and the resulting electrode exhibits superior electrochemical performance The macroporous carbon materials have high pore volume with a diameter greater than 50 nm. This type of materials were formed by interconnected networks, which provide good mechanical strength, and enhance the

electrolyte wettability [26,27]. However, the large pore volume also has a drawback that the dissolved polysulfide can be easily penetrated into the electrolyte solution during the redox process, which results in poor electrochemical performance in the first few cycles.

In addition to the above individual porous carbon materials with specific textural properties, the research is also focused on synthesizing the bimodal structures, which contain both micro and mesoporous carbons in the sample. G. He. et al.[28] has prepared bimodal (2 nm and 5.6 nm pore size) distributed carbon material with high surface area and interconnected pore structures as a host for the sulfur cathode. The smaller pore encapsulates majority of the sulfur mass in it, which suppresses the polysulfide dissolution into the electrolyte. Whereas, the larger pores facilitate fast diffusion of Li^+ ions and the resulting cell exhibits high discharge capacity of 501 mAh g^{-1} even at high current rate of 2 C at 100th cycle.

On the other hand, the porous carbon materials with heteroatom doping, protective coatings and metal doping have also shown the improved electrochemical performance and excellent cycle stability. These types of hybrid composites are anticipated to improve the conductivity of the electrode and also help in trapping the dissolved polysulfides in it by chemical adsorption during the redox process. For instance, H. Wu et al.[29] reported the N/P co-doped graphene/CNT/porous carbon matrix for sulfur cathode. This heteroatom doped carbon has a synergistic effect of physical adsorption of dissolved polysulfide into the porous carbon structures and chemical interaction of the formed polysulfides with the N and P atoms present in the carbon. These heteroatoms in the carbon matrix act as electron withdrawing agents due to their higher electronegativity than that of carbon atom, which promotes chemical bonding with them in the carbon matrix [30]. G. Ma et al.[31] have prepared the conductive polypyrrole-coated mesoporous carbon CMK-8/sulfur composite cathode. The infusion of sulfur into CMK-8 improves the utilization of active material during the redox process. Moreover, the presence of conductive coating on the surface of CMK-8/sulfur composite inhibits the migration of dissolved polysulfides into the electrolyte and also accommodates large volume expansion. F. Sun et al.[32] reported the N_2-doped mesoporous carbon coated with ultrafine La_2O_3 nanoparticles on the surface of carbon for the sulfur cathode. The N_2 atoms immobilise the sulfur and reduce the shuttle phenomena. Whereas, La_2O_3 nanoparticles have strong catalytic effect on sulfur reduction. The synergistic effect of N_2 and La_2O_3 offers high discharge potential and fast reaction kinetics of the electrode. As a result of heteroatom doping, conductive coating and metal oxide doping into the carbon

matrix, the sulfur composites delivered high discharge capacity and showed excellent coluombic efficiency for longer cycles.

Recently, the activated carbon derived from the biomass has been studied as an alternative matrix for the sulfur cathode in a Li-S battery. For example, S. Wei et al.[33] have prepared hierarchical porous carbon from pig bone by using KOH activation process and studied the effect of activation temperature on the textural parameters. The carbon activated at 850 ºC exhibits high surface area of 2157 m^2 g^{-1} and the resulting sulfur composite delivered high discharge capacity due to efficient trapping of dissolved polysulfides into the porous carbon. J. Guo et al.[34] have reported the synthesis of porous carbon nanosheets from corn cobs by the method of chemical activation and used them as matrix for the sulfur cathode. The thin two-dimensional porous sheet-like structure provides high active material utilization, suppresses the shuttle effect and improves rapid ion and electron motilities during the redox process.

Sulfur-Graphene and Sulfur-Graphene oxide

Graphene (2D and one-atom thick layer) made of sp^2 carbon atoms densely arranged in hexagonal structure, has drawn much attention in energy storage systems due to its tremendous electrical conductivity, high surface area, good thermal stability and chemically non-reactive nature at higher electrochemical potential window [35]. Application of graphene and graphene based composite materials in Li-S battery with unique electrode preparation and cell design delivered high electrochemical performance in comparison to pristine sulfur cathode. For instance, G. Zhou et al.[36] have prepared a sandwich-type electrode in which sulfur cathode is initially coated onto a graphene paper (current collector) and a graphene layer is coated on polypropylene membrane used as separator (figure 1.6). Thus, the sulfur is sandwiched between the two graphene layers. The presence of graphene layers on both sides of sulfur provides high electrical conductivity, good flexibility and the voids in the layers can buffer volume expansion during lithiation. In addition, the bottom graphene layer acts as an efficient polysulfide reservoir for sulfur cathode and the top graphene layer reduces the migration of dissolved polysulfides to anode. A long cycle life and good rate capability are achieved by using the sandwich type structure. Later on, the research has been extended to develop heteroatom doped graphene materials to further improve the electrochemical performance of sulfur cathode. For example, G. Zhou et al.[37] reported the synthesis of 3D N and S co-doped graphene sponge for the sulfur cathode and studied the effect of heteroatoms

in anchoring the polysulfide species by DFT calculations. They have concluded from the DFT results that the presence of thionic and pyrrolic groups on the graphene increases the binding strength of lithium polysulfide significantly to $E_b= 2.06$ eV, in comparison to individual doped N_2 ($E_b= 1.43$ eV), S ($E_b= 1.04$ eV) and pristine graphene ($E_b= 0.78$ eV). Hence, the N, S-co-doped graphene sponge can accommodate high active material loading, reduces the electrode polarization and improves the reaction dynamics for longer cycles.
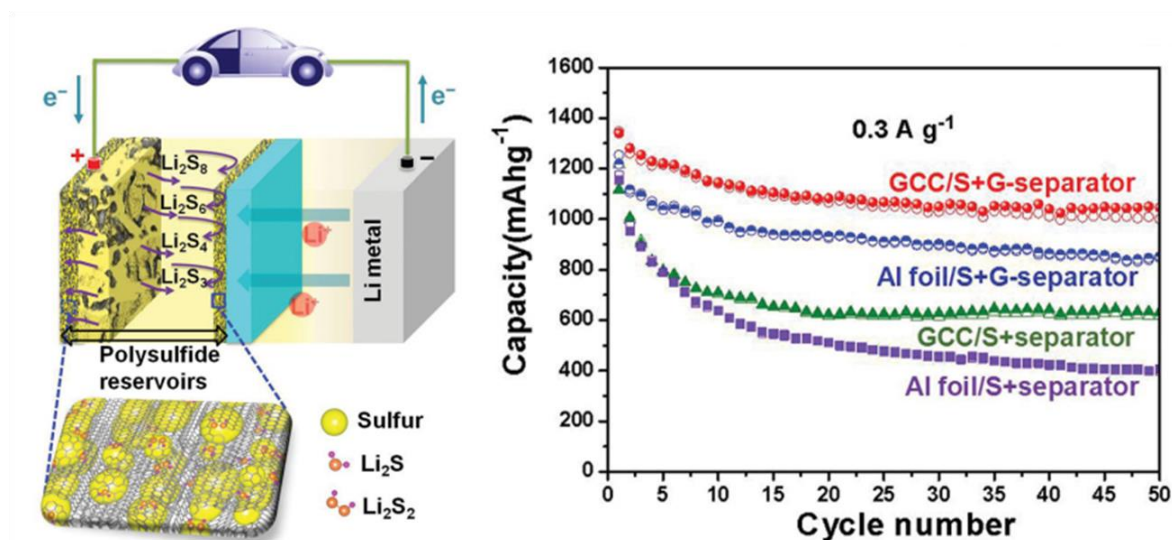
Figure 1.6 Schematic of Li-S battery with novel electrode configuration and the corresponding electrochemical performance (adapted from ref [36]).

Apart from graphene which has physical absorption of polysulfide, the graphene oxide is also used as matrix for the sulfur cathode. L. ji et al.[14] reported that the sulfur and polysulfide have strong binding property with the reactive functional groups present on the surface of graphene oxide. The chemical interaction/chemisorption between them results in good electrochemical stability of the electrode during the redox process with repeated charge/discharge cycles.

Sulfur-CNTs

Like graphene, the carbon nanotubes (CNTs) also play a major role in improving the electrochemical performance of the sulfur cathode. For instance, J. Guo et al.[38] have synthesized the disordered CNTs/sulfur composite by vapour infusion process in vacuum system. At high temperature (500 ºC), the smaller sulfur (S_6 or S_2) molecules diffuse through narrow pore channels of the disordered CNTs to hollow core and form stable S_8 molecules. These narrow pores in the composite reduce the penetration of liquid electrolyte into it, which decreases the polysulfide dissolution and the electrode shows good chemical stability with

cycling. J. Yan et al.[39] assembled the electrode in the form of layer-by layer (multi-layer) coating strategy, wherein the negatively charged S/CNT and positively charged S/PANI are alternatively deposited on the aluminium substrate. The binder free and the sandwich structured electrode acts as chemical and physical barrier that decreases the dissolution of polysulfide into the electrolyte.

Follow-up studies have been made on the development of the CNT composites (such as conductive polymer coatings, metal doping) in order to encapsulate the sulfur cathode. For example, Q. Fan et al.[40] prepared a ternary $CNT/NiFe_2O_4$-S hybrid material. The CNTs in the composite are expected to improve the electronic conductivity and the $NiFe_2O_4$ nanosheets provide strong binding sites for polysulfide intermediate species. A homogenous distribution of small sulfur particles in the composite renders fast Li^+ ion conduction and the cell exhibits high specific capacity with incredible cycle stability.

Sulfur-Carbon Nanofibre

The recent advancements in the field of nanoscience and nanotechnology provide a great opportunity for the development of novel and hybrid structures as host matrix for the sulfur cathode. In this regard, the carbon nanofibres prepared from the electrospinning process have unique textural properties such as high surface area, uniform fibre diameter, high electrical conductivity and mechanical strength due to long interconnected non-wound network [41,42]. For instance, L. Ji et al.[18] reported the synthesis of porous carbon nanofibre matt from polyacrylonitrile/poly(methyl methacrylate) (PAN/PMMA) precursors and used them for encapsulating the sulfur cathode. Wherein, PAN acts as carbon source during the carbonization process and PMMA acts as micropore inducer. The presence of narrow micropores in the carbon nanofibre enhances the electrochemical stability of sulfur cathode by reducing the shuttle effect. In addition, the macropores in the composite increase the wetability of the electrode with electrolyte solution and the nanosized fibre diameter decreases the diffusion length of lithium ions and electrons that provide high rate performance.
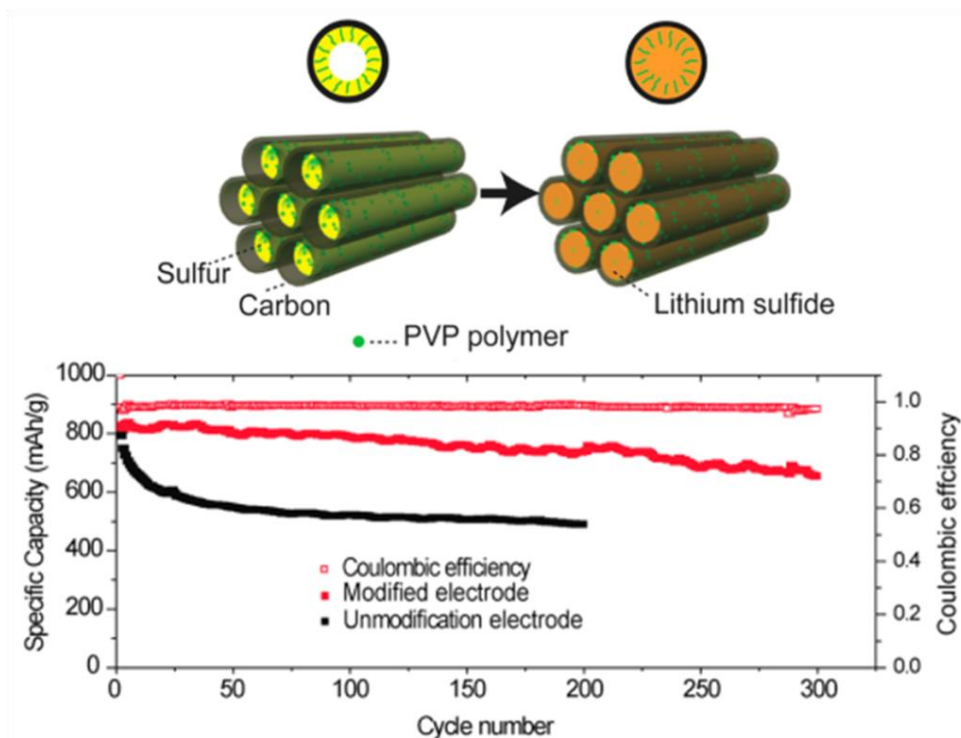
Figure 1.7 Schematic representation of polymer modified hollow carbon nanofiber/sulfur cathode and their cycle performance curves (adapted from the ref [43]).

G. Zheng et al.[43] introduced anodized aluminium oxide (AAO) as a template for the preparation of hollow carbon nanofibres to encapsulate sulfur into it. Furthermore, the surface of hollow carbon nanofibres was also modified with amphiphilic polymers, which provide strong interaction between the polar lithium polysulfides and non-polar carbon during the redox process as shown in the figure 1.7. The polysulfide intermediate species were interfacially trapped in the modified cathode and the cell showed excellent cycle performance with high capacity retention of 80% for over 300 cycles.

1.1.1.1.2 Sulfur-Metal Oxides

A variety of porous carbon based materials with unique properties have been explored for use in Li-S battery in order to trap lithium polysulfides. However, the physical   adsorption of these carbonaceous materials can inhibit the diffusion of polysulfides for only a few cycles. On the other hand, research is also focused on trapping the dissolved polysulfides by chemical interaction [44]. X. Ji et al.[17] employed PEG grafted mesoporous carbon for constraining the dissolved polysulfide in the cathode during charge/discharge process. Later on, the metal oxide composites were also used in Li-S battery due to their strong binding property (polar-polar interactions) with polysulfide species. Z. W. Seh et al.[45] prepared sulfur-TiO_2 yolk-shell (nanostructured) composite as shown in the figure 1.8. The internal void space can

accommodate large volume expansion during the redox process, which decreases disintegration of active material from the current collector and also suppresses the polysulfide dissolution.
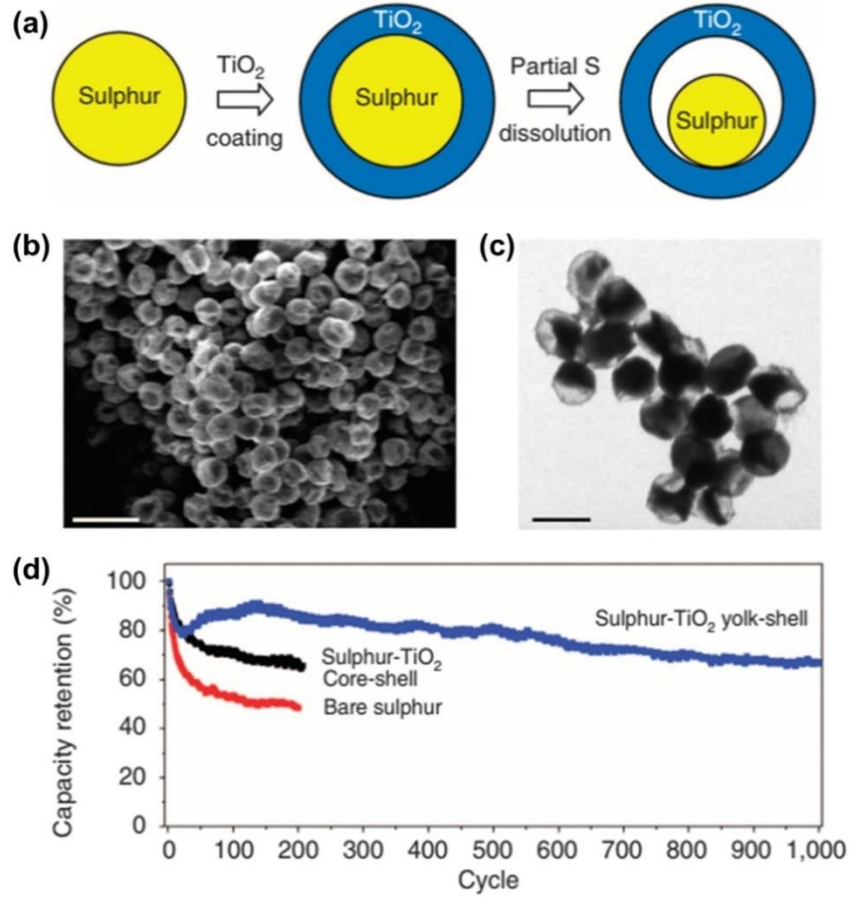
Figure 1.8 (a) Schematic for the synthesis of sulfur-TiO$_2$ yolk shell, (b) SEM image, (c) TEM image, and (d) comparative cycle performance (adapted from the ref [45]).

Q. Pang et al.[46], prepared Ti$_4$O$_7$ (Magneli phase), which has high surface area and excellent conductivity of 2 x 10^3 S cm^{-1}. The presence of polar O-Ti-O bonds in the material shows a strong affinity towards polysulfides and the resulting cell displayed stable cycle performance for 500 cycles. Further, the metal oxide-coated separators were also used in Li-S battery in order to trap the dissolved long chain polysulfide (LCP) intermediates in the cathode. W. Li et al.[47] used V$_2$O$_5$-coated polypropylene separator as a barrier film for the sulfur cathode. This layer inhibits the migration of dissolved polysulfides from the cathode to the anode surface, which improves the active material utilization for prolonged cycles.

1.1.1.1.3 Sulfur-Conductive Polymers

Recently conductive polymers have been explored in energy storage systems to improve the ion and electron transport pathways during the redox process. In Li-S batteries,

conductive polymers play an important role in modifying the structure of the sulfur cathode that prevents the polysulfide dissolution. For example, F. Wu et al.[48] prepared polythiophene/ sulfur core-shell structures by *in-situ* chemical polymerization process, wherein the uniformly coated polythiophene on the surface of sulfur powder acts as conductive additive as well as porous absorbing agent. Hence, the polythiophene/sulfur electrode delivered high electrochemical performance and stable cycle life in comparison to pure sulfur cathode.

Studies have been extended to other conductive polymers for tailoring the architecture of the sulfur cathode. L. Xiao et al.[49] developed a simple and environment friendly process for the preparation of self-assembled polyaliline nanotubes for encapsulating the elemental sulfur. During the heat treatment process at 285 ºC a fraction of sulfur reacts with polyaniline nanotubes and forms a stable three dimensional composite. Moreover, the cross linked inter- and/or intra-chained disulfide bonds formed by *in-situ* vulcanization provide a strong physical and chemical confinement of sulfur and polysulfide species during the redox process. In order to further improve the internal electrical conductivity of the composite materials, the researchers have explored the use of highly conductive MWCNTs, mesoporous carbons, and graphene materials. These materials are intended to decrease the charge transfer resistance of the electrode and the polymers provide strong chemical interaction with polysulfide ions. For example, C. Wang et al.[50] synthesized MWCNTs/S/polypyrrole composite, in which the MWCNTs/S is prepared by acid-based catalysed chemical precipitation of sulfur on MWCNTs. Finally, polypyrrole (PPy) was coated on MWCNTs/S by *in-situ* chemical oxidative polymerization of pyrrole. Hence, the combination of high surface area MWCNTs and conductive polymer coating showed better improvement in the electrochemical performance of sulfur cathode by alleviating the polysulfide dissolution into the electrolyte. In addition, these types of structures are anticipated to accommodate large volume variation during the charge/discharge process.

1.1.1.1.4 Polymerized Sulfur

Pure sulfur cathode suffers from insulating nature and polysulfide dissolution that resulted in low active material utilization and irreversible loss of active material during repeated cycling. The use of various porous carbon materials, metal oxides, 3D current collectors etc., can inhibit the migration of dissolved lithium polysulfides to the anode surface. The research has also been directed towards the use of polymerised sulfur as the cathode material in order to prevent the dissolution of polysulfide species into electrolyte.

J. Wang et al.[51] initiated the synthesis of conductive polymer matrix-embedded sulfur composite material. The elemental sulfur dehydrogenates the polyacrylonitrile (PAN) polymer and forms conductive chain during the heat treatment process. Concurrently, the polar -CN- functional groups cyclise to highly stable heterocyclic compound, wherein the sulfur atoms intercalate. The molecular level interaction of sulfur atoms with conductive backbone prevents the formation of agglomerate structures and also inhibits the dissolution of polysulfide species. N. L. Doan et al.[52] studied the binding mechanism of sulfur with dehydrogenated PAN by varying the sulfur content. The proposed mechanism was based on the size and structure of the polymer backbone, which involves the embedding of 8-membered sulfur with 4 heterocyclic rings of the dehydrogenated polymer. The upper limit of sulfur content in the composite is 56% and with an increase in the sulfur content beyond this, the cell delivers poor electrochemical performance due to superficial deposition of sulfur.

Z. Lin et al.[53] prepared sulfur-rich lithium polysulfidophospate (Li_3PS_{4+n} (0<n<9)) by the chemical reaction of elemental sulfur with lithium thiophospate in tetrahydrofuran solvent. During the reaction the sulfur atoms are added to the sulfur atoms of the charged terminal, PS_4^{3-} anion and form stable S-S bond. This type of compound has high lithium-ion conductivity and the discharge process involves the formation of Li_2S and Li_3PS_4 as by products. The reversible redox reaction with improved intrinsic ionic conductivity renders good chemical and cycle stability of the electrode. Further, W. J. Chung et al.[54] explored the use of processable high sulfur content polymer (poly(sulfur-random-1,3-diisopropylbenzene)) prepared by using inverse vulcanization method. The electrochemical behaviour of this polymer is similar to that of pure elemental sulfur and the electrode showed high capacity retention due to mitigation of the shuttle effect.

1.1.1.1.5 Current Collectors

The substrates also play a prominent role in improving the electrochemical performance of sulfur cathode in Li-S battery. The conventional Li-ion and Li-S batteries use 2D aluminium current collector as a substrate for electrode preparation. Generally, In batteries during prolonged cycling the Al substrate may be prone to corrosion [55]. Moreover, the initial reduction of sulfur involves liquid-liquid transition that leads to loss of active material for the Al current collector and the cell exhibits high internal resistance associated with poor electrochemical performance. Hence, an intense research has been focused on 2D and 3D current collectors such as 3D carbon paper, carbon and metal-coated Al current collector and

free standing electrode (graphene, MWCNTs, carbon nanofibre) in order to improve the long term stability of the cells.

For Instance, S. H. Chung et al.[56] employed porous carbon current collector, which has low density, high porous structure and light weight when compared to Al current collector. These unique features provide high sulfur loading and increase the electrolyte absorption that retained the dissolved polysulfides in the cathode part. In addition to 3D carbon substrates, the metal coated Al (metal= Pt, Au or Ni) with high porous structure, hydrophilic nature and catalyst activity provide strong adsorption towards polysulfide intermediates during the redox process and thereby, eliminate the use of carbon matrix, binder and conductive carbon. Moreover, these substrates decrease the charge transfer resistance, improve the active material utilization and the resulting cell exhibits superior electrochemical performance [57].

Apart from the modified 2D current collectors, another new approach has also been developed i.e., free standing electrode for constraining the polysulfide species in it. However, the ideal requirement of a free standing electrode is that it should be flexible, strong enough during the infusion of active sulfur and must retain its structure after repeated charge/discharge processes [59]. Moreover, the free standing electrodes have unique properties such as light-weight in comparison to conventional Al current collector, high porosity and good electrical conductance due to their continuous network. For example, G. Zhou et al.[58] prepared nitrogen-doped double-shelled hollow carbon spheres infused with sulfur followed by graphene wrapping, which acts as flexible free standing electrode for high power Li-S battery (figure 1.9). The rationally designed structure provides sufficient space to accommodate volume expansion during the cycling process. In addition, the nitrogen atoms present in the carbon matrix can chemically bind with the dissolved polysulfide species and the graphene coating on to the surface of hollow carbon spheres can further immobilize the dissolved polysulfide species in the cathode.
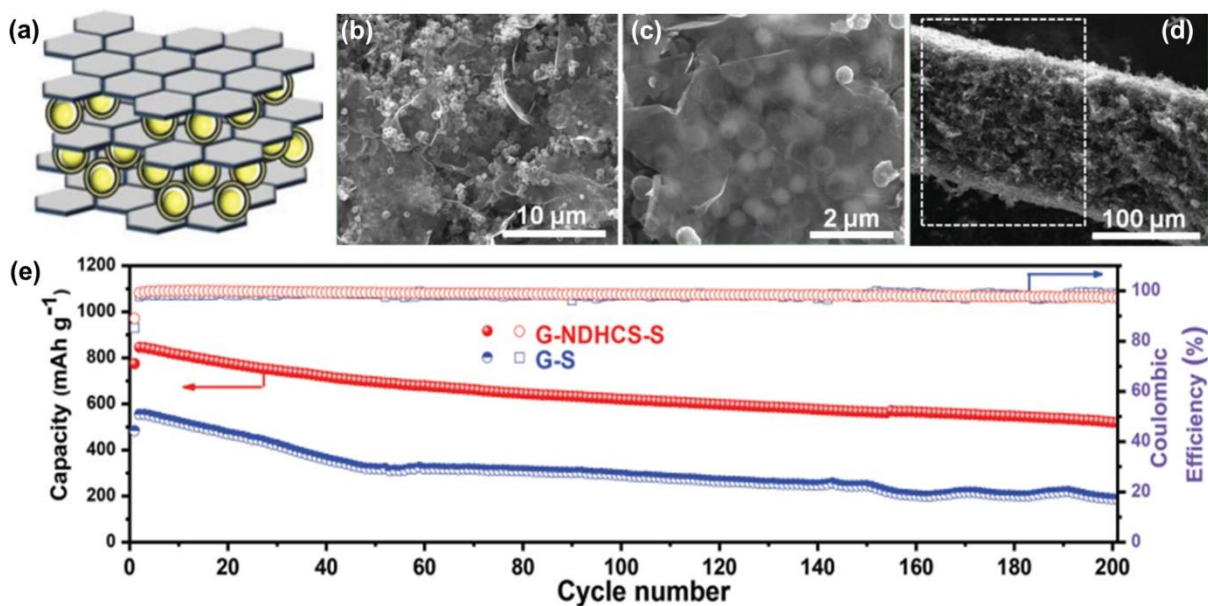
Figure 1.9 (a) Schematic for the of free-standing electrode, (b) and (c) SEM images at different magnifications, (d) SEM-cross sectional images and (e) comparative long-term cycle performance (adapted from the ref [58]).

1.1.1.1.6 Li$_2$S Cathode

The fully lithiated Li$_2$S is the final end discharge product of the sulfur cathode, which is also considered to be the promising candidate for Li-S battery due to its high theoretical capacity (1166 mAh g^{-1}) and high melting point (938 ºC) [60]. The advantage of using Li$_2$S as cathode is that it can be directly paired with high capacity lithium-free anodes (Sn and Si) to form Li-S battery in full-cell configuration. As a result, the energy density of the rechargeable cell dramatically increases. In addition, the use of lithium metal anode in conventional Li-S cell can be avoided, which has severe intrinsic safety issues due to dendrite formation with repeated cycling process [9,60]. Further, the volume expansion of the electrode can be mitigated because the Li$_2$S cathode shrinks to form sulfur as the final product. Therefore, the electrode remains structurally stable for long-term cycles. However, bulk Li$_2$S material is considered to be electrochemically inactive due to its poor ionic and electronic conductivities. Moreover, the Li$_2$S cathode is highly sensitive to moisture and also suffers from polysulfide dissolution. A uniform conductive coating throughout the Li$_2$S particle surface can improve the solid state diffusion of ions and electrons form the bulk material. Z. Lin et al.[61] have synthesized core-shell structured carbon-coated nanosized Li$_2$S cathode followed by additional coating of graphene oxide (GO) onto these particles. The carbon coating on the outer surface of Li$_2$S particles prevents the direct contact with the electrolyte, which inhibits the dissolution

of the formed polysulfide intermediates. The functional groups present on the surface of GO are anticipated to trap the polysulfide species by chemisorption and the resulting electrode exhibits superior electrochemical performance during the fast reaction kinetics. Alternatively, the chemically modified surfaces, and metal oxide coating on Li_2S also enhance the ionic conductivity and chemically traps the dissolved polysulfides in it. For example, Z. W. Seh et al.[62] reported the synthesis of PPy-Li_2S by *in-situ* non-aqueous polymerization process. The N_2 atoms present on PPy possess strong interaction with the Li present on Li_2S, which covers the complete surface of Li_2S particles. As a result of chemisorption, the polysulfide species are trapped in the cathode part, which increases the cycle life of the electrode. Moreover, the conductive coating on the surface of Li_2S particles helps in increasing the ion and electron conductivities during the redox process. Y. Chen et al.[63] have synthesised free-standing porous Al_2O_3-Li_2S-graphene electrode, in which Al_2O_3 was deposited on Li_2S-graphene by atomic layer deposition technique. The porous graphene sheets provide high conductivity and act as physical barrier for polysulfide species. Whereas, a thin layer of Al_2O_3 on the surface of the composite exhibits strong chemical interaction with the polysulfide species, which suppresses the dissolution of polysulfides into the electrolyte.

1.1.1.1.7 Effect of Binders

In general, the electrode for the cathode is prepared by casting active material and conductive additive onto Al current collector by using polymeric binder. The primary role of the binder is to adhere different particles of the active material along with the conductive additive to the substrate. Though the conventional binders such as polyvinylidenedifluoride (PVDF) [64] and polytetrafluoroethylene (PTFE) [65] have high electrochemical stability, they cannot tolerate huge volume expansion during the charge/discharge process. This results in collapse of the electrode structure and formation of Li_2S precipitate onto the surface of the carbon particles. In addition, these binders are inactive to polysulfide species that cannot suppress the shuttle effect.

Recently, water soluble and functional binders have been explored for sulfur cathode as alternatives to the conventional binders in order to create robust electrode structure and improve the polysulfide retention ability. For example, M. He et al.[66] prepared elastomeric water soluble binder containing a mixture of styrene butadiene rubber (SBR) and sodium carboxymethyl cellulose (CMC) in 1:1 ratio for sulfur cathode. The SBR has strong binding property and good flexibility. Whereas, CMC is well known for its high dispersion capability

and acts as thickening agent for aqueous system due to the presence of surface functional groups. This aqueous binder renders a uniform distribution of sulfur and conductive carbon particles, which enhance the electrical conductivity and increases the utilization of active sulfur. J. Wang et al.[67] used highly water soluble carbonyl-β-cyclodextrin as binder for sulfur cathode. This binder has unique properties such as strong bonding strength, moderate viscosity and has wide electrochemical stability window in the range of 0-5 V. The effective binding and uniform dispersion of sulfur particles resulted in maximum utilization of active material upto 92% with good cycle performance. Further, G. Ai et al.[68] studied the effect of conductivity and functional binders on the electrochemical performance of the sulfur cathode by using different polymer binders such as poly(9, 9-dioctylfluorene-co-fluorenone-co-methylbenzoic ester) (PFM), poly(vinylpyrrolidone) (PVP), poly(3,4- ethylene-dioxy-thiophene) and PVDF. Among them, PFM and PVP binders contain carbonyl functional groups, which showed strong binding energy with sulfur atoms that assist the solid-phase precipitation during both charge and discharge processes. This resulted in reducing the shuttle effect and preventing self-discharge in contrast to the other binders with no carbonyl groups (PEDOT and PVDF). Moreover, these binders (PFM and PVP) have improved the conductivity and provide large surface area for the reaction to take place, which in turn enhances the active material utilization for longer cycles.

1.1.1.2 Electrolyte and its Additives

In batteries the electrolyte acts as ion transport medium between the cathode and the anode during the redox process. In a Li-S battery, different types of electrolyte systems have been explored such as liquid, gel-polymer and solid state electrolytes in order to suppress the migration of polysulfide species to the anode surface. Typically, the conventional LIBs use $LiPF_6$ electrolyte (ethylene carbonate (EC)/dimethyl carbonate (DMC) in 1:1 ratio) due to its high ionic conductivity in comparison to other systems [69]. However, in Li-S battery the carbonate based solvents are not used because the polysulfide intermediates are highly reactive to carbonates via. nucleophilic addition or substitution reaction to form irreversible products (figure 1.10) [70]. This parasitic reaction in the cell resulted in loss of active sulfur from the electrode that leads to severe capacity fading with cycling. The ether based solvents such as DME and DOL are considered to be suitable media for Li-S battery. The linear chain in DME increases the solubility of polysulfides and improves the reaction kinetics. Whereas, the cyclic DOL helps in forming stable solid electrolyte interface on the lithium metal and has

limited polysulfide dissolution property, which reduces the reaction kinetics [71,72]. Hence, a mixture of DME/DOL has high solubility of elemental sulfur and also increases the maximum utilization of active material, which enhances the electrochemical performance of Li-S cell. Alternatively, ionic liquids such as N-methyl-N-butylpyrrolidinium bis(trifluoromethylsulfonyl)imide ($Py_{14}TFSI$) [73], equimolar LITFSI in Triglyme/tetraglyme [74], 1-methyl-1-propylpyrrolidinium bis(fluoro-sufonyl)imide (MPP FSI) [75] were also used alone or in combination with DME as solvents. These solvents have low donor ability due to their weak Lewis basicity, which results in suppressing the dissolution of polysulfide species into the electrolyte. Hence, the electrochemical reduction of sulfur involves the solid-state process and most of the intermediate species immobilised onto the electrode. As a result, the Li-S cells delivered an improved electrochemical performance with excellent cycle stability [76].

(a) EC decomposition mechanism
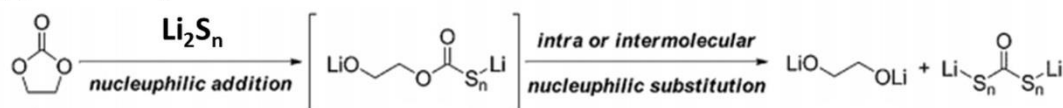
(b) EMC decomposition mechanism
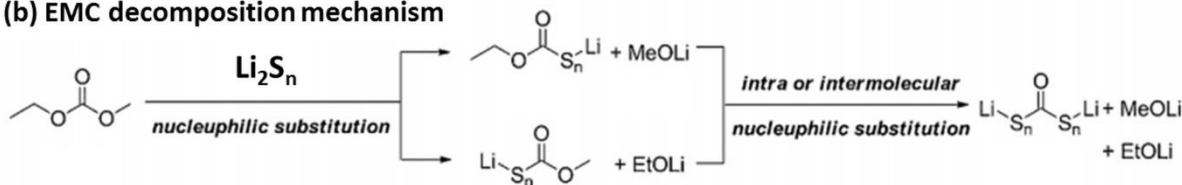
Figure 1.10 Mechanisms for the decomposition of carbonate based solvents with polysulfides species (adapted from the ref [70]).

In addition to the solvent, the chemical compatibility of the lithium salt with the polysulfide species is also an important criterion. A review article by S. S. Zhang.[71] stated that the conventionally used salts such as $LiPF_6$, $LiBF_4$, $LiClO_4$, lithium bisoxalatoborate (LiBOB) etc., are not suitable for the Li-S battery due to their high reactivity towards polysulfide species. So far, $LiN(SO_2CF_3)_2$ salt dissolved in a binary mixture of DME/DOL with volume ratio of 1:1 is considered to be the best electrolyte for the sulfur cathode. This electrolyte has unique properties such as low viscosity, high ionic conductivity, good chemical stability and high polysulfide dissolution property and has negligible corrosion effect on Al current collector. Furthermore, the research has also explored in studying the concentrated electrolyte systems. For instance, L. Sou et al.[77] prepared ultrahigh concentrated

electrolyte namely 7M LITFSI (solvent-in-salt) for the sulfur cathode. They have concluded that in 7M LITFSI electrolyte the dissolution of polysulfides and shuttle effect can be minimised because of low solubility of polysulfides. Moreover, concentrated electrolyte systems suppress the lithium dendrite formation due to their high salt concentration and high viscosity. However, it should be noted that these electrolytes at very high concentrations have negative impact on the cell performance at higher currents due to the decreased ionic transport. The resulting discharge capacity profile of the cell shows severe potential drop due to concentration polarization.

Though the dissolution of polysulfides into the electrolyte is inevitable or even necessary step for the reduction of sulfur cathode during the electrochemical process, the shuttle phenomenon and parasitic side reactions cause passivation of lithium metal (anode) surface with repeated cycling, which decreases the lithium cycling efficiency [78]. Therefore, excessive lithium ions are required for Li-S battery due to severe degradation of lithium metal. The efforts have also been made to enhance the stability of anode by modifying the surface film (SEI) using some of the electrolyte additives. Such breakthrough was done by Y. V. Mikhaylik [79] by introducing $LiNO_3$ into the electrolyte as an additive. The $LiNO_3$ present in the electrolyte passivates the surface of Li anode by forming a stable SEI layer on the surface. Further, S. S. Zhang [80] studied the role of $LiNO_3$ electrolyte additive on both the Li anode and sulfur cathode. On Li anode, this additive not only prevents the chemical reaction between polysulfides and Li metal, but also protects the anode surface by inhibiting the reduction of polysulfide species on the Li anode. On sulfur cathode, $LiNO_3$ undergoes large irreversible reduction at a potential of 1.6 V during the first discharge cycle and gets disappeared in the subsequent cycles. Hence, it is essential to select the discharge cut-off potential of cell (~1.5 V), which can avoid the formation of irreversible reduction products on the cathode surface. As a result, the coulombic efficiency and cycle stability of the electrode are greatly increased. Furthermore, the research has also been extended to use various types of additives. For instance, R. Xu et al.[81] reported the role of polysulfide additive into the electrolyte on sulfur cathode. This additive provides the dynamic equilibrium between the dissolution and precipitation of polysulfide species, which acts as self-healing agent in Li-S battery for longer cycles. F. Wu et al.[82] introduced lithium iodide into the electrolyte, which resulted in the formation of a protective layer on both the electrode surfaces. They have also studied the *in-situ* formation of this protective film by quantum chemistry calculations.

Initially, the I· radical is generated at a potential of ~3 V vs. Li/Li$^+$, which further reacts with dimethoxyethane (DME) in the electrolyte to form DME(-H) radical. Finally, the DME(-H) radical polymerises to form polyether layer on the surface of cathode that inhibits the dissolution of polysulfide species into the electrolyte. Though the concentration of additive in the electrolyte is very low, it plays a major role in changing the bulk properties. It reduces the viscosity, improves the ionic conductivity, protects the lithium anode and thus significantly improves the electrochemical performance of the Li-S cell.

Additionally, the research has also been extended to use gel-polymer and solid-state electrolytes prepared by using new chemical approaches, which have shown decreased polysulfide shuttle phenomenon during the redox process. Moreover, these electrolytes may function as separator and also prevent the formation of lithium dendrite on the surface of anode. For example, K. Jeddi et al.[83] prepared a composite polymer electrolyte containing mesoporous silica particles. S. S. Zhang.[84] reported a free-standing poly(ethylene oxide)/SiO$_2$ based gel-polymer electrolyte. This type of polymer electrolyte not only acts as a medium for facilitating rapid ion movement, but also acts as polysulfide dissolution barrier during charge/discharge process.

M. Nagao et al.[85] fabricated the solid-state Li-S battery by using the solid Li$_2$S-P$_2$S$_5$ electrolyte. Wherein, the ball milled sulfur composite, solid electrolyte and Li-In alloy anode were stacked layer-by-layer to form a solid-state Li-S battery. They have concluded that the cell performance mainly depends on the crystallinity of sulfur, size of the particles and intimate contact between the particles on the electrode. R. C. Xu et al.[86] prepared Li$_7$P$_{2.9}$Mn$_{0.1}$S$_{10.7}$I$_{0.3}$ glass-ceramic solid electrolyte by high energy ball milling process and has shown that it possesses high ionic conductivity of 5.6 S cm^{-1} and high operating voltage of 5 V vs. Li/Li$^+$. The Li-S cells fabricated by using this solid electrolyte exhibited superior capacity and good rate capability. Despite considerable advantages of the gel-polymer and solid-state electrolytes, the low ionic mobility during the rapid charge/discharge processes have negative impact on the cell performance due to sluggish reaction kinetics at the electrode/electrolyte interface.

1.1.1.3 Modified Separators and Membranes

It is well known that the separator in batteries physically isolates the cathode and anode from each other. Basically, the separators used in conventional LIBs are made of polymeric material like polypropylene (PP) or polyethylene (PE) or glass fibre, which permits

only ions through it and blocks the electrons. In addition, they possess good flexibility and high mechanical strength, which protect them from tearing and puncher. However, these separators cannot inhibit the migration of dissolved polysulfides to the anode surface during the charge/discharge process [87]. As a result, the soluble polysulfides shuttle between the electrodes (cathode and anode) and that leads to dynamic capacity fading and poor cycle performance. In order to overcome these issues, the research has also focused on functional separators such as cation selective membrane, modified separator i.e., with additional layer coated on it and interlayer that can effectively trap the polysulfide species.

In the first case, I. Bauer et al.[88] reported the nafion-coated conventional separator as a cation selective membrane, which is expected to localise the dissolved polysulfides in the cathode part. The reason for trapping the polysulfide species is due to the presence of SO_3^- ions in the nafion film, which allows only the positively charged lithium ions through it. Whereas, the negatively charged polysulfide species are repelled due to electrostatic repulsion force. Hence, the coulombic efficiency and cycle stability of the cell increase. But, the main disadvantage of the cation selective membrane is that it decreases the ionic and electronic conductivities of the electrode material, which reduce the electrochemical utilization of the active material.

In case of modified separators, an additional conductive layer was coated onto the polypropylene separator to trap the polysulfide species in the cathode side. For instance, J. Balach et al.[90] synthesized the mesoporous carbon by resorcinol/formaldehyde process by using hard-template process followed by coating on the surface of commercially available polypropylene separator. S. H. Chung et al.[91] coated the commercially available conductive super P carbon on polypropylene separator. These modified separators possess excellent flexibility, good mechanical strength, and act as upper current collectors that confine the active material in it. Therefore, the electrochemical performance of the cell is greatly improved due to physical confinement of the dissolved polysulfide species in it for prolonged cycles. Apart from the modified separator, an interlayer (membrane) is also used as an absorbent for the dissolved polysulfides. Particularly, the light weight carbon based interlayers function as good barriers and effective polysulfide reservoirs that increase the re-utilization of the active material during cycling process [92]. R. Singhal et al.[89] prepared micro and mesoporous carbon nanofiber mat by electrospinning process and used it as an interlayer for sulfur cathode (figure 1.11). The application of interlayer has an advantage that it

decreases the resistance of the cell, inhibits the dissolved polysulfide species and thereby the discharge capacity increases during the cycling process.
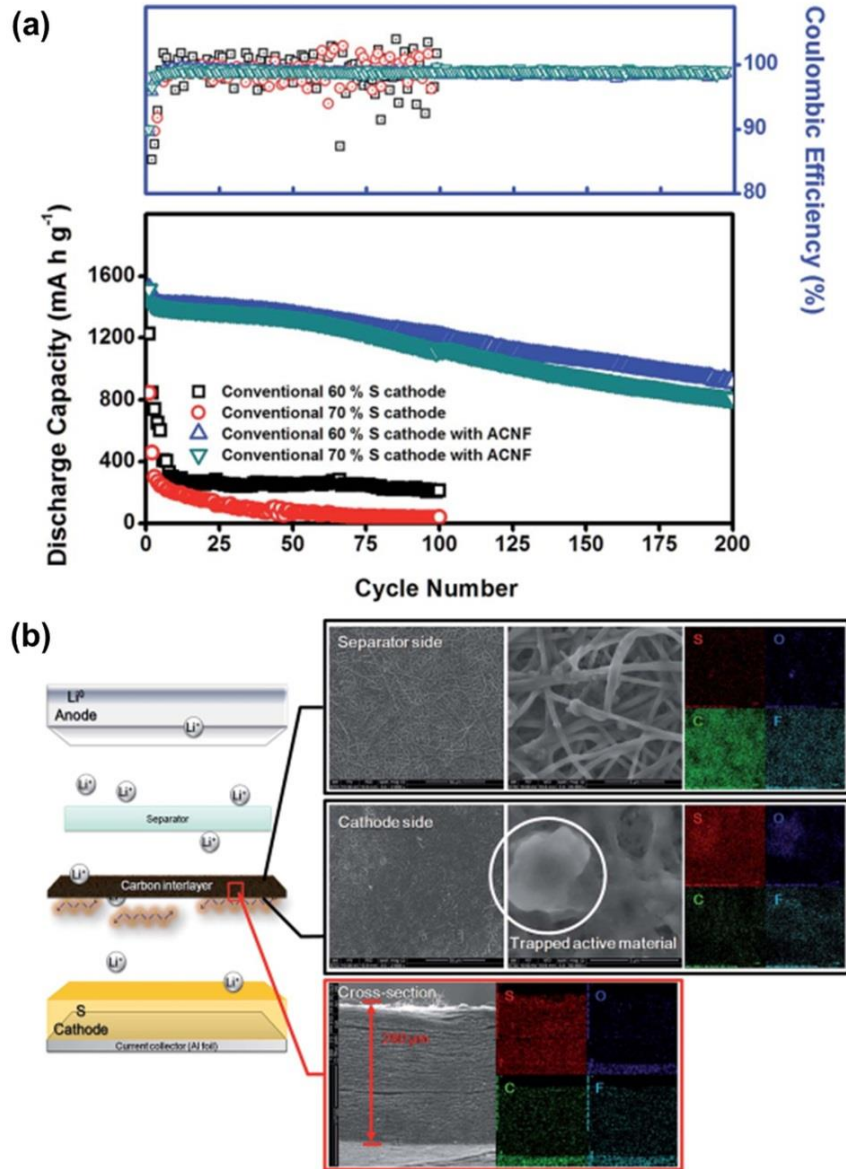
Figure 1.11 (a) Comparative cycle performance curve of with and without carbon fibre interlayer and (b) corresponding SEM-EDS mapping of interlayer after 200 cycles (adapted from the ref [89]).

1.1.1.4 Designing of the Anode Materials

In Li-S battery, the lithium metal is generally used as the reference electrode (anode) due to its high theoretical capacity (3860 mAh g^{-1}), light weight and low operating potential. However, the major drawback of using the lithium metal is that it can form lithium dendrites with repeated charge/discharge process. These dendrites penetrate through the separator that causes internal short circuit and thermal runaway of the cell. Moreover, lithium metal is

sensitive to polysulfide species and forms a passivating layer on the surface of anode, which decreases the lithium ion movement during the fast reaction kinetics [93]. The increase in manufacturing cost and safety concerns are currently hampering the large-scale production of Li-S batteries in addition to aforementioned challenges (section 1.1).

In order to mitigate this issue the research has been focused on *in-situ/ex-situ* protective coating on the surface of lithium metal anode that prevents the reaction between lithium and polysulfides and also reduces the dendrite formation. In the *in-situ* process, the addition of electrolyte additives, solvents and electrolytes of higher concentration play an important role in the formation of a stable SEI layer on the surface of anode [94,95]. For instance, C. Zu et al.[94] used DOL-fuorinated ether (1,1,2,2-tetrafuoroethyl-2,2,3,3-tetra-fuoropropylether, TTE) as the electrolyte for sulfur cathode. They have observed the formation of SEI layer with a composition of LiF, which inhibits the parasitic reaction on the surface of lithium metal anode. Whereas, in the *ex-situ* process, a thin layer of metal is laminated on the surface of lithium anode. A. C. Kozen et al.[96] prepared a 14 nm thick Al_2O_3 coated lithium metal anode by atomic layer deposition process. These types of layers passivate the anode surface that suppresses the reduction of polysulfide species on the Li anode and increases the coulombic efficiency and the cycle stability of the cell.

Alternatively, the pre-lithiated anode materials such as tin and silicon with novel electrode structure and cell design have also been explored in Li-S battery. These anode materials have high theoretical capacity, which can compensate the charge storage capacity of the sulfur cathode and operate at lower potential. Hence, the combination of these electrodes to form a full cell can deliver high specific energy that is 2-3 times higher than conventional Li-ion battery. For instance, B. Duan et al.[97] fabricated a novel Li-S battery by using Sn/C as anode, carbyne polysulfide as cathode, wherein the thin lithium foil placed on the surface of anode acts as lithium source. This battery possesses high energy and high safety, which can overcome the safety issues allied with the lithium metal. C. Shen et al.[98] used the pre-lithiated nafion-coated silicon as an anode for Li-S battery. They have also studied the effect of weight ratios of anode to cathode on the electrochemical performance of Si-S battery. The battery at the optimised cathode to anode ratio of 1.00:1.43 delivered high specific energy of 590 Wh kg^{-1}, which is two times higher than the commercially available Li-ion battery. Furthermore, the research has also been directed towards the construction of lithium metal-free battery. In this case, the Li_2S is used as cathode and silicon/tin as anode and the cell

delivered appreciated electrochemical performance with extended cycle stability. For example, J. Hassoun et al.[9] introduced tin-sulfur battery by using Sn/C as anode, Li_2S/C as cathode and the two electrodes are separated by gel polymer electrolyte. The use of gel polymer electrolyte not only increases the safety, but also prevents the migration of the dissolved polysulfides to the anode surface and the resulting cell exhibited high energy density of 1100 Wh kg^{-1}.

1.2 Supercapacitors

Supercapacitor also known as ultracapacitor and electrochemical capacitor, is an energy storage device that provides high power density, good electrochemical stability and long cycle life. In 1971, the Standard Oil Company and Nippon Electric Company (NEC) were the first to commercialize the double layer capacitor with the name of supercapacitor [99,100]. Later on, this technology has been improved by developing electrode materials, electrolytes and manufacturing processes. Presently, the supercapacitors have been commercialized by the companies such as Maxwell, Panasonic, NEC and so on and find wide-spread applications ranging from portable electronic devices to hybrid electric vehicle technology and energy storage generated by solar cells.

Principle of Supercapacitors

The supercapacitor consists of two electrodes, electrolyte and the separator, which separates both the electrodes. During the charging/discharging process, the opposite charges accumulate on the surface of the electrode forming an electrical double layer for charge storage as shown in the figure 1.12. The supercapacitors use high surface area electrode materials. Therefore, the specific capacitance and energy density dramatically increase due to high surface to volume ratio and smaller distance between the two electrodes.

The specific capacitance (C_s) is calculated by using the equation 1.7.

$$C_s = \varepsilon\, A/D \qquad\qquad (1.7)$$

Where

ε = Dielectric constant of the electrolyte

A = Surface area of the electrode ($m^2\, g^{-1}$)

D = Distance between the electrodes

Based on the energy storage mechanism, the supercapacitors are further divided into three types; (a) Electric double layer capacitor, which undergoes a non-faradaic reaction process, in which the ions are stored on the opposite electrodes at the electrode/electrolyte interface by physical adsorption. Since there is no charge transfer reaction between the electrolyte and electrodes in EDLCs, the energy storage is highly reversible and has longer cycle life. Highly porous carbon materials are used as electrodes for EDLCs, (b) Pseudocapacitor, which involves faradic reactions, wherein the charge transfer is accomplished through the redox reactions between the electrode and electrolyte. Conductive polymers and metal oxides are used as the electrodes for pseudocapacitors and (c) Hybrid capacitor, also known as Li-ion capacitor. The charge storage takes place via both the non-faradaic and faradaic reactions. Hybrid capacitor uses activated carbon as cathode and pre-lithiated carbon (graphite) as anode to attain high output voltage. Hence, the capacitance and energy density of the pseudocapacitor and hybrid capacitor are higher than the EDLCs. But, these have shorter cycle life due to faradic reactions. Moreover, the power capabilities of these devices are relatively lower in comparison to EDLCs due to slow diffusion of ions between the electrodes during the fast reaction kinetics.
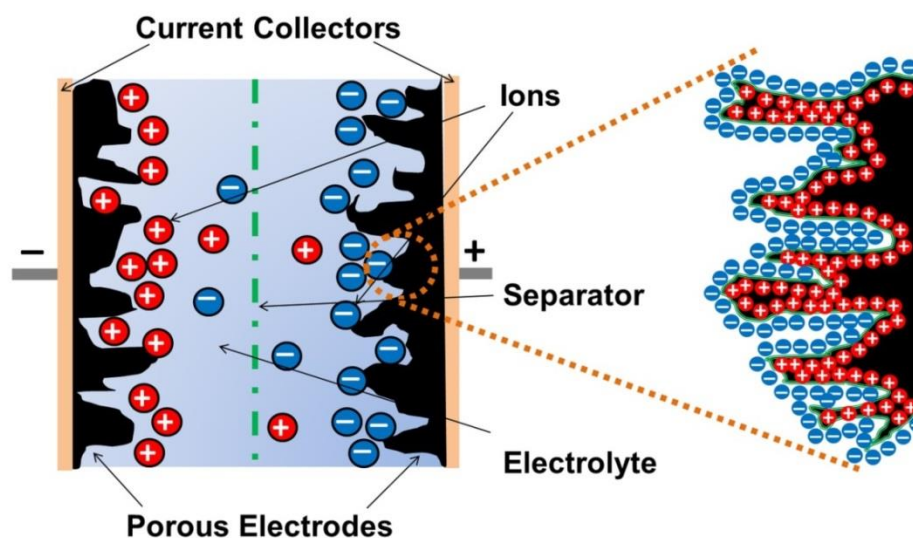
Figure 1.12 Schematic representation of charged supercapacitor.

Challenges in the development of new materials for supercapacitor

Though the supercapacitors are commercially available in the market, there is still a need for improvement in terms of the enhanced energy density and decrease in cost. This leads to the study of fundamental aspects such as designing novel electrode materials and electrolytes [101]. The improvement in the energy density of supercapacitor can be done by increased capacitance and/or voltage. Hence, the development of porous materials with high

specific surface area and suitable pore size distribution, which can deliver high power and energy densities using cost-effective precursor is highly challenging.

1.2.1 Literature Survey on Supercapacitor

The high power density supercapacitor is considered to be one of the potent energy storage systems for use in advanced portable electronic devices and electric vehicles. However, there is a considerable scope to improve the energy density of a supercapacitor by designing novel electrode structures and electrolytes. The research has therefore been directed towards the development of various electrode materials and electrolyte systems in order to enhance the electrochemical performance of supercapacitors.

1.2.1.1 Designing of Electrodes

1.2.1.1.1 Porous Carbon Materials

Since the development of supercapacitors, porous carbon materials have been in use due to their high surface area and good electrochemical stability. In the recent years, various types of carbon materials are used as electrodes for EDLCs such as activated carbons (ACs), graphene and CNT based materials. Among different porous carbon materials, the ACs have drawn attention due to their unique physico-chemical properties such as high surface area, large pore volume and easy to synthesize at low cost. For example, Y. Han et al.[102] prepared activated carbon from fish gills by the method of KOH activation and used it as electrode for supercapacitor. The activated carbon showed high surface area with hierarchical porous structures with the presence of O and N functional groups in them. The electrode prepared from this porous carbon delivered high specific capacitance of 334 F g^{-1} in 6M KOH electrolyte at a current density of 2 A g^{-1}. Zhou et al.[103] synthesized herero atom doped honeycomb-like porous carbon materials from green bristle grass seeds by one-step KOH activation process. The obtained porous carbon materials exhibited high surface area and the sample treated at 800 ℃ delivered high specific capacitance of 391 F g^{-1} at 0.5 A g^{-1} in KOH electrolyte. Moreover, the electrode also showed good capacitance retention of about 97% after 10000 cycles at 20 A g^{-1} current density (figure 1.13).
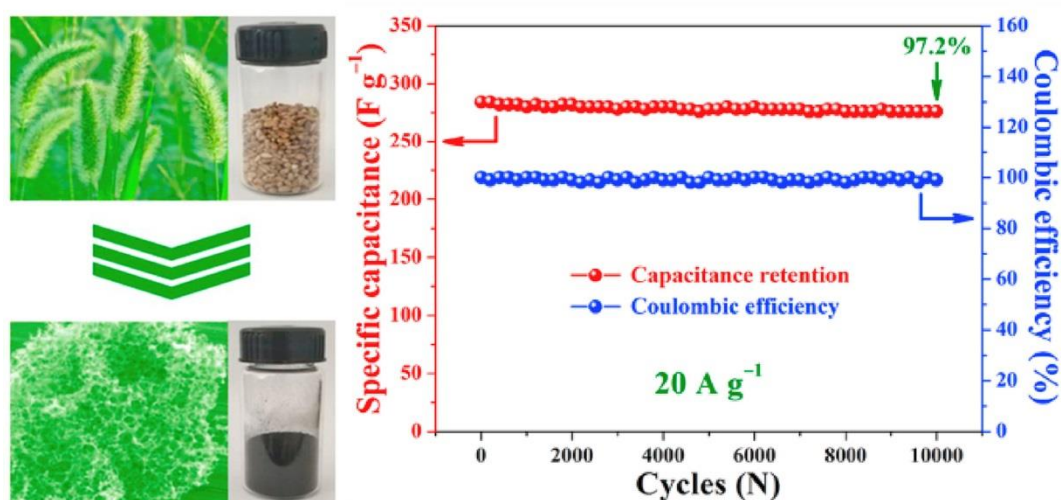
Figure 1.13 Bristle grass seeds-derived activated carbon and its long-term electrochemical performance at 20 A g^{-1} (adopted from ref [103]).

Graphene is also used as an electrode in supercapacitor due to its unique properties such as high electrical conductivity, high surface area and excellent mechanical strength. These properties make graphene and graphene based materials attractive for EDLCs. For instance, L. Jinlong et al.[104] reported the synthesis of porous graphene oxide by hydrothermal assisted H_2O_2 activation process. The electrode delivered a high specific capacitance of 240 F g^{-1} at 1 A g^{-1} and retained a capacitance of 194 F g^{-1} at 20 A g^{-1} with good cycle stability. E. S. Kumar.[105] synthesized nanoporous graphene by using graphene oxide as carbon source and Mg/Zn strip as reducing agent (wet chemical method). The nanoporous graphene electrode delivered high capacitance of 264 F g^{-1} at 1 A g^{-1} in KOH electrolyte. Even at high current rate of 10 A g^{-1}, the electrode displayed 204 F g^{-1} with 95% capacitance retention after 20000 cycles. The enhanced performance is due to unique properties of nanoporous graphene in addition to improved electrical conductivity, which has positive effect in enhancing the electrochemical performance of EDLCs.

Like graphene, CNTs are also used as electrodes in EDLCs due to their unique properties such as excellent electrical conductivity, good chemical stability and reasonable surface area. Y. S Yan et al.[106] prepared a free-standing carbon paper by microporous carbon plate with numerous hetero atoms and acid-treated CNTs. The resulting electrode possesses high surface area with good electrical conductivity and delivered a high specific capacitance of 275 F g^{-1} and 148 F g^{-1} in aqueous (1 M H_2SO_4) and organic ((1-butyl-3-methyl-imidazolium tetrafluoroborate (BMIM BF$_4$)/acetonitrile (AN)) electrolytes respectively.

Although the electrodes prepared from graphene and CNTs have shown an excellent improvement in the electrochemical performance with good power capabilities, the high processing cost is a limiting factor for their commercialization in supercapacitor applications.

1.2.1.1.2 Conductive Polymers

Conductive polymer is another common electrode used in the supercapacitor due to its high conductivity and high charge storage capacity in comparison to porous carbon electrode. The conductive polymers with conjugative double bonds along the polymer backbone render high conductivity. However, the charge storage mechanism of these polymers is different from that of EDLCs. These polymers store charge by redox reactions between the electrodes, which increase the energy and also decrease self-discharge. S. Chaudhari et al.[107] prepared electrospun polyaniline (PANI) nanofiber mat as electrode for supercapacitor and evaluated its electrochemical performance by using three electrolyte systems such as 1M H_2SO_4, 1M Na_2SO_4 and 1M $LiClO_4$ in propylene carbonate. Among them, the PANI electrode in 1M H_2SO_4 exhibited superior performance due to smaller ion hydration number and smaller ionic radius of H^+ ion. In addition, these authors have also studied and compared the electrochemical performance of PANI nanofibers with PANI powder. They have observed that PANI fibers with interconnected network and more electroactive-sites provide fast faradic reactions and delivered higher capacitance of 267 F g^{-1} in comparison to PANI powder (208 F g^{-1}). Despite their considerable advantages, the conductive polymers exhibit relatively low power capabilities due to slow diffusion of ions within the electrodes during the redox process. Further, the research has also been focused on developing conductive polymer composites in order to enhance the power and energy densities of EDLCs. For example, B. Liu et al.[108] synthesized core shell structured $CoNi_2S_4$/polypyrrole on N-doped graphene foam by using hydrothermal process. The $CoNi_2S_4$, polypyrrole and N-doped graphene are electrochemically active in this hybrid structure, which leads to superior electrochemical performance of 730 F g^{-1} at 10 A g^{-1}.

1.2.1.1.3 Metal Oxides

Metal oxides such as RuO_2, TiO_2, MnO_2 were used as electrodes in supercapacitor due to their high conductivity and high charge storage capacity based on redox reactions. Among them, RuO_2 supercapacitors are widely studied because of their wide potential window, high specific capacitance, good chemical and thermal stabilities and long cycle life. For example, Hu et al.[109] developed hydrous RuO_2 ($RuO_2.xH_2O$) electrode in the form of nanotubular array

architecture, which showed an ultrahigh specific capacitance of 1300 F g^{-1}. This behaviour is mainly due to unique properties of the electrode such as high porous structure which facilitates easy penetration of the electrolyte, metallic type conductivity and ease of proton diffusion/exchange during the redox process. As a result, the electrode delivered high capacitance in comparison to porous carbon and conductive polymer electrodes.

Though the RuO_2 based supercapacitor exhibited enhanced electrochemical performance, the high cost of precursors and processing have limited their commercialization. Alternatively, the research has been focused on the other less expensive metal oxides namely TiO_2, MnO_2, SnO_2 and V_2O_5 [110]. Among these, manganese oxide based supercaopacitors are considered to be one of the best alternatives due to their non-toxicity, natural abundance and use of low cost precursors. Y. Chen et al.[111] reported the synthesis of MnO_2 nanosheet like structures on reduced graphene oxide (RGO) by redox reaction between $KMnO_4$ and GO followed by freeze-drying process. The resulting electrode delivered high specific capacitance of 238 F g^{-1} at 0.1 A g^{-1} with good electrochemical stability. This behaviour is due to strong covalent linkage between carbon atom of RGO and oxygen atom of MnO_2 (via. C-O-Mn), which reduces the charge transfer resistance and also overcome the mechanical disintegration of MnO_2 from the RGO.

1.2.1.2 Electrolytes

In general, electrolyte also plays an important role in supercapacitor in enhancing the electrochemical performance. The electrode materials having high surface area with small porous structure can deliver high capacitance and energy [101]. However, if the pores are too small in the electrode, the ions in the electrolyte are unable to reach the inner surface of the electrode for charge storage. This leads to poor specific capacitance and low energy density. Hence, the high surface area electrode materials with pore size similar to that of ions in the electrolyte are necessary to maximise the accessibility of ions for adsorption on the surface of the electrode. The electrolytes used in supercapacitors are classified into three types namely (1) aqueous electrolytes (2) organic electrolytes and (3) ionic liquid electrolytes.

Aqueous electrolytes such as KOH, Na_2SO_4, H_2SO_4 are extensively used in EDLCs due to their low cost and ease of fabrication of device without the need of sophisticated equipments. Moreover, these electrolytes possess high conductivity due to high ionic concentration [107]. However, the low potential window (1.2 V – decomposition voltage of water) of these aqueous electrolytes leads to decrease in energy density of the EDLCs.

Organic electrolytes consist of lithium salts or quaternary ammonium salt dissolved in carbonate based or acetonitrile solvent and have high operating voltage of 2.7 V [100]. Currently, most of the commercial supercapacitors in the market use organic electrolytes due to their higher potential, which increases the energy density of the device. The main disadvantages of the organic electrolytes are low capacitance, higher resistance that decreases the power density. In addition to high cost, the applicability of these electrolytes is associated with safety issues such as toxicity, volatility and flammability of solvents. Moreover, the organic electrolytes are not suitable for high temperature applications because the electrochemical potential window of these electrolytes decreases with an increase in the temperature.

Ionic liquids (ILs), also named as room temperature molten salts, consist of bulky cation with different anions. The ILs are solvent-free electrolytes, which can overcome the safety issues associated with the other electrolyte based on solvents. In addition, they have high thermal and chemical stabilities and high operating potential (3.7 V) [112]. As a result of large potential window, the energy density of EDLCs is significantly increased in comparison to organic and aqueous electrolyte based supercapcitors. But, the high cost, high viscosity and low ionic conductivity have decreased their viability in EDLCs.

1.3 Need, Objectives and Scope of the Present Research Study

1.3.1 Need of the Present Study

High energy denisty Li-S battery and high power density supercapacitor are considered to be promising candidates among the emerging energy storage systems. The Li-S cell, which works on the basis of conversion chemistry, has high energy density, which is 3-5 times higher than that of the currently used LIBs. The sulfur cathode operates at a potential of 2.1 V vs. Li/Li$^+$ with a theoretical specific capacity of 1672 mAh g^{-1} and the energy density of 2600 Wh kg^{-1}. However, commercialization of the Li-S battery is greatly hampered due to polysulfide dissolution, insulating nature of sulfur and large volume expansion as discussed in the section 1.1. Moreover, the use of lithium metal as the anode has serious concern due to dendrite formation with repeated cycling processes that leads to cell short-circuit and thermal runaway.

In the recent years, much focus has been on overcoming the challenges of sulfur cathode by forming composite with conductive matrix. Among the different kinds of matrix used, the micro and mesoporous carbon is considered to be suitable host for sulfur cathode

and for ion adsorption. The micro/mesoporous carbon has unique properties such as high surface area, large pore volume, excellent electrical and mechanical properties [22,113]. Therefore, in Li-S battery the sulfur-infiltered porous carbon material can overcome the insulating behaviour and also help in trapping the dissolved polysulfides in it. In the present research study, focus is made on the synthesis of bio-inspired activated carbon materials by using different naturally available precursors such as neem leaves, tissue paper and jute stalks. Moreover, these precursors are naturally available and the preparation of porous carbon materials involves simple, easy and chemical activation process. The activated carbon/sulfur composite was prepared by the melt-diffusion process. The effect of porous carbon materials and modified separator on sulfur cathode in improving the electrochemical performance and trapping the dissolved polysulfides has been studied. However, the use of lithium metal as an anode in Li-S battery remains a major drawback due to dendrite formation with repeated cycling, which leads to short circuit and thermal runaway of cell. The high capacity lithiated anodes such as lithiated tin and lithiated silicon can compensate the charge storage capacity of the sulfur cathode. In the present study, the investigator focused on synthesizing Sn/Graphene and Si/Graphite anodes and studied their electrochemical performance with sulfur cathode in full cell configuration. Moreover, these anodes have advantages of operating at relatively lower potential, low cost and higher specific capacity in comparison to conventional anodes of LIBs.

In supercapacitor the development of porous carbon materials with good textural parameters from low cost carbon precursors is highly challenging. Therefore, the development of novel electrodes for supercapacitors is the need of the hour. For supercapacitor, the micro and mesoporous carbons provide numerous active sites for ion adsorption, which increase the charge storage capacity of the device. The porous carbon materials developed in the present study are also explored as electrodes for application in supercapacitors.

1.3.2 Objectives of the Present Research Study

The objectives of the present research study are as follows:

1. To synthesize hierarchical (micro and meso) porous carbons from naturally available precursors for application in Li-S battery and supercapacitor.

2. To synthesize high capacity anodes as alternative electrodes to lithium metal anode for Li-S battery.

3. To investigate into the electrochemical performance of the individual electrodes (cathodes and anodes) in half cell configuration by using lithium foil as the reference electrode.

4. To fabricate and study the performance of the Li-S battery in full cell configuration by using the cathode and anode materials of superior electrochemical performance, developed in the present study.

5. To investigate into the electrochemical performance of the porous carbon materials developed in the present study for application in supercapacitors.

1.3.3 Scope of the Present Research Study

The electrochemical studies of cathode, anode and full-cell in Li-S battery have been carried out in two electrode configuration by using 1M lithium bis-(trifluoromethyl-sulfonylimide) (LITFSI) in a mixture of 1,3 dioxalane (DOL) and dimethoxyethane (DME) (DOL:DME as 1:1 by volume) with 5 wt% $LiNO_3$ additive as the electrolyte. In supercapacitor, the electrochemical performance of the porous carbons developed in the present study has been carried out in both the three electrode and two electrode configurations by using 6M KOH (aqueous) as the electrolyte. The studies have been confined to the laboratory experiments and the electrochemical evaluation of the fabricated cells has been done at the room temperature of 25 ± 1 ℃.

References

1. Winter, M. & Brodd, R. J. What are Batteries, Fuel Cells, and Supercapacitors?. *Chem. Rev.* **104**, 4245-69 (2004).

2. Goodenough, J. B. & Park, K. S. The Li-ion Rechargeable Battery: A Perspective. *J. Am. Chem. Soc.* **135**, 1167-76 (2013).

3. Etacheri, V., Marom, R., Elazari, R., Salitra, G. & Aurbach, D. Challenges in The Development of Advanced Li-ion Batteries: A Review. *Energy Environ. Sci.* **4**, 3243 (2011).

4. Manthiram, A., Fu, Y. & Su, Y. S. Challenges and Prospects of Lithium-Sulfur Batteries. *Acc. Chem. Res.* **46**, 1125-1134 (2013).

5. Bruce, P. G., Freunberger, S. A., Hardwick, L. J. & Tarascon, J. M. Li-O$_2$ and Li-S Batteries with High Energy Storage. *Nat. Mater.* **11**, 19-30 (2012).

6. Kim, M. H., Kim, H. K., Xi, K., Vasant Kumar, R., Jung, D. S., Kim, K. B., Roh K. C. Lithium-Sulfur Capacitors. *ACS Appl. Mater. Interfaces* **10**, 6199-6206 (2018).

7. Wang, J., Xie, K. & Wei, B. Advanced Engineering of Nanostructured Carbons for

Lithium-Sulfur Batteries. *Nano Energy* **15**, 413-444 (2015).

8. Wang, D. W., Zeng, Q., Zhou, G., Yin, L., Li, F., Cheng, H. M., Gentle, I. R., Lu, G. Q. M. Carbon-Sulfur Composites for Li–S Batteries: Status and Prospects. *J. Mater. Chem. A* **1**, 9382-9394 (2013).

9. Hassoun, J. Scrosati, B. A High-Performance Polymer Tin Sulfur Lithium Ion Battery. *Angew. Chem. Int. Ed.* **49**, 2371-2374 (2010).

10. Cheng, X. B., Huang, J. Q. Zhang, Q. Review-Li Metal Anode in Working Lithium-Sulfur Batteries. *J. Electrochem. Soc.* **165**, A6058-A6072 (2018).

11. See, K. A., Jun, Y. S., Gerbec, J. A., Sprafke, J. K., Wudl, F., Stucky, G. D., Seshadri, R. Sulfur-Functionalized Mesoporous Carbons as Sulfur Hosts in Li-S Batteries: Increasing the Affinity of Polysulfide Intermediates to Enhance Performance. *ACS Appl. Mater. Interfaces* **6**, 10908-10916 (2014).

12. Li, D., Han, F., Wang, S., Cheng, F., Sun, Q., Li, W. C. High Sulfur Loading Cathodes Fabricated Using Peapodlike, Large Pore Volume Mesoporous Carbon for Lithium-Sulfur Battery. *ACS Appl. Mater. Interfaces* **5**, 2208-2213 (2013).

13. Huang, J. Q. Liu, X. F., Zhang, Q., Chen, C. M., Zhao, M. Q., Zhang, S. M., Zhu, W., Qian, W. Z., Wei, F. Entrapment of Sulfur in Hierarchical Porous Graphene for Lithium-Sulfur Batteries with High Rate Performance from -40 to -60 ºC. *Nano Energy* **2**, 314-321 (2013).

14. Ji, L., Rao, M., Zheng, H., Zhang, L., Li, Y., Duan, W., Guo, J., Cairns, E. J., Zhang, Y. Graphene Oxide as a Sulfur Immobilizer in High Performance Lithium/Sulfur Cells. *J. Am. Chem. Soc* **133**, 18522-18525 (2011).

15. Li, W., Zhang, Q., Zheng, G., Seh, W. & Yao, H. Understanding the Role of Different Conductive Polymers in Improving the Nanostructured Sulfur Cathode Performance. *Nano Lett.* **13**, 5534-5540 (2013).

16. Wang, J., Lu, L., Shi, D., Tandiono, R., Wang, Z., Konstantinov, K., Wang, H. L. A Conductive Polypyrrole-Coated, Sulfur-Carbon Nanotube Composite for Use in Lithium-Sulfur Batteries. *Chempluschem* **78**, 318-324 (2013).

17. Ji, X., Lee, K. T. & Nazar, L. F. A Highly Ordered Nanostructured Carbon-Sulfur Cathode for Lithium-Sulfur Batteries. *Nat. Mater.* **8**, 500-506 (2009).

18. Ji, L. Rao, M., Aloni, S., Wang, L., Cairns, E. J., Zhang Y. Porous Carbon Nanofiber-Sulfur Composite Electrodes for Lithium-Sulfur Cells. *Energy Environ. Sci.* **4**, 50-53 (2011).

19. Moon, S. Jung, Y. H., Jung, W. K., Jung, D. S., Choi, J. W., Kim D. K. Encapsulated Monoclinic Sulfur for Stable Cycling of Li-S Rechargeable Batteries. *Adv. Mater.* **25**, 6547-6553 (2013).

20. Zhang, C. Wu, H. B., Yuan, C., Guo, Z., Lou X. W. D. Confining Sulfur in Double-Shelled Hollow Carbon Spheres for Lithium-Sulfur Batteries. *Angew. Chem.* **124**, 9592-9595 (2012).

21. Tao, X. Zhang, J., Xia, Y., Huang, H., Du, J., Xiao, H., Zhang, W., Gan Y. Bio-Inspired Fabrication of Carbon Nanotiles for High Performance Cathode of Li-S Batteries. *J. Mater. Chem A* **2**, 2290-2296 (2014).

22. Li, X., Cao, Y., Qi, W., Saraf, L. V., Xiao, J., Nie, Z., Mietek, J., Zhang, J. G., Schwenzera, B., Liu, j. Optimization of Mesoporous Carbon Structures for Lithium-Sulfur Battery. *J. Mater. Chem.* **21**, 16603-16610 (2011).

23. Zhang, B., Qin, X., Li, G. R. & Gao, X. P. Enhancement of Long Stability of Sulfur Cathode by Encapsulating Sulfur into Micropores of Carbon Spheres. *Energy Environ. Sci.* **3**, 1531-1537 (2010).

24. Chen, S. R., Zhai, Y. P., Xu, G. L., Jiang, Y. X., Zhao, D. Y., Lia, J. T., Huang, L., Sun, S. G.. Ordered Mesoporous Carbon/Sulfur Nanocomposite of High Performances as Cathode for Lithium-Sulfur Battery. *Electrochim. Acta* **56**, 9549-9555 (2011).

25. Sohn, H. Gordin, M. L., Xu, T., Chen, S., Lv, D., Song, J., Manivannan, A., Wang, D. Porous Spherical Carbon/Sulfur Nanocomposites by Aerosol-Assisted Synthesis: The Effect of Pore Structure and Morphology on Their Electrochemical Performance As Lithium/Sulfur Battery Cathodes. *ACS Appl. Mater. Interfaces* **6**, 7596-7606 (2014).

26. Ding, B., Yuan, C., Shen, L., Xu, G. & Nie, P. Encapsulating Sulfur into Hierarchically Ordered Porous Carbon as a High-Performance Cathode for Lithium-Sulfur Batteries. *Chem. Eur. J.* **19**, 1013-1019 (2013).

27. Agrawal, M., Choudhury, S., Gruber, K., Simon, F., Fischer, D., Albrecht, V., Gobel, M., Koller, S., Stamm, M., Ionov, L. Porous Carbon Materials for Li-S Batteries Based on Resorcinol-Formaldehyde Resin with Inverse Opal Structure. *J. Power Sources* **261**, 363-370 (2014).

28. He, G., Ji, X. & Nazar, L. High 'C' Rate Li-S Cathodes: Sulfur Imbibed Bimodal Porous Carbons. *Energy Environ. Sci.* **4**, 2878-2883 (2011).

29. Wu, H., Xia. L., Ren, J., Zheng, Q., Xu, C., Lin, D., A High-Efficiency N/P Co-Doped Graphene/CNT/Porous Carbon Hybrid Matrix as Cathode Host for High Performance

Lithium-Sulfur Batteries. *J. Mater. Chem. A* **5**, 20458-20472 (2017).

30. Song, J. Xu, T., Gordin, M. L., Zhu,P., Lv, D., Jiang, Y. B., Chen, Y., Duan, Y., Wang, D. Nitrogen-Doped Mesoporous Carbon Promoted Chemical Adsorption of Sulfur and Fabrication of High-Areal-Capacity Sulfur Cathode with Exceptional Cycling Stability for Lithium-Sulfur Batteries. *Adv. Funct. Mater.* **24**, 1243-1250 (2014).

31. Ma, G., Wen, Z., Jin, J., Lu, Y., Rui, K., Wu, X., Wu, M., Zhang, J. Enhanced Performance of Lithium Sulfur Battery with Polypyrrole Warpped Mesoporous Carbon/Sulfur Composite. *J. Power Sources* **254**, 353-359 (2014).

32. Fugen Sun, Jitong Wang, Donghui Long, Wenming Qiao, Licheng Ling, Chunxiang Lv, R. C. A High-Rate Lithium-Sulfur Battery Assisted by Nitrogen-Enriched Mesoporous Carbons Decorated with Ultrafine La_2O_3 Nanoparticles. *J. Mater. Chem. A* **1**, 13283-13289 (2013).

33. Wei, S. Zhang, H., Huang, Y., Wang, W., Xai, Y., Yu, Z. Pig Bone Derived Hierarchical Porous Carbon and its Enhanced Cycling Performance of Lithium-Sulfur Batteries. *Energy Environ. Sci.* **4**, 736-740 (2011).

34. Guo, J., Zhang, J., Jiang, F., Zhao, S., Su, Q., Du, G. Microporous carbon nanosheets derived from corncobs for lithium-sulfur batteries. *Electrochim. Acta* **176**, 853-860 (2015).

35. Zhu, J., Yang, D., Yin, Z., Yan, Q. & Zhang, H. Graphene and Graphene-Based Materials for Energy Storage Applications. *Small* **10**, 3480-3498 (2014).

36. Zhou, G., Pei, S., Li, L., Wang, D. W., Wang, S., Huang, K., Yin, L. C., Li, F., Cheng, H. M. A Graphene-Pure-Sulfur Sandwich Structure for Ultrafast , Long-Life Lithium-Sulfur Batteries. *Adv. Mater.* **26**, 625-631 (2013).

37. Zhou, G., Paek, E., Hwang, G. S. & Manthiram, A. Long-Life Li/Polysulphide Batteries with High Sulfur Loading Enabled by Lightweight Three-Dimensional Nitrogen/Sulfur-Co-doped Graphene Sponge. *Nat. Commun.* **6**, 7760 (2015).

38. Guo, J., Xu, Y. & Wang, C. Sulfur-Impregnated Disordered Carbon Nanotubes Cathode for Lithium-Sulfur Batteries. *Nano Lett.* **11**, 4288-4294 (2011).

39. Yan, J., Liu, X., Yao, M., Wang, X. & Li, B. Long-Life, High-Efficiency Lithium-Sulfur Battery from a Nanoassembled Cathode. *Chem. Mater.* **27**, 5080-5087 (2015).

40. Fan, Q., Liu, W., Weng, Z., Sun, Y. & Wang, H. Ternary Hybrid Material for High-Performance Lithium-Sulfur Battery. *J. Am. Chem. Soc.* **137**, 12946-12953 (2015).

41. Wang, H., Zhang, C., Chen, Z., Kun, H. & Guo, Z. Large-Scale Synthesis of Ordered

Mesoporous Carbon Fiber and its Application as Cathode Material for Lithium-Sulfur Batteries. *Carbon,* **81**, 782-787 (2014).

42. Zu, C., Fu, Y. Manthiram, A. Highly Reversible Li/Dissolved Polysulfide Batteries with Binder-Free Carbon Nanofiber Electrodes. *J. Mater. Chem. A* **1**, 10362-10367 (2013).

43. Zheng, G., Zhang, Q., Cha, J. J., Yang, Y., Li, W., Seh, Z. W., Cui, Y. Amphiphilic Surface Modification of Hollow Carbon Nanofibers for Improved Cycle Life of Lithium Sulfur Batteries. *Nano Lett.* **13**, 1265-1270 (2013).

44. Li, Z., Li, C., Ge, X., Ma, J., Zhang, Z., Li, Q., Wang, C., Yin L. Reduced Graphene Oxide Wrapped MOFs-Derived Cobalt-Doped Porous Carbon Polyhedrons as Sulfur Immobilizers as Cathodes for High Performance Lithium Sulfur Batteries. *Nano Energy* **23**, 15-26 (2016).

45. Seh, Z. W., Li, W., Cha, J. J., Zheng, G., Yang, Y., McDowell, M. T., Hsu, P. C., Cui, Y. Sulfur-TiO$_2$ Yolk-Shell Nanoarchitecture with Internal Void Space for Long-Cycle Lithium-Sulfur Batteries. *Nat. Commun.* **4**, 1331 (2013).

46. Pang, Q., Kundu, D., Cuisinier, M. & Nazar, L. F. Surface-Enhanced Redox Chemistry of Polysulphides on a Metallic and Polar Host for Lithium-Sulfur Batteries. *Nat. Commun.* **5**, 4759 (2014).

47. Li, W., Garner, J. H., Wang, J., Liu, J., Gross, A. F., Sherman, E., Graetz, J., Vajo, J. J., Liu, P. V$_2$O$_5$ Polysulfide Anion Barrier for Long-Lived Li-S Batteries. *Chem. Mater.* **26**, 3403-3410 (2014).

48. Wu, F., Chen, J., Chen, R., Wu, S., Li, L., Chen, S., Zhao, T. Sulfur/Polythiophene with a Core/Shell Structure: Synthesis and Electrochemical Properties of the Cathode for Rechargeable Lithium Batteries. *J. Phys. Chem. C* **115**, 6057-6063 (2011).

49. Xiao, L., Cao, Y., Xiao, J., Schwenzer, B., Engelhard, M. H., Saraf, L. V., Nie, Z., Exarhos, G. J., Liu,J. A Soft Approach to Encapsulate Sulfur: Polyaniline Nanotubes for Lithium-Sulfur Batteries with Long Cycle Life. *Adv. Mater.* **24**, 1176-1181 (2012).

50. Wang, C., Wan, W., Chen, J. T., Zhou, H. H., Zhang, X. X., Yuan, L. X., Huang, Y. H. Dual Core-Shell Structured Sulfur Cathode Composite Synthesized by a One-Pot Route for Lithium Sulfur Batteries. *J. Mater. Chem A* **1**, 1716-1723 (2013).

51. Wang, J., Yanf, J., Xie, J. & Xu, N. A Novel Conductive Polymer-Sulfur Composite Cathode Material for Rechargeble Lithium Batteries. *Adv. Mater.* **050**, 963-965 (2002).

52. Nam, L. D., Ghaznavi, M., Zhao, Y., Zhang, Y., Konarov, A., Sadhu, M., Tangirala,

R., Chen, P. Binding Mechanism of Sulfur and Dehydrogenated Polyacrylonitrile in Sulfur/ Polymer Composite Cathode. *J. Power Sources* **241**, 61-69 (2013).

53. Lin, Z., Liu, Z., Fu, W., Dudney, N. J. & Liang, C. Lithium Polysulfidophosphates: A Family of Lithium-Conducting Sulfur-Rich Compounds for Lithium-Sulfur Batteries. *Angew. Chem. Int. Ed.* **52**, 7460-7463 (2013).

54. Chung, W. J., Griebel, J. J., Kim, E. T., Yoon , H., Simmonds, A. G., Ji, H. J., Dirlam, P. T., Glass, R. S., Wie, J. J., Nguyen, N. A., Guralnick, B, W., Park, J., Somogyi, A., Theato, P., Mackay, M. E., Sung, Y. E., Char, K., Pyun, J. The Use of Elemental Sulfur as an Alternative Feedstock for Polymeric Materials. *Nat. Chem.* **5**, 518-524 (2013).

55. Braithwaite, J. W., Gonzales, A., Nagasubramanian, G., Lucero, S. J., Peebles, D. E., Ohlhausen, J. A., Cieslak, W. R. Corrosion of Lithium-Ion Battery Current Collectors. *J. Electrochem. Soc.* **146**, 448-456 (1999).

56. Chung, S., Manthiram, A. Low-Cost , Porous Carbon Current Collector with High Sulfur Loading for Lithium-Sulfur Batteries. *Electrochem. commun.* **38**, 91-95 (2014).

57. Babu, G., Ababtain, K., Ng, K. Y. S. & Reddy, L. M. A. Electrocatalysis of Lithium Polysulfides : Current Collectors as Electrodes in Li/S Battery Configuration. *Sci. Rep.* **5**, 8763 (2015).

58. Zhou, G., Zhao, Y., Manthiram, A. Dual-Confined Flexible Sulfur Cathodes Encapsulated in Nitrogen-Doped Double-Shelled Hollow Carbon Spheres and Wrapped with Graphene for Li-S Batteries. *Adv. Energy Mater.* **5**, 1402263 (2015).

59. Elazari, R., Salitra, G., Garsuch, A., Panchenko, A. & Aurbach, D. Sulfur-Impregnated Activated Carbon Fiber Cloth as a Binder-Free Cathode for Rechargeable Li-S Batteries. *Adv. Mater.* **23**, 5641-5644 (2011).

60. Yang, Y. McDowell, M. T., Jackson, A., Cha, J. J., Hong, S. S., Cui, Y. New Nanostructured Li_2S/ Silicon Rechargeable Battery with High Specific Energy. *Nano Lett.* **10**, 1486-1491 (2010).

61. Lin, Z., Nan, C Ye, Y., Guo, J., Zhu, J., Cairns, E. J. High-Performance Lithium/Sulfur Cells with a Bi-functionally Immobilized Sulfur Cathode. *Nano Energy* **9**, 408-416 (2014).

62. Seh, Z. W., Wang, H., Hsu, P. C., Zhang, Q., Li, W., Zheng, G., Yao, H., Cui, Y. Facile Synthesis of Li_2S-Polypyrrole Composite Structures for High Performance Li_2S Cathode. *Energy Environ. Sci.* **7**, 672-676 (2014).

63. Chen, Y., Lu, S., Zhou, J., Wu, X., Qin, W., Ogoke, O., Wu, G. 3D Graphene

Framework Supported Li₂S Coated with Ultra-Thin Al₂O₃ Films: Binder-Free Cathodes for High-Performance Lithium Sulfur Batteries. *J. Mater. Chem. A* **5**, 102-112 (2017).

64. Schneider, H., Garsuch, A., Panchenko, A., Gronwald, O., Janssen, N., Novak P. Influence of Different Electrode Compositions and Binder Materials on the Performance of Lithium-Sulfur Batteries. *J. Power Sources* **205**, 420-425 (2012).

65. Zhou, W., Chen, H., Yu, Y.,Wang, D., Cui, Z., DiSalvo, Abruna, H. D. Amylopectin Wrapped Graphene Oxide/Sulfur for Improved Cyclability of Lithium-Sulfur Battery. ACS Nano **7**, 8801-8808 (2013).

66. He, M., Yuan, L. X., Zhang, W. X., Hu, X. L., Huang, Y. H. Enhanced Cyclability for Sulfur Cathode Achieved by a Water-Soluble Binder. *J. Phys. Chem. C* **115**, 15703-15709 (2011).

67. Wang, J., Yao, Z., Monroe, C. W., Yang, J., Nuli, Y. Carbonyl-β-Cyclodextrin as a Novel Binder for Sulfur Composite Cathodes in Rechargeable Lithium Batteries. *Adv. Funct. Mater.* **23**, 1194-1201 (2012).

68. Ai, G., Dai, Y., Ye, Y., Mao, W., Wang, Z., Zhao, H., Chen, Y., Zhu, J., Fu, Y., Battaglia, V., Guo, J., Srinivasan, V., Liu, G. Investigation of Surface Effects Through the Application of the Functional Binders in Lithium Sulfur Batteries. *Nano Energy* **16**, 28-37 (2015).

69. Zhang, S., Ueno, K., Dokko, K., Watanabe, M. Recent Advances in Electrolytes for Lithium-Sulfur Batteries. *Adv. Energy Mater.* **5**, 1500117 (2015).

70. Yim, T., Park, M, S., Yu, J. S., Kim, K. J., Im, K. Y., Kim, J. H., Jeong, G., Jo, Y. N., Woo, S. G., Kang, K. S., Lee, I., Kim, Y. J. Effect of Chemical Reactivity of Polysulfide Toward Carbonate-Based Electrolyte on the Electrochemical Performance of Li-S Batteries. *Electrochim. Acta* **107**, 454-460 (2013).

71. Zhang, S. S. Liquid Electrolyte Lithium/Sulfur Battery: Fundamental Chemistry, Problems, and Solutions. *J. Power Sources* **231**, 153-162 (2013).

72. Wang, L., Byon, H. R. N-Methyl-N-propylpiperidinium bis (trifluoromethanesulfonyl) imide-based organic electrolyte for high performance lithium-sulfur batteries. *J. Power Sources* **236**, 207-214 (2013).

73. Zheng, J., Gu, M., Chen, H., Meduri, P., Engelhard, M. H., Zhang, J. G., Liu, J., Xiao, J. Ionic Liquid-Enhanced Solid State Electrolyte Interface (SEI) for Lithium-Sulfur Batteries. *J. Mater. Chem. A* **1**, 8464-8470 (2013).

74. Ueno, K., Yamazaki, A., Mandai, T., Tachikawa, N., Dokko, K., Watanabe, M., Anionic Effects on Solvate Ionic Liquid Electrolytes in Rechargeable Lithium-Sulfur Batteries. *J. Phys. Chem. C* **117**, 20509-20516 (2013).

75. Salitra, G., Markevich, E., Rosenman, A., Talyosef, Y., Aurbach, D., Garsuch A. High-Performance Lithium-Sulfur Batteries Based on Ionic-Liquid Electrolytes with Bis (fluorolsufonyl)imide Anions and Sulfur-Encapsulated Highly Disordered Activated Carbon. *ChemElectroChem* **1**, 1492-1496 (2014).

76. Park, J. W., Ueno, K., Tachikawa, N., Dokko, K. & Watanabe, M. Ionic Liquid Electrolytes for Lithium-Sulfur Batteries. *J. Phys. Chem. C* **117**, 20531-20541 (2013).

77. Suo, L., Hu, Y., Li, H., Armand, M. & Chen, L. A New Class of Solvent-in-Salt Electrolyte for High-Energy Rechargeable Metallic Lithium Batteries. *Nat. Commun.* **4**, 1481 (2013).

78. Zhang, S. S. New Insight into Liquid Electrolyte of Rechargeable Lithium/Sulfur Battery. *Electrochim. Acta* **97**, 226-230 (2013).

79. Mikhaylik, Y. V. Electrolytes for Lithium Sulfur Cells. *US Pat.* **7**, 354-680 (2008).

80. Zhang, S. S. Role of $LiNO_3$ in Rechargeable Lithium/Sulfur Battery. *Electrochim. Acta* **70**, 344-348 (2012).

81. Xu, R., Belharouak, I., Li, J. C. M., Zhang, X., Bloom, I., Bareno, J. Role of Polysulfides in Self-Healing Lithium-Sulfur Batteries. *Adv. Energy Mater.* **3**, 833-838 (2013).

82. Wu, F., Lee, J. T., Nitta, N., Kim, H., Borodin, O., Yushin, G. Lithium Iodide as a Promising Electrolyte Additive for Lithium-Sulfur Batteries: Mechanisms of Performance Enhancement. *Adv. Mater.* **27**, 101-108 (2015).

83. Jeddi, K., Sarikhani, K., Taheri, N. & Chen, P. Stabilizing Lithium/Sulfur Batteries by A Composite Polymer Electrolyte Containing Mesoporous Silica Particles. *J. Power Sources* **245**, 656-662 (2014).

84. Zhang, S. S. A Concept for Making Poly(ethylene oxide) Based Composite Gel Polymer Electrolyte Lithium/Sulfur Battery. *J. Electrochem. Soc.* **160**, 1421-1424 (2013).

85. Nagao, M., Hayashi, A. & Tatsumisago, M. Sulfur-Carbon Composite Electrode for All-Solid-State Li/S Battery with Li_2S-P_2S_5 Solid Electrolyte. *Electrochim. Acta* **56**, 6055-6059 (2011).

86. Xu, R. C., Xia, X. H., Li, S. H., Zhang, S. Z., Wang, X. L., Tu, J. P. All-Solid-State
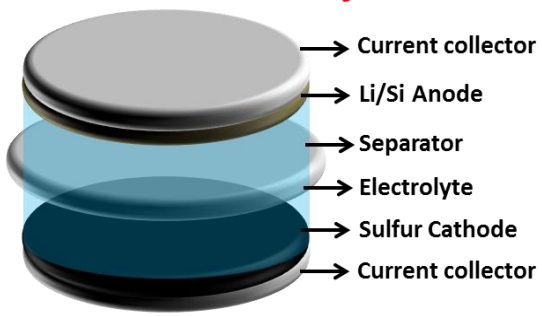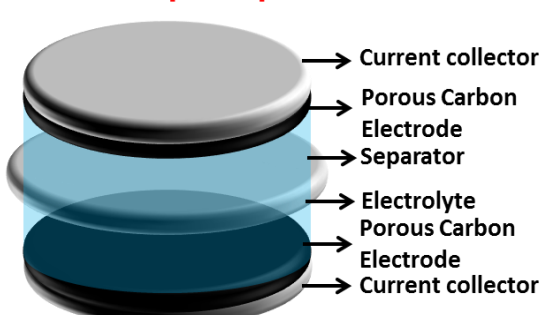
Lithium-Sulfur Batteries Based on a Newly Designed $Li_7P_{2.9}Mn_{0.1}S_{10.7}I_{0.3}$ Superionic Conductor. *J. Mater. Chem. A* **5**, 6310–6317 (2017).

87. Zhu, J., Yanilmaz, M., Fu, K., Chen, C., Lu, Y., Ge, Y., Kim, D., Zhang, X. Understanding Glass Fiber Membrane Used as a Novel Separator for Lithium-Sulfur Batteries. *J. Memb. Sci.* **504**, 89-96 (2016).

88. Bauer, I., Thieme, S., Brückner, J., Althues, H. & Kaskel, S. Reduced Polysulfide Shuttle in Lithium-Sulfur Batteries Using Nafion-Based Separators. *J. Power Sources* **251**, 417-422 (2014).

89. Singhal, R., Chung, S. H., Manthiram, A., Kalra, V. A Free-Standing Carbon Nanofiber Interlayer for High-Performance Lithium-Sulfur Batteries. *J. Mater. Chem. A* **3**, 4530-4538 (2015).

90. Balach, J., Jaumann, T., Klose, M., Oswald, S., Eckert, J., Giebeler, L. Functional Mesoporous Carbon-Coated Separator for Long-Life, High-Energy Lithium-Sulfur Batteries. *Adv. Funct. Mater.* **25**, 5285-5291 (2015).

91. Chung, S., Manthiram, A. Bifunctional Separator with a Light-Weight Carbon-Coating for Dynamically and Statically Stable Lithium-Sulfur Batteries. *Adv. Funct. Mater.* **24**, 5299-5306 (2014).

92. Wang, X., Wang, Z., Chen, L. Reduced Graphene Oxide Film as a Shuttle-Inhibiting Interlayer in a Lithium-Sulfur Battery. *J. Power Sources* **242**, 65-69 (2013).

93. Cao, R., Xu, W., Lv, D., Xiao, J. & Zhang, J. G. Anodes for Rechargeable Lithium-Sulfur Batteries. *Adv. Energy Mater.* **5**, 1-23 (2015).

94. Zu, C., Azimi, N., Zhang, Z., Manthiram, A. Insight into Lithium-Metal Anodes in Lithium-Sulfur Batteries with a Fluorinated Ether Electrolyte. *J. Mater. Chem. A* **3**, 14864-14870 (2015).

95. Barghamadi, M., Best, A. S., Bhatt, A. I., Hollenkamp, A. F., Mahon, P. J., Musameh, M., Ruther, T. Effect of $LiNO_3$ Additive and Pyrrolidinium Ionic Liquid on the Solid Electrolyte Interphase in the Lithium-Sulfur Battery. *J. Power Sources* **295**, 212-220 (2015).

96. Kozen, A. C., Lin, C. F., Pearse, A. J., Schroeder, M. A., Han, X., Hu, L., Lee, S. B., Rubloff, G. W., Noked, M. Next-Generation Lithium Metal Anode Engineering via Atomic Layer Deposition. *ACS Nano* **9**, 5884-5892 (2015).

97. Duan, B., Wang, W., Wang, A., Yu, Z., Zhao, H., Yang, Y. A New Lithium Secondary Battery System: The Sulfur/Lithium-ion Battery. *J. Mater. Chem. A* **2**, 308-314 (2014).

98. Shen, C., Ge, M., Zhang, A., Fang, X., Liu, Y., Rong, J., Zhou, C. Silicon(Lithiated)-Sulfur Full Cells with Porous Silicon Anode Shielded by Nafion Against Polysulfides to Achieve High Capacity and Energy Density. *Nano Energy* **19**, 68-77 (2016).

99. Boos, D. L., Heights, G. Electrolytic Capactor Having Carbon Paste Electrodes. *US Pat. 3536963* (1970).

100. Ko, R., Carlen, M. Principles and Applications of Electrochemical Capacitors. *Electrochim. Acta* **45**, 2483-2498 (2000).

101. Miller, E. E., Hua, Y., Tezel, F. H. Materials for Energy Storage : Review of Electrode Materials and Methods of Increasing Capacitance for Supercapacitors. *J. Energy Storage* **20**, 30-40 (2018).

102. Han, Y., Shen, N., Zhang, S., Li, D., Li, X. Fish Gill-Derived Activated Carbon for Supercapacitor Application. *J. Alloys Compd.* **694**, 636-642 (2017).

103. Zhou, W., Lei, S., Sun, S., Ou, X., Fu, Q., Xu, Y., Xiao, Y., Cheng, B. From Weed to Multi-Heteroatom-Doped Honeycomb-Like Porous Carbon for Advanced Supercapacitors: A Gelatinization-Controlled One-Step Carbonization. *J. Power Sources* **402**, 203-212 (2018).

104. Lv, J., Liang, T. Nanoporous Graphene Obtained by Hydrothermal Process in H_2O_2 and its Application for Supercapacitors. *Chem. Phys. Lett.* **659**, 61-65 (2016).

105. Senthilkumar, E., Sivasankar, V., Kohakade, B. R., Thileepkumar, K., Ramya, M., Sundari, G. S., Raghu, S., Kalaivani, R. A., Synthesis of Nanoporous Graphene and Their Electrochemical Performance in a Symmetric Supercapacitor. *Appl. Surf. Sci.* **460**, 17-24 (2017).

106. Yun, Y. S., Lee, M. E., Joo, M. J., Jin, H. J. High-Performance Supercapacitors Based on Freestanding Carbon-Based Composite Paper Electrodes. *J. Power Sources* **246**, 540-547 (2014).

107. Chaudhari, S., Sharma, Y., Archana, P. S., Jose, R., Ramakrishna, S., Mhaisalkar, S., Srinivasan, M. Electrospun Polyaniline Nanofibers Web Electrodes for Supercapacitors. *J. Appl. Polym. Sci.* **129**, 1660-1668 (2013).

108. Liu, B., Mo, R., Kong, D., Wang, Y., Yang, H. Y. 3D Nitrogen-Doped Graphene Decorated $CoNi_2S_4$@Polypyrrole Electrode for Pseudocapacitor with Ultrahigh Electrochemical Performance. *FlatChem* **6**, 1-10 (2017).

109. Hu, C. C., Chang, K. H., Lin, M. C., Wu, Y. T. Design and Tailoring of the Nanotubular Arrayed Architecture of Hydrous RuO_2 for Next Generation

Supercapacitors. *Nano Lett.* **6**, 2690-2695 (2006).

110. Wang, F., Wu, X., Yuan, X., Liu, Z., Zhang, Y., Fu, L., Zhu, Y., Zhou, Q., Wu, Y., Huang, W. Latest Advances in Supercapacitors: From New Electrode Materials to Novel Device Designs. *Chem. Soc. Rev.* **46**, 6816-6854 (2017).

111. Chen, Y., Zhang, J., Li, M., Yang, C., Zhang, L., Wang, L., Lu, H. Strong Interface Coupling and Few-Crystalline MnO_2/Reduced Graphene Oxide Composites for Supercapacitors with High Cycle Stability. *Electrochim. Acta* **292**, 115-124 (2018).

112. Galinski, M., Lewandowski, A., Stepniak, I. Ionic Liquids as Electrolytes. *Electrochim. Acta* **51**, 5567-5580 (2006).

113. Wang, J., Kaskel, S. KOH Activation of Carbon-Based Materials for Energy Storage. *J. Mater. Chem.* **22**, 23710-23725 (2012).

114. Xu, G., Ding, B., Shen, L., Nie, P., Han, J., Zhang, X. Sulfur Embedded in Metal Organic Framework-Derived Hierarchically Porous Carbon Nanoplates for High Performance Lithium-Sulfur Battery. *J. Mater. Chem. A* **1**, 4490-4496 (2013).

Chapter 2

Materials and Methodology

Li-S Battery

- Current collector
- Li/Si Anode
- Separator
- Electrolyte
- Sulfur Cathode
- Current collector

Supercapacitor

- Current collector
- Porous Carbon Electrode
- Separator
- Electrolyte
- Porous Carbon Electrode
- Current collector

Contents

2.1 Synthesis of New Electrode Materials

2.1.1 Li-S Battery

Cathode Material: Preparation of Porous Carbon/Sulfur Composite

Elemental sulfur powder of commercial grade obtained from Fischers Scientific was used for the preparation of the cathode materials. The complete cathode development in Li-S battery was focused on the preparation of novel carbon/sulfur composite material and cell design. During the preparation of porous carbon/sulfur, the mass of porous carbon material and elemental sulfur were weighed according to the required mass ratio. Then, a small amount of carbon disulphide (CS_2) solvent was added to facilitate homogeneous distribution and

penetration of elemental sulfur into the pores of carbon. The resulting samples were dried at room temperature of 25 ℃ and later thoroughly mixed in a mortar. Finally, the samples were heat treated in alumina crucibles at a preferred temperature of 155 ℃ in a tubular furnace under argon atmosphere. The synthetic procedure of porous carbon/sulfur materials and the heat treatment procedure for the preparation of composites were discussed in detail later in the respective chapters of this thesis.

Anode Material: Preparation of Sn/Graphene and Si/Graphite Anodes

Sn/Graphene and Si/Graphite composites were prepared by electrodeposition and ball milling process respectively. The method of preparation is described in detail later in the corresponding chapter of this thesis.

2.1.2 Supercapacitor

For supercapacitor, the as-prepared porous carbon materials synthesized in the present study were also used for the fabrication of electrodes.

2.2 Techniques for Characterization of Electrode Materials

The morphology, structure, chemical composition and surface area of the synthesized porous carbon materials, sulfur infused porous carbon composites and anode materials were determined by different characterization techniques, which are described hereunder. The detailed explanation and interpretation of the results obtained by different characterization techniques are discussed in the respective chapters.

2.2.1 Field Emission-Scanning Electron Microscopy (FE-SEM)

The morphology of the as-prepared porous carbons, sulfur infused porous carbon materials and anode materials was investigated by using field emission scanning electron microscope (FE-SEM, Hitachi S-4300 SE/N).

2.2.2 Transmission Electron Microscopy (TEM)

The morphology of the as-prepared carbons, sulfur infused porous carbon composites and the presence of graphene and graphite in the anode (electrodeposited Sn/Graphene and ball milled Si/Graphite) were analysed by the transmission electron microscopy, FEI Tecnai T20 equipped with a Gatan Imaging Filter Tridiem using Energy filtered TEM.

2.2.3 BET Surface Area Studies

Nitrogen adsorption-desorption isotherm studies of the porous carbon materials were carried out by using Micromeritics ASAP 2020 analyser and the specific surface areas of the samples were determined by using the BET analysis. Prior to the analysis, the porous carbon

materials were subjected to degasification process at 120 ºC for 6h. Whereas, the degasification of porous carbon/sulfur composites was carried out at 70 ºC for 6h. This technique involves the adsorption and desorption of N_2 gas onto the surface of the porous carbon materials at its boiling point. The amount of gas molecules required to form a monolayer on the surface can be calculated by using the equation (2.1).

$$P/V(P_o-P) = 1/V_m C + C-1/V_m C * P/P_o \qquad (2.1)$$

Where P and P_o are the equilibrium pressure and the saturation pressure of N_2 gas, V is the volume of the gas adsorbed, V_m is the amount of monolayer of N_2 adsorbed, and C is BET constant.

A monolayer of N_2 molecules adsorbed and the BET constant are calculated from the intercept and slope plot between P/V (P_o–P) against P/P_o. The specific surface area of these porous samples can be calculated by using the following equation 2.2.

$$\text{Specific surface area } (m^2 \, g^{-1}) = V_m \, A_m \, N/22414 * W \qquad (2.2)$$

Where A_m is the cross sectional area of N_2 (16.2 x 10^{-20} m^2 for N_2), N is the Avogadro number and W is the weight of the sample (g).

2.2.4 Energy Dispersive X-ray Spectroscopy (EDS)

Elemental mapping of sulfur and carbon in the synthesized composite samples was done by using an energy dispersive X-ray spectrometer (EDS). In order to record the elemental mapping of the electrochemically cycled samples, the cells were decrimped inside a glove box. Later, the electrodes were soaked in 1:1 DME-DOL solvent (by volume) for five minutes. After evaporating the solvent, the electrodes were used for recording the elemental mapping of sulfur and carbon.

2.2.5 Thermogravimetric Analysis

Thermogravimetric analysis was used to study the change in the weight of the sample as a function of temperature under controlled atmosphere. The TGA instrument consists of high sensitive weighing balance, which gives the information about weight loss or gain in the sample. In the present study, the amount of sulfur present in the composites was measured under argon flow by thermogravimetry instrument Netzch (Luxx, sTA, 449 Jupiter Germany) analyser. The weight loss in the TGA curve gives the information about the amount of sulfur present in the composites.

2.2.6 X-ray Diffraction Analysis

X-ray diffraction (XRD) technique is used to determine the crystal structure of the materials. The XRD spectrum is obtained by the interaction of high energy X-ray beam with the crystalline materials, which satisfies the Braggs law.

Braggs Law is expressed by an equation as follows.

$$n\lambda = 2d \sin \theta \qquad (2.3)$$

Where n is the order of diffraction, λ is the wavelength, d is the distance between the planes and θ is the incident angle.

The universal database also known as Joint Committee on Powder Diffraction Standards (JCPDS) is used to identify the crystal structures of the materials. The JCPDS is a collection of standard XRD patterns, which corresponds to the interplanar distances of specific crystallographic properties of the materials. In the present study, the X-ray diffraction patterns of both the sulfur infused porous carbon composites and anodes were recorded by the XRD instrument, Bruker D8 Advance, Germany using Cu-kα (λ=1.54 A°) radiation and the data are collected in the 2θ range of 10-80°.

2.2.7 Raman Spectroscopy

Raman spectroscopy is a powerful technique used to identify the chemical and structural properties of the materials. The Raman scattering is obtained when a monochromatic laser light interacts with the electron cloud of the sample. If the energies of the incident and scattered photons are equal, it is named as Rayleigh scattering (elastic scattering). Whereas, if the energy of the scattered photons is less than that of the incident photons, it is known as stokes line and if the energy of the scattered photons is higher than that of the incident photon, it is known as anti-stokes line. These two types of scattering are Raman active (inelastic scattering) and the peaks in the spectrum are characteristic of the specific material.

The Raman shift is calculated by using the following equation:

$$\text{Raman shift } (\Delta_\omega) = (1/\lambda_0 - 1/\lambda_1) \qquad (2.4)$$

Where λ_0 is the excitation wavelength and λ_1 Raman spectral wavelength.

In the present study, the structural features of the as-prepared carbons, sulfur infused composite materials and the presence of graphene in anode materials were analysed by

Raman spectrometer (Model: Horiba JobinYvon Lab Ram HR-800), with an argon ion laser as a source at an excitation wavelength of 514 nm.

2.2.8 X-ray Photoelectron Spectroscopy

X-ray photoelectron spectroscopy is a surface analytical technique used to determine the oxidation states and chemical composition of the elements in the samples. When a beam of X-ray is irradiated on the sample, the electrons are ejected from the surface and the kinetic energy of the ejected electrons is calculated by using the equation 2.5.

$$\text{Kinetic energy} = h\upsilon - BE - \varphi_s \qquad (2.5)$$

Where $h\upsilon$ is the energy of photon, BE is the binding energy of electron and φ_s is the work function.

The survey scan spectrum was obtained by passing the energy of 187.9 eV and the deconvolution spectra were recorded for the elements of interest namely C 1s and S 2p with a step of 0.1 eV. The XPS instrument was calibrated using Au foil for which the characteristic binding energy value of 4f electron is 84.1 eV. In the present study, the oxidation state and the chemical composition of sulfur incorporated porous carbon samples were analysed by the Omicron X-ray photoelectron spectrometer model ESCA 2SR Germany using Mg-Kα radiation as the excitation source. The high resolution spectra were obtained by passing the energy of 20 eV with an energy step of 0.1 eV.

2.3. Electrochemical Studies

2.3.1 Electrode Preparation and Cell Fabrication

2.3.1.1 Electrode Preparation

Li-S Battery

The working electrodes (cathode) were prepared by using active material, conductive additive (super P carbon) and binder in the weight ratio of 80:10:10. Super P carbon is procured from TIMCAL Ltd., Switzerland. The super P carbon is a very fine powder and has some of the specific characteristics such as high electrical conductivity, high BET surface area, density of 160 kg m^{-3} and has low moisture content (0.1%). The co-electrodeposited Sn/graphene composite is directly used as anode, while the Si/graphite electrodes were prepared by using active material, conductive additive and binder in the weight ratios as 60:20:20. Firstly, the binder is dissolved in the suitable solvent followed by the addition of conductive carbon and active material. Then, all these were thoroughly ground in a mortar.

The homogeneous mixed slurry was coated on a current collector and then dried in vacuum oven at 60 °C for 12 h. Finally, the electrodes were punched into 12 mm discs with the help of a disc cutter and used for cell fabrication.

Supercapacitor

For the three-electrode system, the working electrode was prepared by mixing active material, acetylene black and polytetrafluoroethylene (PTFE) binder in the weight ratio of 80:10:10 respectively and the homogenous mixture was subsequently coated onto the Ni foam (current collector) and dried at 100 ºC for 12 h. For the two electrode system, the working electrode was prepared by mixing active material, acetylene black and PVDF binder in N-methyl-2-pyrrolidone (NMP) solvent in the weight ratio of 80:10:10 respectively. The slurry was uniformly coated onto stainless steel current collector and was dried in an oven at 100 ºC for overnight.

2.3.1.2 Electrolyte Preparation

Li-S Battery

The laboratory reagent grade (L.R) materials namely bis(triflouromethane)-sulfonamide lithium salt (LITFSI), 1,3-dioxalane (DOL) and dimethoxyethane (DME), procured from M/S Sigma Aldrich were used for the preparation of electrolyte. The electrolyte preparation has been done in an argon filled glove box. A 1M electrolyte solution was prepared by dissolving LITFSI in a mixture of DOL and DME in 1:1 ratio by volume. After dissolution of the salt in the solvent, $LiNO_3$ (5 wt %) was added as an additive and the solution was stirred until the additive was dissolved completely in the solvent.

Supercapacitor

Potassium hydroxide (KOH) (L.R grade) was obtained from M/S Fischer Scientific. A 6M KOH solution was prepared and used as an electrolyte for both the three and two electrode configuration systems.

2.3.1.3 Cell Fabrication Procedure

Li-S Battery

Two electrode system either in the form of 2032 coin cell or swagelok cell was employed for the fabrication of Li-S cells and all the cells were assembled in argon-filled glove box. The 2032 coin cells were procured from MTI corporation, USA and the SWAGELOK cells (SS 316L grade) from SWAGELOK Bangalore, India. The current collector coated with the active material was used as the working electrode and a lithium

metal foil was used as the reference electrode. The two electrodes were separated by polypropylene membrane (celgard-2400). 1M LITFSI containing 5 wt % of $LiNO_3$ as additive was used as an electrolyte and the schematic representation of cell fabrication process is shown in the figure 2.1. It may be noted that for the fabrication of half cells (individual cathode or anode), the lithium metal was used as a reference electrode. Whereas, for the full-cell fabrication, a thin lithium foil placed on the surface of Si/graphite was used as the anode and the sulfur infused porous carbon was used as the cathode. The modification in the electrode fabrication with modified separators and the amount of lithium used for full cell measurements were described in the respective chapters of this thesis. Before evaluating the electrochemical performance, the fabricated cells were kept for stabilization at room temperature (25 ºC) for 4-6 h.
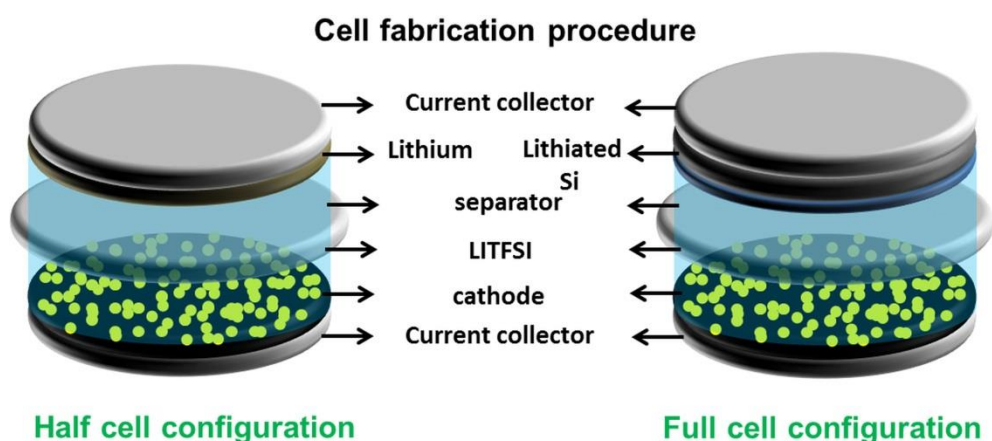
Figure 2.1 (a) Schematic representation for the fabrication Li-S cell.
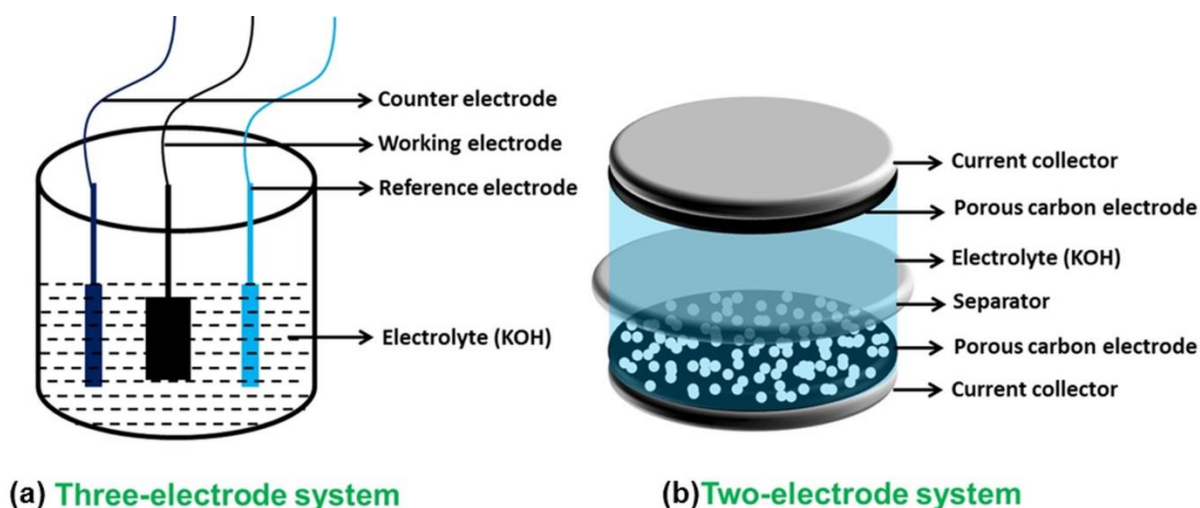
Figure 2.2 Schematic representation of (a) Three-electrode set-up and (b) Two-electrode set-up for supercapacitor.

Supercapacitor

For the three-electrode system, the Pt foil and Ag/AgCl (1M KCl) were used as the counter and reference electrode respectively. The Ni foil coated with porous carbon acted as the working electrode and 6M KOH was used as the electrolyte. Whereas, the two electrode systems were prepared using swagelok cells with symmetrical carbon electrodes separated by glass microfibre filter paper (Grade GF/D) separator with 6M KOH as the electrolyte. The fabricated cells were kept for stabilization at room temperature (25 ℃) for 4-6 h prior to the electrochemical studies. The schematic representation for the three and two electrode set-ups is given in figure 2.2a and b.

2.3.2 Cyclic Voltammetry Studies

Cyclic voltammetric studies of the electrodes were carried out by the Solatron 1260 impedance/gain phase analyzer. In Li-S battery, the cathode and anode materials were tested in the potential range of 1.5 to 2.8 V and 0.01 to 1.5 V, respectively at a scan rate of 0.1   mV s^{-1}. Whereas, full-cells were tested in the potential range of 1.0 to 2.6 V at a scan rate of 0.1 mV s^{-1}. For supercapacitor, the CV studies for the three and two electrode configurations were performed in the potential range of -1.0 to 0.0 V and 0.0 to 1.0 V, respectively, at different scan rates.

2.3.3 Galvanostatic Charge/Discharge Studies

For Li-S battery, the galvanostatic charge/discharge measurements were carried out by using battery testing station (Arbin instruments, Model: BT2000) in the voltage range of 1.5-2.8 V vs. Li/Li^{+} for sulfur half cells, 0.01-1.5 V vs. Li/Li^{+} for anode (Sn and Si) half cells and 1.0-2.6 V for lithiated Si-S full cells, respectively at different current rates. Whereas, the charge/discharge studies of the symmetric supercapacitor were done in the potential range of 0.0 to 1.0 V at different current densities.

2.3.4 Electrochemical Impedance Spectroscopy (EIS)

The AC impedance studies of the electrodes (Li-S battery and supercapacitor) were carried out by impedance/gain phase analyzer, Solartron-1260 in the frequency range of 100 kHz to 0.01 Hz with an ac signal amplitude of 10 mV.

2.3.5 Calculations

Li-S Battery:

Capacity: The total number of ampere-hours or watt-hours that can be withdrawn from a fully charged cell or battery under specified condition of discharge.

The specific capacity of the cells (C_{CD}) was calculated by using a formula given in the equation (2.6).

Specific capacity $C_{CD} = I * \Delta t / m * 3600$ mAh g^{-1} (2.6)

Where, I is the charge/discharge current in amperes, Δt is the discharge time in seconds and m is the active material mass in grams.

Gravimetric energy density: Energy density is the measure of the energy storage efficiency of a battery, usually expressed in watt-hours per kilogram (Wh kg^{-1}).
The energy density (ED) of the cells was calculated by using a formula given in the equation (2.7).

Gravimetric energy density = Battery voltage * Specific capacity Wh kg^{-1} (2.7)

Gravimetric power density: Power density is the measure of power delivered by a battery (per unit mass), usually expressed in watt per kilogram (W kg^{-1})

The power density (PD) of the cells was calculated by using a formula given in the equation (2.8).

Gravimetric power density = Energy density / time (h) W kg^{-1} (2.8)

Supercapacitor:

For a three electrode system, the specific capacitance was calculated from the discharge profile using the equation (2.9).

Specific capacity $C_{s,CD} = I * \Delta t / m * \Delta V$ (2.9)

Where *I* is the charge/discharge current (A), Δt is the discharge time (s), *m* is the active material mass (g), and ΔV is the voltage change (V) excluding the IR drop during the discharge process.

The specific capacitance (C_s) for the two electrode configuration based on the mass of single electrode was calculated from the discharge profile using the equation (2.10).

Specific capacity $C_{s,CD} = 2 (I * \Delta t / m * \Delta V)$ (2.10)

Where *I* is the discharge current (A), Δt is the discharge time (s), ΔV is the voltage change (V) excluding the IR drop and m is the mass of carbon (g) at each electrode. A factor of two is used as multiplication factor due to the series capacitance formed in the two-electrode system.

Chapter 3

Synthesis and Electrochemical Studies of High Capacity Cathodes for Li-S Battery

Contents

Introduction

A variety of strategies have been implemented in recent years to overcome the insulating behaviour of sulfur cathode and polysulfide dissolution in a Li-S cell. These include the designing of novel cathode structures such as mesoporous carbon/sulfur, graphene/sulfur and metal oxide/sulfur nanocomposites as discussed in the chapter 1 (Section 1.1.1) [1,2,3]. These types of composites help in improving the electrochemical performance of the sulfur cathode by constraining the dissolved polysulfide species in them. Among these, the micro and mesoporous carbon materials with unique physicochemical properties such as high specific surface area, excellent electrical conductivity, good chemical and thermal stabilities played a significant role in enhancing the electrical conductivity, trapping of dissolved polysulfide into the pores and accommodating large volume expansion during the redox process. Though these carbon materials exhibited promising electrochemical performance with improvement in the specific capacity and cycle stability, the preparation of

these porous carbon materials involves tedious experimental conditions and complex procedures which also make the process expensive [4,5,6,7].

Recently activated carbons (ACs) derived from biomass is attracting attention owing to its unique advantages such as environmental friendliness, facile synthetic process and low cost [8,9]. Further, high surface area, good electrical conductivity and well developed porous structure of AC led to promising electrochemical stability during charge/discharge process[10,11]. For example, S. Wei et al.[12] have prepared AC derived from pig bone and used it as a matrix for sulfur cathode, which delivered initial discharge capacity close to 1265 mAh g^{-1}. The heteroatom doped AC material prepared from soyabean residue exhibited excellent electrical conductivity and high specific surface area and showed promising electrochemical performance in terms of capacity and cyclability [11]. Subsequently, the activated carbons derived from various biomass precursors such as olive stone [13], corncob [9], fish scale [14] and pomelo peel [15] have been explored in Li-S battery and these have shown significant improvement in the active material utilization during the redox process.

In this background, the investigator focused on the synthesis of activated carbon materials from biomass namely neem leaves, tissue paper and jute stalks in order to further enhance the electrochemical performance of the sulfur cathode in Li-S battery. A simple and cost effective KOH chemical activation process has been adopted in the present study and the reaction mechanism for the formation of porous structures by KOH activation is presented hereunder.

Reaction Mechanism of KOH Activation:

The reaction of KOH with carbon proceeds via solid-solid reaction and also solid-liquid reaction. The mechanism proposed for the formation of porous structures depends on a large number of variables such as operating temperature, precursors used and the amount of the activating agent [16]. The mechanism involves reduction of potassium compounds (KOH, K_2CO_3, K_2O) to elemental potassium and oxidation of carbon to carbonates, accompanied by the evolution of a large number of gasses like CO, CO_2 and H_2O (g). D. L. Castello et al.[17] have studied the reaction between KOH and carbon by combining the experimental and theoretical data and proposed a series of reactions as given in the equations (3.1) to (3.6). Initially, at about 400 ℃, KOH reacts with carbon to form K_2CO_3 (eqn 3.1), which further decomposes to K_2O and CO_2 as the temperature increases to 800 ℃ (approximately)

(equations 3.2 and 3.3). Concurrently, the as-formed K_2CO_3 (eqn 3.1), CO_2 and K_2O (eqns 3.2 and 3.3), further react with carbon to produce CO and metallic potassium at this higher temperature (~800 ℃) (eqns 3.4 to 3.6).

$$6KOH + 2C \rightarrow 2K + 3H_2 + 2K_2CO_3 \tag{3.1}$$
$$2KOH \rightarrow K_2O + H_2O \tag{3.2}$$
$$K_2CO_3 \rightarrow K_2O + CO_2 \tag{3.3}$$
$$CO_2 + C \rightarrow 2CO \tag{3.4}$$
$$K_2CO_3 + 2C \rightarrow 2K + 3CO \tag{3.5}$$
$$C + K_2O \rightarrow 2K + CO \tag{3.6}$$

Based on the above reactions, three types of activation mechanisms have been proposed. Firstly, the redox reaction between various potassium compounds and carbon framework (eqns 3.1, 3.5 and 3.6) is called the chemical activation process. This leads to the formation of a large number of porous structures during the heat treatment process. Secondly, The H_2O and CO_2 formed during the activation process also act as additional pore generating agents by gasification of C (physical activation) as given in the equations 3.2 and 3.4. Thirdly, the metallic K formed (eqns 3.1, 3.5 and 3.6) during the activation process, intercalates into the carbon matrix, which results in the expansion of carbon lattice. During acid washing, the intercalated K based compounds diffuse out from the carbon matrix and thus additional microporosity will be generated in this process. The comprehensive effects of chemical activation, physical activation and lattice expansion of carbon result in the formation of micro and mesoporous structures with high specific surface area and large pore volume in the carbon matrix.

The present chapter is divided into four sections, which comprise the experimental details, results and discussion of micro and mesoporous carbon synthesized from fallen neem leaves (section 3.1), micro and mesoporous carbon synthesized from tissue paper (section 3.2), micro and mesoporous carbon synthesized from jute stalks (section 3.3) and their application as hosts for sulfur cathode in a Li-S battery. The Section 3.4 presents a comparison of the developed porous carbons in the present study and with those reported in the literature.

Section 3.1 Neem Leaves-Derived Micro and Mesoporous Carbon as an Efficient Polysulfide Inhibitor for Sulfur Cathode

The preparation of most of the activated carbon (AC) materials involves a two-step process. The biomass materials were initially pre-carbonized at a lower temperature to remove the volatile organic compounds followed by soaking the pre-carbonized powders into an activating agent and final carbonization at high temperatures. Considering commercial point of view, it is essential to adopt the methods that are quick, easy and simple to synthesize micro and mesoporous carbon materials. *In-situ* KOH activation is one such way to simplify the process to prepare AC materials and very few literature reports on this method are available [18,19]. The aim of the present study is to synthesize micro and mesoporous carbon from neem leaves (Azadirachta Indica) by the method of *in-situ* KOH activation and study its performance as polysulfide inhibitor for sulfur cathode in Li-S battery.

3.1.1 Synthesis of NLMC and NLMC/S Cathode

Synthesis of NLMC

The fallen neem leaves were collected from the local neem trees and thoroughly cleaned with deionised (DI) water followed by drying in an oven at 80 °C. These dried neem leaves were ground in a mortar to form a powder and this powder was soaked in 25 ml of KOH solution with different weight ratios of NLMC to KOH in grams as 1:0, 1:0.2, 1:0.3 and 1:0.4. The KOH soaked powders were dried in an oven at 100 °C. The dried samples were heat treated in a tubular furnace at 1000 °C for 4 hours in an argon atmosphere at a heating rate of 10 °C per minute. The black powders thus obtainded were washed with 1M HCl and 1M HF followed by DI water and finally dried in an oven at 100 °C. The resulting samples prepared with the powder of neem leaves to KOH ratios of 1:0, 1:0.2, 1:0.3 and 1:0.4 were labeled as NLMC-1, NLMC-2, NLMC-3 and NLMC-4, respectively. The investigator also made an attempt to prepare the NLMC with wt ratio of neem leaves powder to KOH in grams as 1:0.5. In this experiment, it was found that the yield of activated carbon is much lower than NLMC-4. The reason may be that at this concentration of KOH, more carbon is oxidized to CO_2 and CO. Therefore, the studies are limited up to NLMC-4.
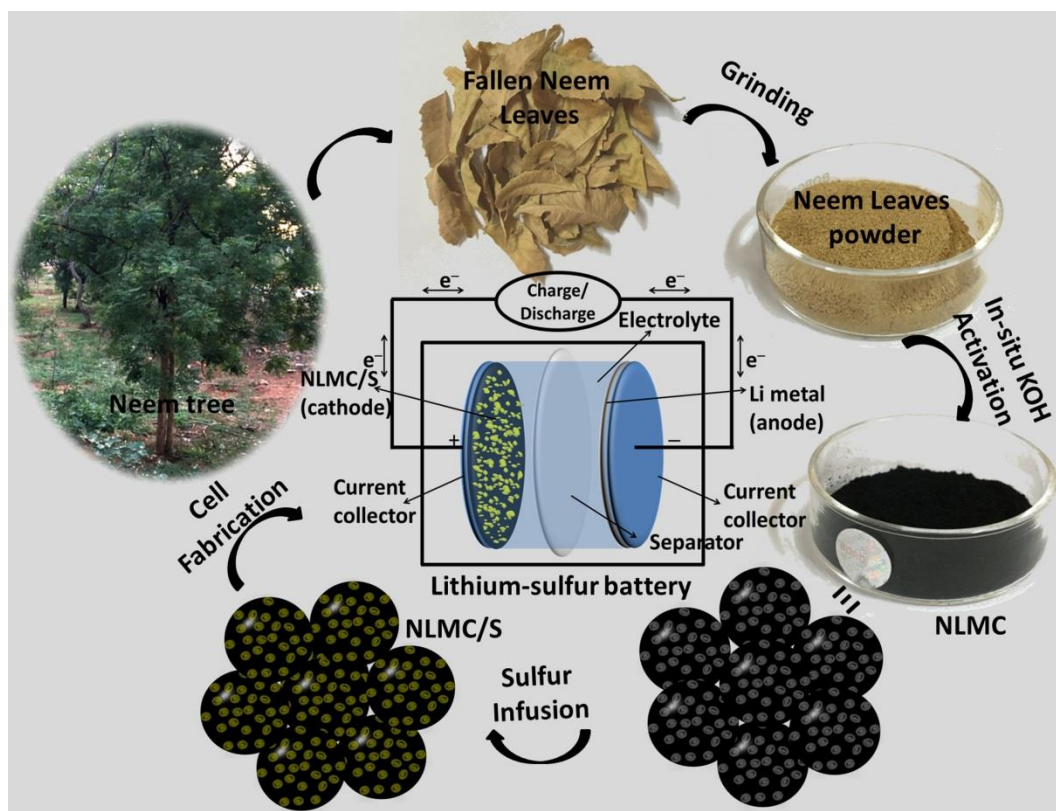
Figure 3.1.1 Schematic representation for the synthesis of NLMC/S cathode and cell fabrication process.

Synthesis of NLMC/S Cathode

Initially, the elemental sulfur powder was dissolved in minimum amount of carbon disulfide (CS_2) solvent and the resulting solution was mixed with as-prepared carbon materials (NLMC-1, NLMC-2, NLMC-3 and NLMC-4) to form a final weight ratio of 3:1. The preliminary studies were made in order to prepare the NLMC/S composites with much higher sulfur loading into porous carbon matrix. According to the literature reports, L. Y. Li et al.[20] has synthesized porous carbon/sulfur composite with the initial weight ratios of sulfur to porous carbon as 3:1 to obtain a composite with 58 wt % of sulfur and studied its electrochemical performance. C. P. Yang et al.[21] prepared the porous carbon/sulfur composite with 53 wt% of sulfur in the carbon matrix by using the weight ratios of sulfur to carbon as 2.4:1. Therefore, in the present study, the investigator has chosen the mass ratio of 3:1 during the synthesis of NLMC/S composites. The sulfur diffuses into the micro and mesopores of the NLMC. As the CS_2 gets evaporated, the sulfur gets precipitated in the micro and mesopores of the NLMC. The powders were heated initially at 155 °C for 12 hours and then finally at 300 °C for 2 hours in closed alumina crucibles at a heating rate of 5 °C per min. At 155 °C, most of the molten sulfur gets penetrated into the porous carbon and in final heating stage at

300 °C, maximum content of exposed sulfur on the outer surface is evaporated. Thus, as-obtained sulfur infused carbon materials were named as NLMC-1/S, NLMC-2/S, NLMC-3/S and NLMC-4/S, respectively. Further, the sulfur loading into NLMC-4 was also done by increasing the amount of elemental sulfur into NLMC-4 by keeping the different ratios of sulfur to carbon (NLMC), i.e., 3:1 and 5:1. X. Tao et al.[22] have prepared kapok fiber-derived carbon nanotile/sulfur composites with difference in the initial mass ratios of sulfur to porous carbon as 3:1 and and 15:1, respectively, to study the effect of higher sulfur loading on the electrochemical performance of sulfur cathode. In the present study, the sulfur to NLMC-4 with difference in weight ratios of 3:1 and 5:1 were labelled as NLMC-4/S50 and NLMC-4/S67, respectively, as in the former 50 wt% has been infused into carbon and in the later case, 67 wt% has been infused into carbon.

Two electrode systems were constructed using standard 2032 coin cells by using NLMC/S as the cathode, lithium foil as the reference electrode and 1M LITFSI with 5 wt% $LiNO_3$ as electrolyte. The assembled cells were kept for stabilization for 4 h at room temperature. The Schematic illustration for the preparation of NLMC/S cathode and the cell fabrication process are given in the figure 3.1.1.

3.1.2 Results and Discussion: Characterization of NLMC and NLMC/S Cathode

3.1.2.1 Morphological Analysis:

The morphological studies of the as-prepared NLMC samples were analyzed by FE-SEM and TEM. Figure 3.1.2 shows the SEM, TEM and the corresponding HR-TEM images of the as-prepared NLMC-1, NLMC-2, NLMC-3 and NLMC-4. All the samples show similar type of morphological characteristics with macropores, which are expected to improve the wettability of the electrode, and increase the ionic mobility during the charge/discharge process. It is interesting to note that the *in-situ* KOH activated NLMC has more mesopores and macropores in comparison to NLMC sample as shown in the figure 3.1.2. As the neem leaves contain trace amounts of elements such as Ca, K, Mg, Si, O [23], the excessive addition of KOH to the sample induces additional mesopore sturctures as well as an increase in the graphitic nature of the sample during the heat treatment process.
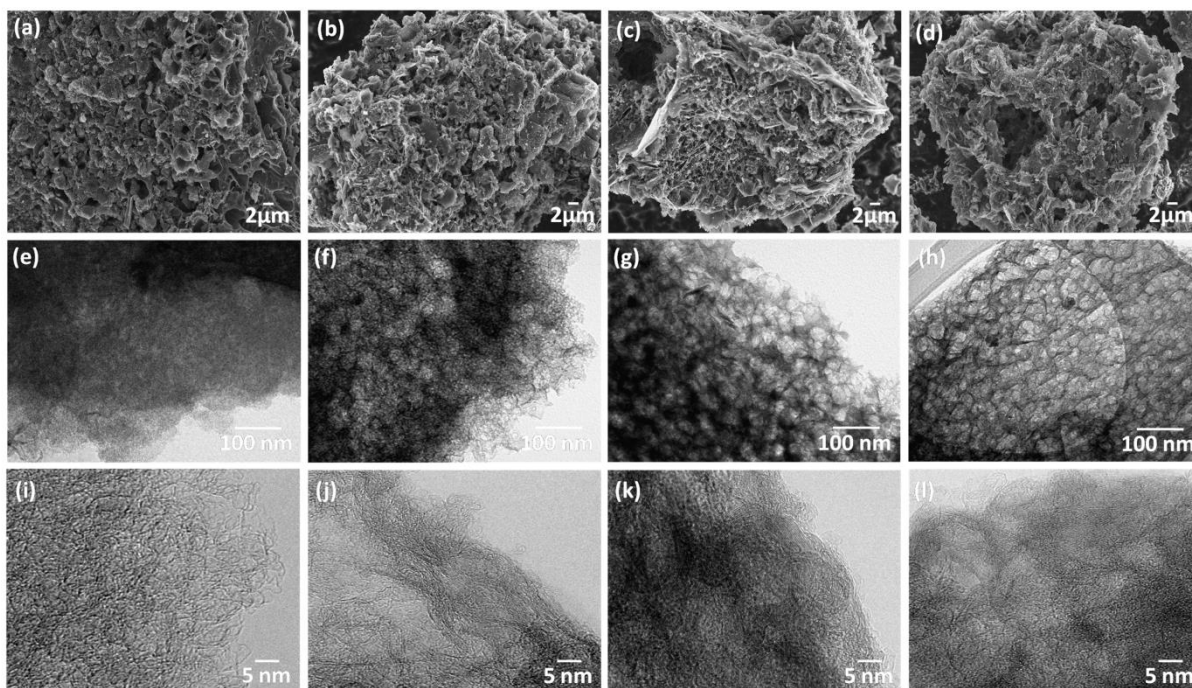
Figure 3.1.2 FE-SEM (a-d) and TEM images (e-h) of NLMC-1, NLMC-2, NLMC-3 and NLMC-4 respectively and the corresponding HR-TEM images (i-l).

3.1.2.2 N_2 Adsorption/Desorption Analysis:

N_2 adsorption/desorption studies were conducted to analyse the textural properties of the as-prepared NLMC-1, NLMC-2, NLMC-3 and NLMC-4 samples (figure 3.1.3). All the samples represent the type IV isotherm, which is characteristic of the mesopore structures in the samples [9]. Further, the linear feature of the isotherm at low relative pressure indicates the presence of micropores (figure 3.1.3a). It can be seen from the table 3.1 that the as-prepared NLMC-1 displays the lowest specific surface area, which increases with an increase in the amount of KOH used in the activation process. The pore size distribution of all the NLMC samples (figure 3.1.3b) was analysed by using 2D non-local density functional theory (NLDFT), which showed the presence of micropores in the range of 0.8 to 1.0 nm, in addition to the presence of mesopores in the range of 3-4 nm. NLDFT is a non-local density functional theory, which is used to determine the pore size distribution ranging from micro to mesopores in the sample. More precisely, the presence of microporous structures (< 2nm) in the as-prepared activated carbon materials [24,25]. From the data, the pore volumes are calculated and presented in the table 3.1. It is interesting to note that the increase of mass ratio of KOH-carbon evidently makes the micropores broaden and the formation of large mesopores is observed as shown in the figure 3.1.2b for NLMC prepared with KOH-carbon ratio of 0.4:1. The surface area and pore volume of KOH treated NLMC (2-4) samples are significantly

higher than those of NLMC-1, indicating that the *in-situ* activation of KOH plays an important role in inducing significant fraction of micro and mesoporous structures in the carbon. The high surface area and large pore volume are advantageous for the carbon as it can uptake high amount of sulfur, which improves the overall lithium ion kinetics during redox reactions via easy access of electrolyte into the pores [26]. Further, the presence of mesoporous structure not only acts as polysulfide dissolution barrier, but also accommodates volume expansion during the discharging process.
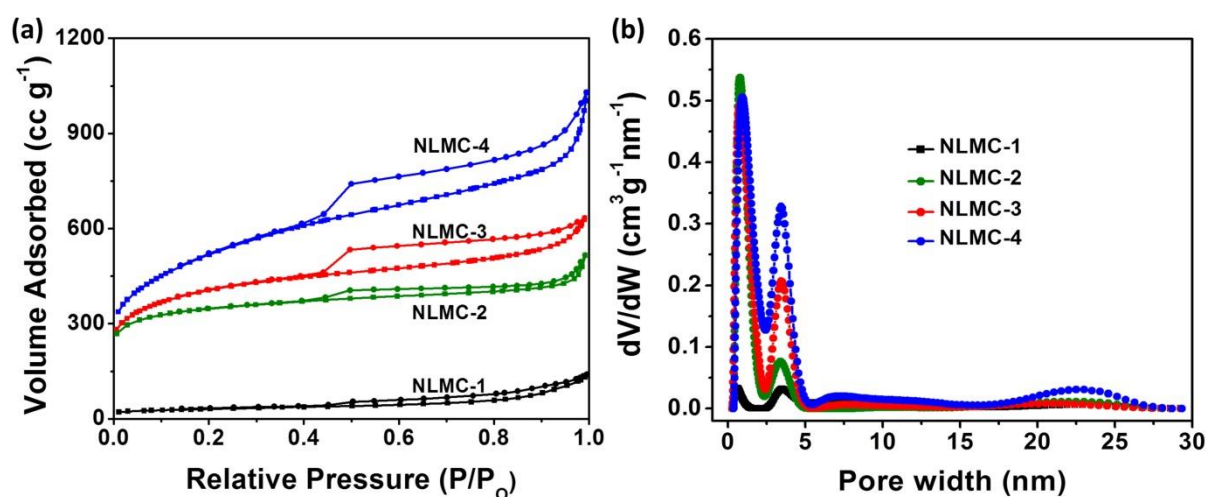
Figure 3.1.3 (a) N_2 adsorption/desorption isotherms and (b) Corresponding pore size distribution curves of NLMC-1-4.

Table 3.1.1 Comparison of surface area and pore size distribution of NLMC-1-4

Activated carbon sample	Surface area $(m^2\,g^{-1})$	Pore volume $(cc\,g^{-1})$
NLMC-1	93	0.17
NLMC-2	1175	0.67
NLMC-3	1411	1.09
NLMC-4	1872	1.59

3.1.2.3 EDS Elemental Mapping and TG Analysis:

The distribution of sulfur in NLMC samples was analyzed by EDS elemental mapping and the results show the homogenous distribution of sulfur throughout the carbon matrix (figure 3.1.4). Further, the thermogravemetric (TG) curves of sulfur infused NLMC 1-4 samples (figure 3.1.5) show a weight loss in the temperature range of 200 to 350 °C. The NLMC-1/S showed the weight loss at lower temperature range, following the trend

corresponding to the weight loss of elemental sulfur. However, the sulfur infused NLMC-2-4 samples displayed a weight loss in the TG curves at a higher temperature range indicating that the sulfur present in the micro and mesoporous structure diffused slowly in contrast to the NLMC-1/S [9]. From the TG curves the sulfur contents in the NLMC-1/S, NLMC-2/S, NLMC-3/S, NLMC-4/S50 and NLMC-4/S67 are calculated to be 38.6, 46.6, 48.8 and 50.1 % respectively.
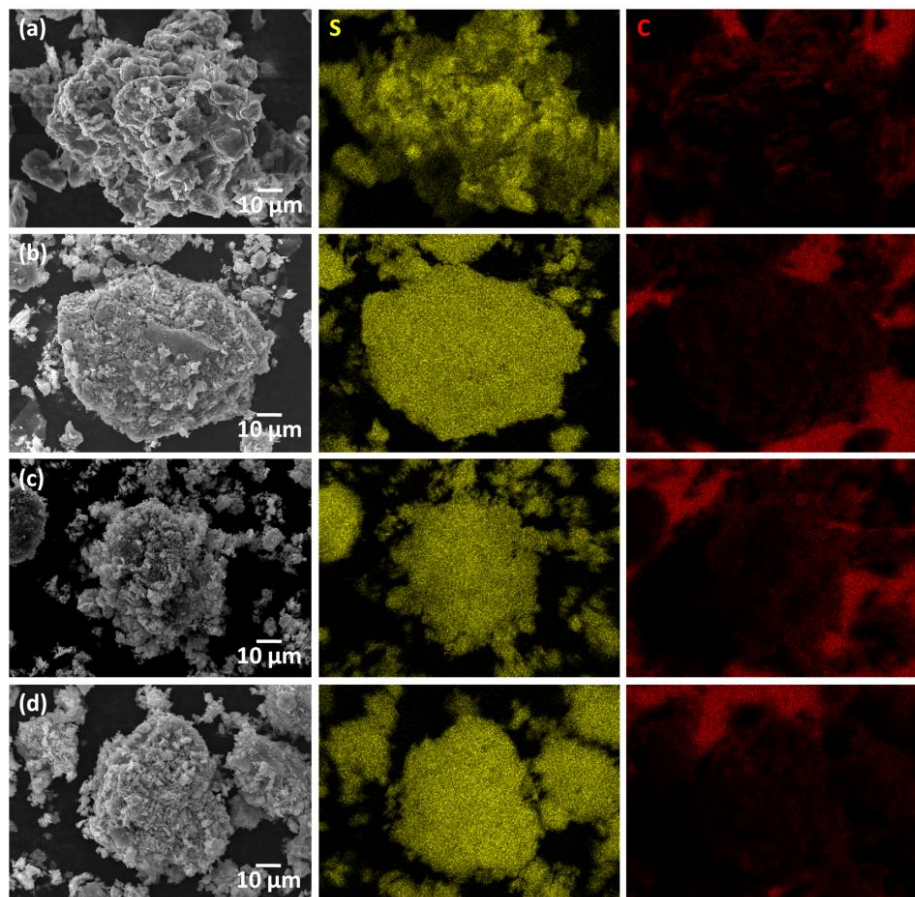
Figure 3.1.4 SEM images of sulfur infused NLMC-1, NLMC-2, NLMC-3 and NLMC-4 (a-d) with the corresponding elemental map of sulfur (yellow) and carbon (red).
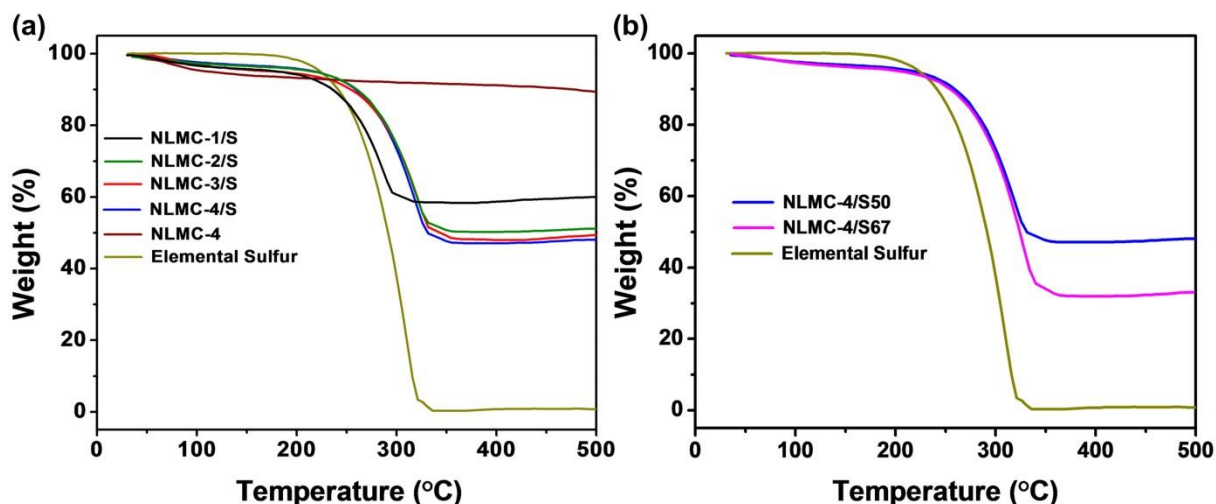
Figure 3.1.5 (a) TG curves of sulfur infused NLMC1-4-S composites and (b) TG curves of NLMC-4/S50 and NLMC-4/S67.

3.1.2.4 Raman Spectral Analysis:

Figures 3.1.6a and b show the Raman spectra of the as-prepared NLMC1-4 and the corresponding sulfur infused composites. The Raman spectra of these samples display peaks at 1350 cm^{-1}, which correspond to the characteristic D band and are assigned to the A_{1g} mode of defective carbon atoms. These spectra also show peaks at 1590 cm^{-1} corresponding to G band, which are assigned to the E_{2g} vibration mode of graphitic carbon atoms [27]. The elemental sulfur shows the Raman scattering in the low wave number region (<500 cm^{-1}), which corresponds to the characteristic vibration mode of sulfur atoms [22]. This elemental sulfur peak is missing in sulfur infused NLMC-1-4 composites. D. Wang et al. [28], also observed similar Raman spectra for the samples after sulfur infusion into micro and mesoporous structures and concluded that the sulfur is completely confined into the porous carbon matrix. Thus, from the Raman spectra of the samples in the present study, it may be inferred that the sulfur is diffused into the micro and mesoporous carbon matrix during the heat treatment process.
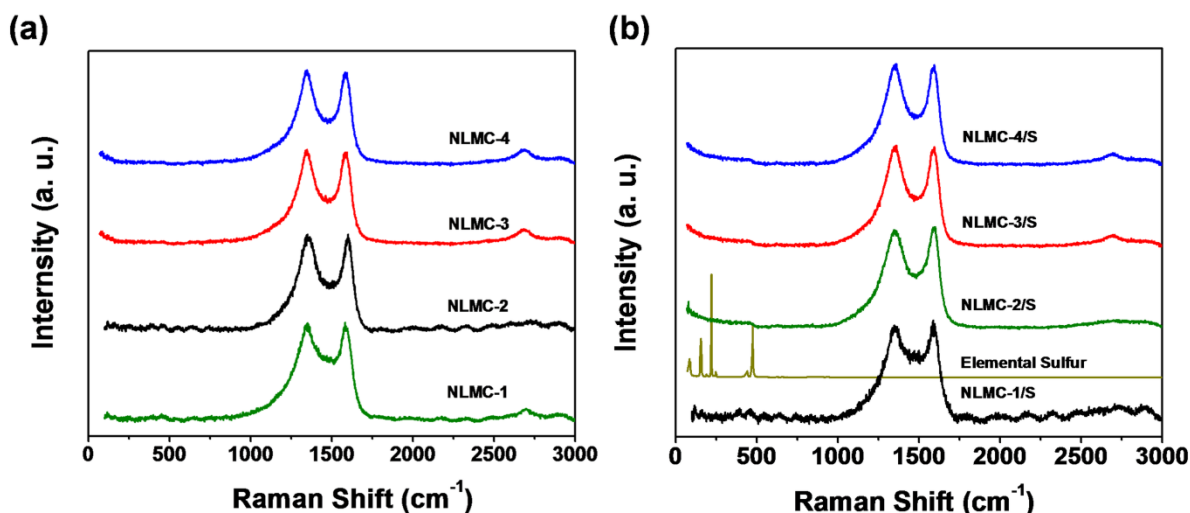
Figure 3.1.6 Raman spectra of (a) as-prepared and (b) sulfur infused NLMC-1-4 composites.

3.1.3 Results and Discussion: Electrochemical Studies (CV, C/D, CY and EIS) of NLMC/S Cathode

The electrochemical performance of NLMC/S cathode materials was evaluated with respect to Li anode in the potential range of 1.5 to 2.8 V. In order to select the composite material with superior electrochemical performance, a comparison of the discharge profiles of all the prepared materials is made at 0.1 C rate as shown in the figure 3.1.7. The NLMC-1/S, NLMC-2/S, NLMC-3/S and NLMC-4/S cathodes delivered initial discharge capacities of 424 mAh g^{-1}, 868 mAh g^{-1}, 1185 mAh g^{-1} and 1396 mAh g^{-1} respectively. Thus, the *in-situ* activated NLMC/S cathodes delivered high specific discharge capacities due to high surface to volume ratio of carbon that improves the ionic and electrical conductivities, which in turn increase the utilization of active material during the redox process.

The NLMC-1/S cathode shows poor cycle performance with low discharge capacity of 167 mAh g^{-1} at 50th cycle due to low surface area with negligible pore volume. Even after 50 charge/discharge cycles the NLMC-2/S, NLMC-3/S and NLMC-4/S cathodes exhibit the discharge capacities of 540 mAh g^{-1}, 774 mAh g^{-1} and 901 mAh g^{-1}, respectively. Among all the electrodes, NLMC-4/S exhibits the highest discharge capacity even after 50 charge/ discharge cycles. This is attributed to large pore volume, trapping the soluble polysulfides into the porous carbon matrix and also accommodating large volume expansion. It is reported in the literature that the presence of micro/mesoporous structures in the carbon matrix helps in entrapping the dissolved polysulfide species in the cathode part and improves the electrochemical performance of sulfur cathode for longer cycles [29]. For example, G. Lu et al.[30], prepared porous graphitic carbon material with high surface area, large pore

volume and the resulting sulfur composite exhibited high discharge capacity for longer cycles. This behaviour is due to efficient trapping of dissolved polysulfide species in the porous structures and improved ionic and electronic conductivities.
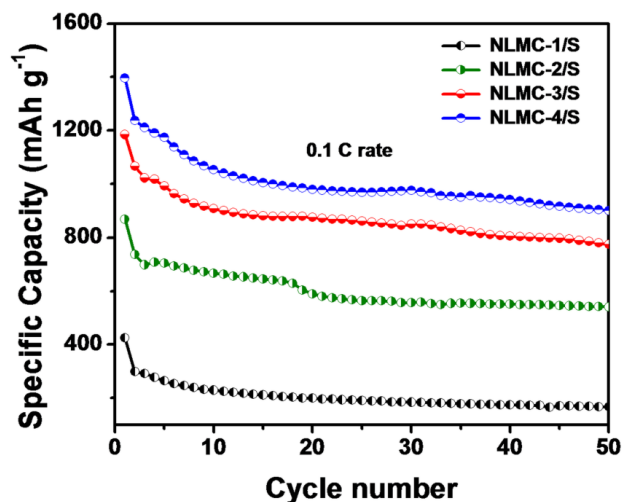
Figure 3.1.7 Comparative cycle performance of NLMC-1/S, NLMC-2/S, NLMC-3/S and NLMC-4/S cathodes measured in the voltage range of 1.5-2.8 w.r.t Li anode at 0.1 C rate.

As the NLMC-4/S showed the highest discharge capacity, it was selected for higher loading of sulfur and for further electrochemical studies. The cyclic voltammetric (CV) studies were conducted in order to study the electrochemical behaviour of NLMC-4/S50 cathode, which contains 50% by weight of sulfur (figure 3.1.5) in the composite material. Figure 3.1.8 shows the CV profile of NLMC-4/S50 for the initial 10 cycles carried out at a scan rate of 0.1 mV s^{-1} in the potential range of 1.5 to 2.8 V vs. Li/Li^{+} electrode. It is well known that the oxidation/reduction reaction of the sulfur cathode with lithium involves stepwise and complex reactions [12,31]. During the cathodic scan, the composite shows a pair of peaks at about 2.3 V and 2.1 V, which can be assigned to formation of long chain polysulfide (Li$_2$S$_n$, n= 4 to 8) and its reduction to short chain polysulfides (Li$_2$S$_2$ and Li$_2$S) as the final discharge product. In the anodic scan, a sharp oxidation peak is observed at a potential of 2.4 V, which is attributed to reversible conversion of lithium sulfide to elemental sulfur [32,33]. In the subsequent scan upto 10 cycles, no changes are observed in redox peaks, suggesting high electrochemical stability of NLMC-4/S50 composite cathode.
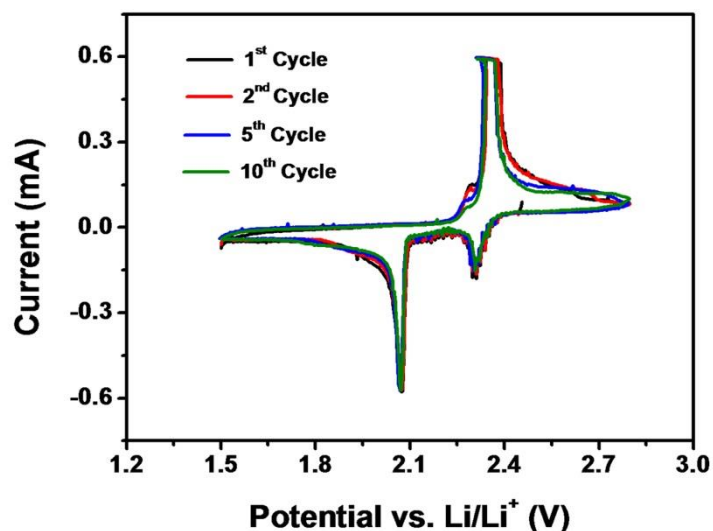
Figure 3.1.8 (a) CV profile of NLMC-4/S50 carried out at 0.1 mV S^{-1} scan rate.

Figure 3.1.9a shows the schematic representation for the fabrication of NLMC-4/S cell, wherein, NLMC/S is used as cathode and lithium metal as the reference electrode. Further, the electrochemical performance of sulfur infused NLMC-4 cathode with higher loading of sulfur (NLMC-4/S50 and NLMC-4/S67) has also been studied at 0.1 C rate and the initial charge/discharge curves are shown in the Figure 3.1.9b. A two-stepped plateau is observed in the discharge profiles for both the cells, which corresponds to multi-electron transfer reaction between elemental sulfur and lithium. The flat charge curves indicate the reversible conversion of polysulfide intermediates to sulfur. These results are in good agreement with those of CV studies. Initially, the NLMC-4/S50 and NLMC-4/S67 electrodes delivered high discharge capacities of 1391 mAh g^{-1} and 1096 mAh g^{-1}, respectively. After, 50 charge/discharge cycles (Figure 3.1.9c), the NLMC-4/S50 cell displays much higher capacity of 896 mAh g^{-1} than that of NLMC-4/S67 (544 mAh g^{-1}), indicating that the higher loading of active material into the porous carbon matrix decreases the electrochemical performance of sulfur cathode during redox process [34]. This behavior is mainly due to the deposition of excess sulfur on the surface of porous carbon, which increases dissolution of soluble polysulfide species into the electrolyte. Moreover, the presence of excess active material may also reduce the ion and electron motilities due to a decrease in the pore volume or blockage of pores. Hence, it is inferred that the NLMC-4/S50 with 50 wt % of sulfur loading exhibits superior electrochemical performance in comparison to NLMC-4/S67 with 67 wt%.
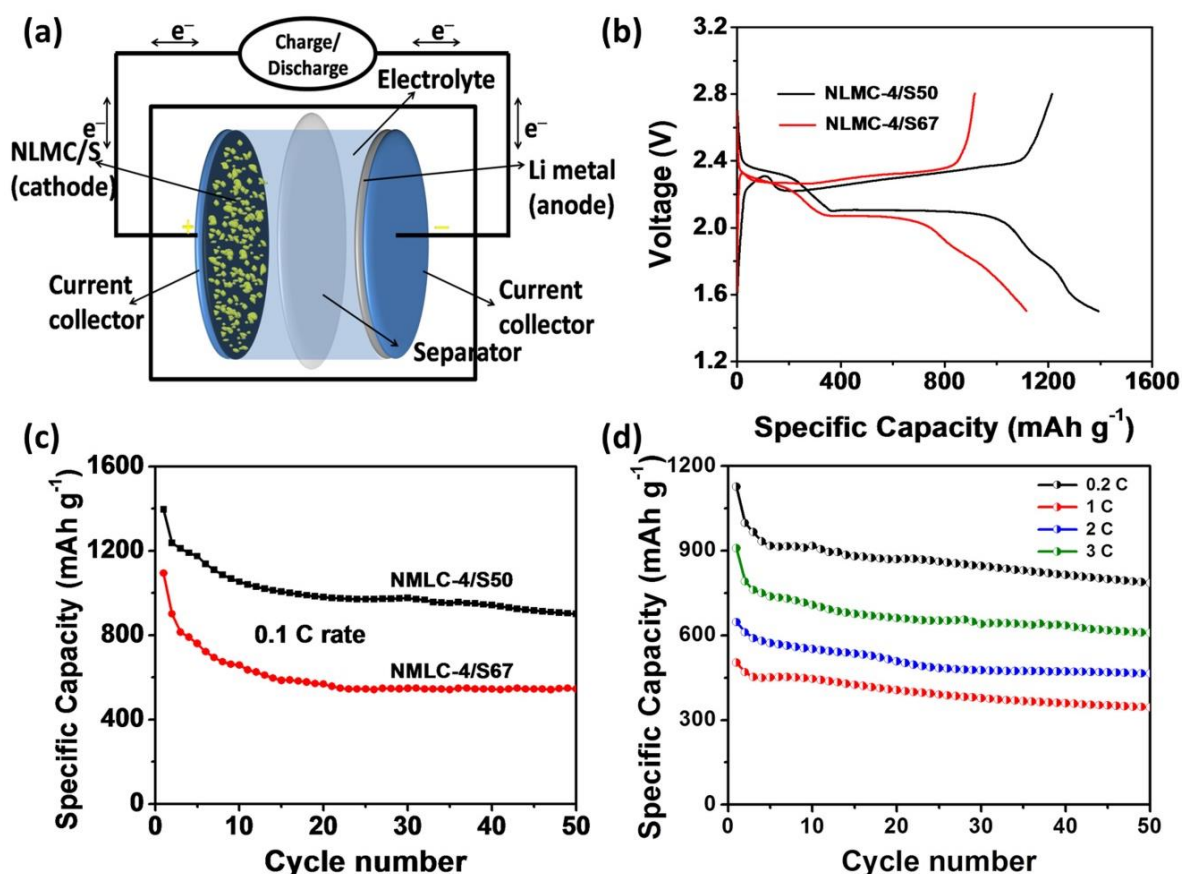
Figure 3.1.9 (a) Schematic representation for the fabrication of NLMC/S cell, (b) and (c) are the charge/discharge, cycle performance curves of NLMC-4/S50 and NLMC-4/S67, respectively and (d) cycle performance curve of NLMC-4/S50 cathode measured at different current rates (0.2 C, 1 C, 2 C and 3 C) for over 50 cycles.

B. Zhang et al.[26] also prepared hierarchically porous carbon microfibers/sulfur composites with different sulfur loading of 48 wt% and 66 wt% into porous carbon matrix. They have observed an improved electrochemical performance of the sulfur cathode with 48 wt% of sulfur infusion into porous carbon matrix in comparison to 66 wt%. The reduced performance is due to higher sulfur loading, which increases the dissolution of dissolved polysulfide species into the electrolyte. Further, the NLMC-4/S50 cathode delivered discharge capacities of 784 mAh g^{-1}, 608 mAh g^{-1}, 464 mAh g^{-1} and 344 mAh g^{-1} at different current rates of 0.2 C, 1 C, 2 C and 3 C, respectively even after 50 cycles (figure 3.1.9d) demonstrating the rate capability and electrochemical stability of NLMC-4/S50.

The difference in electrochemical performances of NLMC-4/S50 and NLMC-4/S67 was also validated by EIS and the Nyquist plots are shown in the Figure 3.1.10. The plots of both the electrodes showed depressed semicircles in the high frequency region, which

corresponds to charge transfer region at the electrode/electrolyte interface. These are also characterized by the Warburg impedance in the low frequency region, which is associated with the diffusion of lithium ions from the electrode surface into the electrolyte [20]. The experimental results fitted well with the equivalent circuit shown in the in-set of figure 3.1.10. R_s represent the resistance of the electrolyte, R_{ct} is the charge transfer resistance, CPE is the constant phase element and W_o is the Warburg resistance caused by the diffusion of lithium ions in the porou electrode. The NLMC-4/S50 electrode displayed lower R_{ct} of 29.8 Ω in comparison to NLMC-4/S67 with an R_{ct} of 56.6 Ω. X. Gu et al.[29] also observed an increase in R_{ct} value with an increase in sulfur loading into carbon matrix, which is mainly due to the presence of higher content of sulfur on the electrode resulting in higher cell resistance. This result confirms that an improved charge transfer process takes place with optimum sulfur loading into the carbon matrix and thus the resulting cell achieves an enhanced electrochemical performance.
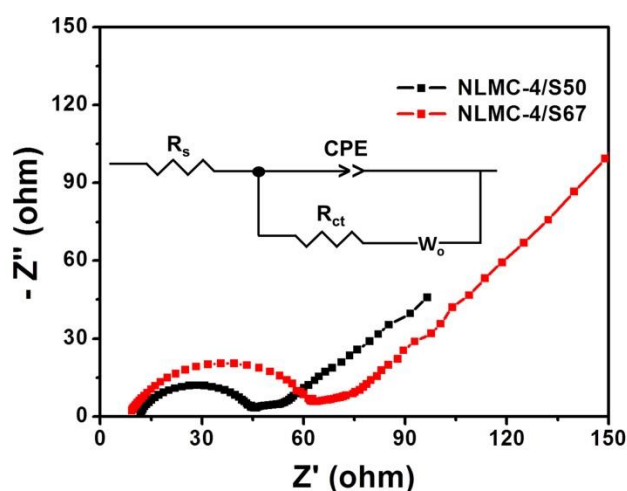
Figure 3.1.10 Nyquist plots of NLMC-4/S50 and NLMC-4/S67 electrodes.

The longer cycle performance tests for the sulfur infused NLMC samples with and without *in-situ* KOH activation were also conducted at 1 C rate (figure 3.1.11). Initially, the NLMC-4/S50 cell showed a higher discharge capacity of 939 mAh g^{-1}, in comparison to NLMC-1/S (279 mAh g^{-1}), inferring that the porous carbon with high surface area provides enough space for sulfur infiltration during the heat treatment process, which can overcome the insulating behavior of sulfur cathode and improve the active material utilization during fast reaction kinetics. Even after 200 cycles the NLMC-4/S50 cell exhibits appreciated discharge capacity of 506 mAh g^{-1} with good columbic efficiency. Whereas, the NLMC-1/S electrode displayed poor cycle performance and exhibited a specific capacity of 30 mAh g^{-1} after 200th

cycle. These results confirm that the presence of micro and mesoporous carbon matrix effectively traps the dissolved polysulfide species into the pores and improves the electrochemical performance of the cell with repeated charge/discharge processes.
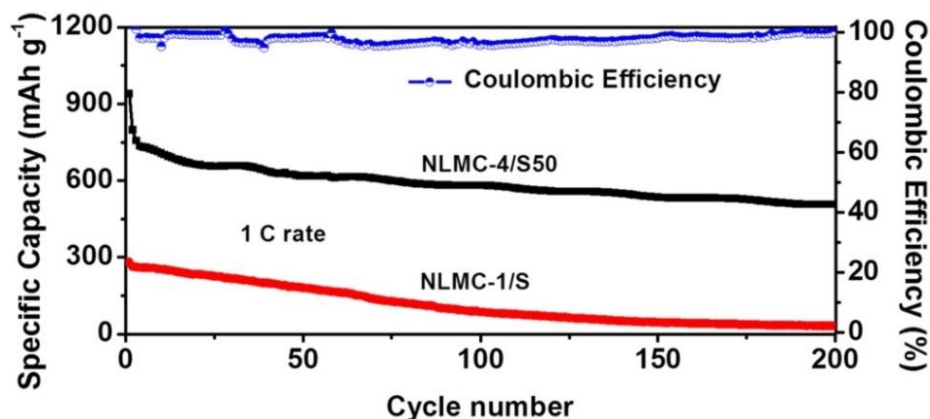
Figure 3.1.11 Comparative cycle performance curve of NLMC-4/S50 and NLMC-1/S measured at 1 C for 200 cycles.

Further, attempt has been made to analyse the dissolved polysulfides in electrolyte solution after cycling process by adopting the procedure as follows: Initially, the Li-S cells (NLMC-4/S50 and NLMC-4/S67) were assembled using Swagelok cell and tested at a current rate of 1 C for 10 charge/discharge cycles. Then, the Li-S cells were de-crimped inside the glove box for visual identification of colour change on the separator. The polypropylene separator used in Li-S cell with NLMC-4/S50 electrode showed pale yellow colour, whereas the colour contrast slightly increased for the separator used in Li-S cell with NLMC-4/S67 cathode as shown in images of figure 3.1.12. The above observation clearly indicates that the polysulfide dissolution into the electrolyte increases with an increase in the amount of sulfur loading into the NLMC-4 and hence, NLMC-4 with optimum sulfur loading (NLMC-4/S50) showed better electrochemical performance than NLMC-4/S67.
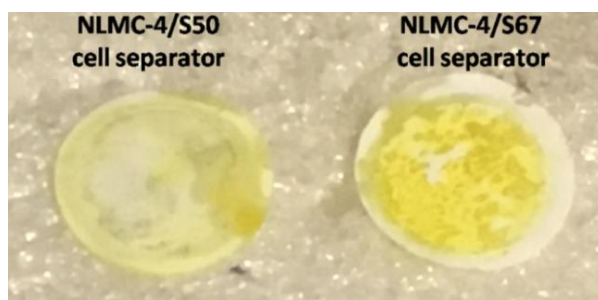
Figure 3.1.12 Photo image of separators of the cells prepared by using NLMC-4/S50 and NLMC-4/S67 electrodes.
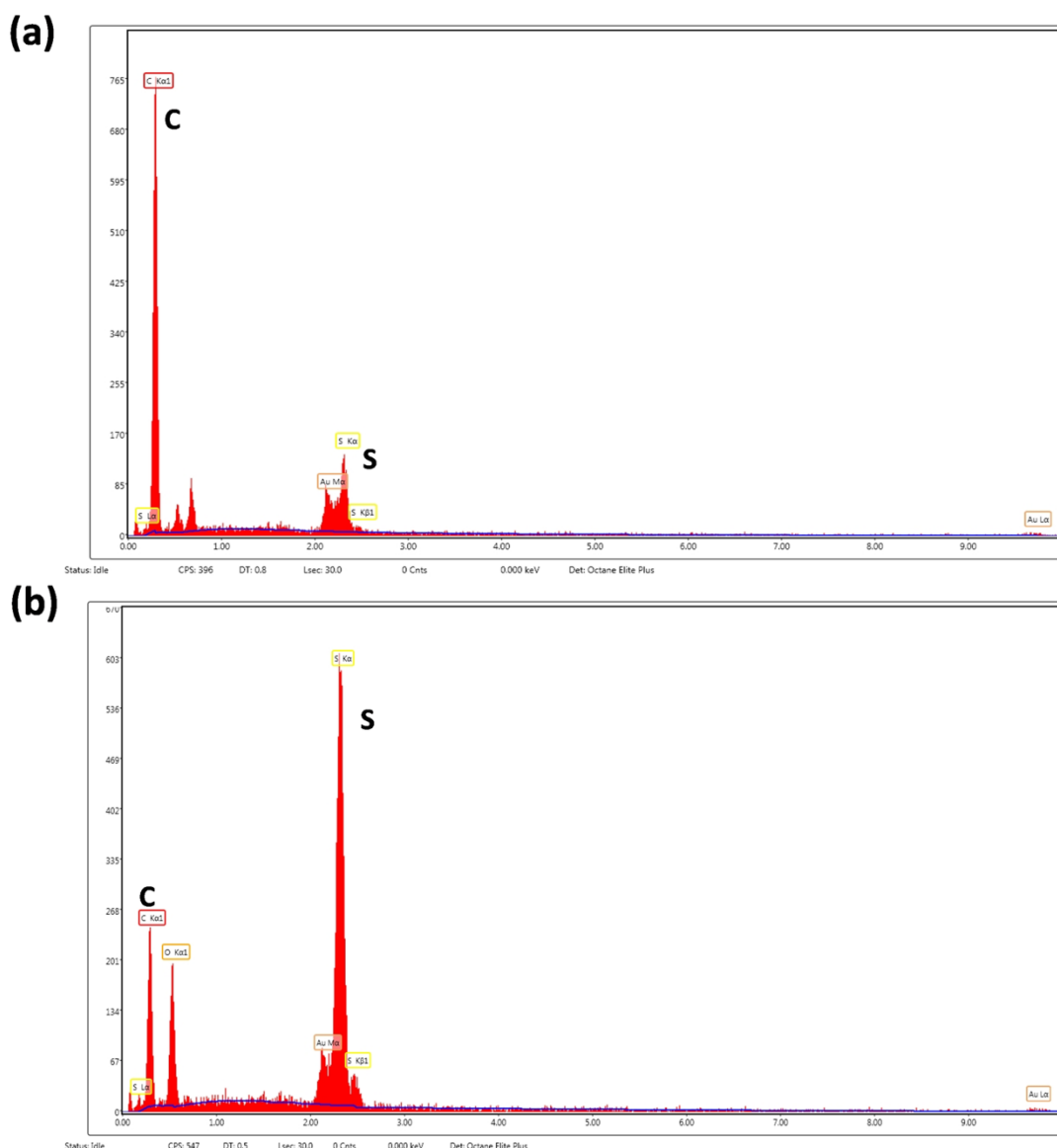
Figure 3.1.13 EDS spectra of separators (a) of the de-crimped NLMC-4/S50 and (b) of the de-crimped NLMC-4/S67 cells after 10 cycles.

Furthermore, the separators used in the NLMC-4/S50 and NLMC-4/S67 cells were subjected to EDS analysis and elemental mapping and the results are shown in the Figures 3.1.13 and 3.1.14 respectively. Though carbon and sulfur are present in separators of NLMC-4/S50 and NLMC-4/S67 electrodes, the intensity of sulfur peak in the former is less than the later (Figure 3.1.13), demonstrating that dissolution of polysulfide into the electrolyte is reduced in NLMC-4/S50 in comparison to NLMC-4/S67 electrode. These EDS results are consistent with the elemental mapping of the separators used in NLMC-4/S50 and NLMC-4/S67 electrodes, as the sulfur concentration is found to be less in NLMC-4/S50 than in NLMC-4/S67. The results of these experiments confirm that the dissolution of polysulfide

into the electrolyte is reduced NLMC-4 with optimum sulfur loading (NLMC-4/S50), inferring that NLMC-4 carbon effectively traps polysulfides in its micro and mesoporous structure and thus increases the cycle life of the Li-S cell.
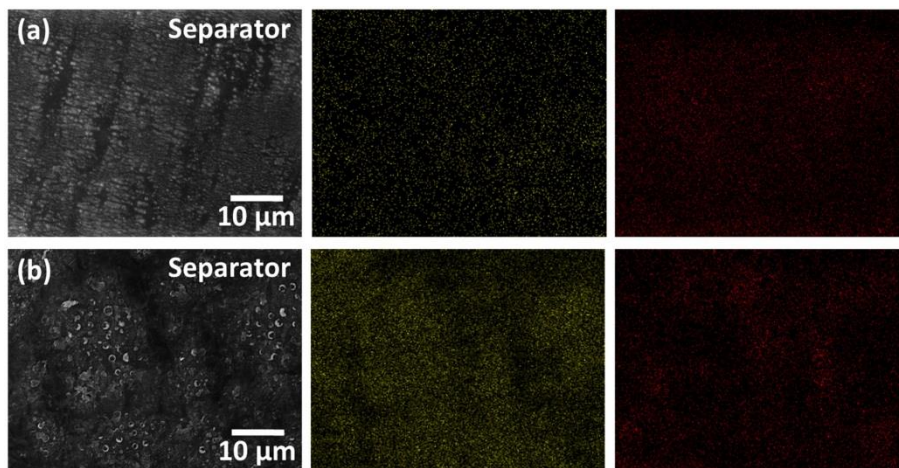
Figure 3.1.14 Elemental mapping of separators (a) NLMC-4/S50 and (b) NLMC-4/S67 cells de-crimped after 10 charge/discharge cycles.

3.1.4 Conclusions

The as-prepared NLMC-4 exhibited higher surface area of 1872 m^2 g^{-1} and large pore volume of 1.59 cc g^{-1} in comparison to other NLMC samples. The sulfur infused NLMC-4 with 50 wt% of sulfur loading delivered highest discharge capacity of 1396 mAh g^{-1} and retained 896 mAh g^{-1} after 50 cycles at 0.1 C rate. When the cells were tested at 1 C rate, the NLMC-4/S50 exhibited superior electrochemical performance and delivered a discharge capacity of 506 mAh g^{-1} in comparison to NLMC-1/S cathode (33 mAh g^{-1}) at 200th cycle. Hence, it is concluded that the micro and mesoporous carbon derived from neem leaves acts as an efficient matrix for sulfur cathode in a Li-S battery due to efficient trapping of polysulfide species into the pores of carbon.

Section 3.2 Tissue Paper-Derived Porous Graphitic Carbon Sheets as Polysulfide Inhibitor for Sulfur Cathode

In the present study, the investigator has prepared porous graphitic carbon sheet (p-GCS) from a tissue paper by a facile one-step *In-situ* chemical activation process and used as a host as well as barrier film for the sulfur cathode in a Li-S battery. The detailed synthetic process, material characterization and the electrochemical studies are discussed hereunder.

3.2.1 Synthesis of p-GCS and p-GCS/S Cathode

Synthesis of p-GCS

The chemicals used in the synthesis of p-GCS were received from Fischer Scientific and tissue papers were purchased from the local market. The synthesis of p-GCS was carried out by a facile one-step process as illustrated in the figure 3.2.1. The tissue paper and aqueous potassium hydroxide (KOH) solution were mixed in a beaker at different mass ratios of 1:0, 1:1 and 1:2. The KOH-soaked tissue paper pulp in each of the beakers was dried in an oven at 100 °C for overnight. The resulting solid mass was later heat-treated in a tubular furnace at 900 °C for one hour under argon atmosphere at a heating rate of 10 ºC per minute. After cooling to the room temperature, the black coloured powders were repeatedly washed with 1M HCl solution and 1M HF followed by DI water. The resulting samples were finally dried in an oven at 80 °C for overnight in order to obtain porous carbon material. The as-synthesized powder without KOH activation was labeled as p-TPC (pristine tissue paper carbon), and the *in-situ* activated carbon samples synthesized by using tissue paper and KOH in the mass ratios of 1:1 and 1:2 were named as p-GCS-1 and p-GCS-2, respectively.

Synthesis of Sulfur Infused p-GCS Cathode

Initially, the porous carbon (p-TPC/p-GCS-1/p-GCS-2) materials and elemental sulfur were mixed at the mass ratio of 1:3, and then a small amount (1 ml) of carbon disulfide (CS_2) solvent was added to the mixture for the homogeneous distribution of elemental sulfur. As the CS_2 solvent gets evaporated, the sulfur present in the micro and mesopores of carbon gets precipitated in the pores. The resulting samples were dried and later thoroughly mixed in a mortar. Then, the samples were heat-treated in closed alumina boats in a tubular furnace at 155 °C under argon atmosphere for 15 h. Henceforth, these three sulfur incorporated carbon materials are denoted as p-TPC/S, p-GCS-1/S and p-GCS-2/S, respectively.

The electrochemical studies of the synthesized composite samples were carried out using a two electrode system with lithium metal as the reference electrode and 1M LITFSI containing 5 wt% of $LiNO_3$ as an electrolyte. The working electrodes were prepared by using

the active material, conductive additive (super P carbon) and binder (polyvinylidene-difluoridine) in the weight ratios of 80:10:10 with N-Methyl-2 pyrrolidone (NMP) as a solvent for the slurry preparation.
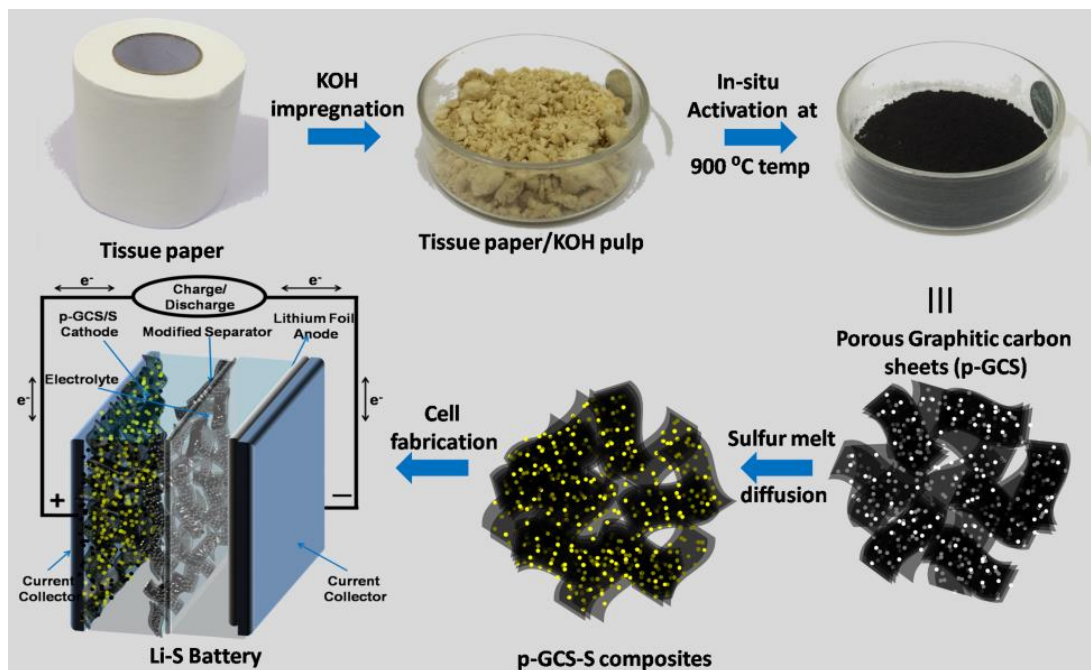
Figure 3.2.1 Schematic representation for the preparation of p-GCS/S electrode for Li-S battery application.

3.2.2 Results and Discussion: Characterization of p-GCS and p-GCS/S Cathode
3.2.2.1 Morphological Analysis:

The microstructures of the *in-situ* activated carbon samples were analyzed by using FE-SEM and HR-TEM and the images are shown in figure 3.2.2. The SEM and TEM images (figures 3.2.2a and 2.2d) of p-TPC reveal the presence of fibre like structured carbon. Whereas, the SEM images of the *in-situ* KOH activated carbons (figures 3.2.2b and 2.2c) display sheet-like structures illustrating that the KOH plays a significant role in breaking the cellulose bond of tissue paper during soaking and in the formation of carbon sheets during heat treatment process. The bright-field TEM images (figures 3.2.2e and 2.2f) show the presence of wrinkles and scrolls in the as-prepared samples indicating the typical graphitic sheet-like morphology.
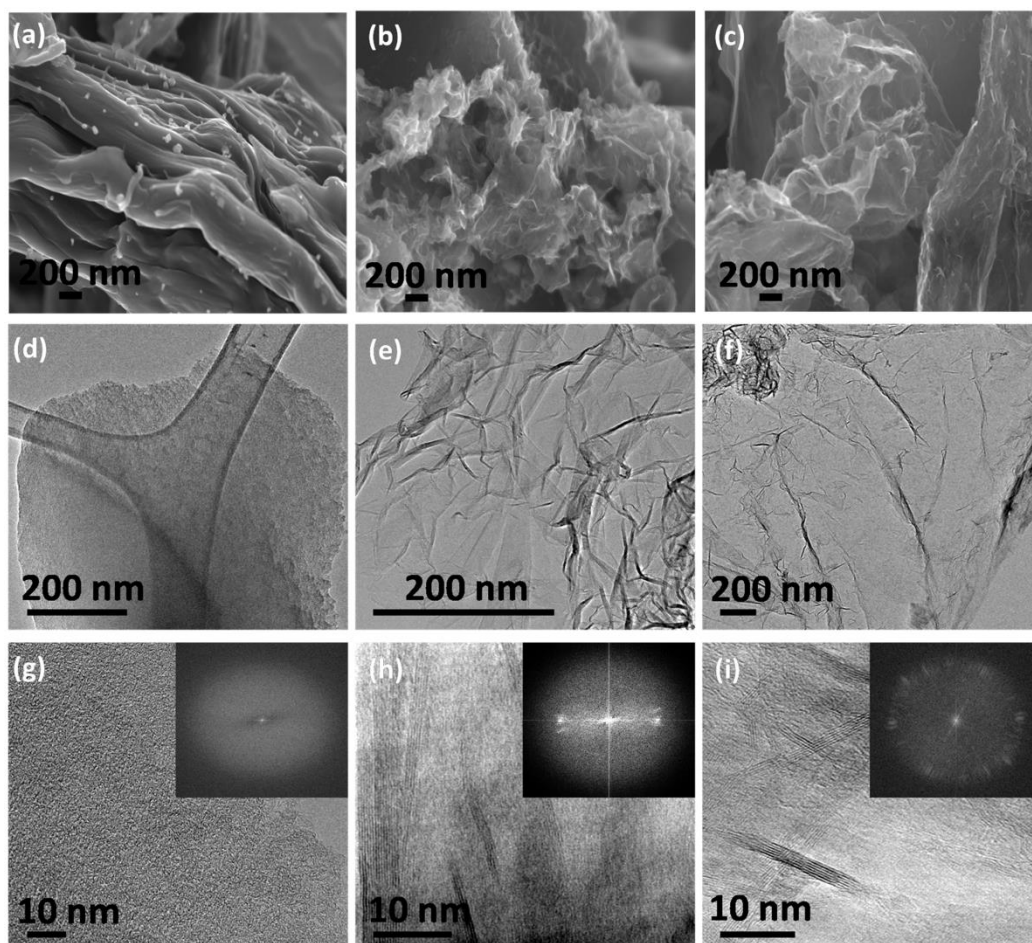
Figure 3.2.2 SEM and TEM images of p-TPC (a and d), p-GCS-1 (b and e) and p-GCS-2 (c and f), and their corresponding HR-TEM images with in-set of FFT patterns (g-i).

Furthermore, the HR-TEM images (figures 3.2.2h, 2.2i and their insets) and the corresponding fast Fourier transformations (FFT's) confirm the presence of graphene sheets with ordered carbon structures in the samples. In contrast, the HR-TEM micrograph from the p-TPC (figure 3.2.2g and the inset) and the corresponding FFT clearly indicate amorphous nature of carbon. The metrics from the FFT's inset of figures 3.2.2h and 2.2i are 0.34 nm typically corresponding to the d-values from graphitic carbon (002). This is also confirmed by the EEL spectra (figure 3.2.3). Figure 3.2.3 shows the EELS C-K edge of the p-TPC, p-GCS-1 and p-GCS-2. The C K-edge in EEL spectrum typically shows two features for the near edge fine structure. A narrow peak at around 285 eV (transition from 1s to π^* states) and a sequence of peaks, ranging from 292 eV to 310 eV (transitions from the 1s to the unoccupied σ^*) are observed in the p-GCS-1 and p-GCS-2 samples, which are characteristic of sp^2-hybridized carbon atoms. R. Raccichini et al. [35] also reported the similar type of peaks at 285 eV and 292 eV to 311 eV for multi-layered graphene grafted Fe_2O_3 particles and

assigned them to the presence of ordered graphitic structures in the sample. The shape and the intensity of the peaks fit well with those of amorphous (p-TPC) and ordered graphitic structure (p-GCS-1 and p-GCS-2), thus supporting the HRTEM and the FFT analysis. The existence of graphene-like structured carbon in *in-situ* KOH activated carbon is expected to improve the electronic and ionic conductivities during the electrochemical processes [36].
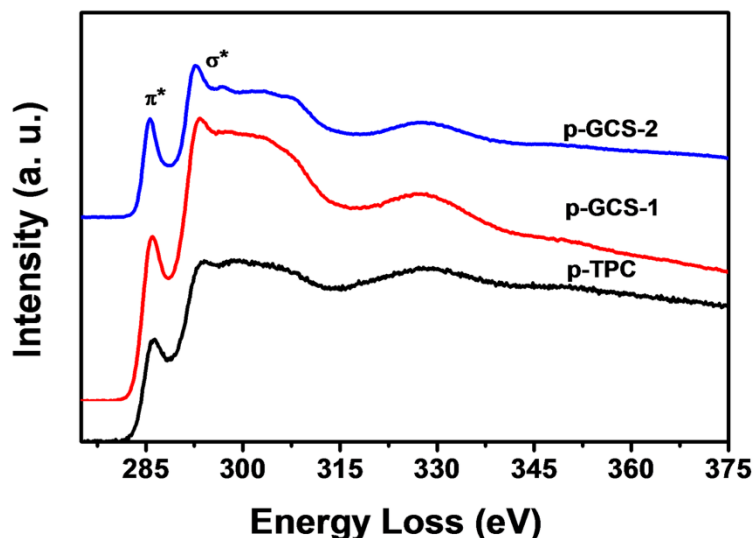
Figure 3.2.3 EELS spectra of p-TPC, p-GCS-1 and p-GCS-2.

3.2.2.2 N_2 Adsorption/Desorption Analysis:

The N_2 adsorption/desorption isotherms were recorded for as-prepared p-TPC, p-GCS-1 and p-GCS-2 in order to characterize their textural parameters and the results are shown in the figure 3.2.4. The p-GCS-1 and p-GCS-2 materials show the presence of both type I and type IV isotherms (figure 3.2.4a), which are characteristic of micro and mesoporous material [26]. Precisely, the adsorption isotherm at low relative pressure (p/p_o) indicates the presence of micropores, whereas, a hysteresis loop observed at medium relative pressure (p/p_o) reveals the formation of mesopores during the chemical activation process. The specific surface area and pore volume of p-GCS-1 and p-GCS-2 are given in the table 3.2.1. Further, the pore size distribution of these materials indicates the presence of both micro and mesoporous carbon in the *in-situ* activated carbon materials (figure 3.2.4b). In contrast, the p-TPC shows the isotherm distinct from that of the *in-situ* activated carbons, which is characteristic of the non-porous materials (type II isotherm) [37].The p-TPC exhibits very low surface area with negligible pore volume as given in the table 3.2.1. This result indicates that the *in-situ* activation of KOH increases the surface area and the total pore volume with graphene-like structured carbon. In Li-S battery, the porous morphology with graphene-like

structured carbon is expected to trap the dissolved polysulfides, in addition to improved electrical conductivity. Moreover, the porous carbon has an advantage that the electrolyte can get easily accessed into the porous structure and enhances the ionic conductivity during high current rates [29].
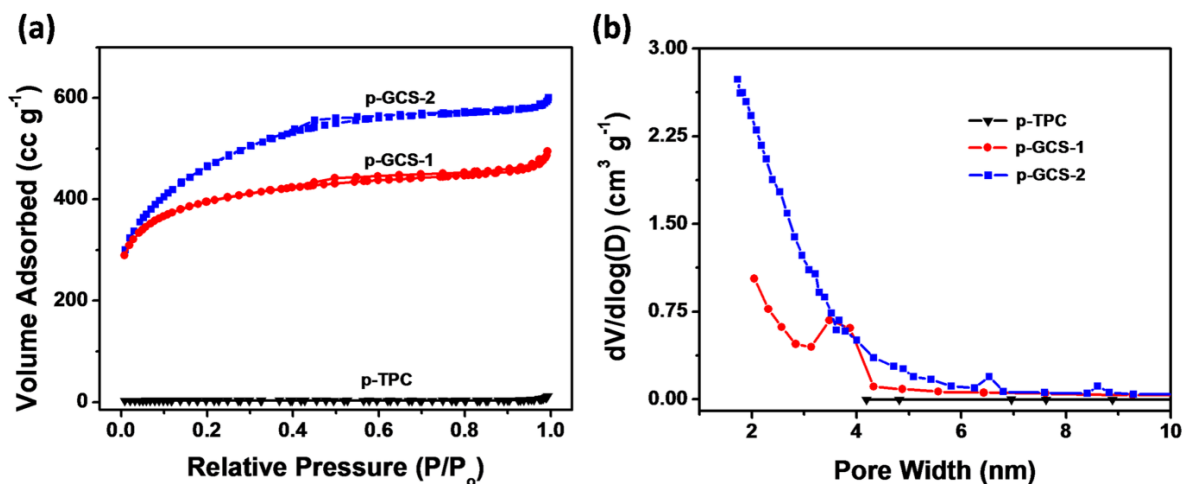
Figure 3.2.4 (a) N_2 adsorption-desorption isotherms of p-TPC, p-GCS-1 and p-GCS-2 and (b) the corresponding DFT pore size distribution curves.

Table 3.2.1   Comparison of surface area and pore size distribution of p-TPC, p-GCS-1 and p-GCS-2.

Activated carbon sample	Surface area $(m^2 \ g^{-1})$	Pore volume $(cc \ g^{-1})$
p-TPC	4	0.01
p-GCS-1	1423	0.76
p-GCS-2	1673	0.92

3.2.2.3 EDS Elemental Mapping and TG Analysis:

The sulfur incorporated p-TPC, p-GCS-1 and p-GCS-2 materials were subjected to EDS elemental mapping in order to know the distribution of sulfur in the carbon matrix. Figure 3.2.5 shows the EDS elemental map of the composite materials and the corresponding SEM images. The elemental mapping of all the composites shows the presence of sulfur and also reveals that sulfur is homogeneously distributed throughout the carbon matrix. Further, TG analysis was also carried out for these composites in order to know the amount of sulfur present in them (figure 3.2.6). The TG curves of p-TPC/S, p-GCS-1/S and p-GCS-2/S composites show a consistent weight loss from 200 ºC to 350 ºC, indicating that the rapid

weight loss is due to the decomposition of these composites. The p-GCS-1/S and p-GCS-2/S displayed a weight loss in the TG curves at higher temperature range, which corresponds to sluggish diffusion of elemental sulfur present in the micro and mesoporous structure of carbon matrix [38]. In contrast, the p-TPC/S showed the weight loss at lower temperature range indicating rapid removal of sulfur due to the non-porous nature of p-TPC. The sulfur content calculated from the TG curves for p-TPC/S, p-GCS-1/S and p-GCS-2/S are 54%, 56%, and 64%, respectively. The highest sulfur content present in p-GCS-2/S may be due to high surface to volume ratio of p-GCS-2, which helps in trapping the molten sulfur into the micro and mesopores of the carbon matrix.
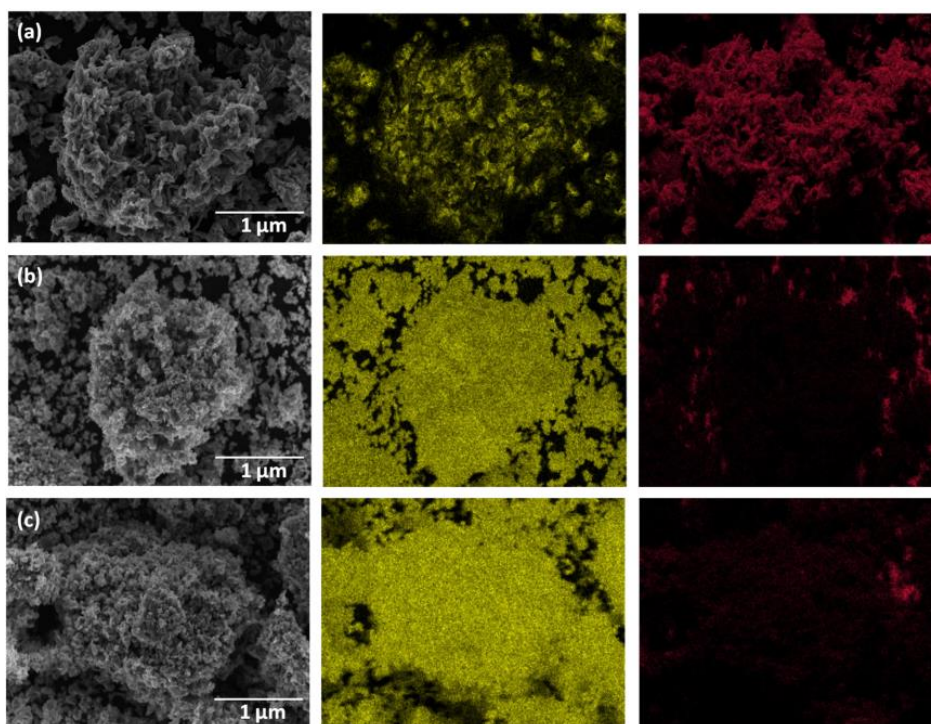
Figure 3.2.5 The SEM images of sulfur infused (a) p-TPC, (b) p-GCS-1 and (c) p-GCS-2 composite materials with the corresponding EDS elemental map of elemental sulfur (yellow) and carbon (red).
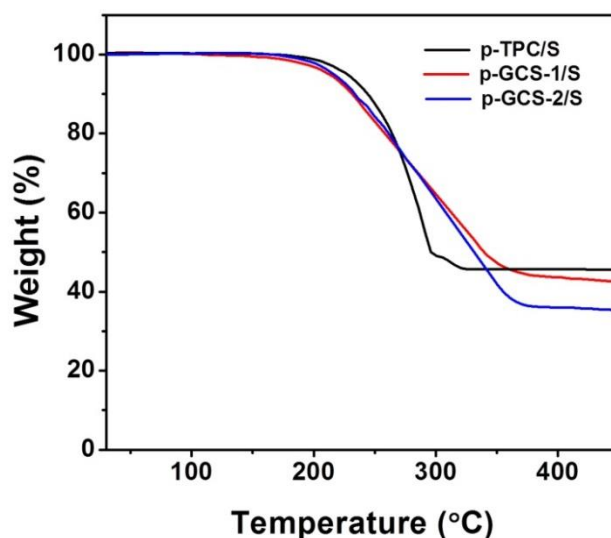
Figure 3.2.6 TG curves of sulfur infused p-TPC, p-GCS-1 and p-GCS-2 composites.

3.2.2.4 X-ray Diffraction Analysis:

The crystal structures of the as-prepared p-TPC, p-GCS-1 and p-GCS-2 were obtained by x-ray diffraction analysis and the pattern are shown in the figure 3.2.7. The XRD patterns of p-TPC shows a broad peak, which infers the disordered structure of carbon. Whereas, the XRD patterns of p-GCS-1 and p-GCS-2 samples display a narrow peak around 2θ value of 26º, which indicates the graphitic nature of carbon. The peaks at ~26º and ~44º correspond to the reflections of (002) and (100) planes of carbon [39]. However, the patterns of p-GCS-1 and p-GCS-2 samples show a small peak shift towards higher angle at (002) plane in comparison to p-TPC. This type of behavior has also been observed for KOH activated carbon and the peak shift has been interpreted due to the decrease in the interlayer distance [40]. As a result, the graphene layers stack to form nano-crystalline clusters of carbon. Sharp and well-defined peaks are observed for elemental sulfur, which indicate that sulfur exists in crystalline orthorhombic form. Moreover, the composite materials also display diffraction peaks corresponding to crystalline nature of sulfur. B. Zhang et al.[26] also reported similar type of XRD patterns for sulfur infiltered carbon material even after heat-treatment process. This is mainly due to overloading of elemental sulfur into the carbon material. Hence, most of the sulfur is distributed into the pores of carbon matrix as well as on the outer surface of carbon. However, the expected carbon peaks at ~26º and ~44º are not observed clearly in p-TPC/S, p-GCS-1/S and p-GCS-2/S due to the high intense peaks of crystalline sulfur [40]. Q. Zeng et al. [41] in their studies on carbon nanocapsules/sulfur composite also have not observed the carbon peaks in the XRD pattern. Thus, the XRD analysis has given clear evidence for the presence

of sulfur in p-GCS-1 and p-GCS-2 and also for the crystalline nature of the composite materials before and after the infusion of sulfur.
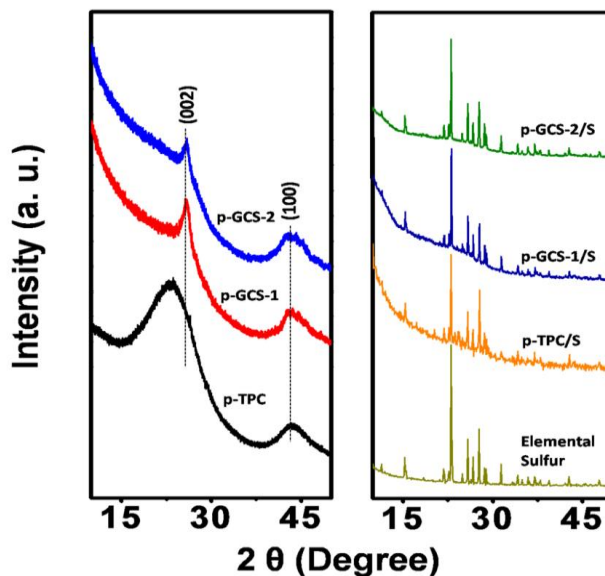
Figure 3.2.7 X-ray diffraction patterns of p-TPC, p-GCS-1, p-GCS-2, elemental sulfur and the corresponding sulfur infused composite materials.

3.2.2.5 Raman Spectral Analysis:

Raman spectroscopy has been used to analyze the type of carbon and degree of graphitization in these samples. Figure 3.2.8 shows the Raman spectra of the p-TPC, p-GCS-1 and p-GCS-2 and the sulfur infused p-GCS composite materials. The spectra of p-TPC and p-TPC/S show the D and G bands at ~1350 cm^{-1} and ~1590 cm^{-1} respectively, indicating both the crystalline and amorphous nature of carbon. Whereas, the Raman spectra for p-GCS and p-GCS/S samples display sharper D and G peaks at ~1350 cm^{-1} and ~1590 cm^{-1} respectively. Nevertheless, the intensity of the D peak is much less and the intensity of G peak is much higher in the *in-situ* activated carbon materials. This indicates more graphitic carbon in p-GCS-1 and p-GCS-2. The D peak represents the A_{1g} breathing modes of sp^2 disordered carbon, while the sharper G peak represents the E_{2g} C-C bond stretching mode of sp^2 carbon. In addition to D and G peaks, a more important peak appears at ~2700 cm^{-1}, which can be assigned to the presence of multi-layered graphene-like structures in the sample [42]. Thus, Raman spectra infer that the *in-situ* KOH activation of tissue paper plays a significant role in the formation of graphene-like structures in the carbon. These results are well consistent with the HR-TEM and EELS spectrum. The Raman spectrum of elemental sulfur exhibits a sequence of characteristic Raman peaks in the low wavenumber region, which represents the vibration mode of S-S bonds [43]. On the contrary, the p-GCS-1/S and p-GCS-2/S do not show

any peak corresponding to elemental sulfur indicating that the sulfur penetrates into pores of carbon material during the heat treatment process. Recently, F. Sun et al.[42] have reported the effect of activation temperature on the degree of graphitization in the biomass-derived chemically activated carbon material and concluded that the carbon treated at 900 ^{0}C showed higher graphitic nature in comparison to low activation temperature processes (700 ^{0}C and 800 ^{0}C). This result infers that the precursors, activating agent and activation temperature play a significant role in the crystallization of carbon. The intensity ratios of D and G peaks (I_D/I_G ratio) for p-TPC, p-GCS-1 and p-GCS-2 are 1.05, 0.23 and 0.31, respectively. The reduced I_D/I_G values suggest that the *in-situ* KOH activation increases the graphitic nature in the samples. Moreover, the intensity and profile of the 2D peak reflect the presence of multi-layer graphene-like structured carbon, which is expected to improve the electrical conductivity of the sulfur infused p-GCS composites as well as the overall electrochemical performance of the cell during charge/discharge process. It is also noted that there is a small increase in the I_D/I_G ratio for p-GCS-2 when compared to p-GCS-1 revealing that the graphitic structures are slightly destroyed with higher amount of KOH. K. G. Raj et al.[39] also observed similar trend in the activated carbon samples and reported that the higher amount of KOH suppresses the stacking order of graphitic carbon. They have also concluded that the presence of K metal catalyzes the localized graphitization of carbon at higher temperature.
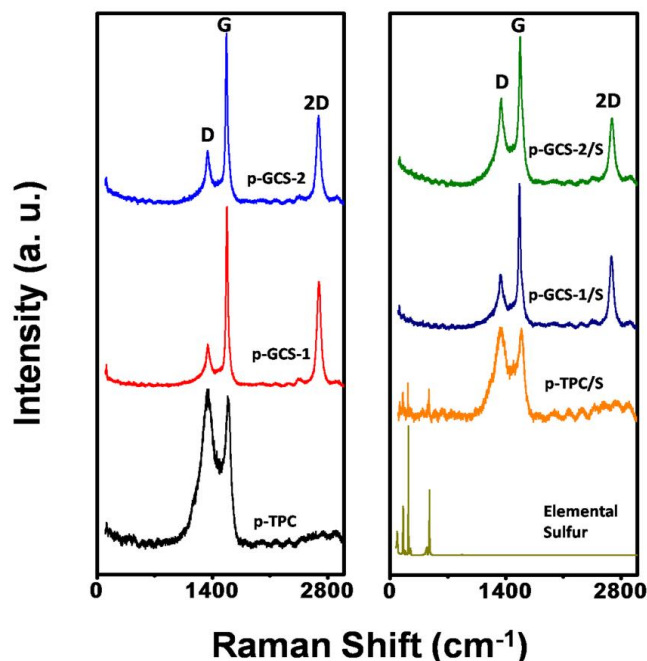
Figure 3.2.8 Raman spectra of p-TPC, p-GCS-1, p-GCS-2, elemental sulfur and sulfur infused composite materials.

3.2.2.6 X-ray Photoelectron Spectroscopic (XPS) Analysis:

XPS was carried out in order to investigate the chemical composition of the p-GCS-1/S composite. The overall survey spectrum and the computer deconvolution spectra of C1s, S2p of p-GCS-1/S are shown in the figure 3.2.9.
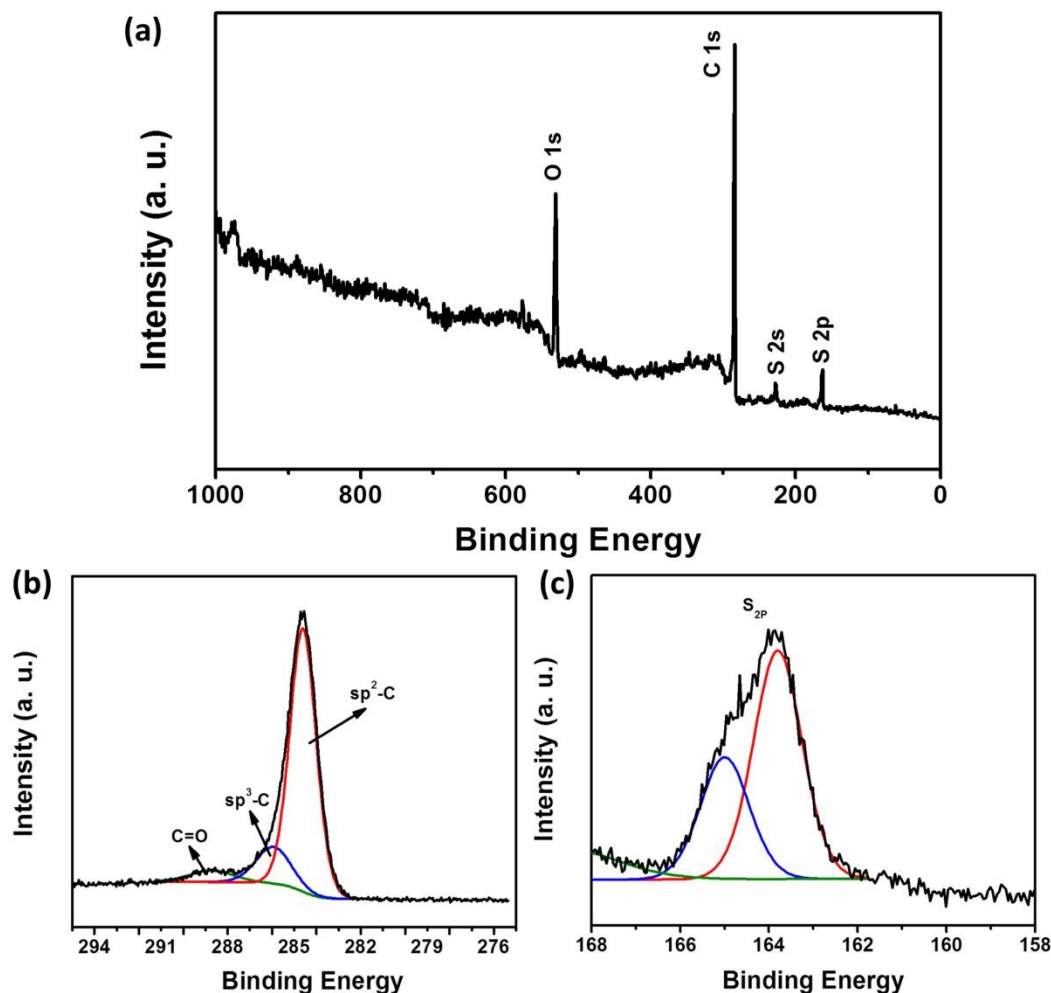
Figure 3.2.9 (a) XPS survey spectrum, and computer deconvolution spectra of (b) C1s and (c) S2p of p-GCS-1/S composite.

The survey spectrum shows the presence of C, O, S elements in the sample (figure 3.2.9a). The computer deconvolution spectrum of C1s shows three peaks at 284.6 eV, 285.9 eV, and 288.7 eV corresponding to sp^2, sp^3 and carbon in C=0, respectively (figure 3.2.9b). It is interesting to note that the C1s spectrum shows a prominent peak at 284.5 eV, which corresponds to highly graphitic nature (sp^2) of carbon. This result further supports the inference made by Raman spectra. The S 2p spectrum displays a peak at 164 eV, which is deconvoluted into two peaks at 163.9 eV and 165.0 eV, respectively as shown in the figure 3.2.9c. The binding energies of these two peaks can be assigned to spin orbital coupling of

S $2p_{3/2}$ and S $2p_{1/2}$,[44] confirming the presence of elemental sulfur in the composite. It may be noted that the characteristic elemental binding energy of sulfur is 164 eV [45]. As p-GCS-2/S is also a similar composite material with graphitic nature of carbon, in which sulfur is infused, same analysis of XPS holds good for the p-GCS-2/S composite also.

In the present study, the investigator also made an attempt to prepare the p-GCS with mass ratio of tissue paper to KOH in grams as 1:3. In this experiment, it was found that the yield of activated carbon is much lower than p-GCS-2. The reason may be that at this concentration of KOH, more carbon is oxidized to CO_2 and CO. Therefore, the studies are limited up to p-GCS-2. It may be noted that with an increase in KOH concentration, the degree of graphitization decreases due to generation of more pores in the carbon matrix.

3.2.3 Results and Discussion: Electrochemical Studies (CV, C/D, CY and EIS) of p-GCS/S Cathode

The electrochemical performance of p-GCS/S composite materials has been evaluated by cyclic voltammetry and charge/discharge profiles using lithium foil as the reference electrode. Figure 3.2.10 shows the cyclic voltammogram of p-GCS-2/S cathode for the first five cycles obtained by applying a voltage in the range of 1.5-2.8 V at a scan rate of 0.1 mV s^{-1}. In general, the redox reactions of elemental sulfur with lithium involve multi-electron transfer reactions [31]. During the cathodic scan, the composite materials show two redox peaks at 2.3 V and 2.1 V, which are characteristic of formation of the soluble long chain polysulfides (Li_2S_x, x = 4≤x≤8) and short chain precipitated polysulfides (Li_2S_2, Li_2S) due to ring opening of elemental sulfur and reduction of long chain polysulfides, respectively. These results are consistent with the those reported in the literature [46]. In the anodic scan, a single peak appears at 2.5 V, which corresponds to the oxidation of short chain polysulfides to crystalline sulfur through long chain polysulfide intermediate products. Further, it is interesting to note that there is not much change in the CV profile of p-GCS-2/S electrode in the successive cycles, indicating good electrochemical stability. It may be noted that the CV profiles of p-TPC/S and p-GCS-1/S are similar to those of p-GCS-2/S.
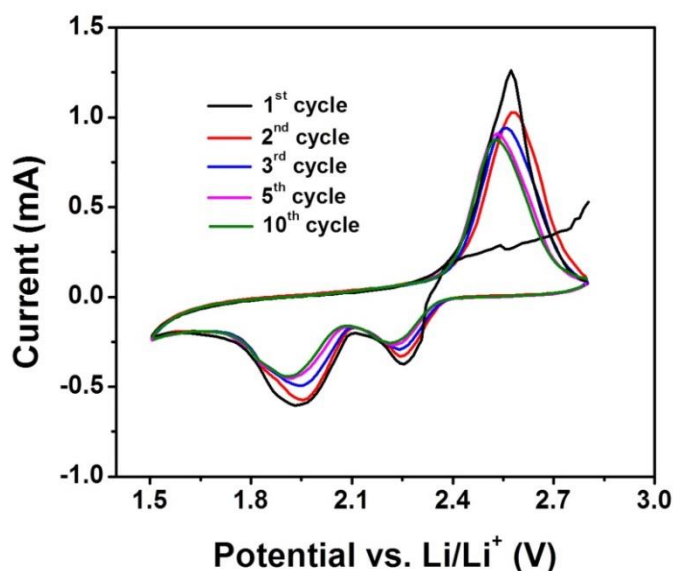
Figure 3.2.10 CV profile of p-GCS-2/S cathode obtained at a scan rate of 0.1 mV s^{-1}.

Figure 3.2.11a shows the galvanostatic charge/discharge profiles of sulfur infused p-TPC/S, p-GCS-1/S and p-GCS-2/S composite materials measured at 0.1C rate. The discharge curve of all the samples represents a typical two-step curve indicating the reduction of sulfur involved in a series of electron transfer reactions [9]. Whereas, the flat curve in the charging process corresponds to a reversible conversion of lithium polysulfides to elemental sulfur, which is in agreement with the results of CV studies. The charge and discharge capacities calculated from the charge/discharge profiles of p-TPC/S, p-GCS-1/S and p-GCS-2/S composite materials are 586 mAh g^{-1} & 639 mAh g^{-1}, 1263 mAh g^{-1}& 1446 mAh g^{-1} and 1312 mAh g^{-1}& 1497 mAh g^{-1}, respectively. The cyclic stability curves of these composite materials measured at 0.1 C rate are shown in figure 3.2.11b. Though a decrease in discharge capacity is observed in the initial cycles owing to polysulfide dissolution, the discharge capacity gets stabilized in the later cycles as most of the polysulfide species are trapped in the mesoporous carbon matrix. The p-GCS-1/S and p-GCS-2/S composite materials delivered high discharge capacities of 759 mAh g^{-1} and 821 mAhg^{-1}, respectively, even after 40 cycles. However, p-TPC/S delivered a low discharge capacity of 33 mAh g^{-1} only at 40th cycle. The superior electrochemical performance of the sulfur infused p-GCS/S materials may be due to improved ionic and electrical conductivities, which are further discussed in detail in the successive EIS section. The poor electrochemical performance of p-TPC/S is mainly due to the low graphitic nature of carbon that decreases the electronic conductivity and limited porous structures that lead to polysulfide shuttle phenomenon. X. Liang et al.[47] compared the electrochemical performance of the sulfur infused ordered mesoporous carbon (OMC) and

pristine sulfur cathodes. They have observed that the OMC/S cathode exhibited superior performance, whereas, the pristine sulfur cathode delivered poor cycle performance. The enhanced electrochemical performance of OMC/S is mainly due to large surface area of OMC, which inhibits the dissolution of polysulfide species into the electrolyte. Moreover, the uniform distribution of sulfur into the nanopores can successfully elevate the volume expansion created during the lithiation process. Results of the present study inferred that p-GCS/S material showed superior electrochemical performance in terms of high specific capacity and cyclic stability in comparison with p-TPC/S.
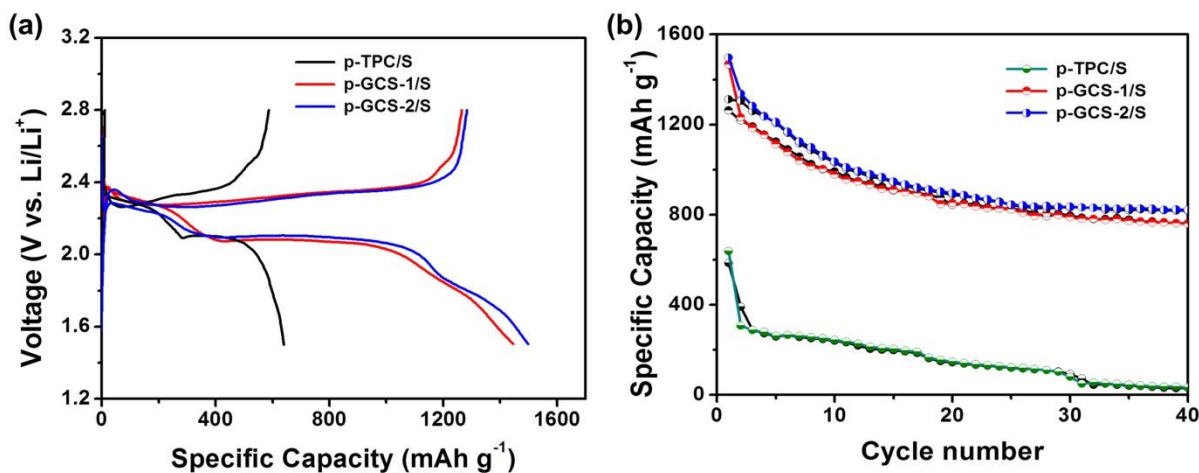
Figure 3.2.11 (a) Charge/discharge and (b) cycle performance curves of p-TPC/S, p-GCS-1/S and p-GCS-2/S composite materials measured at 0.1 C rate.

Figure 3.2.12 shows the comparative Nyquist plots for the p-TPC/S, p-GCS-1/S and p-GCS-2/S composite materials measured before electrochemical cycling. The plots in case of all these samples show depressed semicircle in the mid frequency region, which corresponds to charge transfer region at the electrode-electrolyte interface. An inclined line is also observed in all the plots in the low frequency region, which corresponds to the Warburg impedance. This is associated with the diffusion of lithium ions within the sulfur cathode. The experimental results are fitted well with the equivalent circuit shown in the in-set of figure 3.2.12. The p-GCS-1/S and p-GCS-2/S cathodes exhibits lower R_{ct} values of 39.5 Ω and 35.3 Ω respectively in comparison with pristine p-TPC/S, which has an R_{ct} value of 105.2 Ω. These results demonstrate that the p-GCS materials with hierarchical porous structured carbon can effectively reduce the charge transfer resistance of the cell. F. Wu et al.[48] observed an improved charge transfer process for polythiophene-coated sulfur cathode in comparison to pristine sulfur due to enhanced conductivity of the electrode. X. Liang et al.[47] studied the electrochemical performance of sulfur infused ordered mesoporous carbon (OMC) and

pristine sulfur cathodes. They have reported that the pristine sulfur electrode exhibited higher R_{ct}, whereas, the OMC/S electrode displayed much lower R_{ct} due to improved interfacial compatibility with the electrolyte. The results of the present study infer that the sulfur infusion into p-GCS with homogenous distribution can effectively enhance the charge transfer process and thus the resulting cell displayed an enhanced electrochemical performance.
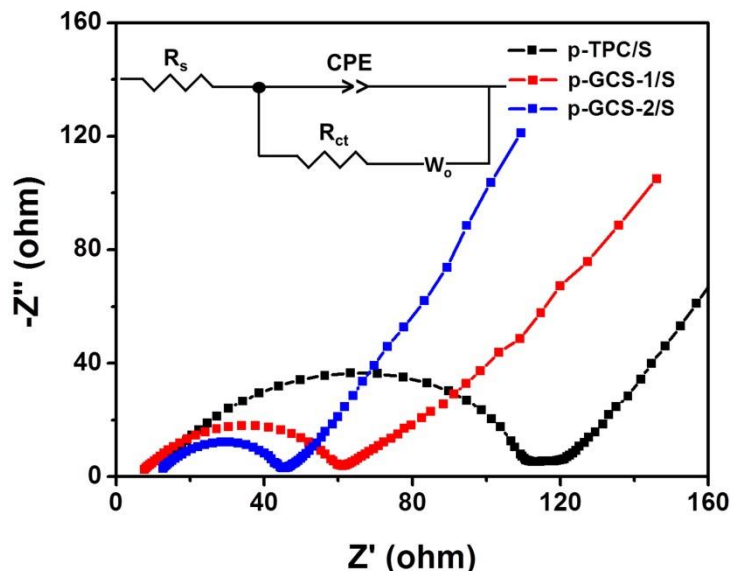
Figure 3.2.12 Nyquist plot of sulfur infused p-TPC, p-GCS-1, p-GCS-2 composites.

The sulfur infused p-GCS-2 cathode exhibited high initial discharge capacity, which is attributed to high surface area and excellent graphitic nature that enhances the electrical conductivity of sulfur cathode. However, the polysulfide dissolution into the electrolyte cannot be prevented during repeated charge/discharge cycles. It has been reported in the literature that an increased amount of sulfur loading in the composites resulted in decreased discharge capacities during prolonged cycling [34]. The reason for the decay in the discharge capacity is attributed to the deposition of excess sulfur on the surface of porous carbon material, which may block the pores or reduce the pore volume that resulted in decrease of the lithium ion uptake and electron transport pathways. Therefore, the cell experiences reduced electrochemical performance due to disintegration of active material from the cathode and migration of the dissolved polysulfide species to the anode. Furthermore, the electrochemical performance of the p-GCS-2/S cathode was studied with modified separator in order to enhance the electrochemical performance of the cell. The modified separator is prepared by coating the as-prepared p-GCS-2 on to the polypropylene separator. Figure 3.2.13 shows the charge/discharge and cycle performance curves of the p-GCS-2/S electrode measured at 0.1 C rate. Initially, the p-GCS-2/S cathode delivered high discharge and charge capacities of

1633 mAh g^{-1} and 1458 mAh g^{-1}, respectively, which are higher in comparison to the charge and discharge capacities obtained for the p-GCS-2/S with pristine polypropylene separator. The improved electrochemical performance of p-GCS-2/S with modified separator is mainly due to the formation of sandwich-type structure, in which highly conductive carbon increases the utilization of sulfur to a maximum. Further, the electrode also exhibited an improved performance at a current rate of 0.2 C and retained a high discharge capacity of 992 mAh g^{-1} even after 50 cycles. These results indicate that the p-GCS coated separators play an important role in enhancing the electrochemical performance of the sulfur infused p-GCS composites. Moreover, the p-GCS on the separator inhibits the dissolution of dissolved polysulfides into the electrolyte and increases the reutilization of active material during cycling. J. Wang et al. [49] used electrospun activated carbon nanofiber interlayer (ACNF) for sulfur cathode. The high porous structure of ACNF helped in inhibiting the migration of the dissolved polysulfide from the cathode to the anode surface and the continuous 3D network rendered fast electron conduction during redox process. X. Wang et al. [50] also prepared carbon particles-anchored reduced graphene oxide film as a barrier for sulfur cathode and achieved an improved electrochemical performance. The presence of functional groups on the RGO anchors the soluble polysulfides in it and the carbon particles provide channels for the electrolyte penetration and also improve the electrical conductivity.

The long-term cycle performance test was also conducted for the p-GCS-2/S electrode with pristine and modified separators at a high current rate of 1 C for 200 cycles (figure 3.2.13c). Interestingly, the p-GCS-2/S electrode with modified separator displayed higher discharge capacity of 652 mAh g^{-1}, even after 200 cycles with good coulombic efficiency. The superior electrochemical performance of this electrode is attributed to high surface area, large pore volume and good electrical conductivity of the as-prepared p-GCS-2 sample that acts as an efficient matrix as well as an interlayer for sulfur cathode.
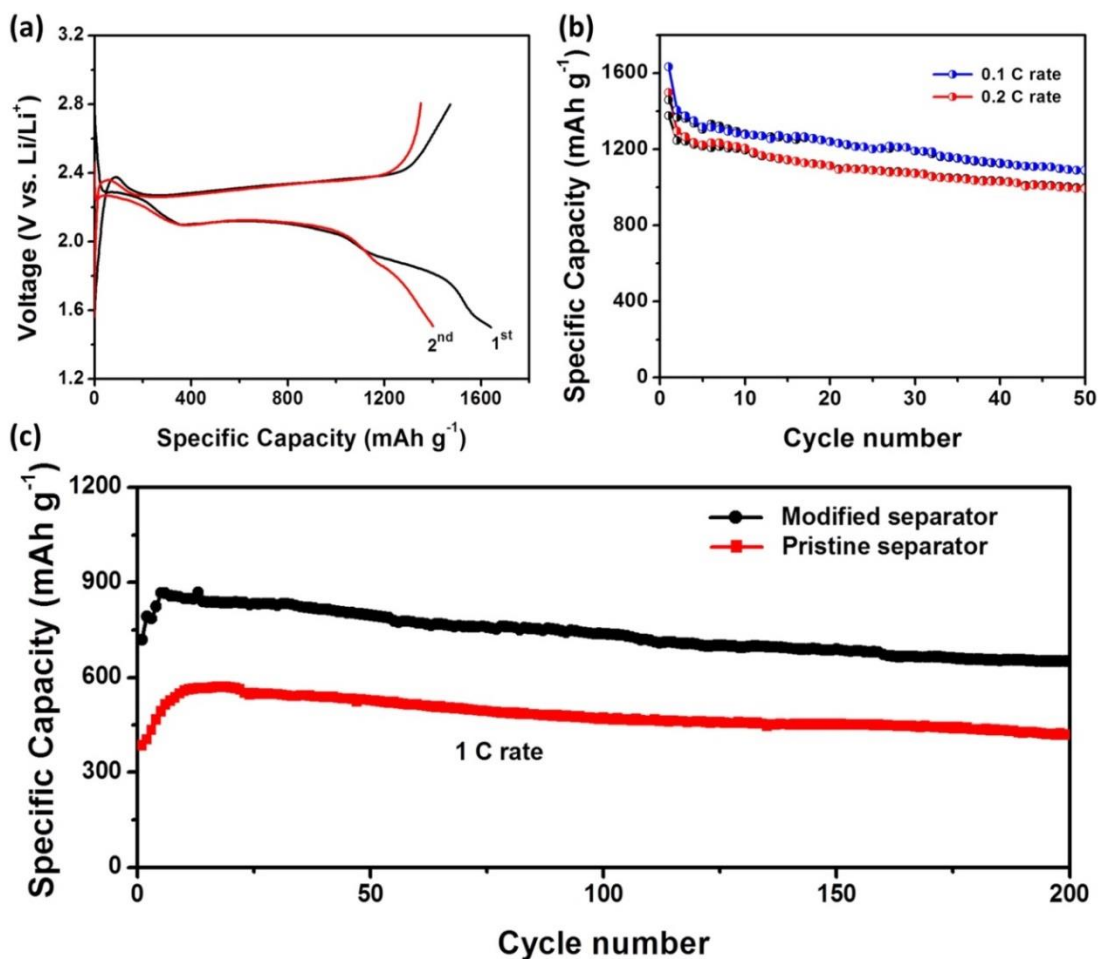
Figure 3.2.13 (a) and (b) are the charge/discharge and cycle performance curves of p-GCS-2/S electrode with modified separator measured at 0.2 C rate, and (c) comparative long-term cycle performance tests at 1 C rate.

Li-S cells fabricated using p-GCS-2/S cathode with modified separator and lithium metal anode, have been used in order to demonstrate their functioning for the lightening of LED (figure 3.2.14). Two such cells are connected in series to give an output voltage of ~4.2 V in order to lighten 40 LEDs connected in parallel. The *in-situ* activated carbon prepared from tissue paper with tunable pore structure and unique graphitic nature exhibited promising electrochemical performance for Li-S battery application and was successfully used for powering the small electronic component. Hence, p-GCS is considered to be the potential carbon matrix for high energy density Li-S battery. Moreover, a straight forward and facile methodology to synthesize p-GCS makes it feasible for large scale production.
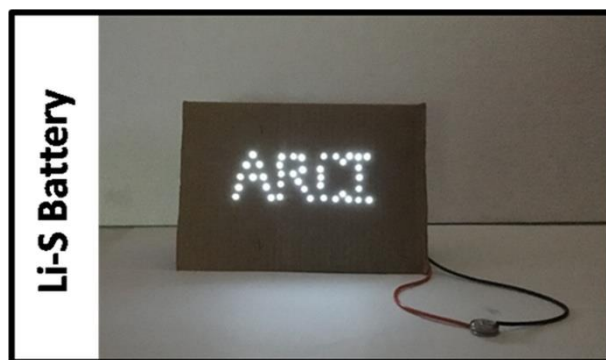
Figure 3.2.14 Photo image of LED lights with two Li-S batteries connected in series.

3.2.4 Conclusions

The investigator successfully adopted a facile one-step process to synthesize porous p-GCS from tissue paper. Characterization of p-GCS materials confirms the presence of graphene-like structured carbon with excellent textural parameters. The p-GCS-2/S electrode with modified separator delivered a high initial discharge capacity of 1633 mAh g^{-1} at 0.2 C rate. Even at a high charge/discharge rate of 1 C, the electrode delivered excellent discharge capacity of 652 mAh g^{-1} after 200 cycles with good coulombic efficiency. These results confirm that the p-GCS functions as an efficient host as well as an interlayer for sulfur cathode by constraining the dissolved polysulfides in it and also improves the ionic and electronic conductivities during the redox process.

Section 3.3 Jute Stalks-Derived Micro and Mesoporous Carbon as an Efficient Polysulfide Inhibitor for Sulfur Cathode

It is well understood from the above sections (3.1 and 3.2) and from the literature (section 1.1.2) that activated carbons with high surface area and large pore volume facilitate higher amount of sulfur loading into carbon matrix, which enhances the electrochemical performance of the sulfur cathode. Therefore, the investigator has also explored a two-step chemical activation process for the synthesis of micro and mesoporous graphitic carbon sheets (MGC) from jute stalks (Corchorus Olitroius). The as-prepared activated carbon is used as matrix as well as barrier film (modified separator) to evaluate the electrochemical performance of the sulfur cathode in a Li-S battery. The synthetic process, characterization and the electrochemical studies of the sulfur infused MGC cathode are discussed hereunder.

3.3.1 Synthesis of MGC and Sulfur Infused MGC Cathode

Synthesis of MGC

The Jute stalks were received from the local farm land and thoroughly washed with deionised water and then dried in an oven at 80 ºC. The dried stalks were crushed into fine powder and pre-carbonized at 350 ºC in argon atmosphere for 2 h at a heating rate of 5 ºC per minute. The pre-carbonized powder of 5g was mixed with 25 ml of aqueous KOH in a beaker thoroughly with mass ratio of pre-carbonised jute stalk powder to KOH as 1:4 and kept in an oven at 100 ºC for overnight. The obtained solid was heat-treated at 1000 ºC in a tubular furnace at a heating rate of 5 ºC per minute under argon atmosphere for 1 h. After cooling down to room temperature, the resulting black powder was repeatedly washed with 1M HCl followed by DI water and finally dried in an oven at 100 ºC for overnight. Henceforth, the as-synthesized KOH activated jute stalks powder is named as micro and mesoporous graphitic carbon sheets (MGC).

Synthesis of Sulfur Infused MGC Cathode

The sulfur infused MGC composite material was synthesized by using the as-prepared MGC and sulfur powder of laboratory reagent grade as shown in the figure 3.3.1. The surface area and pore volume of MGC are found to be much higher than those of the NLMC and p-GCS. Therefore, it was thought of studying the electrochemical performance of MGC/S cathode with relatively higher loading. In the present study, the amount of sulfur loading into the MGC was varied in the mass ratio of sulfur to MGC as 1.5:1, 3.0:1 and 5.5:1. In each of the three samples, 0.5 g of MGC, required amount of sulfur as per the mass ratio and 1ml of carbon disulfide (CS_2) were mixed thoroughly for homogenous distribution of sulfur into the

carbon matrix. The resulting powders were then dried at room temperature. As the solvent evaporates, the sulfur gets precipitated into the micro and mesopores of carbon matrix. Later, these samples were thoroughly mixed in a mortar and heat treated in alumina crucible at 155 ºC for 10 h under argon atmosphere. After cooling down to room temperature, the sulfur infused MGC composites were obtained. The composites with different amounts of sulfur loading in the mass ratio of sulfur to MGC as 1.5:1, 3.0:1 and 5.5:1 are denoted as MGC/S-1, MGC/S-2 and MGC/S-3 respectively.
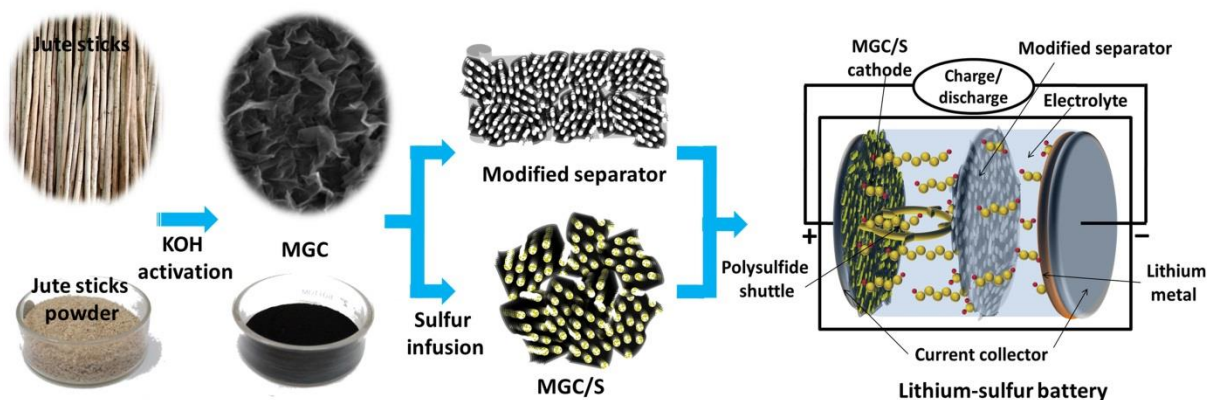
Figure 3.3.1 Schematic illustration for the synthesis of MGC, modified separator and Li-S cell fabrication.

The electrochemical performance of sulfur infused MGC samples was evaluated by using lithium foil as the reference electrode and 1M LITFSI with 5 wt% $LiNO_3$ as the electrolyte in 2032 coin cells. The working electrode (cathode) was prepared by mixing sulfur infused MGC samples, conductive additive (super P carbon) and binder (polyvinylidene-difluoridine) in the weight ratios of 80:10:10 with N-Methyl-2 pyrrolidone (NMP) as the solvent. Further, the modified separator is prepared by coating a thin layer of as-prepared MGC dispersed in PVDF/NMP solvent on polypropylene separator.

3.3.2 Results and Discussion: Characterization of MGC and MGC/S

3.3.2.1 Morphological Analysis:

The surface morphology of the as-prepared MGC and sulfur infused MGC has been studied using FE-SEM and TEM, which are shown in the figures 3.3.2 and 3.3.3. The FE-SEM of the as-prepared MGC and sulfur infused MGC/S display a thin sheet-like structured carbon (figures 3.3.2a-3.2d). This type of structures has an advantage of improving the electrode wetability and causing fast ion movement. Further, the bright field TEM images (figures 3.3.3a-3.3d) show the presence of wrinkles and scroll in the samples, which indicate the typical graphene sheet-like morphology. In addition, the HR-TEM images shown in the

figures 3.3.3e-h infer the presence of graphene-like structures with highly ordered carbon in the samples. The existence of graphene sheet-like structures in the samples may improve the electrode reaction kinetics during fast charge/discharge process [51].
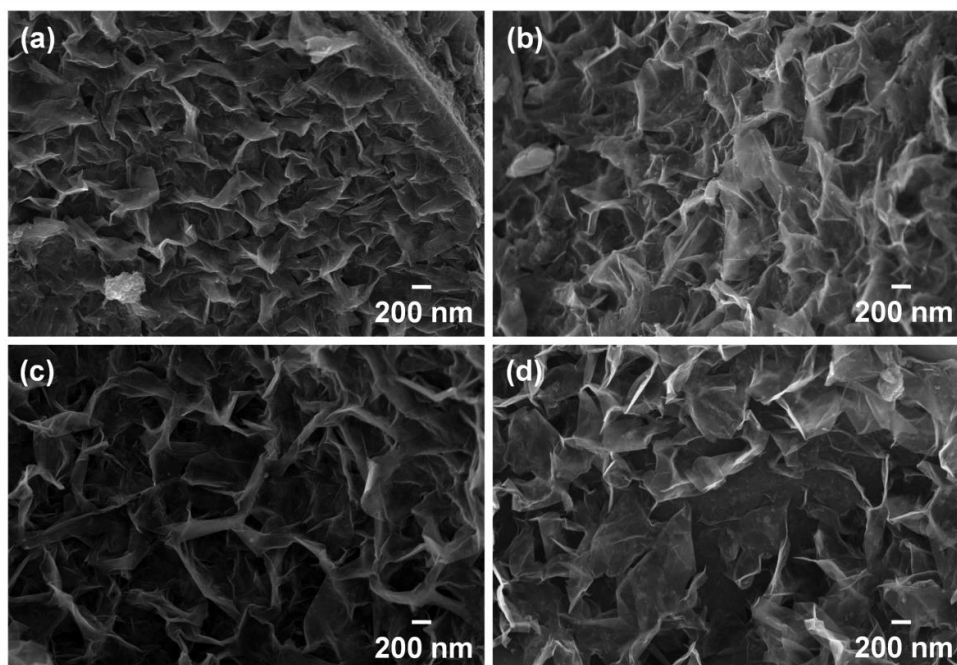
Figure 3.3.2 FE-SEM images (a) as-prepared MGC, (b) MGC/S-1, (c) MGC/S-2, and (d) MGC/S-3.
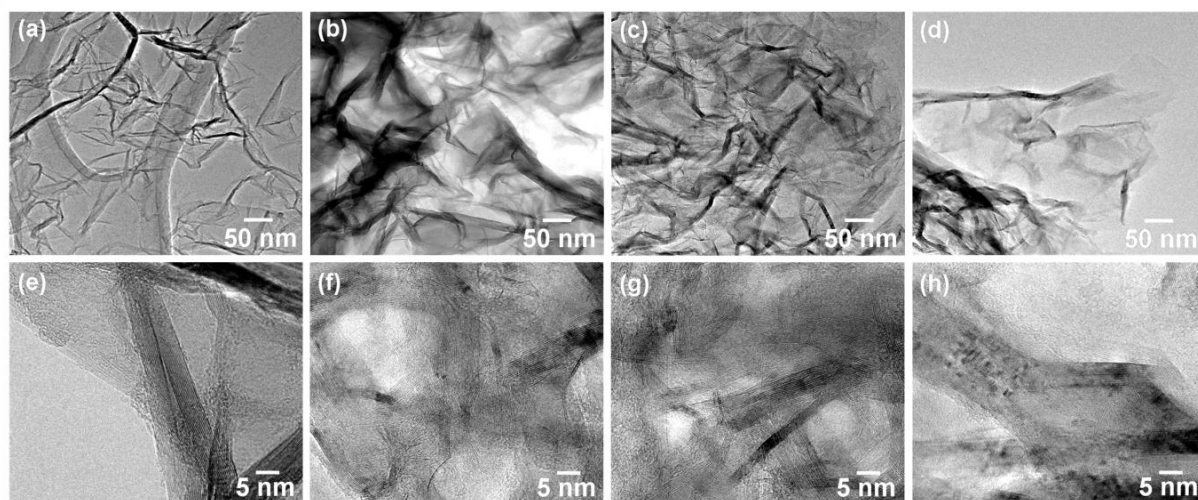
Figure 3.3.3 TEM images (a) as-prepared MGC, (b) MGC/S-1, (c) MGC/S-2 and (d) MGC/S-3 and the corresponding HR-TEM images (e-h), respectively.

3.3.2.2 N$_2$ Adsorption/Desorption Analysis:

N$_2$ adsorption/desorption isotherms have been recorded in order to characterize the textural parameters of the as-prepared MGC, MGC/S-1, MGC/S-2 and MGC/S-3 (figure

3.3.4a). The as-prepared MGC displays typical adsorption isotherm, containing the features of both type I and type IV isotherms. This result reveals the presence of both micropores and mesopores in the sample [52]. In particular, the adsorption at low relative pressure (P/P_o~0) suggests the presence of micropores, whereas, a hysteresis loop in the moderate relative pressures (P/P_o~0.4) indicates the existence and formation of mesoporous structures during the chemical activation process. It can be seen from the table 3.3.1 that the as-prepared MGC exhibits high surface area with a large pore volume. This result infers that the addition of KOH induces significant fraction of micro and mesopores in the activated carbon. After the sulfur infusion into the as-prepared MGC, the surface area decreases due to filling of elemental sulfur throughout the micro and mesopores of carbon. It can also be observed from the figure 3.3.4a that MGC-S/1 displays an isotherm similar to type IV with the existence of mesopores in the sample even after sulfur infiltration. However, with a further increase in the sulfur loading into MGC, the surface area decreases and the resulting samples show characteristic type II isotherms as observed in the case of MGC/S-2 and MGC/S-3. G. Xu et al.[53] also observed the similar trend after the sulfur infusion into hierarchically porous carbon nanoplates (HPCN). They have concluded that the decrease in specific surface area is due to penetration of molten sulfur into the voids of HPCN by capillary forces and gets solidified in it during the cooling process. As a result, the sample exhibited type II isotherm with non-porous nature. Consequently, the pore volume also decreases with an increase in sulfur loading as observed in the present study (figure 3.3.4b). Thus, the MGC/S-1, MGC/S-2 and MGC/S-3 exhibited low pore volume as shown in the Table 3.3.1. This is indirect evidence that the pores are completely filled with elemental sulfur during the melt-diffusion process. It is expected that the thin graphene sheet-like structured morphology with high surface area helps in trapping the dissolved polysulfide species in the carbon matrix during the electrochemical process.
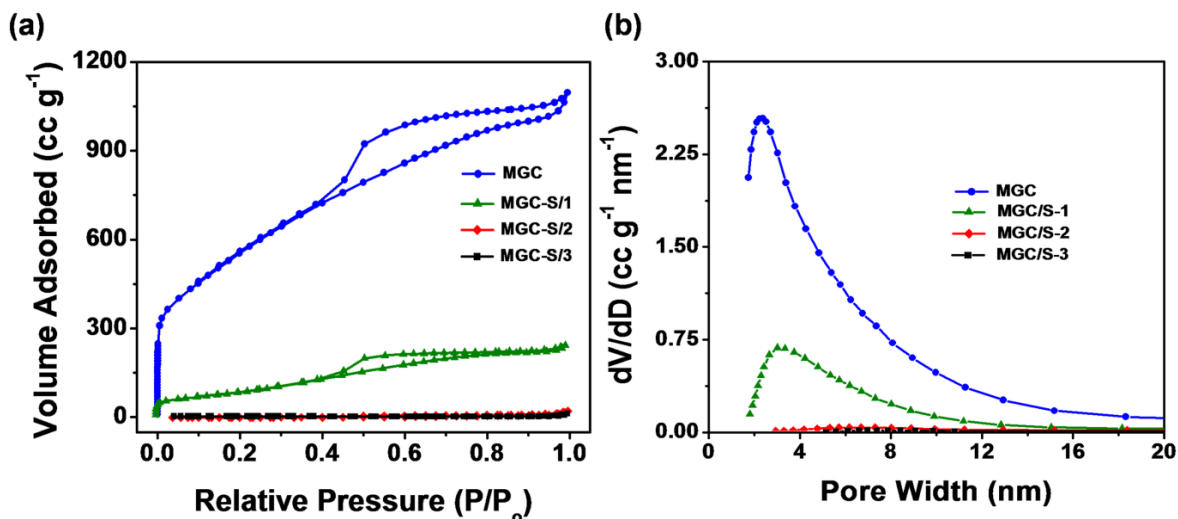
Figure 3.3.4 (a) N$_2$ adsorption/desorption isotherms and (b) corresponding pore size distribution curves of MGC/S-1, MGC/S-2 and MGC/S-3.

Table 3.3.1   Comparison of surface area and pore size distribution of the as-prepared MGC and sulfur infused MGC composites.

Activated carbon sample	Surface area ($m^2\ g^{-1}$)	Pore volume ($cc\ g^{-1}$)
As-prepared MGC	2047.4	1.69
MGC/S-1	317.8	0.37
MGC/S-2	8.9	0.03
MGC/S-3	0.1	0.01

3.3.2.3 EDS Elemental Mapping and TG Analysis:

In order to study the distribution of elemental sulfur in MGC/S-1, MGC/S-2 and MGC/S-3, all the samples have been subjected to EDS elemental mapping and the elemental maps of carbon and sulfur are shown in the figure 3.3.5. It can be observed that sulfur is homogenously distributed throughout the MGC matrix. Further, the sulfur infused MGC samples have also been subjected to thermogravimetric analysis in order to study the amount of sulfur present in them. Figure 3.3.6 shows the TG curves of MGC/S-1, MGC/S-2 and MGC/S-3 recorded under the argon atmosphere. All the samples show a continuous weight loss in the temperature range of 200 ºC to 450 ºC, which corresponds to the evaporation of elemental sulfur. J. Guo et al. [9] also observed the weight loss in the temperature range of about 200 ºC to 520 ºC for the sulfur infiltered porous carbon nanosheets. This phenomenon is

due to slow weight loss of the elemental sulfur confined in the micropores, which requires more driving force to overcome the capillary forces and hence the weight loss occurs at higher temperature. The amounts of sulfur present in the samples that are calculated from the TG analysis are 48%, 64% and 76% for MGC/S-1, MGC/S-2 and MGC/S-3, respectively.
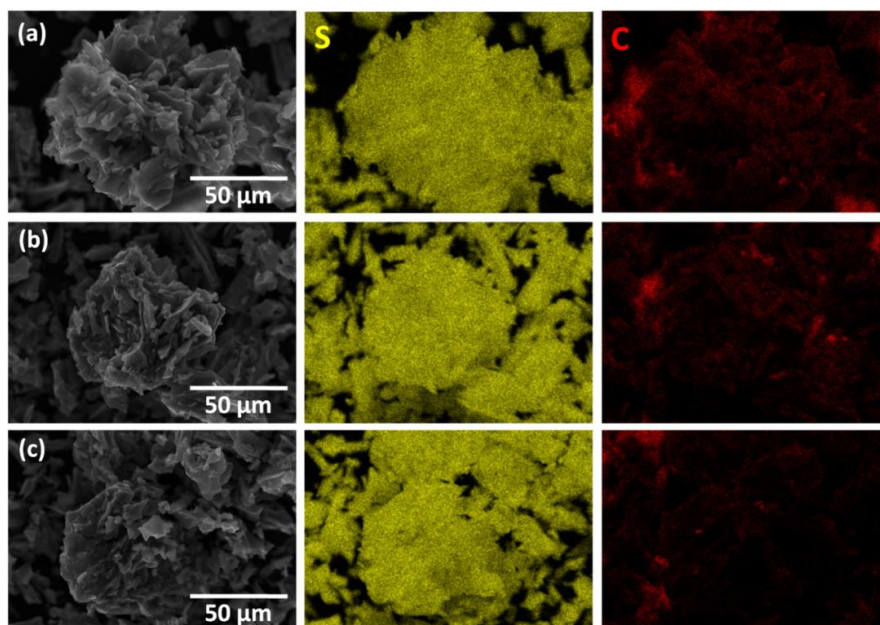
Figure 3.3.5 EDS elemental map of MGC/S-1 (a), MGC/S-2 (b) and MGC/S-3 (c) with sulfur (yellow) and carbon (red).
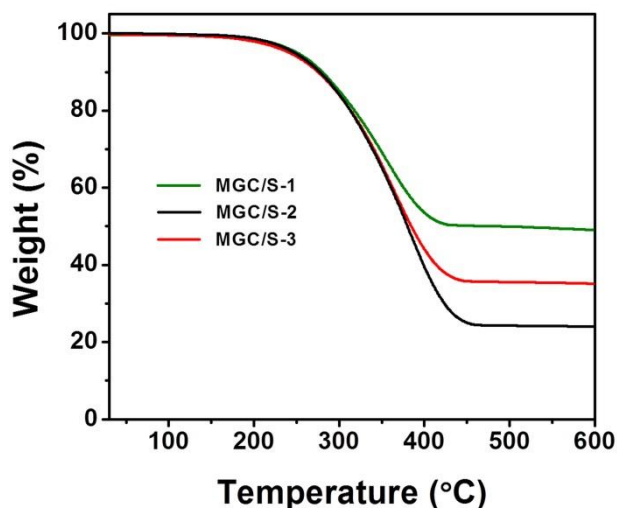
Figure 3.3.6 Thermogravimetric curves of MGC/S-1, MGC/S-2 and MGC/S-3 composites.

3.3.2.4 Raman Spectral Analysis:

The MGC and the sulfur infused MGC samples have been subjected to analysis by Raman spectroscopy in order to study the type of carbon present in the samples (Figure 3.3.7). The Raman spectrum of the as-prepared MGC shows a sharp peaks at 1342 cm^{-1}, which is

attributed to the D band that arises from the A_{1g} mode of disordered carbon and also a peak at 1587 cm^{-1}, which is assigned to the G band, that represents the E_{2g} mode of ordered carbon [54]. The intensity ratio of I_D/I_G is 0.63, which indicates the presence of more graphitic structures in the sample. Moreover, an additional peak at 2700 cm^{-1} is observed in the as-prepared MGC, which is attributed to the presence of multi-layered graphene in the sample. This inference supports the HR-TEM images showing multi-layered graphene-like structure. F. Sun et al.[42] reported that the degree of graphitization increases with an increase in temperature. At 900 ºC, the KOH activated sample displays a prominent peak at 2700 cm^{-1} in addition to the peaks at 1350 cm^{-1} and 1600 cm^{-1}, which corresponds to the presence of multi-layered graphene-like structures in the sample. The Raman spectrum of pure sulfur shows a sequence of characteristic peaks at low wavenumber region of <520 cm^{-1}, that can be assigned to vibration modes of sulfur atoms [22]. The MGC/S-1, MGC/S-2 and MGC/S-3 samples also show a similar type of Raman scattering that corresponds to the carbon atoms of the as-prepared MGC. However, the characteristic peak of sulfur is not detected in these samples. That means, the elemental sulfur is completely penetrated into the pores during the heat treatment process [9]. This phenomenon is in accordance with the BET isotherms and inference from the pore volume data. The presence of graphene-like structures with high surface area in the sample can help in overcoming the insulating behaviour of sulfur cathode as well as trapping the dissolved polysulfide species in it.
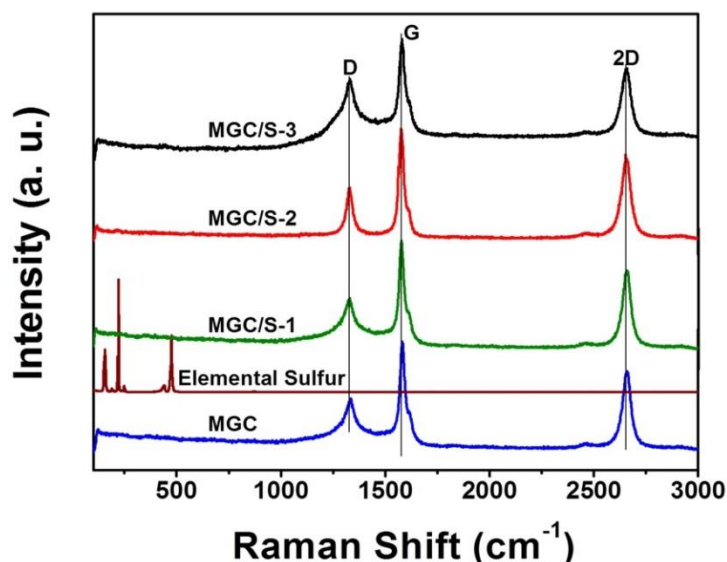
Figure 3.3.7 Raman spectra of the as-prepared MGC, elemental sulfur, MGC/S-1, MGC/S-2 and MGC/S-3.

3.3.3 Results and Discussion: Electrochemical Studies (CV, C/D, CY and EIS) of MGC/S Cathode

The electrochemical performance of sulfur infused MGC has been evaluated with pristine polypropylene separator using a lithium foil as the reference electrode. Figure 3.3.8a shows the initial charge/discharge curves of MGC/S-1, MGC/S-2 and MGC/S-3 electrodes obtained between 1.5-2.8 V at a current rate of 0.2 C. The thickness of the samples of MGC/S-1, MGC/S-2 and MGC/S-3 was so adjusted that the sulfur loading in each of these samples is approximately equal to 2 mg cm^{-2}. All the samples display a two-stepped discharge plateau, which indicates the multi-electron transfer reaction of the elemental sulfur with lithium [55]. Whereas, the flat profile in the charging process represents the reversible conversion of lithium polysulfide species to sulfur. The specific discharge capacities calculated from the charge/discharge curves of MGC/S-1, MGC/S-2 and MGC/S-3 are 1476 mAh g^{-1}, 1227 mAh g^{-1} and 962 mAh g^{-1}, respectively. The initial high discharge capacity exhibited by MGC/S-1 is mainly due to homogenous distribution of sulfur throughout the carbon matrix. Moreover, the minimum sulfur loading into the conductive host improves the active material utilization more efficiently. However, with an increase in the amount of sulfur loading into MGC there is a decrease in the specific capacity during the redox process [34]. This behaviour is mainly due to excessive deposition of elemental sulfur onto the surface of carbon, which completely blocks or decreases the pore volume that ultimately reduces the reaction kinetics of the electrode. In addition, the active material deposited on the surface is prone to severe polysulfide dissolution into the electrolyte. As a result, the cell displayed low specific capacity and poor cycle performance. Even after 40 cycles, (figure 3.3.8b) the MGC/S-1, MGC/S-2 and MGC/S-3 electrodes delivered high discharge capacities of 939 mAh g^{-1}, 868 mAh g^{-1} and 651 mAh g^{-1}, respectively. Among them, the higher sulfur loading into MGC/S-2 with 64% of sulfur is found to be optimal due to its stable and improved electrochemical performance. Moreover, the higher sulfur loading into the cell has an advantage that it increases the specific energy of the cell. It has been reported in the literature that the optimum sulfur loading into porous conductive carbon host enhances the active material utilization, traps the dissolved polysulfide and also increases the ionic and electronic transport pathways during charge/discharge process [34,56].
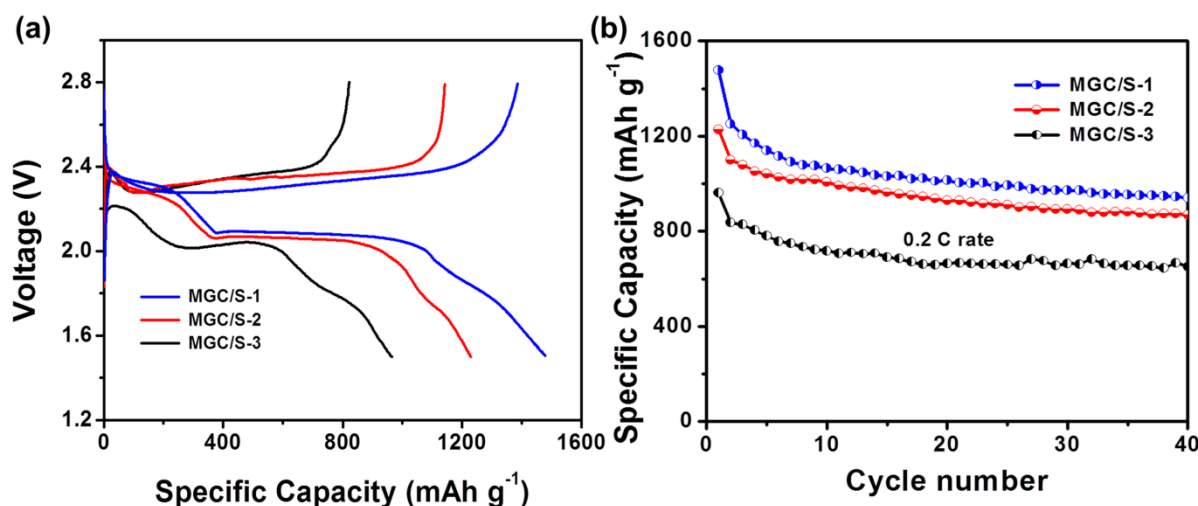
Figure 3.3.8 (a) Galvanostatic charge/discharge profiles and (b) cycle performance curves of MGC/S-1, MGC/S-2 and MGC/S-3 obtained between 1.5-2.8 V at 0.2 C rate with pristine polypropylene separator.

Furthermore, the studies have also been made in order to improve the electrochemical performance of the MGC/S-2 electrode by using modified separator. As mentioned in the introduction under the section 1.1.1.3, that the cycle life of Li-S battery can be further improved by introducing a thin layer of membrane between the cathode and separator or by modifying the separator. The interlayer or modified separator acts as a polysulfide reservoir that inhibits the migration of dissolved polysulfide intermediates to the anode surface. Moreover, it also enhances the reutilization of trapped active material during the repeated charge-discharge process by means of physical or chemical absorption. As a result, the electrochemical performance and cycle life of the cell increases, in comparison to the cell fabricated by using pristine sulfur cathode. For example, H. Yao et al. [57], prepared a modified separator by coating a thin layer of highly conductive carbon (super P carbon) on to the conventional polypropylene separator and studied its influence on the electrochemical performance of sulfur cathode. They reported that the large surface area of conductive carbon helps in trapping the dissolved polysulfides in this layer and improves the active material utilization during the electrochemical process. Thus, the cell fabricated by using sulfur cathode and modified separator exhibited high discharge capacity upto 500 cycles. In the present study, the investigator focus on preparing modified separator by using the as-prepared MGC as a carbon source and study its electrochemical performance on the MGC/S-2 cathode. It is expected that the dual confinement (MGC as host matrix as well as interlayer) of sulfur and its dissolved polysulfide species in MGC may improve the discharge capacity and the

cycle life of Li-S battery. Initially, the cyclic voltammetry test was conducted for the MGC/S-2 electrode in order to study the electrochemical behaviour with modified separator for 10 cycles in the potential range of 1.5-2.8 V at 0.1 mV s^{-1} scan rate (figure 3.3.9). During the discharge process, a pair of peaks are observed at the potentials of 2.3 V and 2.0 V, which correspond to the formation of long chain lithium polysulfides (Li_2S_n; $4 \leq n \leq 8$) accompanied by the transformation of sulfur from solid to liquid phase. Further, the long chain polysulfides finally get reduced to short chain lithium sulfides (Li_2S_2/Li_2S) [15]. Whereas, during the charging process, the peak at 2.5 V is attributed to the oxidation of Li_2S_2/Li_2S to elemental sulfur via long chain polysulfide intermediates. In the subsequent 10 cycles, no considerable change is observed in the redox reaction of the MGC/S-2 electrode. This result indicates good electrochemical stability of the cathode with modified separator.
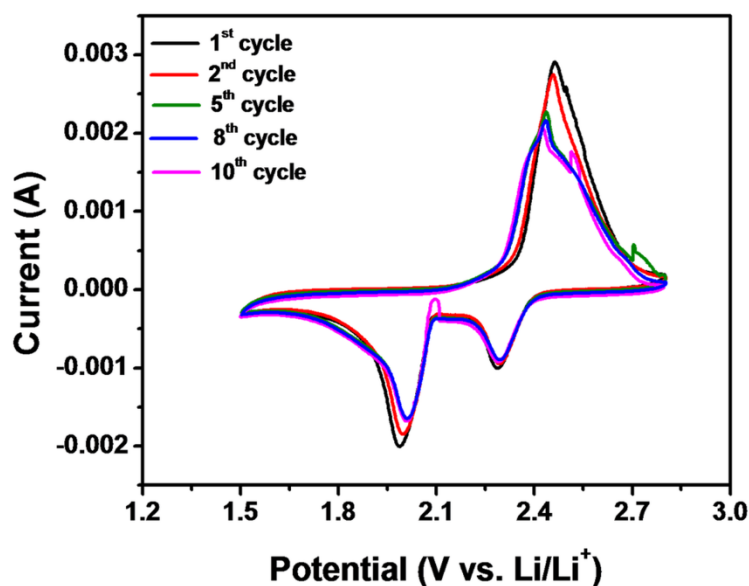
Figure 3.3.9 CV profile of MGC/S-2 electrode with modified separator measured at a scan rate of 0.1 mV s^{-1}.

Figure 3.3.10a shows the schematic representation for the fabrication of Li-S cell with modified separator. It is expected that the modified separator acts as a barrier film, which inhibits the dissolution of polysulfide species and its diffusion to the anode surface. Moreover, it also acts as upper current collector that increases the reutilization of the active material during the redox process. The galvanostatic charge/discharge profile of MGC/S-2 electrode measured in the potential range of 1.5-2.8 V at 0.2 C rate is shown in the in-set of figure 3.3.10b. The charge/discharge curve of MGC/S-2 electrode shows one flat charge curve and two stepped discharge curves, which are indicative of the typical redox reaction of sulfur. Initially, the cell delivered a high discharge capacity of 1542 mAh g^{-1}. Even after 50

cycles, the cell retained a discharge capacity of 1016 mAh g⁻¹ with good coulombic efficiency (figure 3.3.10b). The enhanced electrochemical performance is because MGC does more than one function. It acts as matrix as well as barrier film that helps in trapping the dissolved polysulfide species and also improves the active material utilization during the redox process [58]. Moreover, it can also accommodate the large volume variation during lithiation and has enhanced ionic and electronic conductivities.
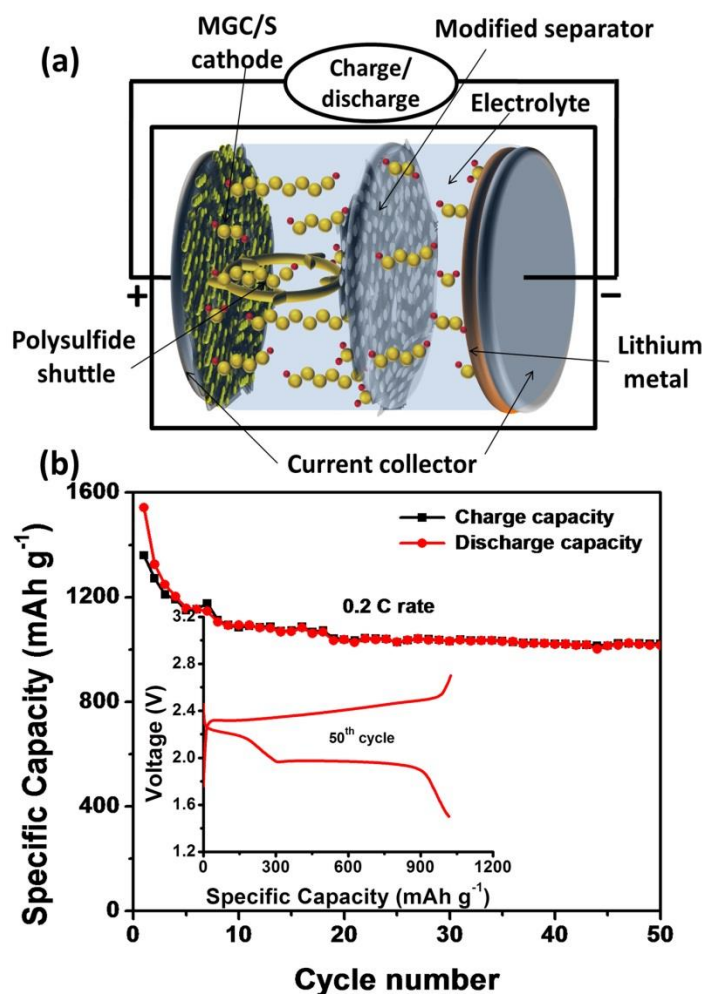
Figure 3.3.10 (a) Schematic representation of Li-S cell with modified separator and (b) cycle performance of MGC/S-2 electrode with modified separator measured in the voltage range of 1.5-2.8 V at 0.2 C rate (with in-set of charge/discharge profile).

The long term cycle performance test has also been conducted in order to show the electrochemical stability of the electrode at higher current rate of 1 C and the results are shown in the figure 3.3.11. The photo image of the modified separator is shown in the in-set of figure 3.3.11. The flexible nature of this separator makes it feasible for the preparation of Li-S cells for large-scale applications. The MGC/S-2 electrode with modified separator delivered high discharge capacity of 663 mAh g⁻¹ at 200ᵗʰ cycle in comparison to 481 mAh g⁻¹

with the pristine separator. These results infer that the modified separator acts as a barrier film that confines the dissolved lithium polysulfide in it and also increases the reutilization of the trapped active material during the prolonged cycles.
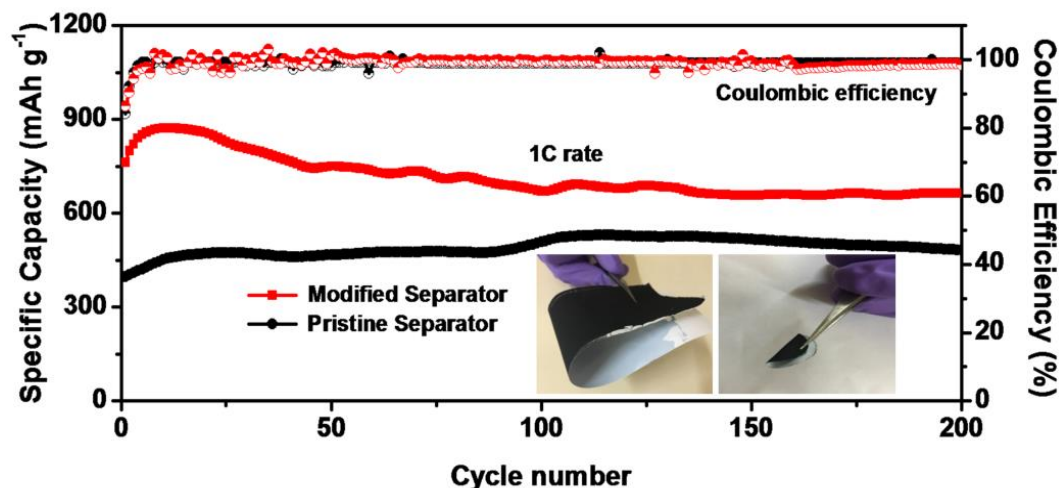
Figure 3.3.11 Comparative long term cycle performance of MGC/S-2 electrode with pristine and modified separator measured at 1 C rate.

However, the high areal sulfur loading on the electrode in Li-S batteries is an important parameter for practical applications in order to provide the volumetric energy density comparable with that of the conventional lithium-ion batteries. Therefore, the investigator has studied the electrochemical performance of the MGC/S-2 electrode with high active material loading. Figure 3.3.12a shows the charge/discharge profiles of the MGC/S-2 electrode with sulfur loading of 5.4 mg cm^{-2} and 9.3 mg cm^{-2}, measured at 0.2 C rate. It can be seen from the figure 3.3.12a that the discharge profiles show a similar trend even at high sulfur loading as the discharge profile of electrode with 2 mg cm^{-2}. Initially, the cells with active material loading of 5.4 mg cm^{-2} and 9.3 mg cm^{-2} delivered high discharge capacities of 1177mAh g^{-1} and 984 mAh g^{-1}, respectively. Even after 50 cycles, the cells displayed appreciated discharge capacities of 871 mAh g^{-1} and 632 mAh g^{-1} with good coulombic efficiency (figure 3.3.12b). It is observed from the figure 3.3.12 that with increase in active material loading on the electrode, the polarization of the electrode also increases due to sluggish reaction kinetics at the electrode, which reduces the electrochemical performance of the cell [59]. MGC/S-2 electrode with modified separator can be used even with higher sulfur loading in order to increase the overall capacity of the Li-S cell.
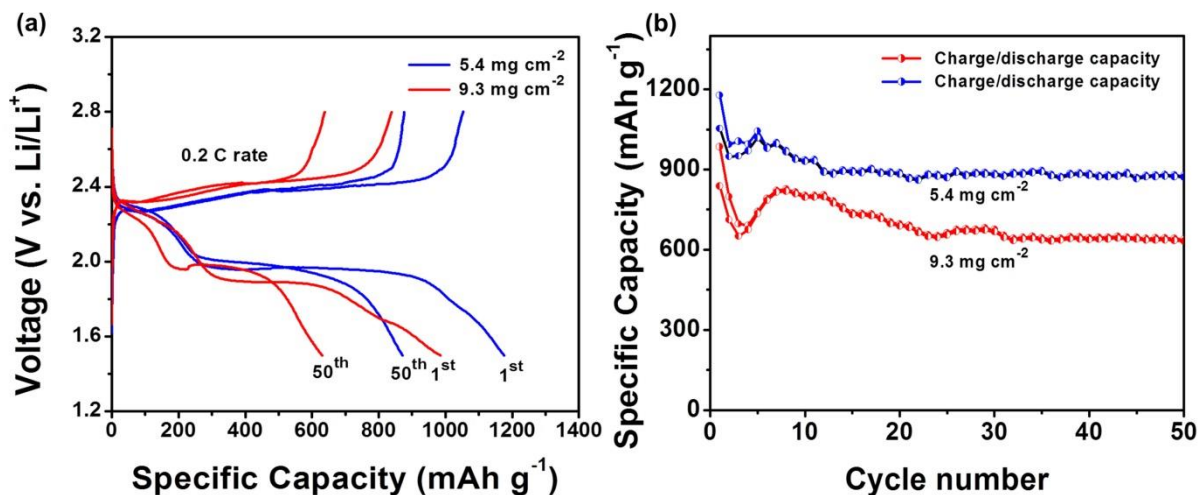
Figure 3.3.12 (a) Charge/discharge profiles and (b) cycle performance curves of MGC/S-2 electrode with high active material loading of 5.4 mg cm^{-2} and 9.3 mg cm^{-2} fabricated by using modified separator and measured in the potential range of 1.5-2.8 V at 0.2 C rate.
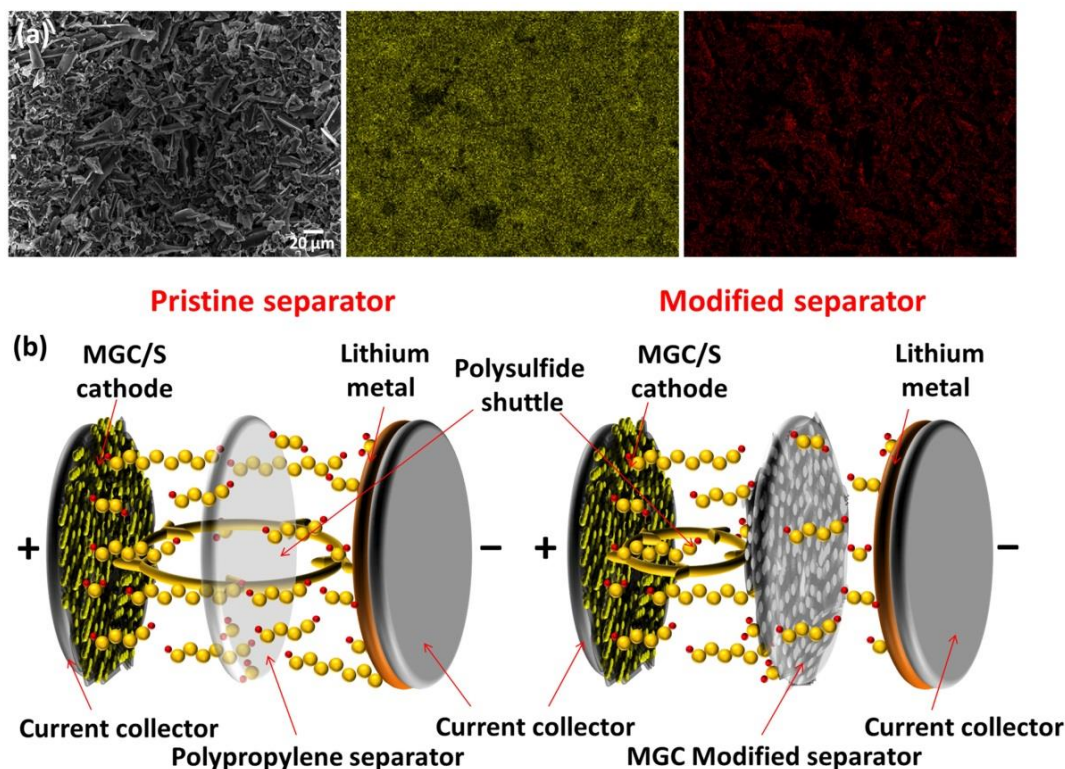
Figure 3.3.13 (a) EDS elemental map of modified separator of de-crimped MGC/S-2 electrode (9.3 mg cm^{-2}), after 50 charge/discharge cycles with sulfur (yellow) and carbon (red), and (b) schematic representation of Li-S cell fabricated with pristine and modified separator.

Furthermore, the de-crimping studies have also been carried out on the MGC/S-2 electrode (S=9.3 mg cm^{-2}), in order to show the effect of the modified separator in improving the electrochemical performance. Figure 3.3.13a shows the EDS-elemental map of the modified separator analysed after 50 charge/discharge cycles. It can be seen from the elemental map that the elemental sulfur is distributed uniformly throughout the carbon matrix, which infers that the soluble polysulfides formed during the redox process are trapped in it. This resulted in the efficient reutilization of the active material. Figure 3.3.13b shows the schematic representation of Li-S cell fabricated with pristine and modified separators. The modified separator acts as a barrier film that suppresses the migration of the dissolved polysulfide intermediates to the anode and also operates like upper current collector in enhancing the overall electrochemical performance of the MGC/S-2 electrode.

3.3.4 Conclusions

The as-prepared MGC exhibits high surface area of 2047 m^2 g^{-1} with a large pore volume of 1.69 cc^3 g^{-1} and also has highly graphitised carbon structure with graphene-like morphological appearance. The MGC/S-2 electrode with optimum sulfur loading and using a modified separator delivered a high initial discharge capacity of 1542 mAh g^{-1} at 0.2 C rate and retained a discharge capacity of 1016 mAh g^{-1} after 50 cycles with good coulombic efficiency. Further, the MGC/S-2 electrode with high active material loading of 5.4 mg cm^{-1} and 9.3 mg cm^{-1} delivered discharge capacities of 871 mAh g^{-1} and 632 mAh g^{-1} at 0.2 C rate at 50th cycle. The Li-S battery fabricated by using low cost activated carbon material such as MGC and high sulfur loading shows a path for large scale commercialization of this battery.

Section 3.4 Comparison of the Micro and Mesoporous Carbon Materials Developed in the Present Study and with those reported in the Literature

This section compares the electrochemical performance of the sulfur infused micro and mesoporous carbons derived from neem leaves, tissue paper and jute stalks and with the carbons reported in the literature in the form of table 3.4.1 and 3.4.2.

Table 3.4.1 Comparison of the electrochemical performance between the sulfur infused micro and mesoporous carbons developed in the present study.

KOH activated carbon Materials as a host for sufur cathode					
Carbon source/ carbon material	Sulfur content (%)	Sulfur loading (mg cm^{-2})	Initial capacity (mAh g^{-1})	Final capacity (mAh g^{-1})	C-rate
Neem leaves	50	1.3-1.5	1143	784 (50th cycle)	0.2
			939	506 (200th cycle)	1
Tissue paper (with modified separator)	64	~1.5	1497	992 (50th cycle)	0.2
			844 (5th cycle)	652 (200th cycle)	1
Jute stalk (with modified separator)	64	~2.0	1527	1016 (50th cycle)	0.2
		5.4	1177	871 (50th cycle)	0.2
		9.3	984	632 (50th cycle)	0.2
		~2.0	859 (5th cycle)	663 (200th cycle)	1

It can be seen from the table 3.4.1 that the micro and mesoporous carbon derived from jute stalks exhibited superior electrochemical performance in comparison to the activated carbons obtained from neem leaves and tissue paper. The improved electrochemical performance is due to the unique properties of the as-prepared MGC such as high surface area, large pore volume and good graphitic carbon content. The high surface area with large pore volume helps in trapping the dissolved polysulfide species and the presence of highly graphitised carbon structures improves the electrical conductivity during the redox process. Further, the electrochemical performance of the MGC/S-2 electrode is enhanced by using

modified separator. The modified separator acts as a barrier film that inhibits the migration of dissolved polysulfide species to the anode surface and increases the reutilization of the active material during repeated charge/discharge process. Moreover, the high surface area of the as-prepared MGC also offers high sulfur loading and thus the resulting cell delivered a higher discharge capacity even after 50 cycles (table 3.4.1).

This section also presents a comparison of the results reported in the literature prepared from conventional carbon materials and the activated carbons synthesized from biomass in the form of a table 3.4.2. For example, X. Chen et al. [55] prepared sulfur infused nitrogen-doped carbon nanofibers (CNF) impregnated with Mn_3O_4 nanoparticles. The electrode contains 50 wt% of sulfur with 11 mg of sulfur loading onto the electrode and the resulting cell delivered a discharge capacity of 744 mAh g^{-1} at 0.2 C rate after 100 cycles. The presence of porous structures in the CNF acts as media for physical entrapping of dissolved polysulfide species. Whereas, the Mn_3O_4 nanoparticles chemically trap the dissolved polysulfides and supress the migration of polysulfide species towards the anode surface. J. Zhang et al. [15] prepared a binder-free porous activated carbon foam (ACF)/sulfur composite electrode with 60 wt% of sulfur infusion in it. The electrode with sulfur loading of 5.1 mg cm^{-2} delivered a high discharge capacity of 750 mAh g^{-1} at 0.2 C rate even after 100 cycles. This behaviour is due to the presence of large internal porosity and continuous three-dimensional network of ACF renders efficient utilization of active material and improves the electrical conductivity during the charge/discharge process. G. Ren et al. [60] prepared O and N doped hierarchical porous carbon from soyabean residue by using KOH activation process. They have prepared an electrode, which contain 80 wt% of sulfur in the composite and the sulfur loading was 5.5 mg cm^{-2} on the electrode. The resulting composite electrode delivered a high initial discharge capacity of 950 mAh g^{-1} and retained a discharge capacity of ~770 mAh g^{-1} at 0.2 C rate even after 100 cycles. The improved electrochemical performance is due to the synergetic effect as explained below. The presence of a large number of micropores in the activated carbon helps in trapping the dissolved polysulfide species and the heteroatoms (O and N) in the carbon can chemically bind the dissolved polysulfides.

Table 3.4.2 comparative electrochemical performance of the micro and mesoporous carbons developed in the present study with those of the carbons reported in the literature.

Conventional carbon materials						
Carbon source/ Carbon material	Sulfur % in carbon	Sulfur loading (mg cm^{-2})	Initial capacity (mAh g^{-1})	Final capacity (mAh g^{-1})	C-rate/ current density (A g^{-1})	Ref
Porous carbon	59	0.5-0.6	1181	~820	0.1 C	[61]
Al-S-VGCF (Interlayer)	95	~5	1100	650 (100th cycle)	0.05 A g^{-1}	[62]
ACAF	70	~7	~1180	788 (90th cycle)	0.1 C	[63]
Ti$_2$S/C Composite	65	12	~950	659 (200th cycle)	0.2 C	[64]
Mn$_3$O$_4$@CNF (Interlayer)	50	11	~1200	744 (100th cycle)	0.2 C	[55]
RGO-HCS	90	~5	860 at 5th cycle	662 (78th cycle)	0.1 C	[36]
KOH activated biomass-derived porous carbon materials						
Olive stone	70	2-2.5	930	670 (50th cycle)	0.1 A g^{-1}	[13]
Corncob	44	-	1600	554 (50th cycle)	0.1 C	[9]
Crude soyabean	80	5.5	950	~770 (100th cycle)	0.2 C	[60]
Fish scale	58	0.8-1.0	1039	1023 (70th cycle)	1.0 C	[14]
Pomelo peel	60	5.1	1258	750 (100th cycle)	0.2 C	[15]
Neem leaves	50	1.3-1.5	1143	784 (50th cycle)	0.2 C	This work
Tissue paper	64	~1.5	1497	992 (50th cycle)	0.2 C	This work
Jute stalk	64	5.4	1177	871 (50th cycle)	0.2 C	This work
		9.3	984	632 (50th cycle)	0.2 C	

The discharge capacities delivered by the cathodes developed in the present study are comparable with the porous carbon-based materials prepared by the conventional methods and activated carbons derived from the biomass reported in the literature. Moreover, the present study also gives a scope for the development of low-cost electrode materials, which has shown a path for large-scale commercial use of these materials for Li-S battery.

References

1. Song, R., Fang, R., Wen, L., Shi, Y., Wang, S., Li, F. A Trilayer Separator With Dual Function for High Performance Lithium-Sulfur Batteries. *J. Power Sources* **301**, 179-186 (2016).

2. Wu, H. B., Wei, S., Zhang, L., Xu, R., Hng, H. H., Lou, X. W. D. Embedding Sulfur in MOF-Derived Microporous Carbon Polyhedrons for Lithium-Sulfur Batteries. *Chem. A Eur. J.* **19**, 10804-10808 (2013).

3. Zhang, D. A., Wang, Q., Wang, Q., Sun, J., Xing, L. L., Xue, X.Y. High Capacity and Cyclability of Hierarchical MoS_2/SnO_2 Nanocomposites as the Cathode of Lithium-Sulfur Battery. *Electrochim. Acta* **173**, 476-482 (2015).

4. Chen, S. R., Zhai, Y. P., Xu, G. L., Jiang, Y. X., Zhao, D. Y., Li, J. T., Huang, L., Sun, S. G. Ordered Mesoporous Carbon/Sulfur Nanocomposite of High Performances as Cathode for Lithium-Sulfur Battery. *Electrochim. Acta* **56**, 9549-9555 (2011).

5. Jayaprakash, N., Shen, J., Moganty, S. S., Corona, A., Archer, L. A. Porous Hollow Carbon @ Sulfur Composites for High-Power Lithium-Sulfur Batteries. *Angew. Chem. Int. Ed.* **50**, 5904–5908 (2011).

6. Nitze, F., Fossum, K., Xiong, S., Matic, A., Palmqvist, A. E. C. Sulfur-Doped Ordered Mesoporous Carbons : A Stability-Improving Sulfur Host for Lithium-Sulfur Battery cathodes. *J. Power Sources* **317**, 112-119 (2016).

7. Sun, F., Wang, J. Chen, H., Li, W., Qiao, W., Long, D., Ling L. High Efficiency Immobilization of Sulfur on Nitrogen-Enriched Mesoporous Carbons for Li-S Batteries. *ACS Appl. Mater. Interfaces* **5**, 5630-5638 (2013).

8. Zhang, S., Zheng, M., Lin, Z., Li, N., Liu, Y., Zhao, B., Pang, H., Cao, J., He, P., Shi, Y. Activated Carbon with Ultrahigh Specific Surface Area Synthesized from Natural Plant Material for Lithium-Sulfur Batteries. *J. Mater. Chem. A* **2**, 15889-15896 (2014).

9. Guo, J., Zhang, J., Jiang, F., Zhao, S., Su, Q., Du, G. Microporous Carbon Nanosheets Derived from Corncobs for Lithium-Sulfur Batteries. *Electrochim. Acta* **176**, 853-860 (2015).

10. Zhou, W., Lei, S., Sun, S., Ou, X., Fu, Q., Xu, Y., Xiao, Y., Cheng, B. From weed to multi-heteroatom-doped honeycomb-like porous carbon for advanced supercapacitors: A gelatinization-controlled one-step carbonization. *J. Power Sources* **402**, 203-212 (2018).

11. Chen, F., Yang, J., Bai, T., Long, B., Zhou, X. Biomass Waste-Derived Honeycomb-Like Nitrogen and Oxygen Dual-Doped Porous Carbon for High Performance Lithium-Sulfur Batteries. *Electrochim. Acta* **192**, 99-109 (2016).

12. Wei, S. Zhang, H., Huang, Y., Wang, W., Xai, Y., Yu, Z. Pig Bone Derived Hierarchical Porous Carbon and its Enhanced Cycling Performance of Lithium-Sulfur Batteries. *Energy Environ. Sci.* **4**, 736-740 (2011).

13. Moreno, N., Caballero, A., Herna, L., Morales, J. Lithium-Sulfur Batteries with Activated Carbons Derived from Olive Stones. *Carbon* **70**, 241-248 (2014).

14. Zhao, S., Li, C., Wang, W., Zhang, H., Gao, M,. Xiong, X., Wang, A., Yuan, K., Huang, Y., Wang, F. A Novel Porous Nanocomposite of Sulfur/Carbon Obtained from Fish Scales for Lithium-Sulfur Batteries. *J. Mater. Chem A* **1**, 3334-3339 (2013).

15. Zhang, J., Xiang, J., Dong, Z., Liu, Y., Wu, Y., Xu, C., Du, G. Biomass Derived Activated Carbon with 3D Connected Architecture for Rechargeable Lithium-Sulfur Batteries. *Electrochim. Acta* **116**, 146-151 (2014).

16. Wang, J., Kaskel, S. KOH Activation of Carbon-Based Materials for Energy Storage. *J. Mater. Chem.* **22**, 23710-23725 (2012).

17. Lozano-Castello, D., Calo, J. M., Cazorla-Amoros, D., Linares-Solano, A. Carbon Activation with KOH as Explored by Temperature Programmed Techniques, and the Effects of Hydrogen. *Carbon* **45**, 2529–2536 (2007).

18. Guo, N., Li, M., Wang, Y., Sun, X., Wang, F., Yang, R N-Doped Hierarchical Porous Carbon Prepared by Simultaneous-Activation of KOH and NH_3 for High Performance Supercapacitors. *RCS Advnaces* **6**, 101372-101379 (2016).

19. Nagaraju, G., Cha, S. M., Yu, J. S. Ultrathin Nickel Hydroxide Nanosheet Arrays Grafted Biomass-Derived Honeycomb-Like Porous Carbon with Improved Electrochemical Performance as a Supercapacitive Material. *Sci. Rep.* **7**, 45201 (2017).

20. Li, L., Chen, Y., Zhong, B. Synthesis and Electrochemical Performance of a Simple and Low-Cost Sulfur/Porous Carbon Composite Cathode for Rechargeable Lithium Sulfur Battery. *Compos. Part A* **62**, 26-31 (2014).

21. Yang, C., P., Yin, Y. X., Ye, H., Jiang, K. C., Zhang, J., Guo, Y. G. Insight into the

Effect of Boron Doping on Sulfur/Carbon Cathode in Lithium-Sulfur Batteries. *ACS Appl. Mater. Interfaces* **6**, 8789-8795 (2014).

22. Tao, X., Zhang, J. Xia, Y., Huang, H., Du, J., Xiao, H., Zhang, W., Gan, Y. Bio-Inspired Fabrication of Carbon Nanotiles for High Performance Cathode of Li-S Batteries. *J. Mater. Chem A* **2**, 2290-2296 (2014).

23. Biswal, M., Banerjee, A., Deo, M., Ogale, S. From Dead Leaves to High Energy Density Supercapacitors. *Energy Environ. Sci.* **6**, 1249-1259 (2013).

24. Ojeda, M. L., Esparza, J. M., Campero, A., Cordero, S., Kornhauser, I., Rojas, F., On comparing BJH and NLDFT pore-size distributions determined from N_2 sorption on SBA-15 substrata, Phys. Chem. Chem. Phys., 5, 1859-1866 (2003).

25. Kupgan, G., Arachchi, T. P. L., Colina, C. M., NLDFT Pore Size Distribution in Amorphous Microporous Materials, Langmuir 33, 11138-11145 (2017).

26. Zhang, B., Xiao, M., Wang, S., Han, D., Song, S., Chen, G., Meng, Y. Novel Hierarchically Porous Carbon Materials Obtained from Natural Biopolymer as Host Matrixes for Lithium-Sulfur Battery Applications. *ACS Appl. Mater. Interfaces* **6**, 13174-13182 (2014).

27. Han, Y., Shen, N., Zhang, S., Li, D., Li, X. Fish Gill-Derived Activated Carbon for Supercapacitor Application. *J. Alloys Compd.* **694**, 636-642 (2017).

28. Wang, D. W., Zhou, G., Li, F., Wu, K. H., Lu, G. Q. M., Cheng, H. M., Gentle, I. R. A Microporous-Mesoporous Carbon with Graphitic Structure for a High-Rate Stable Sulfur Cathode in Carbonate Solvent-Based Li-S Batteries. *Phys. Chem. Chem. Phys.* **14**, 8703-8710 (2012).

29. Gu, X., Wang, Y., Lai, C., Qiu, J., Li, S., Hou, Y., Martens, W., Mahmood, N., Zhang, S. Microporous Bamboo Biochar for Lithium-Sulfur Batteries. *nano Res.* **8**, 129-139 (2015).

30. Xu, G., Xu, Y. F., Fang, J. C., Peng, X. X., Fu, F., Huang, F., Li, J. T., Sun, S. G., Porous Graphitic Carbon Loading Ultra High Sulfur as High-Performance Cathode of Rechargeable Lithium-Sulfur Batteries. *ACS Appl. Mater. Interfaces* **5**, 10782-10793 (2013).

31. Yamin, H., Gorenshtein, A., Penciner, J., Sternberg, Y., Peled, E., Lithium Sulfur Battery -Oxidation/Reduction Mechanisms of Polysulfides in THF Solutions, *Journal of The Electrochemical Society*, **135**, 1045-1048 (1988).

32. Manan S. A. N., Aldous, L., Alias, Y., Murray, P., Yellowlees, L. J., Lagunas, M. C.,

Hardacre, C., Electrochemistry of Sulfur and Polysulfides in Ionic Liquids, *J. Phys. Chem. B*, **115**, 13873-13879 (2011).

33. Wang, J., Cheng, S., Li,W., Zhang,S., Li, H., Zheng, Z., Li, F., Shi, L., Lin, H., Zhang, Y. Simultaneous Optimization of Surface Chemistry and Pore Morphology of 3D Graphene-Sulfur Cathode via Multi-ion Modulation. *J. Power Sources* **321**, 193-200 (2016).

34. Li, X., Cao, Y., Qi, W., Saraf, L. V., Xiao, J., Nie, Z., Mietek, J., Zhang, J. G., Schwenzera, B., Liu, j. Optimization of Mesoporous Carbon Structures for Lithium-Sulfur Battery Applications. *J. Mater. Chem* **21**, 16603-16610 (2011).

35. Raccichini, R., Varzi, A., Sai, V. C. K., Kubel, C., Passerini, S. Boosting the Power Performance of Multilayer Graphene as Lithium-ion Battery Anode via Unconventional Doping with In-Situ Formed Fe Nanoparticles. *Sci. Rep.* **6**, 23585 (2016).

36. Liu, S., Li, Y., Hong, X., Xu, J., Zheng, C., Xie, K. Reduced Graphene Oxide-Hollow Carbon Sphere Nanostructure Cathode Material with Ultra-High Sulfur Content for High Performance Lithium-Sulfur Batteries. *Electrochim. Acta* **188**, 516-522 (2016).

37. Noelia Moreno, Caballero, A., Morales, J., Rodriguez-Castellon, E. Improved Performance of Electrodes Based on Carbonized Olive Stones/S Composites by Impregnating with Mesoporous TiO_2 for Advanced Li-S Batteries. *J. Power Sources* **313**, 21-29 (2016).

38. Gong, Y., Li, D., Luo, C., Fu, Q., Pan, C. Highly Porous Graphitic Biomass Carbon as Advanced Electrode Materials for Supercapacitors. *Green Chem.* **19**, 4132-4140 (2017).

39. Govind Raj, K., Joy, P. A. Role of Localized Graphitization on the Electrical and Magnetic Properties of Activated Carbon. *J. Am. Ceram. Soc.* **100**, 5151-5161 (2017).

40. Xu, J., Shui, J., Wang, J., Wang, M., Liu, H. K., Dou, S. X., Jeon, I. Y., Seo, J. M., Baek, J. B., Dai. L. Sulfur-Graphene Nanostructured Cathodes via Ball-Milling for High-Performance Lithium-Sulfur Batteries. *ACS Nano* **8**, 10920-10930 (2014).

41. Zeng, Q. R., Wang, D. W., Wu, K. H., Li, Y., Godoi, F. C. D., Gentle, I. R. Synergy of Nanoconfinement and Surface Oxygen in Recrystallization of Sulfur Melt in Carbon Nanocapsules and the Related Li-S Cathode Properties. *J. Mater. Chem A* **2**, 6439-6447 (2014).

42. Sun, F., Gao, J. Zhu, Y., Pi, X., Wang, L., Liu, X., Qin, Y. A High Performance

Lithium ion Capacitor Achieved by the Integration of a Sn-C Anode and a Biomass-Derived Microporous Activated Carbon Cathode. *Sci. Rep.* **7**, 40990 (2017).

43. Wang, B., Wen, Y., Ye, D., Yu, H., Sun, B., Wang, G., Jurcakova, D. H., Wang. L. Dual Protection of Sulfur by Carbon Nanospheres and Graphene Sheets for Lithium-Sulfur Batteries. *Chem. A Eur. J.* **20**, 5224-5230 (2014).

44. Zheng, S., Han, P., Han, Z., Zhang, H., Tang, Z., Yang, J. High Performance C/S Composite Cathodes with Conventional Carbonate-Based Electrolytes in Li-S Battery. *Sci. Rep.* **4**, 4842 (2014).

45. Qie, L., Chen, W., Xiong, X., Hu, C., Zou, F., Hu, P., Huang, Y. Sulfur-Doped Carbon with Enlarged Interlayer Distance as a High-Performance Anode Material for Sodium-Ion Batteries. *Adv. Sci.* **2**, 1500195 (2015).

46. Gao, X., Li, J., Guan, D., Yuan, C. A Scalable Graphene Sulfur Composite Synthesis for Rechargeable Lithium Batteries with Good Capacity and Excellent Columbic Efficiency. *ACS Appl. Mater. Interfaces* **6**, 4154-4159 (2014).

47. Liang, X., Wen, Z., Liu, Y., Zhang, H., Huang, L., Jin, J. Highly Dispersed Sulfur in Ordered Mesoporous Carbon Sphere as a Composite Cathode for Rechargeable Polymer Li/S Battery. *J. Power Sources* **196**, 3655-3658 (2011).

48. Wu, F., Chen, J., Chen, R., Wu, S., Li, L., Chen, S., Zhao, T. Sulfur/Polythiophene with a Core/Shell Structure: Synthesis and Electrochemical Properties of the Cathode for Rechargeable Lithium Batteries. *J. Phys. Chem. C* **115**, 6057-6063 (2011).

49. Wang, J., Yang, Y., Kang, F. Porous Carbon Nanofiber Paper as an Effective Interlayer for High-Performance Lithium-Sulfur Batteries. *Electrochim. Acta* **168**, 271-276 (2015).

50. Wang, X., Wang, Z., Chen, L. Reduced Graphene Oxide Film as a Shuttle-Inhibiting Interlayer in a Lithium-Sulfur Battery. *J. Power Sources* **242**, 65-69 (2013).

51. Zhou, L., Zong, Y., Liu, Z., Yu, A. A Polydopamine Coating Ultralight Graphene Matrix as a Highly Effective Polysulfide Absorbent for High-Energy Li-S Batteries. *Renew. Energy* **96**, 333-340 (2016).

52. Liang, C., Bao, J., Li, C., Huang, H., Chen, C., Lou, Y., Lu, H., Lin, H., Shi, Z., Feng, S. One-Dimensional Hierarchically Porous Carbon from Biomass with High Capacitance as Supercapacitor Materials. *Microporous Mesoporous Mater.* **251**, 77-82 (2017).

53. Xu, G., Ding, B., Shen, L., Nie, P., Han, J., Zhang, X. Sulfur Embedded in Metal

Organic Framework-Derived Hierarchically Porous Carbon Nanoplates for High Performance Lithium-Sulfur Battery. *J. Mater. Chem. A* **1**, 4490-4496 (2013).

54. Li, Y., Wang, G., Wei, T., Fan, Z., Yan, P. Nitrogen and Sulfur Co-Doped Porous Carbon Nanosheets Derived from Willow Catkin for Supercapacitors. *Nano Energy* **19**, 165-175 (2016).

55. Chen, X., Yuan, L., Hao, Z., Liu, X., Xiang, J., Zhang, Z., Huang, Y., Xie, J. Free-Standing Mn_3O_4@CNF/S Paper Cathodes with High Sulfur Loading for Lithium-Sulfur Batteries. *ACS Appl. Mater. Interfaces* **10**, 13406-13412 (2018).

56. Lyu, Z., Xu, d., Yang, L., Che, R., Feng, R., Zhao, J.,Li, Y., Wu, Q., Wang, X., Hu, Z. Hierarchical Carbon Nanocages Confining High-Loading Sulfur for High-Rate Lithium-Sulfur Batteries. *Nano Energy* **12**, 657-665 (2015).

57. Yao, H., Yan, K., Li, W., Zheng, G., Kong, D., Seh, Z. W., Narasimhan, V. K., Liang, Z., Cui, Y., Improved lithium–sulfur batteries with a conductive coating on the separator to prevent the accumulation of inactive S-related species at the cathode-separator interface, *Energy Environ. Sci.*, **7**, 3381-3390 (2014).

58. Chung, S., Manthiram, A. Bifunctional Separator with a Light-Weight Carbon-Coating for Dynamically and Statically Stable Lithium-Sulfur Batteries. *Adv. Funct. Mater.* **24**, 5299-5306 (2014).

59. Yu, M., Ma, J., Xie, M., Song, H., Tian, F., Xu, S., Zhou, Y., Li, B., Wu, D., Qiu, H., Wang R. Freestanding and Sandwich-Structured Electrode Material with High Areal Mass Loading for Long-Life Lithium–Sulfur Batteries. *Adv. Energy Mater.* **7**, 1602347 (2017).

60. Ren, G., Li, S., Fan, Z. X., Warzywoda, J., Fan, Z. Soybean-Derived Hierarchical Porous Carbon with Large Sulfur Loading and Sulfur Content for High-Performance Lithium-Sulfur Batteries. *J. Mater. Chem. A* **4**, 16507-16515 (2016).

61. Sohn, H., Gordin, M. L., Xu, T., Chen, S., Lv, D., Song, J., Manivannan, A., Wang, D. Porous Spherical Carbon/Sulfur Nanocomposites by Aerosol-Assisted Synthesis: The Effect of Pore Structure and Morphology on Their Electrochemical Performance As Lithium/Sulfur Battery Cathodes. *ACS Appl. Mater. Interfaces* **6**, 7596-7606 (2014).

62. Zhang, Y., Li, K., Li, H., Peng, Y., Wang, Y., Wang, J., Zhao, J. High Sulfur Loading Lithium-Sulfur Batteries Based on a Upper Current Collector Electrode with Lithium-ion Conductive Polymers. *J. Mater. Chem. A* **5**, 97-101 (2017).

63. He, N., Zhoug, L., Xiao, M., Wang, S., Han, D., Meng, Y. Foldable and High Sulfur

Loading 3d Carbon Electrode for High-Performance Li-S Battery Application. *Sci. Rep.* **6**, 33871 (2016).

64.   Chung, S. H., Luo, L., Manthiram, A. TiS$_2$-Polysulfide Hybrid Cathode with High Sulfur Loading and Low Electrolyte Consumption for Lithium-Sulfur Batteries. *ACS Energy Lett.* **3**, 568-573 (2018).

Chapter 4

Synthesis and Electrochemical Studies of High Capacity Tin/Graphene and Silicon/Graphite Composite Anodes and Fabrication of Lithiated Si-S Full Cell

Contents

Introduction

The Li-S battery with sulfur cathode has a high theoretical specific capacity of 1672 mAh g^{-1}, which is 3-5 times higher than the conventional cathodes used in the lithium ion batteries. However, the commercialization of this system is greatly hindered due to several issues such as poor electrical conductivity of the elemental sulfur and its end discharge products, polysulfide dissolution into the electrolyte and huge volume expansion. These factors result in loss of active material from the cathode, which leads to low discharge capacity and poor cycle life [1]. Recently, tremendous work has been done on sulfur cathode to address these issues as discussed in the chapter 1 (Section 1.1.1.4). Novel high capacity sulfur cathodes based on activated carbon derived from neem leaves, tissue paper and jute stalks developed in the present study have been discussed in the chapter 3.
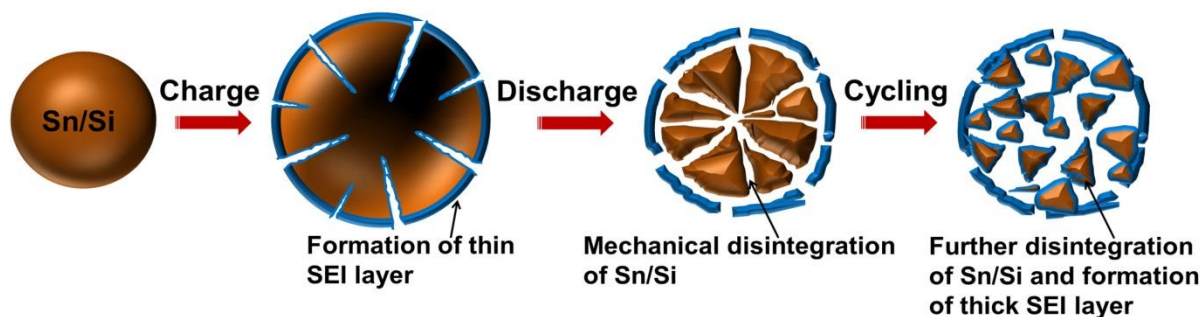
Figure 4.1 Schematic representation of Sn or Si anode during charge/discharge process.

Nevertheless, the use of lithium metal as the anode during the fabrication of Li-S cells remains a major drawback due to the formation of lithium dendrites upon repeated charge-discharge processes. This results in internal short-circuit of the cell which may undergo thermal runway [2]. In addition to this drawback, elemental lithium is toxic and highly expensive. The graphite with theoretical specific capacity of 372 mAh g^{-1}, is the most commonly used anode material in lithium-ion batteries. The graphite anode with low charge/discharge capacity cannot compensate the high charge storage capacity of the sulfur cathode. Hence, the research has been directed towards high capacity anode materials. Among them, high capacity tin (Sn) and silicon (Si) are considered to be good anode materials, which can replace the use of lithium metal anode in Li-S battery [3]. According to the phase diagram, five silicon or tin atoms can accommodate twenty two lithium atoms in order to achieve high theoretical capacities of 4200 mAh g^{-1} for Si and 994 mAh g^{-1} for Sn, respectively [4]. Moreover, these anode materials operate at low potential window, which make them applicable for the fabrication of Li-S full cell. Nevertheless, these anodes have not been explored in commercial rechargeable batteries because the bulk material displays poor cycle performance during lithiation/delithiation process. This is mainly due to the generation of huge mechanical stress during large volume expansion (300%) that eventually results in pulverization, disintegration of active material from the current collector, and loss of electrical contact between the adjacent particles as shown in the figure 4.1 [5,6].

In the present study, the investigator focused on the synthesis of Sn/graphene and Silicon/graphite composites for use as anodes in place of lithium in the Li-S battery. This chapter has been divided into four sections, which include a brief introduction, experimental details, results and discussion of electrodeposition of dendritic porous Sn/Graphene structures (Section 4.1), Si/Graphite prepared by ball milling process (Section 4.2) and fabrication of lithiated Si-S full cell (Section 4.3). Section 4.4 shows the comparison of the electrochemical performance of lithiated Si-S cell developed in the present study with those reported in the literature.

Section 4.1 Graphene Modified Electrodeposited Dendritic Porous Tin Structures as Binder Free Anode Material

Several attempts have been made to mitigate huge volume variation of Sn during lithiation/delithiation process in order to achieve an improved electrochemical performance for longer cycles [7,8]. In the recent years, the Sn-based intermetallic alloys [9,10] and Sn-carbon composites [11,12] have gained much interest owing to their excellent electrochemical stability. On the other hand, Sn-based three dimensional (3D) porous structure fabricated by electrodeposition method as anode material has shown an excellent electrochemical performance [13,14]. The main advantage with electrodeposition method is that, no binder or conductive additive is required during the cell fabrication process [15]. Moreover, the microstructural and chemical properties can easily be manipulated by optimising the deposition parameters. Recently, J. Jeun et al.[16] reported the use of 3D dendritic Sn/C composite prepared by a two-step electrodeposition, which delivered an improved discharge capacity. J. Park et al.[17] have shown that Sn, co-electrodeposited with carbon particles, displayed a maximum discharge capacity of 620 mAh g^{-1} at 100 mA g^{-1} current density. G. Wang et al.[18] reported 3D nano-architecture of Sn/graphene (Sn/G) composite prepared by the chemical reduction method which delivered a stable and highly reversible lithium storage capacity of about 508 mAh g^{-1}, up to 100 cycles. The development of graphene based hybrid nanostructures such as Sn/G, [19,20] Fe_3O_4/G, [21,22] SnO_2/G [23,24] and Co_3O_4/G [25,26] have shown promising electrochemical performance. During the charge/discharge process, presence of highly conductive graphene, due to its sheet-like structure in the composite can maintain an intimate electrical contact between the fractured particles for good electron transport. In addition, it can also accommodate large volume expansion during cycling. However, the fabrication procedures either include time consuming and complex techniques or use of toxic chemicals. The need for a simple technique to develop the electrode materials which can provide high capacity retention and good cyclic performance motivated the investigator to carry out the present study. In the present study, the investigator has developed a sandwich type of highly porous electrodeposited binder free Sn/G/RGO composite anode and evaluated its electrochemical performance.

4.1.1 Synthesis of Sn/Graphene Composite

Graphene oxide (GO) was synthesized by electrochemical exfoliation method as reported in the literature [27] and then reduced thermally by heating at 600 ℃ for 1 h in argon atmosphere in order to obtain reduced graphene oxide (RGO). Electrodeposition was performed by using a two electrode system in aqueous electrolyte solution. Carbon paper rinsed with deionised water followed by ethanol, was used as the substrate (cathode) for electrodeposition of pristine Sn and Sn/G composite. Whereas, a platinum foil was used as the anode and the electrodes were separated by a distance of 6 mm. Sn/G composite was co-electrodeposited at a constant current of 2 A cm^{-2} by using power supply (Dynatronix, DuPR 10-3-6) for 10 seconds at room temperature of 25 ℃. In a typical synthesis, 0.2 g of GO nanosheets was dispersed in a 250 ml electrolytic solution containing 5.36 g of SnSO$_4$ and 13.5 ml of conc. H$_2$SO$_4$ (68-70%). During the co-electrodeposition process, the electrolyte solution was continuously stirred for better dispersion of GO. For the purpose of comparison, pristine Sn was also electrodeposited using the same procedure but without the addition of graphene oxide. Both the materials, (viz. electrodeposited Sn and co-electrodeposited Sn/G) were coated with reduced graphene oxide by drop casting method to form sandwich structures. The schematic illustration of the process is shown in the figure 4.1.1. After the electrodeposition, the samples were rinsed with deionised water followed by heating at 170 ℃ in a tubular furnace under inert atmosphere for 2 hours. The amounts of pristine Sn and Sn/G composite loaded on the carbon paper substrate are in the range of 3.0-3.5 mg cm^{-2}. The RGO content in the sandwich structures is in the range of 2.2-2.6 mg cm^{-2} and the thickness of the electrode (current collector + anode material) is 400 μm.

The electrochemical studies have been carried out using 2032 coin cells, which were assembled in an Ar filled glove box. The electrodeposited anode materials on carbon paper were used as binder free working electrodes and the lithium foil was used as the reference electrode. Two types of electrolyte solutions were employed in the present study. Firstly, A solution of 1 M LiPF$_6$ in a mixture of ethylene carbonate and dimethyl carbonate (EC:DMC) in 50:50 v/v (which is the most commonly used electrolyte for Li-ion batteries) was used. Secondly, 1 M bis(trifluoromethane) sulfonimide lithium salt (LiTFSI) in a mixture of 1,3-dioxalane (DOL) and dimethoxyethane (DME) (DOL:DME, 1:1 by volume) with 5 wt% lithium nitrate as additive was exclusively used in Li-S batteries due to its high electrochemical stability towards dissolved polysulfide species. As mentioned in the chapter 1, the conventionally used carbonate based electrolyte solution cannot be employed in

Li-S cell due to nucleophilic addition or substitution reaction with lithium polysulfides, which leads to severe capacity decay within a few charge-discharge cycles [28].
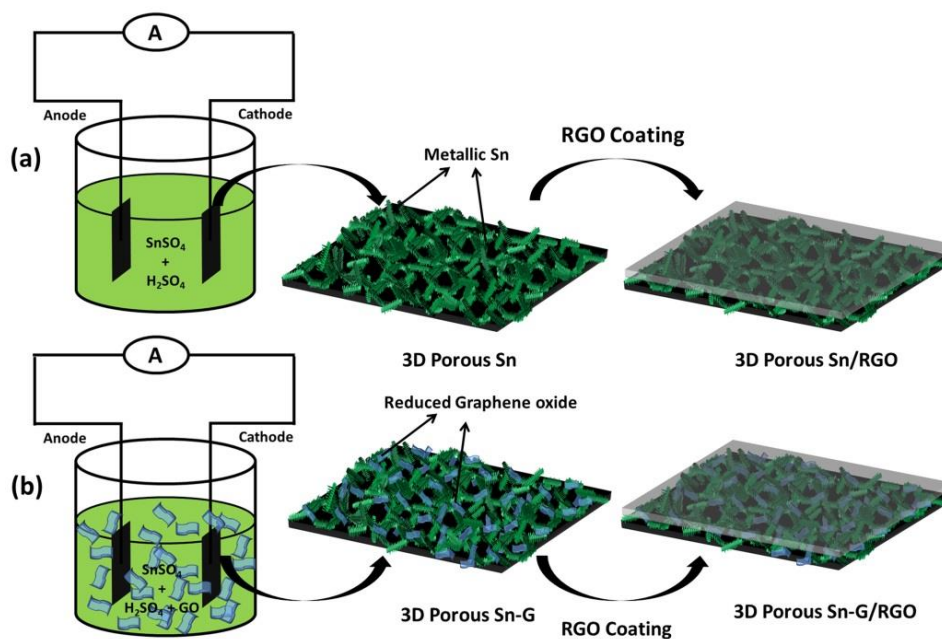
Figure 4.1.1 Schematic representation of the preparation of sandwich type porous 3D structures of (a) Sn/RGO and (b) Sn-G/RGO composite.

4.1.2 Results and Discussion: Characterization of the Tin/Graphene Anode Material

Initially, pristine Sn and Sn-graphene (Sn-G) composite were fabricated on carbon paper substrate (used as current collector) by electrodeposition and co-electrodeposition processes, respectively as shown in the figure 4.1.1. During electrodeposition, a highly porous metallic pristine Sn was directly deposited on the cathode surface (carbon paper) to form dendrite-like structure. During electrodeposition, hydrogen bubbles act as dynamic template for the formation of 3D dendritic Sn on the substrate by selecting suitable parameters such as applied current density and the concentration of precursor materials [29]. *In-situ* incorporation of graphene during the electrodeposition has an advantage of improved electrical conductivity of the electrode material. It is apparent that due to the presence of more oxygen functional groups on bare GO, the electrodeposition may not take place on the negative electrode (cathode). However, in the co-electrodeposition process of both GO and Sn, a small quantity of GO also undergoes deposition along with Sn. During the process, stannous ions were adsorbed on the surface of the GO by electrostatic forces of attraction, followed by migration to the cathode surface. Whereas, the reduction of Sn^{2+} to Sn occurs on the substrate along with the partial reduction of GO to graphene to form Sn-G composite.

4.1.2.1 Morphological Analysis:

The morphologies of the electrodeposited Sn and Sn-G composite were studied using SEM (figure 4.1.2). Figure 4.1.2a and b show the photo image and SEM image of the carbon paper substrate, respectively. The carbon paper substrate appears as a three dimensional network with good interconnectivity, which facilitates high electron transport [30]. In addition, the 3D carbon substrate can facilitate high material loading and also tightly holds the active material during the electrodeposition process.
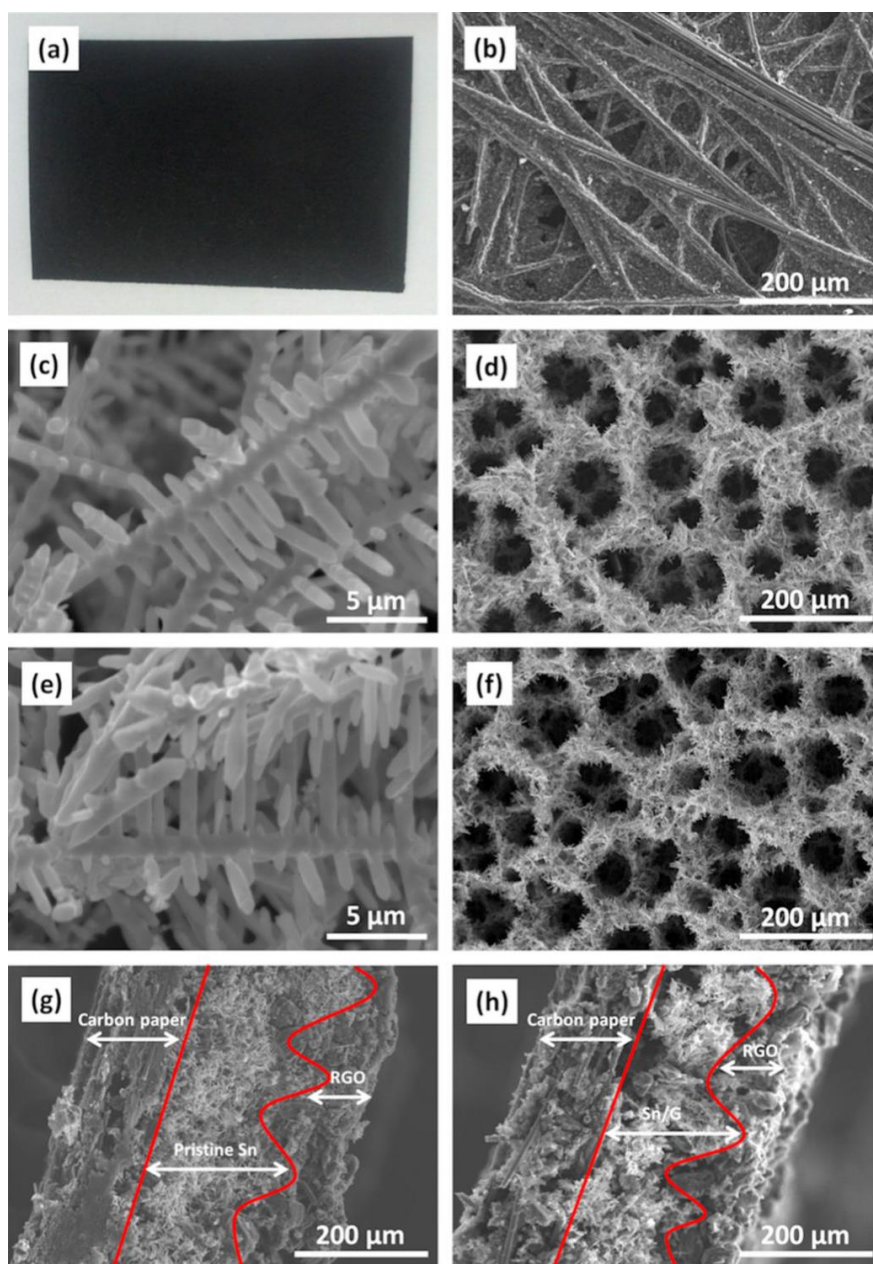
Figure 4.1.2 (a) Photo image of carbon paper and SEM image of (b) carbon paper, (c–d) Sn, (e–f) Sn-G composite at different magnifications, (g and h) cross sectional images of Sn/RGO and Sn-G/RGO.

Figures 4.1.2 (c,d) and (e,f) display the SEM images of highly porous 3D Sn and Sn-G samples at two different magnifications respectively. Both Sn and Sn-G composite show similar type of morphological characteristics with each dendrite being in the range of a few hundred nanometers. Figure 4.1.2 (g and h) shows the cross sectional images of the RGO coated on Sn (Sn/RGO) as well as on Sn-G composite (Sn-G/RGO) electrodes. The cross sectional images of both the samples show zig-zag type morphological appearance with high porosity. These sandwich type structures are expected to offer advantage in terms of compensating large volume change during the charge/discharge processes. Moreover, RGO coating on the surface of pristine Sn or Sn-G composite may protect the active material from the direct contact with the electrolyte to form progressive SEI during cycling.

4.1.2.2 X-ray Diffraction Analysis:

Representative X-ray diffraction patterns of Sn, Sn/RGO, Sn-G and Sn-G/RGO composites are shown in the figure 4.1.3. All the diffraction peaks of the electrochemically deposited tin samples can be assigned to pure phase of metallic tin (JCPDF: 00-04-673, tetragonal) with no other impurity [31]. The graphene peak at around 2θ of 26 degrees is not observed in the Sn-G composite (figure 4.1.3a), which clearly indicates that the high intensity peaks of Sn completely dominate the peak of graphene sheets. Recently, S. Ding et al.[24] have also reported that no diffraction pattern was observed for graphene based hybrid electrode material and the results suggested that very small amount of graphene was present in the sample with homogenous distribution. Whereas, the Sn/RGO and Sn-G/RGO samples exhibit broad peak at around 26º indicating the presences of RGO.

In order to observe the presence of graphene in the co-electrodeposited Sn-G composite, a small proportion of Sn was leached with dilute sulphuric acid (H_2SO_4). The FE-SEM images of the resulting Sn-G composite clearly displayed graphene-like nanostructures. Figure 4.1.3 (b and c) show the FE-SEM images of Sn and Sn-G, respectively. It can be seen from figure 4.1.3c that the growth of Sn dendrites is initiated on the surface of the graphene sheets. FE-SEM image of same sample in another area shows that the Sn dendrites are wrapped with graphene (in-set of figures 4.1.3c). This result was further supported by the TEM images as shown in figure 4.1.4. The TEM images indicate that the graphene is co-deposited along with Sn on the substrate. The presence of graphene in the sample is expected to improve the electrical conductivity of the electrode during the electrochemical process.
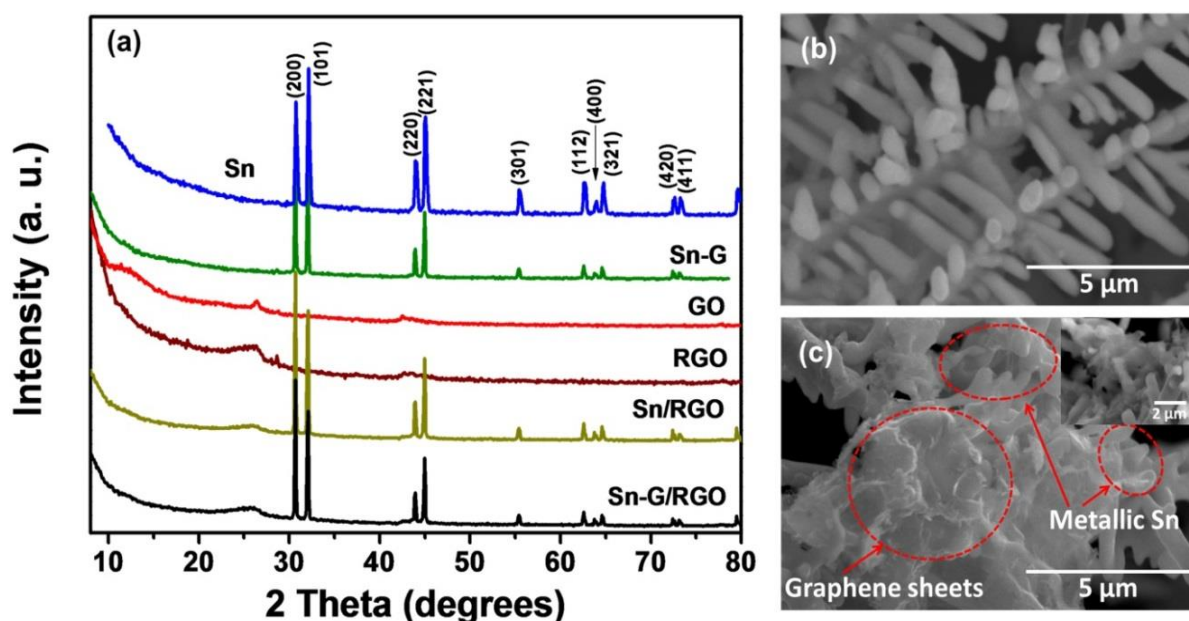
Figure 4.1.3 (a) X-ray diffraction patterns of Sn, RGO, GO, Sn-G, Sn/RGO and Sn-G/RGO composites, FE-SEM images (b) Sn and (c) Sn-G composite material after leaching in the presence of dilute H_2SO_4.
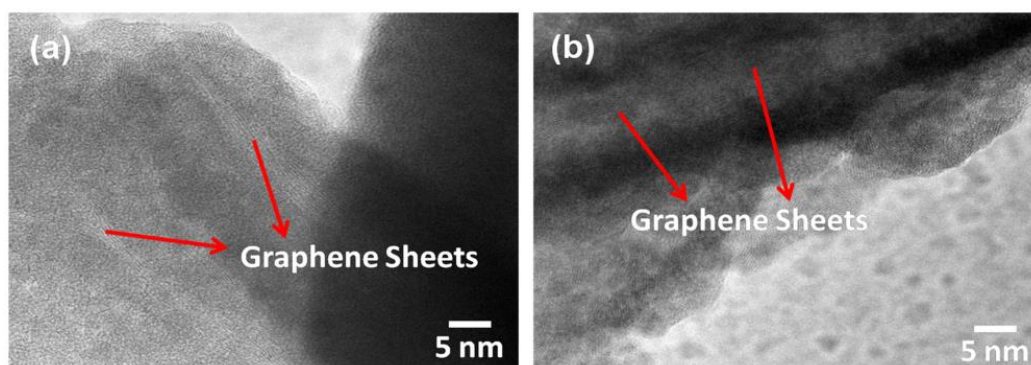
Figure 4.1.4 TEM images of Sn-G composite at two different locations showing the presence of graphene sheets.

4.1.2.3 Raman Spectral Analysis

The presence of graphene in the co-electrodeposited sample was confirmed by Raman spectra. Figure 4.1.5 shows the Raman spectra of RGO, GO, Sn, Sn/RGO, Sn-G and Sn-G/RGO composite electrodes. Raman spectrum of the reduced graphene oxide shows intense peaks at 1573 cm^{-1} and 1344 cm^{-1}, which correspond to the G and D bands of carbon, respectively [32]. The low intensity ratio I_D/I_G (0.42) for RGO indicates more graphitic nature of the sample. When Sn and GO are co-electrodeposited (figure 4.1.5), the intensity peak ratio of D and G bands slightly decreased ($I_D/I_G = 0.89$) when compared to GO ($I_D/I_G = 1.27$). This decrease in the intensity ratio indicates partial reduction of GO to graphene during cathodic

deposition. The presence of disordered structure of graphene in Sn-G composite has synergistic effect, i.e., it increases storage capacity and access of lithium ion diffusion during the charge/discharge process [33]. The Raman spectral analysis of Sn/RGO and Sn-G/RGO has also shown the features similar to that of the RGO spectrum, which infers the presence of highly graphitic carbon on the surfaces.
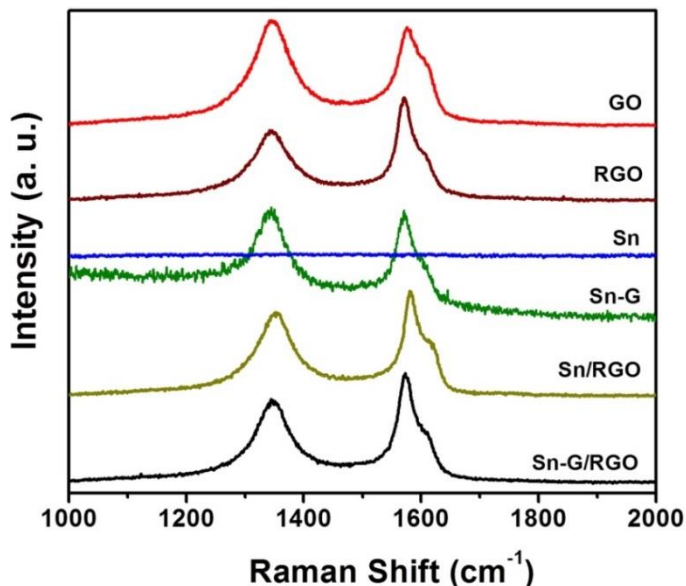
Figure 4.1.5 Raman spectra of GO, RGO, Sn, Sn/RGO, Sn-G and Sn-G/RGO samples.

4.1.3 Results and Discussion: Electrochemical Studies of the Tin/Graphene Anode Materials

The electrochemical performance of all the samples was evaluated by using lithium foil as the reference electrode and $LiPF_6$ as the electrolyte. Figure 4.1.6 represents the electrochemical performance of the anodes measured in the voltage range of 0.02-1.5 V vs. Li/Li$^+$ at 0.1 C rate. All the electrodes are binder free and carbon paper is used as the current collector. Figure 4.1.6 shows the charge-discharge cycle comparison of RGO, Sn, Sn/RGO, Sn-G and Sn-G/RGO composites. Initial discharge capacities of 1114 mAh g^{-1}, 878 mAh g^{-1}, 2249 mAh g^{-1}, 1113 mAh g^{-1} and 2035 mAh g^{-1} are obtained for RGO, Sn, Sn/RGO, Sn-G and Sn-G/RGO, respectively. Sn has shown rapid specific capacity decay and after 20 cycles it retained a capacity of only 97 mAh g^{-1}. The poor cycle performance of Sn is due to large volume expansion that resulted in degraded microstructure, which led to loss of electrical contact between the adjacent particles [34]. Although, porous dendritic structure of Sn facilitates the compensation for volume change due to Li alloying, the mechanical fracture that occurs during delithiation could not be controlled due to submicron structures. Freshly generated fractured Sn surface is prone to SEI formation on each cycle leading to progressive capacity

126

fading. It was reported that the smaller Sn nanoparticles perform better capacity retention due to minimum mechanical fracture and controlled SEI formation [35]. However, simple, scalable, and low cost methods like electrodeposition cannot yield very fine particles in nanometer scale. Only morphological features can be controlled in this process. The rapid capacity decay can be minimized by incorporating graphene into 3D Sn porous nanostructure by coelectrodeposition. The co-electrodeposited 3D Sn-G composite has shown better electrochemical performance and it retained a specific capacity of 270 mAh g^{-1} even after 20 cycles. Improved performance of the Sn-G electrode is mainly due to the presence of highly conductive graphene in the composite. The graphene oxide (GO) dispersed in the electrolyte gets partially reduced to graphene during the electrochemical deposition of Sn at the cathode in addition to hydrogen evolution. Electrochemical reduction of GO was also observed during the electrochemical deposition of Cu-RGO composites [27]. Interestingly, when RGO was coated on the surface of both pristine Sn (pristine Sn/RGO) and Sn-G (Sn-G/RGO), the cells retained high discharge capacities of 413 mAh g^{-1} and 769 mAh g^{-1}, respectively, after 20 cycles. The reasonable capacity retention of RGO coated samples may be due to the presence of a protective RGO layer on the surface that prevents the electrolyte from direct contact with Sn and major amount of SEI layer is expected to form on RGO. Among these two electrodes, Sn-G/RGO composite exhibited higher reversible capacity and cycle performance due to the presence of graphene in the co-electrodeposited Sn-G nanostructure that can further improve the electronic conductivity.
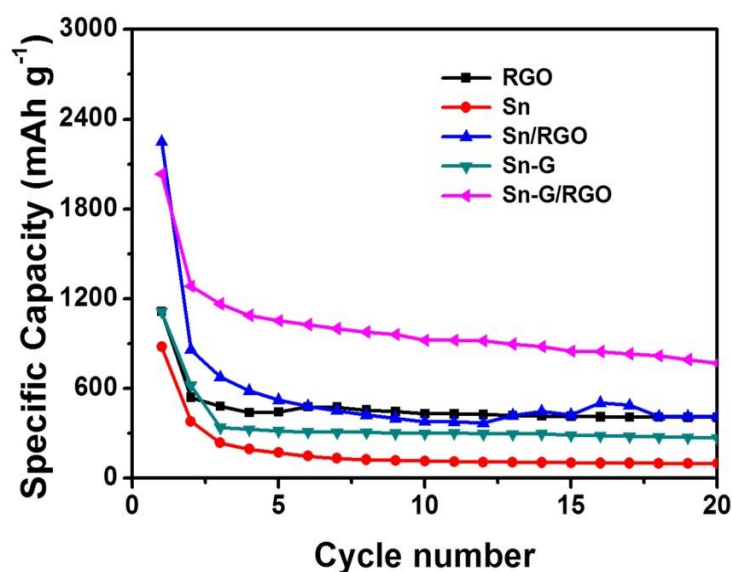
Figure 4.1.6 Comparative cycle performance curves of RGO, Sn, Sn/RGO, Sn-G and Sn-G/RGO measured at 0.1 C rate.

The improved electrochemical performance of these electrodes was further supported by the electrochemical impedance measurements. Figure 4.1.7 shows the Nyquist plots of Sn, Sn/RGO, Sn-G and Sn-G/RGO measured after two charge/discharge cycles. In the high frequency region, Sn/RGO, Sn-G and Sn-G/RGO samples show a depressed semicircle, which corresponds to charge transfer resistance (R_{ct}) in the cell at the electrode-electrolyte interface. Whereas, the Nyquist plot of Sn electrode showed two depressed semicircles in the high and medium frequency regions. The former semicircle corresponds to R_{ct} and the latter one is due to the formation of a thick SEI layer on the surface of anode. This result is in agreement with the electrochemical performance of Sn anode, which showed poor cycle stability after the first cycle. Y. Liu et al.[36], also observed that the use of reduced graphene oxide enhances the charge transfer process, which reduces the internal resistance of the cell. An inclined line is observed in Nyquist plots of all the samples at low frequency region, which corresponds to the Warburg impedance. The Warburg impedance is associated with the diffusion of lithium ions between the electrodes. The experimental results are fitted well with the equivalent circuits as shown in the figure 4.1.7. R_s represent the electrolyte resistance, R_{ct} is the charge transfer resistance, CPE is the constant phase element and W_o is the Warburg resistance associated with diffusion of ions.
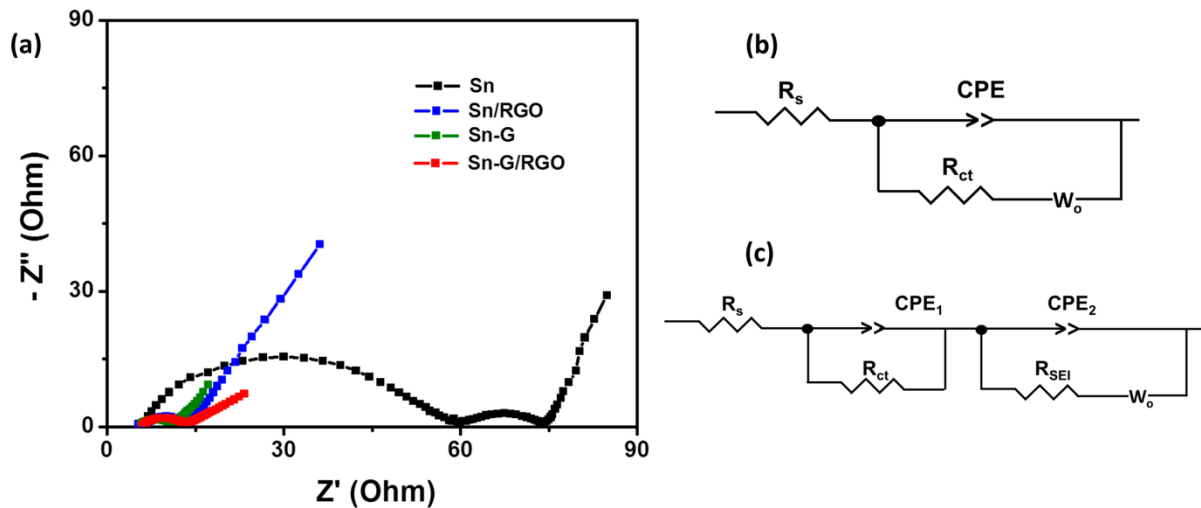
Figure 4.1.7 (a) Nyquist plots of Sn, Sn/RGO, Sn-G and Sn-G/RGO electrodes measured after two charge/discharge cycles, (b) Equivalent circuit for Sn/RGO, Sn-G and Sn-G/RGO and (c) Equivalent circuit for Sn.

The charge transfer resistance values of Sn, Sn/RGO, Sn-G and Sn-G/RGO composites are calculated to be 53.47Ω, 10.12Ω, 5.92Ω and 7.34Ω, respectively. The lower

charge transfer resistance (R_{ct}) of graphene containing Sn electrodes in comparison to pure Sn electrode indicates the fast Li-ion diffusion kinetics during the redox process and thus the cell exhibits superior electrochemical performance. A slight increase in R_{ct} value of Sn-G/RGO electrode in comparison to Sn/G electrode is due to increase in thickness of the electrode after coating with RGO [37].
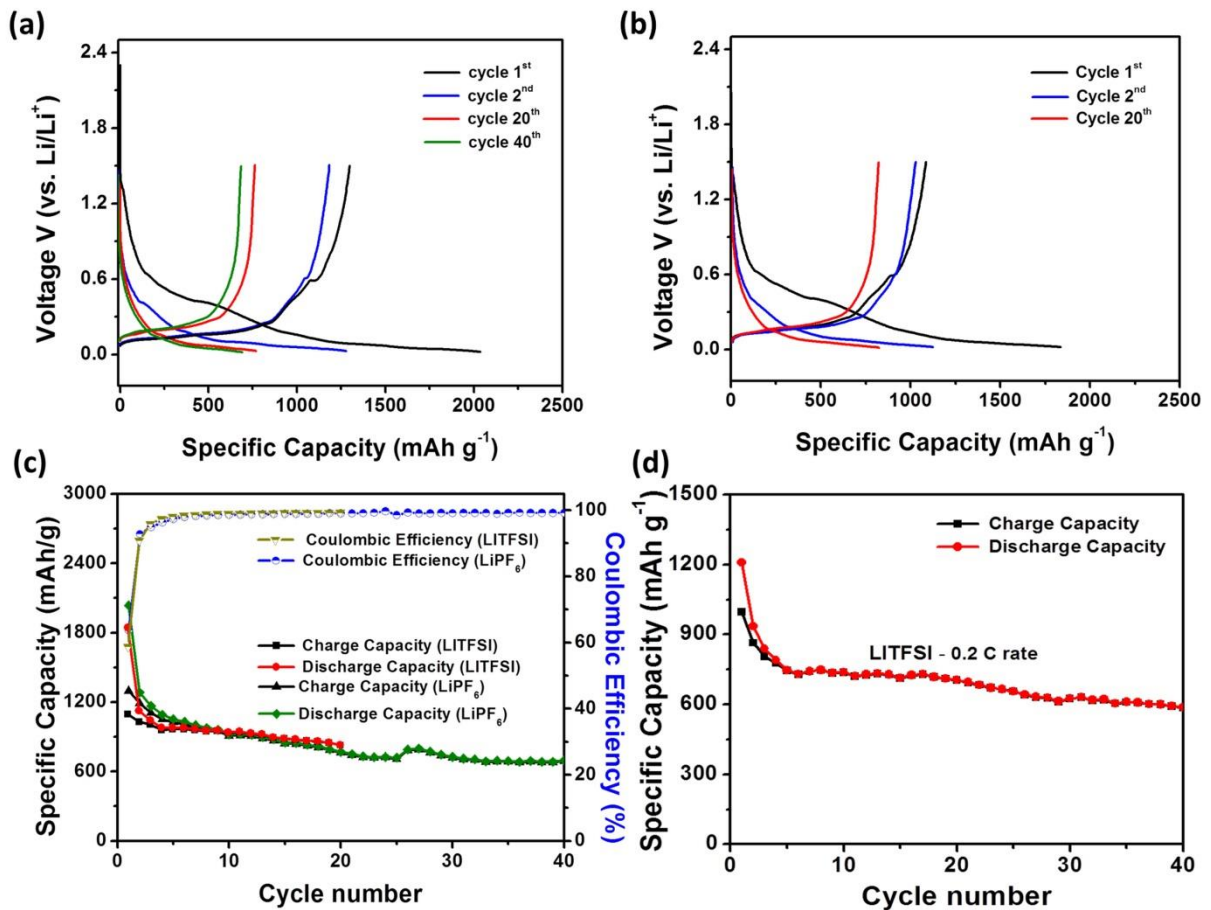
Figure 4.1.8 (a) Charge-discharge profiles of Sn-G/RGO anode with 1M LiPF$_6$ (EC:DMC) and (b) 1M LITFSI electrolyte with 5 wt% of LiNO$_3$ additive measured at 0.1 C rate in the potential range 0.02 to 1.5 V, (c) comparative cyclic performance of Sn-G/RGO electrode in both the electrolyte solutions and (d) Cycle performance of Sn-G/RGO electrode measured at 0.2 C rate.

As the Sn-G/RGO electrode exhibited the highest discharge capacity, it was further selected for comparing the electrochemical performance with 1M LITFSI electrolyte. Figure 4.1.8a shows the typical charge-discharge profiles of the sandwich type Sn-G/RGO composite measured at 0.1 C rate in the voltage range of 0.02-1.5 V using 1M LiPF$_6$ as the electrolyte. During the first cycle, the Sn-G/RGO composite delivered very high discharge and charge capacities of 2035 mAh g^{-1} and 1298 mAh g^{-1} respectively. The initial cycle shows an

irreversible capacity loss of about 37%. The large irreversible capacity loss is attributed to SEI layer formation and the excess lithium ions stored in the active sites of 3D porous Sn and disordered structure of graphene sheets due to the high surface to volume ratio [35,38]. In the second cycle, the irreversible capacity loss was reduced to 11% and after 40 cycles, the anode material still retained a specific capacity of 696 mAh g^{-1}, with a coulombic efficiency of more than 98%. The electrochemical performance of Sn/G/RGO electrode was also measured with 1M LITFSI electrolyte with 5 wt% of LiNO$_3$ additive for the purpose of comparison (Figure 4.1.8b), as this electrolyte is used in Li-S battery due to its high electrochemical stability towards polysulfide species. Initially, the cell delivered high discharge and charge capacities of 1833 mAh g^{-1} and 1086 mAh g^{-1}, respectively and are comparable with that of the cell measured in 1 M LiPF$_6$ electrolyte solution. Even after 20 cycles, the anode displayed high specific capacity of 819 mAh g^{-1} and the coulombic efficiency is close to 100% (Figure 4.1.8c). Further, the Sn-G/RGO electrode was also tested at 0.2 C rate in 1M LITFSI electrolyte containing 5 wt% of LiNO$_3$. The resulting cell delivered a high discharge capacity of 587 mAh g^{-1}, even after 40 cycles as shown in figure 4.1.8d.

The rate capability of Sn-G/RGO electrode was studied at different current rates by using both the electrolyte solutions, as shown in the figure 4.1.9. It can be observed that the electrodes delivered comparable electrochemical responses at different current rates. The electrode with 1M LiPF$_6$ (EC:DMC) delivered the discharge capacities of 1243 mAh g^{-1}, 758 mAh g^{-1}, 233 mAh g^{-1} at current rates of 0.1 C, 0.2 C and 0.5 C, respectively, while the corresponding values observed for 1M LITFSI electrolyte with 5 wt% of LiNO$_3$ additive are 1091 mAh g^{-1}, 621 mAh g^{-1}, 164 mAh g^{-1}. Furthermore, when the current rate is changed from 0.5 C to 0.1 C, the cells retained discharge capacities of 902 mAh g^{-1} with 1M LiPF$_6$ and 926 mAh g^{-1} with 1M LITFSI containing 5 wt% of LiNO$_3$. Excellent capacity retention of Sn-G/RGO may be because of the synergistic effect of the presence of graphene in the Sn-G composite and RGO coating on the surface. This synergistic effect is explained hereunder. The presence of graphene in the co-electrodeposited Sn-G composite acts as a matrix for the mechanically disintegrated Sn particles and increases the electrical conductivity of the electrode. Whereas, the RGO coating on the surface of Sn-G electrode also acts as a conductive matrix, accommodates large volume expansion and protects the surface from the formation of thick SEI layer. In addition, the large open porous structure facilitates easy access of the electrolyte throughout the electrode and allows rapid transport of lithium ions during the redox process. The discharge capacity delivered by the electrodeposited Sn-

G/RGO composite is higher than the values reported in the literature on electrodeposited Sn based composites [13,14,16] and comparable with the other chemically synthesized Sn/graphene composites [10,18]. Thus, the simple, cost-effective and easy synthetic process developed in the present study may find a path for large scale commercialization of the Sn-G/RGO composite material for energy storage application.
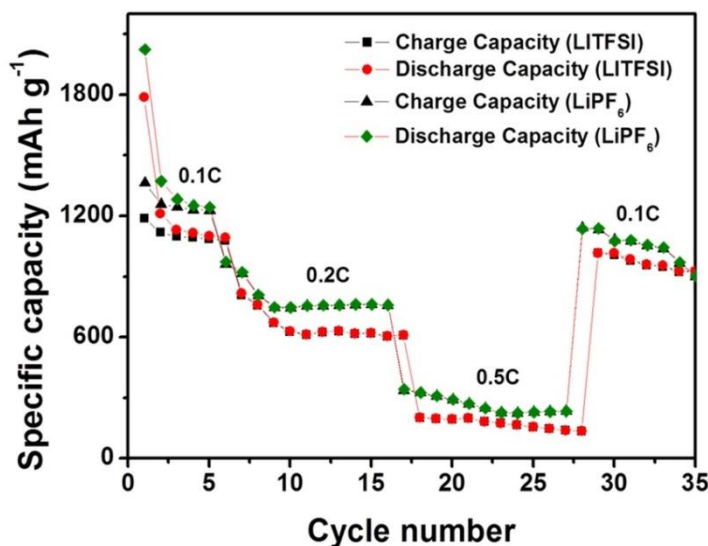
Figure 4.1.9 Rate capability of Sn-G/RGO electrode measured in 1M $LiPF_6$ (EC:DMC) and 1M LITFSI electrolyte with 5 wt% of $LiNO_3$ additive at different current rates.

4.1.4 Conclusions

A simple and cost effective electrodeposition method was employed for the synthesis of the high capacity anode materials. The fabricated anodes are binder-free with 3D highly porous dendritic structures. A protective RGO layer is coated onto the surface of Sn-G composite in order to minimize the progressive SEI layer formation. As a result, an excellent electrochemical performance was obtained for the Sn-G/RGO anode in both the $LiPF_6$ and LITFSI plus 5 wt % of $LiNO_3$ electrolyte systems. The optimal performance exhibited by the Sn-G/RGO anode is mainly due to the synergistic effect of the presence of highly conductive graphene in Sn-G matrix and RGO coating on the surface.

Section 4.2 Synthesis of Silicon/Graphite Composite as an Anode Material

Development of nanostructured silicon based composites reduces the disintegration of active material from the current collector due to smaller size of Si particles and also decreases the volume expansion created during lithiation. The novel electrode structures such as Si/graphene [39,40], Si/CNT [41,42], Si nanosheets [43], Si/conductive polymers [44], Si nanowires [45], mesoporous Si and hollow structures [46,47] have shown an improved electrochemical performance over long cycles. However, the preparation of these materials involves tedious experimental conditions, use of toxic chemicals and high cost precursors, which limit the commercialization of this system. Among the different approaches employed for the fabrication of nanostructured Si, the ball-milling method is considered to be a cost-effective and simple process [48]. The ball-milled Si-graphite (Si/G) composite has been explored for Li-ion batteries by using $LiPF_6$ as electrolyte and has shown an excellent electrochemical stability for longer cycles. For example, J. Nzabahimana et al. [49] synthesized silicon/carbon composite, wherein the porous nanostructured silicon is prepared by ball-milling and chemical etching process followed by carbon coating on it. They have studied the effect of milling time (1h, 2h, 3h, 4h and 5h) on the morphology, crystallinity and electrochemical performance of these composites. The 2 h milled sample delivered the highest discharge capacity of 834 m Ah g^{-1} at 2 A g^{-1} at 200th cycle. S. Huang et al. [50] synthesized phosphorous doped Si/graphite composite by two-stepped ball milling process. The P-doped Si and graphite with 1:1 weight ratio on the electrode exhibited the highest discharge capacity of 883 mAh g^{-1} at 0.2 A g^{-1} current density even after 200 cycles. To the best of the investigator's knowledge, the electrochemical performance of Si/graphite composite has not been studied with LITFSI electrolyte, which motivated the investigator to study this system for Li-S battery application.

3.2.1 Synthesis of Si/Graphite Composite

The laboratory reagent grade silicon and graphite powders were used for the preparation of Si/G composites. The silicon and graphite powders were weighed in the mass ratios of silicon:graphite as 0:1, 0.3:0.7, 0.5:0.5, 0.7:0.3 and 1:0, the total mass being equal to 2 g. Then 2 ml of ethanol was added to the weighed powders and the resulting mixtures were ball milled by using planetary ball mill at 250 rpm for 10 h. Figure 4.2.1 Show the schematic representation for the synthesis of Si/G composites and the cell fabrication process. The resulting samples were washed with 0.1 M HF and then washed several times with DI water

in order to remove surface oxides of silicon followed by drying in an oven at 80 ℃. The ball milled Si/G composites with weight ratios of 0:1, 0.3:0.7, 0.5:0.5, 0.7:0.3 and 1:0 are labelled as G, Si3/G7, Si5/G5, Si7/G3 and Si, respectively.

The electrochemical performance of these composites has been evaluated by using lithium foil as the reference electrode and 1M LITFSI containing 5wt% $LiNO_3$ as electrolyte. The working electrode for anodes was prepared by mixing the active material, super P carbon and sodium alginate (binder) in the weight ratios of 60:20:20 in DI water. The homogenously mixed slurry was coated on the carbon paper (current collector) followed by drying in an oven at 60 °C for 12 h. After drying, the electrodes were punched into 12 mm discs and used for the fabrication of the cells. The amount of active material loading onto the electrode is about 1.2-1.5 mg cm^{-2}. The detailed methodology for characterization and electrochemical studies has been presented in the chapter 2.
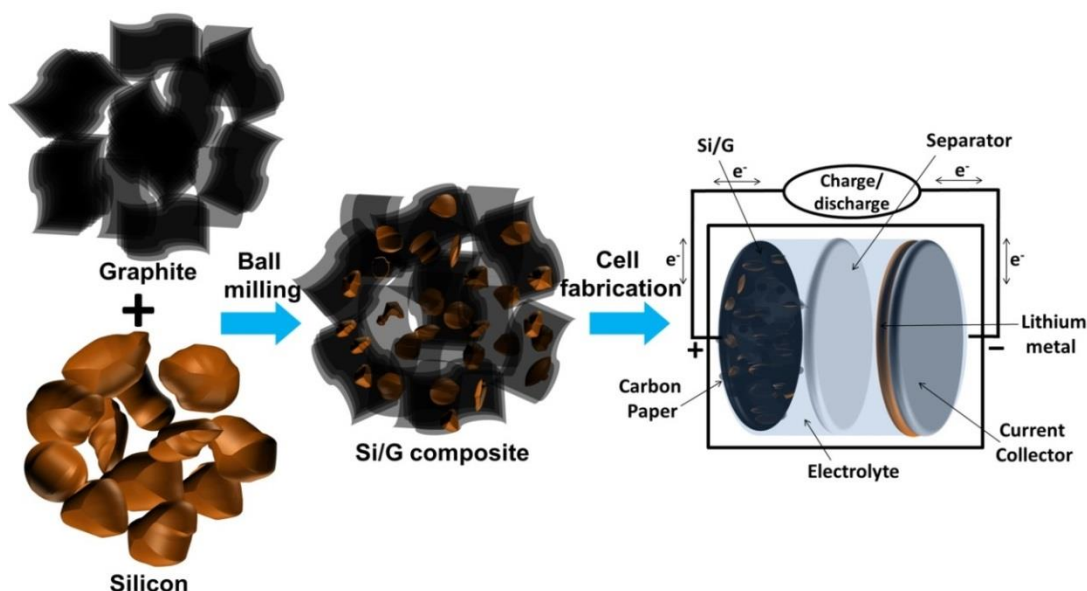
Figure 4.2.1 Schematic representation for the synthesis of Si/G composite and the cell fabrication process.

4.2.2 Results and discussion: Characterization of the Silicon Based Anodes
4.2.2.1 Morphological Analysis:

The morphology and the particle size of the samples have been investigated by using FE-SEM and TEM. Figure 4.2.2 shows the SEM and TEM images of G, Si3/G7, Si5/G5, Si7/G3 and Si composites. It can be seen from the figure 4.2.2 that the particle size of silicon decreases during ball-milling process, indicating proper blending of both the materials. This has been further confirmed by the TEM analysis, in which small silicon particles are well distributed on the graphite sheets. The uniform distribution of silicon with graphite is

expected to improve the electrical conductivity of the electrode during the charge/discharge process.
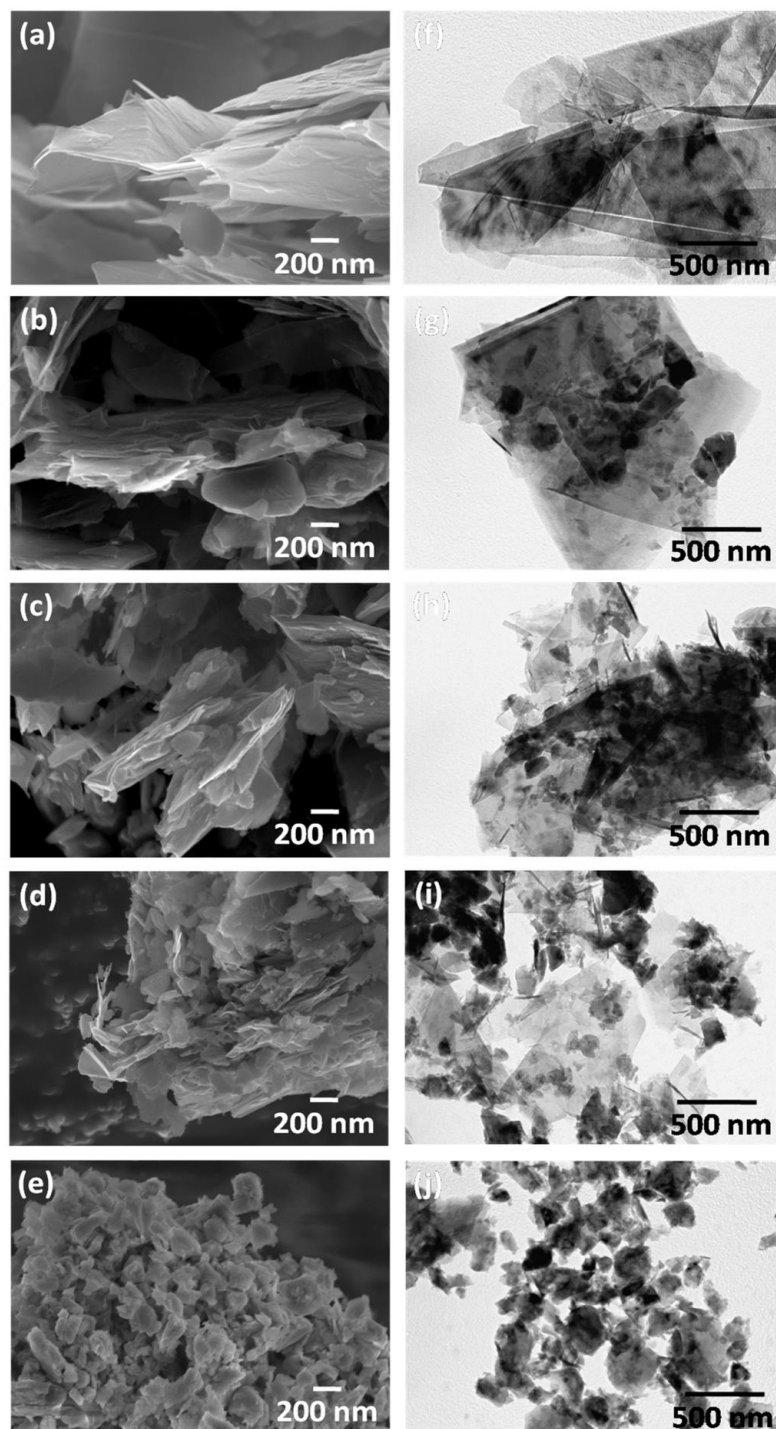
Figure 4.2.2 SEM and TEM images of G (a and f), Si3/G7 (b and g), Si5/G5 (c and h), Si7/G3 (d and i) and Si (e and j).

4.2.2.2 EDS Elemental Mapping:

The EDS elemental mapping was conducted on the composite materials in order to study the distribution of silicon and graphite in the samples. It is clearly observed from the figure 4.2.3 that the silicon is homogenously distributed throughout the graphite matrix.
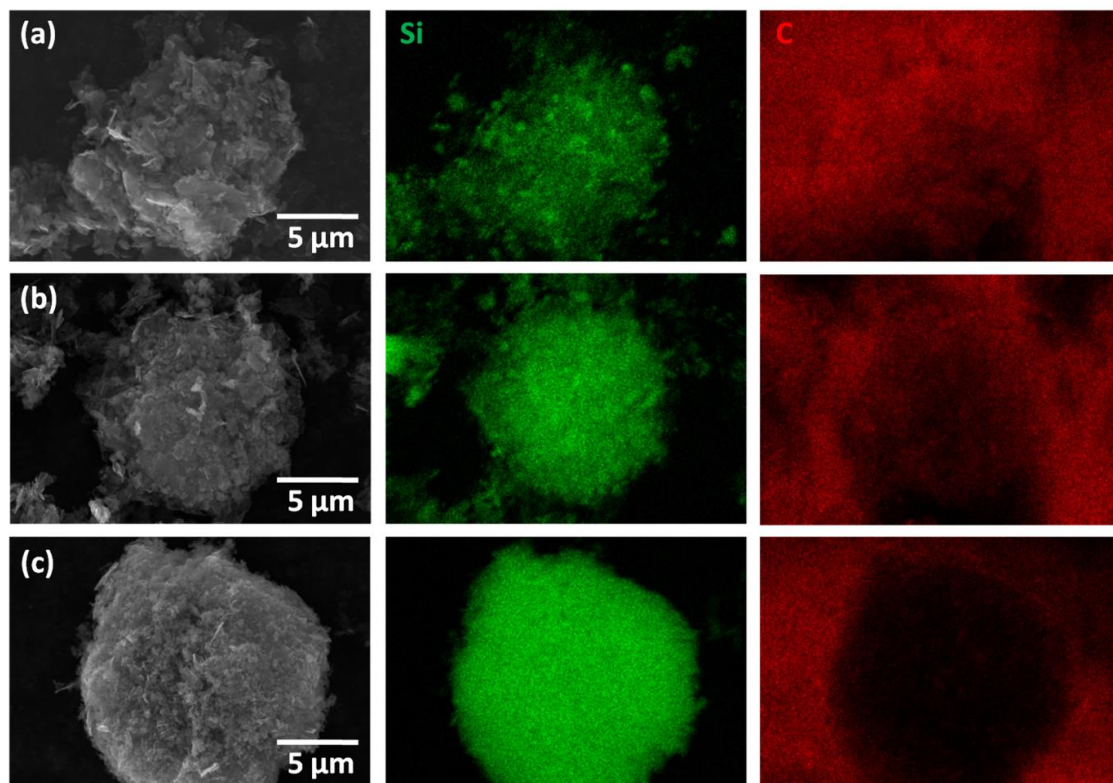
Figure 4.2.3 EDS elemental map of Si3/G7 (a), Si5/G5 (b) and Si7/G3 (c) composites with silicon (green) and graphite (red).

4.2.3.3 X-ray Diffraction Analysis:

The X-ray diffraction patterns of the synthesized G, Si3/G7, Si5/G5, Si7/G3 and Si materials are shown in the figure 4.2.4. The graphite showed one sharp peak at two theta value of 26º, which corresponds to (002) plane of the crystalline form of graphite (JCPDF 75-1621) [51]. In the case of silicon, three distinct peaks appeared at 28º, 47º and 56º, which are attributed to (111), (220) and (311) planes of the crystalline silicon (JCPDF 27-1402). T. Schott et al. [52] also observed similar type of XRD patterns for silicon in the composite. Whereas, the X-ray diffraction patterns of composite materials (Si3/G7, Si5/G5, Si7/G3) displayed the peaks corresponding to polycrystalline silicon and graphite. Moreover, it is also observed that the peak intensity of silicon increases with an increase in silicon content in the composite. This result confirms the existence of both silicon and graphite in crystalline form even after the ball milling process.
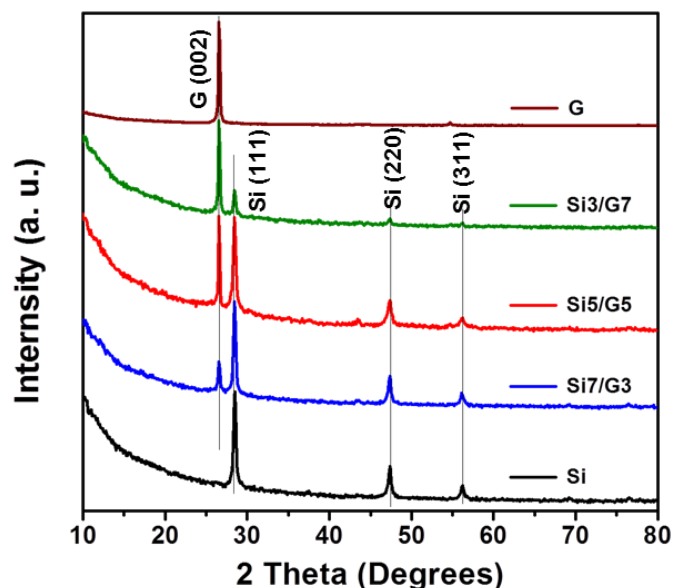
Figure 4.2.4 XRD patterns of G, Si3/G7, Si5/G5, Si7/G3 and Si.

4.2.2.4 Raman Spectral Analysis

In order to further confirm the existence of silicon and graphite in the composite materials and also study the graphitic nature of carbon, the synthesized samples have been subjected to Raman spectral analysis. Figure 4.2.5 shows the Raman spectra of G, Si3/G7, Si5/G5, Si7/G3 and Si materials. The Raman spectrum of graphite displayed two characteristic peaks at 1350 cm^{-1} and 1600 cm^{-1}, which correspond to the D and G peaks, respectively. The former peak can be assigned to A_{1g} vibration mode of defective carbon atoms. Whereas, the later peak in the spectrum resulted from the E_{2g} vibration mode of nanocrystalline graphite [53]. Moreover, a 2D peak appeared at a Raman shift of 2700 cm^{-1} in the sample, which infers the presence of multi-layered graphene-like structure in the sample [54]. The I_D/I_G ratios of graphite such as 0.20, 0.19 and 0.28 for Si3/G7, Si5/G5 and Si7/G3 composites, indicate the presence of more graphitic structure in the sample even after the ball-milling process. Pure silicon exhibits a sharp peak of high intensity at a wavenumber of 515 cm^{-1} and two peaks of less intensity at 295 cm^{-1} and 950 cm^{-1}, which are characteristic of nanostructured silicon [55]. The composite materials also display the peaks corresponding to nanostructured silicon in addition to the D and G bands of the carbon atoms. These results infer the existence of both silicon and graphite in the composites and the presence of graphite is expected to improve the electrical conductivity during the redox process.
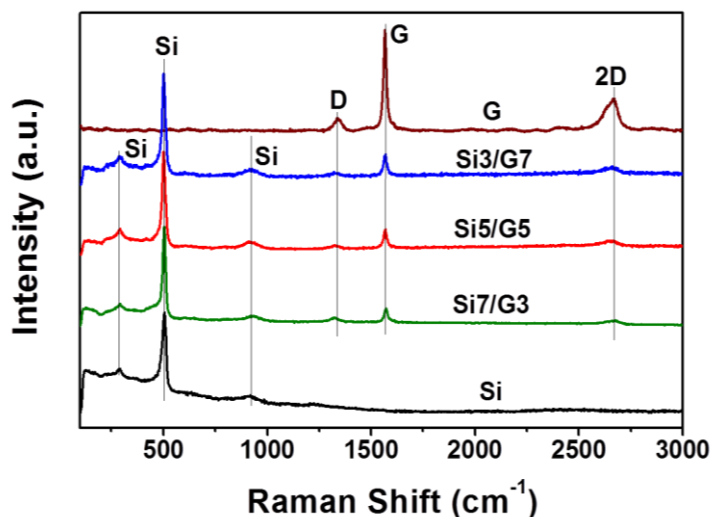
Figure 4.2.5 Raman spectral of G, Si3/G7, Si5/G5, Si7/G3 and Si composites.

4.2.3 Results and Discussion: Electrochemical Studies of Silicon Based Anodes

The electrochemical performance of G, Si3/G7, Si5/G5, Si7/G3 and Si anodes has been evaluated by using lithium metal as the reference electrode and LITFSI as the electrolyte. Figure 4.2.6 shows the comparative cycle performance curves of these anodes measured in the voltage range of 0.01-1.5 V at 0.2 C rate. The carbon paper is used as the current collector for these materials. The three dimensional continuous networks of carbon provide high electrical conductivity, while the internal voids in the carbon paper accommodate large volume variation during the lithiation process [30]. As a result, the electrode showed good electrochemical stability and the cell exhibited improved electrochemical performance upon repeated charge/discharge processes. Initial discharge capacities of 674 mAh g^{-1}, 2248 mAh g^{-1}, 3581 mAh g^{-1}, 3881 mAh g^{-1}, and 4373 mAh g^{-1} are obtained for G, Si3/G7, Si5/G5, Si7/G3 and Si, respectively. Though the pure silicon delivered the highest discharge capacity, the volume expansion during charge/discharge process leads to poor cycle performance and the cell retained a discharge capacity of only 673 mAh g^{-1} after 40 cycles. Whereas, the discharge capacity of graphite is reduced from 674 mAh g^{-1} to 316 mAh g^{-1} after 40 cycles. The poor electrochemical performance of the silicon anode after 40 cycles is due to mechanical disintegration of the active material from the current collector. Therefore, the fractured particles with fresh surfaces are prone to formation of SEI layer on each cycle, which leads to an increase in the thickness of the SEI layer and thus the cell showed severe capacity fading with repeated charge/discharge processes [52]. Whereas, the composites delivered an enhance performance with the specific capacities of 884 mAh g^{-1}, 1496 mAh g^{-1} and 1264 mAh g^{-1} for Si3/G7, Si5/G5, Si7/G3 electrodes, respectively after 40 cycles. The

presence of graphite in the composite, acts as a matrix for the mechanically fractured silicon particles during lithiation. Moreover, it can also accommodate huge volume expansion. Among the composites, the Si5/G5 electrode exhibited the highest discharge capacity due to optimised weight ratio of silicon and graphite in the composite.
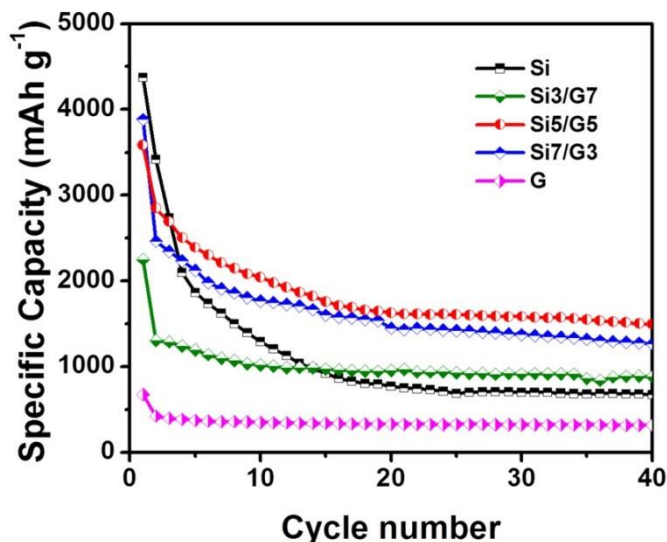
Figure 4.2.6 Comparative cycle performance curves of G, Si3/G7, Si5/G5, Si7/G3 and Si electrodes measured at 0.2 C rate in the potential range, 0.02 to 1.5 V.

The Si5/G5 electrode has been further evaluated by CV studies as shown in the figure 4.2.7. During the initial cathodic scan, a broad band from 0.4 V to 0.7 V is observed, which corresponds to the decomposition of the organic electrolyte and the formation of SEI layer on the surface of the electrode [56]. This band is not observed in the subsequent cycles indicating the good chemical stability of the electrode. In the anodic scan, the peaks at 0.32 V and 0.51 V correspond to the de-alloying of the lithiated silicon [57]. In the subsequent cycles the cathodic peak observed at 0.19 V indicates the alloying of silicon with lithium during the lithiation process. In these cycles, same delithiation peaks are obtained during the anodic scan ant lithiation peak is obtained during the cathodic scan. Thus, the CV studies establish the reversible nature of the Si5/G5 electrode.
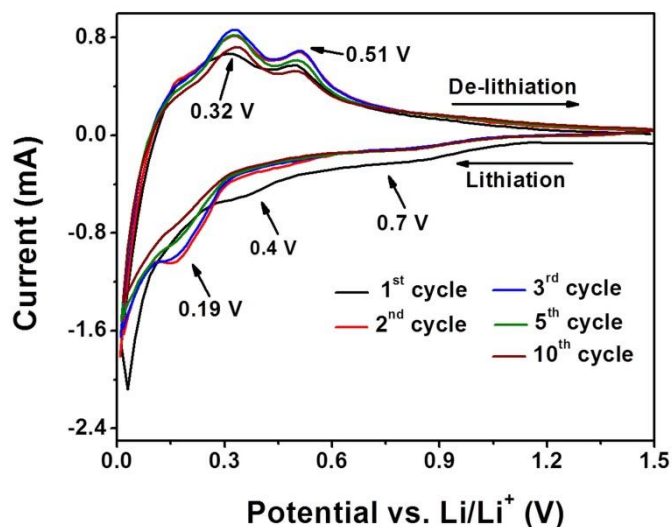
Figure 4.2.7 Cyclic voltammetric profile of Si5/G5 electrode measured in the potential range of 0.01-1.5 V at 0.1 mV s^{-1} scan rate.

Figure 4.2.8a shows the galvanostatic charge/discharge profile for the first three cycles of Si5/G5 anode. The cell delivered high initial discharge capacity of 3574 mAh g^{-1} at 0.2 C rate. Large irreversible capacity loss is observed in the first cycle, which is due to the formation of SEI layer on the surface of the electrode. A long flat discharge curve is observed at a plateau less than 0.15 V, which corresponds to delithiation from the lithiated silicon particles. The electrode showed a capacity fading in the initial cycles and gets stabilized after a few cycles. Even after 50 charge/discharge cycles, the Si5/G5 electrode displayed a high discharge capacity of 1443 mAh g^{-1} (figure 4.2.8b). Furthermore, when the current rate is increased to 1 C, the electrode exhibited a discharge capacity of 816 mAh g^{-1} even at 200th cycle (figure 4.2.8c). The remarkable electrochemical performance delivered by this electrode is mainly due to smaller particle size of silicon and its homogeneous distribution throughout the conductive graphite. Moreover, the use of carbon paper substrate has synergistic effect in improving the electrochemical performance of the cell i.e., it can accommodate large volume expansion during alloying/de-alloying processes and also act as fast electron transport medium. The discharge capacity delivered by the Si/graphite composite with LITFSI electrolyte is comparable with discharge capacity of the ball milled Si based composites with LiPF$_6$ electrolyte [48,49,53,55]. Thus, the simple, cost-effective and easy synthetic process developed in the present study may find a path for large scale commercialization of this system as anode material in a Li-S battery.
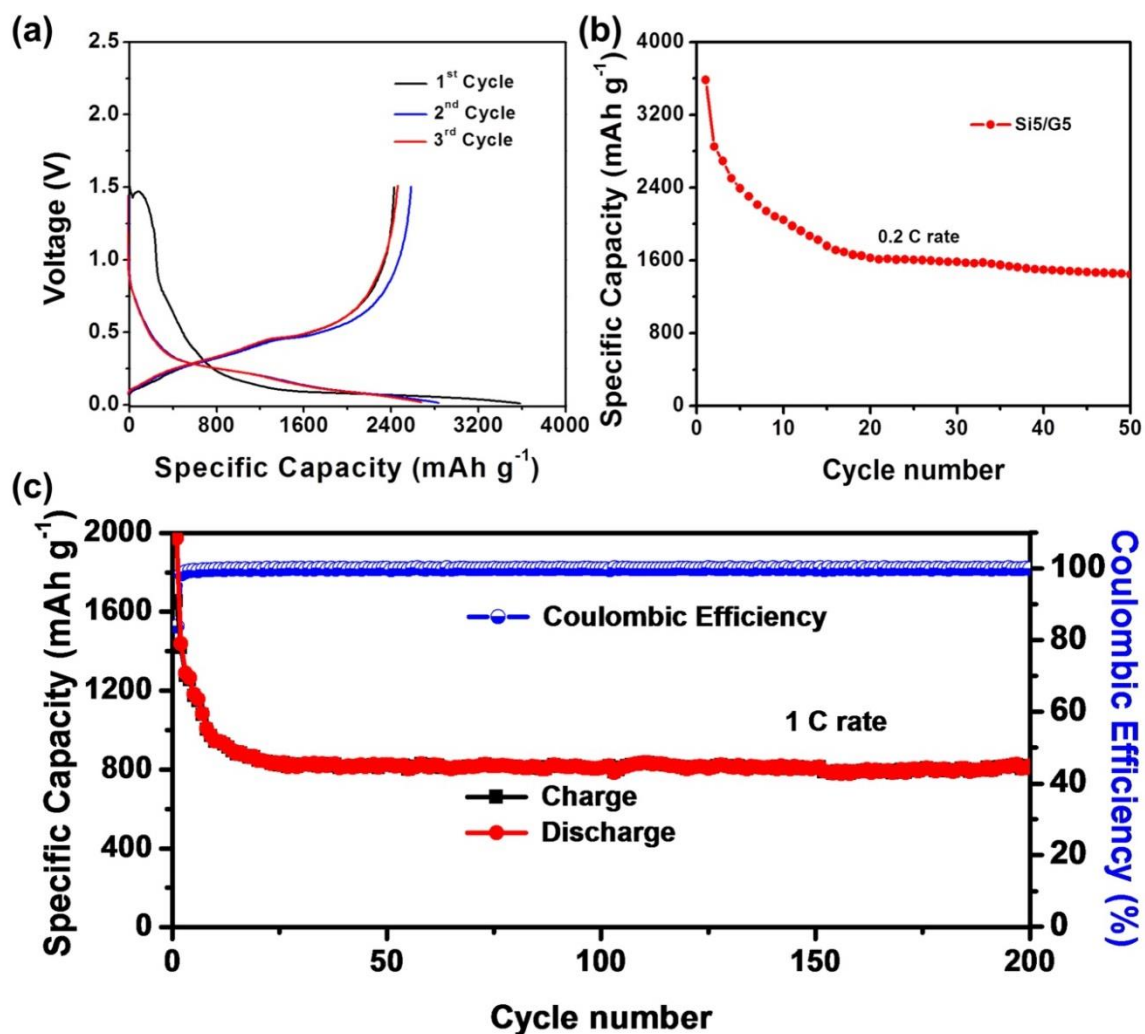
Figure 4.2.8 (a) Charge/discharge profile, (b) cycle performance curve of Si5/G5 electrode measured at 0.2 C rate, and (c) cycle performance curve of Si5/G5 electrode measured at 1 C rate for 200 cycles.

4.2.4 Conclusions

The electrochemical performance of the ball milled Si/graphite composite with different weight ratios has been evaluated by using 1M LITFSI with 5 wt % LiNO$_3$ as electrolyte. The Si5/G5 composite anode prepared by using 1 g of silicon and 1 g of graphite, delivered highest initial discharge capacity of 3574 mAh g^{-1} and retained the capacity of 1443 mAh g^{-1} even after 50 cycles at 0.2 C rate. Further, when the current rate is increased to 1 C, the electrode exhibited high discharge capacity of 816 mAh g^{-1} even at 200th cycle.

Section 4.3 Fabrication of Lithiated Si-S Full Cell using Porous Carbon/Sulfur Cathode and Lithiated Silicon/Graphite Anode

The fabrication of Li-S battery in full cell configuration without the use of lithium metal anode is highly challenging. One such breakthrough was made by J. Hassoun et al.[58] wherein the lithium metal-free Sn-S battery was fabricated by using Li_2S/C cathode and Sn/C anode with gel polymer electrolyte. The resulting cell operating at 2.5 V delivered high discharge capacity of about 1200 mAh g^{-1} (calculated using the mass of Li_2S only) at 0.01 C rate. Y. Yang et al.[3] assembled a Li_2S-Si battery with Li_2S/mesoporous carbon cathode and silicon nanowire anode with bis(triflouromethane)sulfonamide lithium salt (LITFSI) dissolved in 1:1 v/v 1,3-dioxalane (DOL) and dimethoxyethane (DME) electrolyte. This cell delivered a high initial discharge capacity of 423 mAh g^{-1} at 0.3 C rate with an average voltage of 1.7 V. The research has also been directed towards the use of pre-lithiated anodes, which have shown excellent improvement in the electrochemical performance [59,60]. The capacity delivered by the Li-S cell is 3-5 times higher than the currently used Li-ion batteries as shown in the figure 4.3.1.
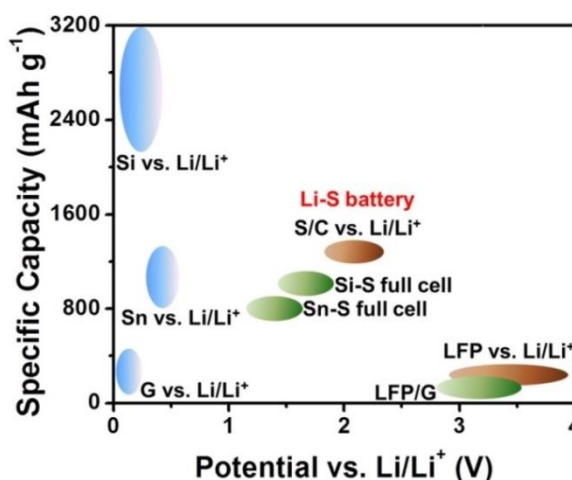
Figure 4.3.1 Specific capacity vs. voltage profiles of half cells and full cells used in Li-S and Li-ion batteries respectively.

Though the Li-S full cell with novel cell configuration exhibits improved electro-chemical performance over the repeated the charge/discharge processes, the synthetic process for the preparation of the electrode materials involved the use of expensive chemicals, complex procedures and tedious experimental conditions [59,61,62]. Therefore, the investigator aimed to develop a simple and cost effective approach to fabricate high performance Li-S battery in full cell configuration by using the best performed MGC/S-2 cathode and Si5/G5

anode developed in the present study. Moreover, the low operating voltage of Si based composite has an advantage that it increases the cell voltage when coupled with the sulfur cathode. The resulting cell also exhibited high energy density.

4.3.1 Fabrication of Lithiated Si-S Full Cell:

Preparation of the Electrodes

The detailed synthesis of the electrode materials, characterization and processing of the electrode have been discussed in their respective chapters. The MGC/S-2 electrode is discussed in the chapter 3 under the section 3.3 and the Si5/G5 electrode is discussed in the chapter 4 under the section 4.2.

Fabrication of Lithiated Si-S Full Cells

The electrochemical studies of the full cells were carried by using MGC/S-2 as the cathode, Si5/G5 as the anode and 1M LITFSI dissolved in a mixture of 1:1 v/v DOL and DME solvents with 5 wt % of $LiNO_3$ additive as the electrolyte. The two electrodes were separated by polypropylene membrane (celgard-2400) and all the cells were assembled in argon filled glove box. A similar procedure has been employed for the fabrication of lithiated Si-S full cell as used in case of sulfur cathode half cell described in the chapter 2, except that a known amount of very thin lithium foil is placed on the surface of the Si5/G5 anode. The electrodes were punched into 12 mm discs. The amount of active material loading on the cathode (sulfur) is in the range of 2.0-2.4 mg. The amount of Si5/G5 composite material is in the range of 1.2-1.5 mg on the anode. The amount of active material loading on the anode is varied according to the amount of active material loading on the cathode for systematic studies of the full cell. The mass ratios of S, Li and Si are given under section 4.3.2: electrochemical studies. All the fabricated cells were kept for stabilization for 24 h before the commencement of the testing of the cells. The capacities were calculated, based on the mass of active sulfur present on the electrode.

4.3.2 Results and Discussion: Electrochemical Studies (CV, CD and CY) of the Lithiated Si-S Cell

The electrochemical performance of the lithiated Si-S battery has been evaluated by using the MGC-2/S cathode and lithiated Si5/G5 as anode. The thin lithium foil placed on the anode is the source of lithium ions. This type of novel cell configuration was reported in the literature and the resulting full cell delivered an improved electrochemical performance with cycling [63]. This simple approach helps in systematic study of lithium introduction into the

cell, rather than pre-lithiated anodes. Figure 4.3.2a and b show the schematic representation of lithiated Si-S full cell assembled before and after the cycle performance. During the discharging, the lithium foil placed on the surface of the anode (figure 4.3.2a) undergoes oxidation and disappears from the anode as shown in the figure 4.3.2b. As a result, the lithium dendrite formation can be eliminated. Moreover, the use of the modified separator has an advantage that it helps in trapping the dissolved polysulfides species in the cathode part, which may improve the active material utilization during the repeated charge/discharge processes.
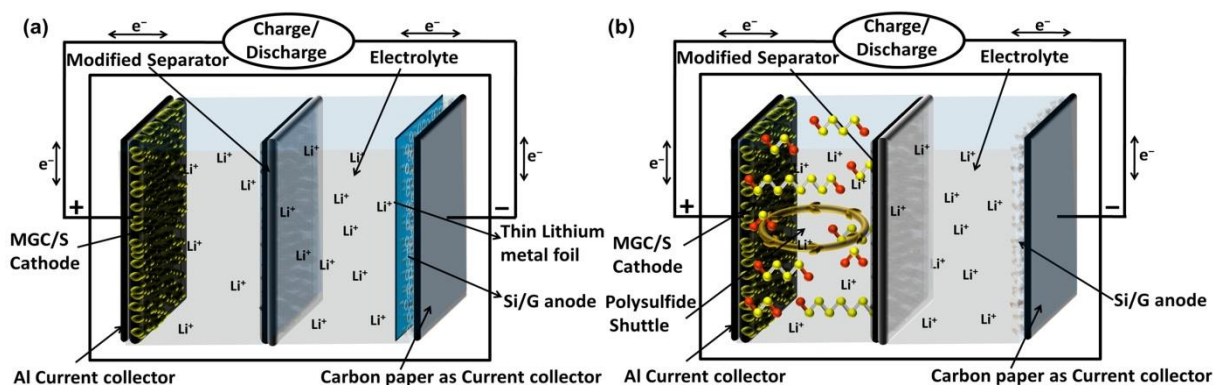
Figure 4.3.2 Schematic representation of lithiated Si-S full cell (a) before and (b) after a few charge/discharge cycles.

In order to achieve a stable and improved electrochemical performance, the optimized weight ratios of the anode, lithium and cathode are necessary. Herein, the investigator has systematically studied the effect of the weight ratios of the anode to cathode on the electrochemical performance of the lithiated Si-S full cell by maintaining the lithium weight ratio constant as discussed hereunder. The galvanostatic charge/discharge studies have been performed in the potential range of 1.0 to 2.6 V at 0.2 C rate. Figure 4.3.3a shows the cycle performance curve of lithiated Si-S full cells with different mass ratios of S:Li:Si as 1:0.5:0.5, 1:0.5:0.7 and 1:0.5:1. Among these, the lithiated Si-S full cell with 1:0.5:0.7 delivered higher discharge capacity of 768 mAh g^{-1}, in comparison to the other two cells with 1:0.5:0.5 and 1:0.5:1 mass ratios delivering 513 mAh g^{-1} and 698 mAh g^{-1} respectively over 50 cycles. It is observed from the figure 4.3.3a that with decreasing weight ratio of anode to cathode active material, the cell discharge capacity decreases, over 50 cycles. Whereas, the cell with equal mass ratios of the anode to cathode also exhibits a similar trend as the cell with lower anode loading. This behaviour is mainly due to irreversible reaction by a few lithium ions during the redox process. C. Shen et al.[59] studied the effect of the weight ratios of lithiated silicon anode to the sulfur cathode on the electrochemical performance of the full cell. The cell at optimised

weight ratio of S:Si as 1.00:1.43 delivered the highest discharge capacity. Moreover, the nafion coating on the surface of the anode acts as a barrier film that inhibits the migration of dissolved polysulfides to the anode surface. Therefore, an optimum amount of active material loading on both the electrodes is an important parameter to achieve superior electrochemical performance. Figure 4.3.3b shows the charge/discharge profile of lithiated Si-S full cell (1:0.5:0.7) measured at 0.2 C rate. It can be seen from the figure 4.3.3b, that the cell showed a two-stepped discharge curve and one flat charge curve indicating the multi-electron transfer reaction of sulfur with lithium [64]. Moreover, the cell operates at a potential of about 1.8 V, which corresponds to the electrochemical reactions occurring at the lithiated Si5/G5 anode and sulfur cathode.
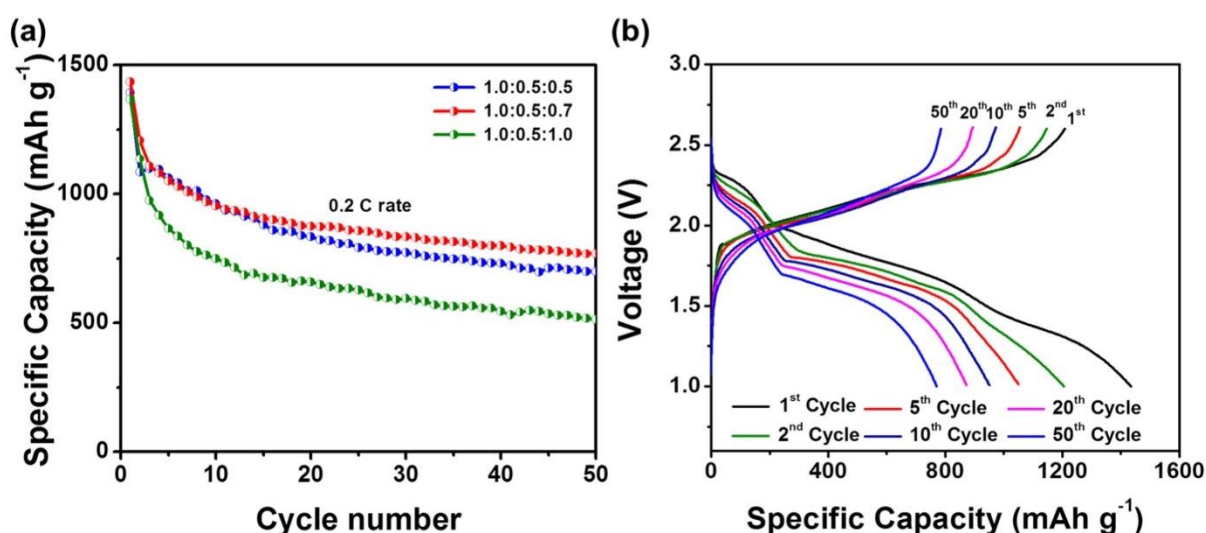
Figure 4.3.3 (a) Comparative cycle performance curves of lithiated Si-S full cell with different mass ratios of cathode, lithium and anode and (b) galvanostatic charge/discharge profile of lithiated Si-S full cell (with mass ratio of S:Li:Si of 1:0.5:0.7) measured in the potential range of 1.0 to 2.6 V at 0.2 C rate.

Further, the electrochemical performance of the lithiated Si-S full cell (with cathode to anode weight ratio of 1.0 to 0.7) can be improved by introducing an excess amount of lithium ions into the system. Therefore, the electrochemical performance of lithiated the Si-S full cell has been evaluated by using the weight ratios of cathode, lithium and anode as 1.0:0.7:0.7. The CV studies were conducted in order to study the electrochemical behaviour of the full cell (figure 4.3.4). During the cathodic scan, a pair of peaks are observed at 2.0 V and 1.6 V. The former peak at 2.0 V corresponds to the reduction of sulfur via ring opening elemental sulfur to long chain polysulfide species. The later peak at 1.6 V indicates the conversion of the long chain polysulfide intermediates to short chain polysulfides as the final discharge

products. In the anodic scan, one oxidation peak is observed at a potential of 2.2 V, which corresponds to the reversible conversion of the formed lithium sulfide back to elemental sulfur [65]. The output voltage of the cell is about 1.8 V, which is in agreement with the cell potential obtained using the half cell potentials of MGC-2/S cathode and Si5/G5 anode. This result confirms that the thin lithium foil placed on the surface of the anode is completely reacted at the anode, which acts as lithium source during the redox process. In the subsequent scan upto 10 cycles, no change is observed in the redox peaks, suggesting the high electrochemical stability of the electrodes.
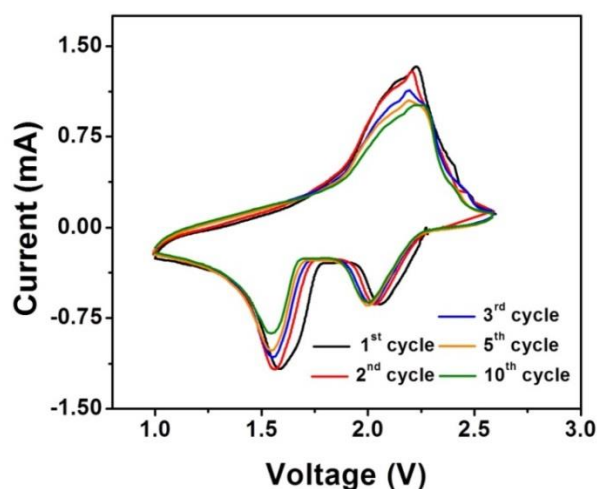
Figure 4.3.4 Cyclic voltammetric profile of lithiated Si-S full cell (1:0.7:0.7) measured at a scan rate of 0.1 mV s^{-1}.

Figure 4.3.5a shows the charge/discharge profile of the lithiated Si-S full cell (1:0.7:0.7) measured at 0.2 C rate. The charge/discharge profile of this cell showed a two-step reduction and one flat oxidation revealing multi-electron transfer reaction. Initially, the cell delivered a high discharge capacity of 1527 mAh g^{-1} at 0.2 C rate. During the first few cycles the cell showed capacity fading, which gets stabilised later and retained a high discharge capacity of 824 mAh g^{-1} after 50 cycles (figure 4.3.5b). The specific energy density calculated, based on the weight of active sulfur alone without carbon and with carbon (carbon + S) are 1483 Wh kg^{-1} and 948 Wh kg^{-1} respectively. The energy density delivered by the present Si-S cell is compared with the theoretical energy density of Li-ion battery (LiFePO$_4$/graphite) and the results are given in table 4.3.1. The energy density delivered by Si-S cell is almost twice that of the conventional LIBs, which shows the practical importance of this system. It is interesting to note that the charge/discharge capacities and specific energy exhibited by lithiated Si-S full cell are comparable with the values reported in the literature for Li-S batteries [60,59,63]. Furthermore, there is considerable scope in improving the

electrochemical performance of Li-S battery by designing novel electrode structure, modified electrolytes and separators.
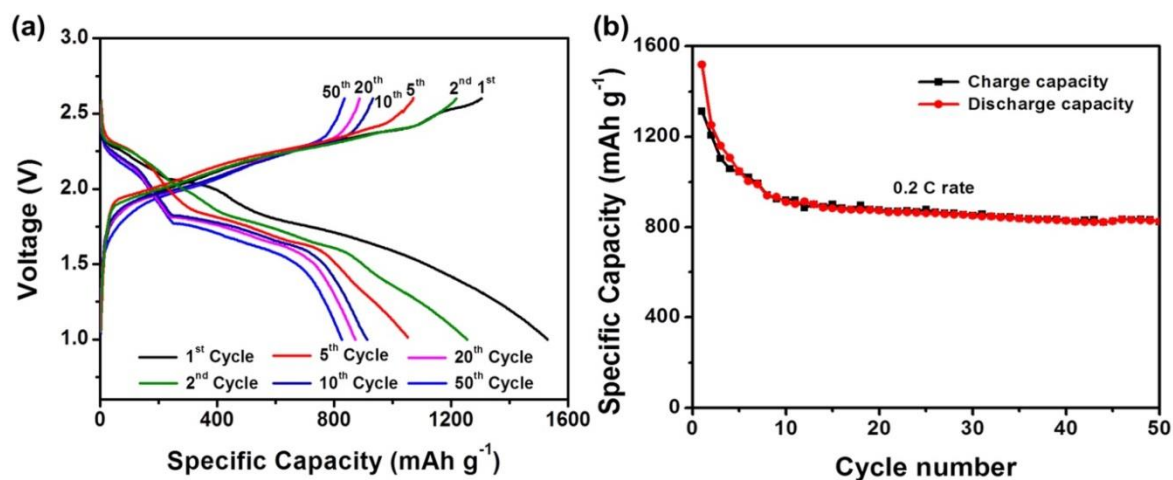
Figure 4.3.5 (a) Charge/discharge profile, (b) cycle performance curve of lithiated Si-S full cell (1:0.7:0.7) measured in the potential range of 1.0 to 2.6 V at 0.2 C rate.

Table 4.3.1   Comparison of energy densities of present Si-S cell with conventional Li-ion battery.

System	Operating Potential (V)	Specific Capacity (mAh g^{-1})	Energy Density (Wh kg^{-1})
LiFePO$_4$/Graphite	3.2	170	544
Lithiated Si-S cell (present study)	1.8	824	948

The test for cycle performance was also conducted at a high current rate of 1 C (figure 4.3.6). The performance for the first two cycles was measured at 0.5 C rate, and the performance for the subsequent cycles upto 300, was measured at 1 C rate. In the first cycle, the lithiated Si-S cell delivered high discharge capacity of 976 mAh g^{-1}. Even after 300 cycles the cell displayed high discharge capacity of 411 mAh g^{-1} with about 99% coulombic efficiency. This result reveals that the presence of micro and mesoporous structures in the cathode helps in trapping the dissolved polysulfide species in it. Moreover, the modified separator acts as a barrier that increases the reutilization of the active material of the cathode and the carbon paper with coated Si5/G5 accommodates huge volume expansion. Thus, the disintegration of the active material from the current collector is suppressed and the

conductivity of the system is enhanced. As a result, the cell displayed improved electrochemical performance over repeated charge/discharge processes.
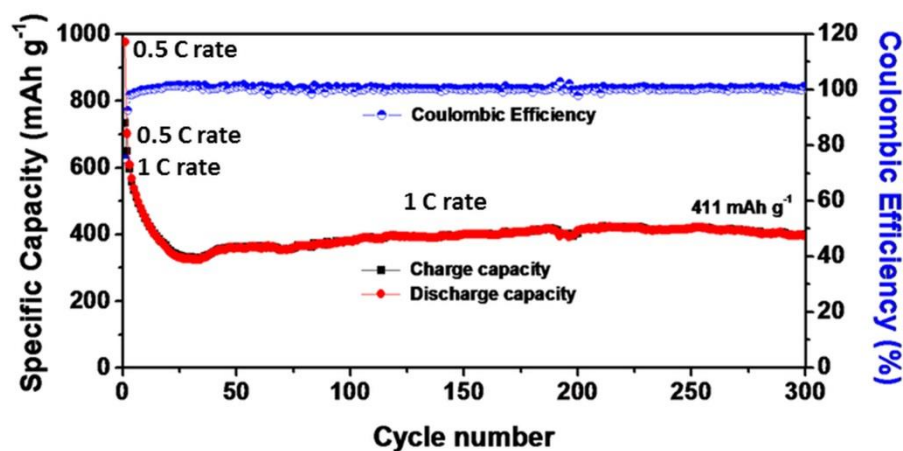
Figure 4.3.6 Long-term cycle performance curve of Si-S cell (1:0.7:0.7) measured at 1 C rate.

The lithiated Si-S cell was decrimped in order to confirm the absence of the lithium foil on the surface of the anode. Figure 4.3.7a shows the photo image of the de-crimped Si-S in swagelok cell after 10 cycles. The decrimped cell shows the absence of lithium foil on the surface of the anode, suggesting complete utilization of lithium during the charge-discharge processes.
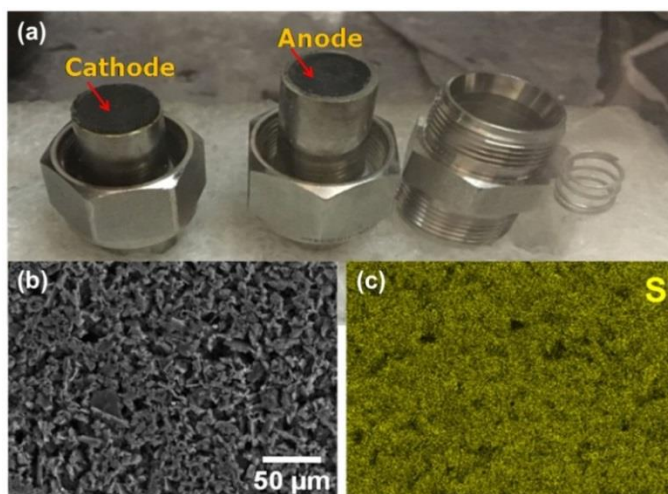
Figure 4.3.7 (a) Photo image of the cathode and anode of the decrimped lithiated Si-S cell (1:0.7:0.7) (b) FE-SEM of the modified separator and (c) corresponding elemental mapping of sulfur (yellow), after 10 charge/discharge cycles.

Further, the investigator has also analysed the modified separator by EDS elemental mapping. Figures 4.3.7b and c show the FE-SEM image and the corresponding elemental map of the modified separator analysed after 10 cycles. The EDS elemental mapping confirms the presence of sulfur element all over the surface of the modified separator with homogenous

distribution. This result suggests that the polysulfide formed during the charge/discharge process gets trapped into MGC modified separator that increases the reutilization of active material and the resulting cell exhibited high capacity retention for longer cycles.

As the lithiated Si-S cell showed an improved electrochemical performance for longer cycles in the coin cell, it motivated the researcher to fabricate the lithiated Si-S pouch cell. The assembled Si-S pouch cells were used for demonstrating the small electronic components such as LEDs and fan as shown in the figure 4.3.8. Two such cells are connected in series to get an output voltage of ~3.6 V to lighten 40 LEDs connected in parallel (figure 4.3.8a). Similarly, the same cells are connected in parallel, which increases the output current to run a fan (figure 4.3.8b). This type of novel cell configuration avoids the use of lithium metal as anode, which has negative impact on the cell due to safety issues such as internal short-circuit and thermal runaway. Moreover, the simple and easy fabrication process of lithiated Si-S full cell shows a path for the large scale commercialization of this system for practical applications.
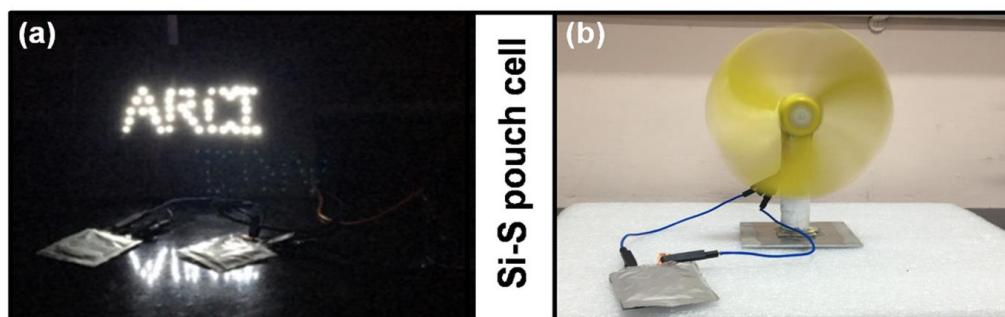
Figure 4.3.8 Photo images of (a) two lithiated Si-S pouch cells connected in series to lighten 40 LEDs connected in parallel and (b) two lithiated Si-S pouch cells connected in parallel to run a fan.

4.3.3 Conclusions

Lithiated Si-S full cells are fabricated by using MGC-2/S cathode and Si5/G5 electrode with a very thin lithium foil on its surface as anode. Experimental studies have been made to optimise the mass ratios of the anode, lithium and cathode in order to achieve good electrochemical performance. The lithiated Si-S cell at the mass ratios of cathode, lithium and anode as 1:0.7:0.7, delivered high initial discharge capacity of 1527 mAh g^{-1} and retained a discharge capacity of 824 mAh g^{-1} after 50 cycles at 0.2 C rate. The energy density exhibited by the lithiated Si-S cell developed in the present study is 948 Wh kg^{-1}, which is nearly twice that of the conventional Li-ion battery (544 Wh kg^{-1}). Moreover, the lithiated Si-S pouch cells fabricated in the present study are used for powering small electronic components.

Section 4.4 Comparison of the Electrochemical Performance of Lithiated Si-S Cell Developed in the Present Study with those reported in the Literature

This section compares the electrochemical performance of lithiated Si-S cell fabricated in the present study by using low-cost and high performing MGC/S-2 cathode and lithiated Si5/G5 anode with those reported in the literature. The specific capacity delivered by the present Si-S cell is comparable with those reported in the literature and the values are tabulated in the form of a table 4.4.1. For instance, X. Pu et al.[61] fabricated Li_xSi-S (LSS) battery by using S/CMK-8 cathode, lithiated mesoporous silicon/carbon composite as the anode and 1M LITFSI containing 1 wt% of $LiNO_3$ additive as the electrolyte. The LSS cell with CNT interlayer placed between the cathode and separator delivered a high initial discharge capacity of 970 mAh g^{-1} and retained a discharge capacity of 780 mAh g^{-1} at 0.5 C rate even after 100 cycles. The improved performance of the cell is due to the presence of CNT interlayer, which acts as polysulfide reservoir that traps the dissolved polysulfides and it also acts as upper current collector that increases the electrical conductivity of the electrode during the redox process.

B. Duan et al.[63] prepared the sulfur/lithium-ion battery by using carbyne polysulfide as the cathode, lithium/Sn-C composite as anode and 1M $LiPF_6$ as electrolyte. The resulting ccell delivered a high discharge capacity of 500 mAh g^{-1} at 0.2 A g^{-1} even after 50 cycles. The presence of smaller sulfur molecules (S_x, $1 \leq x \leq 4$) in the polymer backbone renders a solid phase reaction mechanism with lithium ions during the charge/discharge process. As a result, polysulfide dissolution into the electrolyte can be eliminated and thus, the electrode delivered an improved electrochemical performance. Shen et al.[59] reported the fabrication of Si-S full cell using prelithiated Nafion-coated silicon composite as the anode and S/CNF/G composite as the cathode. A 1M LITFSI containing 5 wt % of $LiNO_3$ additive is used as electrolyte. The sulfur cathode with 50 wt% of sulfur content in it, delivered a high discharge capacity of 610 mAh g^{-1} at 0.1 C rate even after 100 cycles.

The lithiated Si-S cell developed in the present study exhibited superior electrochemical performance due to the application of good electrochemically stable electrodes and novel cell configuration. The discharge capacity delivered by the present Si-S cell is comparable with the Li-S based full cells reported in the literature. In addition to this, the Si-S pouch cells fabricated in the present study give a scope for the development of this system for practical applications.

Table 4.4.1 Comparison of the electrochemical performance of the lithiated Si-S cell fabricated in the present study with those of reported literature.

Li-S battery in full cell configuration								
Cathode	Anode	Electrolyte	Sulfur content (%)	Sulfur loading (mg)	Initial discharge capacity (mAh g^{-1})	Final discharge capacity (mAh g^{-1})	C rate/ current density (A g^{-1})	Ref
S/CMK-8 (CNT interlayer)	Prelithiated mesoporous Si	1M LITFSI (1 wt% LiNO$_3$)	48	~1	970	780 (100th cycle)	0.5 C	61
Li$_2$S-MCMB	Si-O-C composite	LITFSI and TEGDME in 1:4 ratio	50	-	~400	280	0.23 A g^{-1}	65
S/CNF/G	Prelithiated porous Si	1M LITFSI (5 wt% LiNO$_3$)	~50	-	~1000	610 (100th cycle)	0.1 C	59
HCS/S	Prelithiated Si-C	1M LITFSI (0.25M LiNO$_3$)	53	1.3-1.5	1470	~370 (1400th cycle)	0.83 A g^{-1}	60
Carbyne polysulfide	Lithiated Sn/C	1M LiPF$_6$	54	-	~770	500 (50th cycle)	0.2 A g^{-1}	63
MGC/S-2 (MGC modified separator)	Lithiated Si5/G5	1M LITFSI (5 wt% LiNO$_3$)	64	2.0-2.4	1527	824 (50th cycle)	0.2 C	This work
					976 (0.5 C) (5th cycle)	411 (300th cycle)	1 C	

References

1. Wang, J., Xie, K., Wei, B. Advanced Engineering of Nanostructured Carbons for Lithium-Sulfur Batteries. *Nano Energy* **15**, 413-444 (2015).

2. Zu, C., Azimi, N., Zhang, Z., Manthiram, A. Insight Into Lithium-Metal Anodes in Lithium-Sulfur Batteries with a Fluorinated Ether Electrolyte. *J. Mater. Chem. A* **3**, 14864-14870 (2015).

3. Yang, Y. McDowell, M. T., Jackson, A., Cha, J. J., Hong, S. S., Cui, Y. New Nanostructured Li$_2$S/ Silicon Rechargeable Battery with High Specific Energy. *Nano Lett.* **10**, 1486-1491 (2010).

4. Guidotti, R. A., Masset, P. J. Thermally Activated ('thermal') Battery Technology. Part IV. Anode Materials. *J. Power Sources* **183**, 388-398 (2008).

5. Menkin, S., Barkay, Z., Golodnitsky, D., Peled, E. Nanotin Alloys Supported by Multiwall Carbon Nanotubes as High-Capacity and Safer Anode Materials for EV Lithium Batteries. *J. Power Sources* **245**, 345-351 (2014).

6. Derrien, B. G., Hassoun, J., Panero, S., Scrosati, B. Nanostructured Sn-C Composite as an Advanced Anode Material in High-Performance Lithium-Ion Batteries. *Adv. Mater.* **19**, 2336-2340 (2007).

7. Yu, Y., Gu. L., Wang, C., Dhanabalan, A., Doz., P. A. A. P., Mair. J. Encapsulation of Sn-Carbon Nanoparticles in Bamboo-like Hollow Carbon Nanofibers as an Anode Material in Lithium-Based Batteries. *Angew. Chem. Int. Ed.* **48**, 6485-6489 (2009).

8. Ni, W., Wang, Y., Xu, R. Formation of Sn-C Yolk-Shell Nanospheres and Core-Sheath Nanowires for Highly Reversible Lithium Storage. *Part. Part. Syst. Charact.* **30**, 873-880 (2013).

9. Zhuo, K., Jeong, M., Chung, C. Highly Porous Dendritic Ni-Sn Anodes for Lithium-ion Batteries. *J. Power Sources* **244**, 601-605 (2013).

10. Yang, H., Li, L. Tin-Indium/Graphene with Enhanced Initial Coulombic Efficiency and Rate Performance for Lithium ion Batteries. *J. Alloys Compd.* **584**, 76-80 (2014).

11. Tan, Z., Sun, Z., Wang, H., Guo, Q., Su, D. Fabrication of Porous Sn-C Composites with High Initial Coulomb Efficiency and Good Cyclic Performance for Lithium ion Batteries. *J. Mater. Chem. A* **1**, 9462-9468 (2013).

12. Meschini, I. Nobili, F., Mancini, M., Marassi, R., Tossici, R., Savoini, A., Focarete, M. L., Croce. F. High-Performance Sn@Carbon Nanocomposite Anode for Lithium Batteries. *J. Power Sources* **226**, 241-248 (2013).

13. Shin, H., Liu, M. Three-Dimensional Porous Copper-Tin Alloy Electrodes for Rechargeable Lithium Batteries. *Adv. Funct. Mater.* **15**, 582-586 (2005).

14. Jiang, T., Zhang, S., Qiu, X., Zhu, W. & Chen, L. Preparation and characterization of tin-based three-dimensional cellular anode for lithium ion battery. *J. Power Sources* **166**, 503–508 (2007).

15. Uchiyama, H., Hosono, E., Honma, I., Zhou, H., Imai, H. A Nanoscale Meshed Electrode of Single-Crystalline SnO for Lithium-ion Rechargeable Batteries. *Electrochem. commun.* **10**, 52-55 (2008).

16. Jeun, J., Kim, W., Hong, S. Electrophoretic Deposition of Carbon Nanoparticles on Dendritic Sn Foams Fabricated by Electrodeposition. *Mater. Lett.* **112**, 109-112 (2013).

17. Park, J., Eom, J., Kwon, H. Fabrication of Sn-C Composite Electrodes by Electrodeposition and Their Cycle Performance for Li-ion Batteries. *Electrochem. commun.* **11**, 596-598 (2009).

18. Wang, G., Wang, B., Wang, X., Park, J., Dou, S., Ahn, H., Kim, K. Sn/Graphene

Nanocomposite with 3D Architecture for Enhanced Reversible Lithium Storage in Lithium ion Batteries. *J. Mater. Chem* **19**, 8378-8384 (2009).

19. Luo, B., Wang, B., Li, X., Jia, Y., Liang, M., Zhi, L Graphene-Confined Sn Nanosheets with Enhanced Lithium Storage Capability. *Adv. Mater.* **24**, 3538-3543 (2012).

20. Zhou, X., Zou, Y., Yang, J. Periodic Structures of Sn Self-Inserted Between Graphene Interlayers as Anodes for Li-ion Battery. *J. Power Sources* **253**, 287-293 (2014).

21. Chen, D., Ji, G., Ma, Y., Lee, J. Y., Lu, J. Graphene-Encapsulated Hollow Fe_3O_4 Nanoparticle Aggregates As a High-Performance Anode Material for Lithium Ion Batteries. *ACS Appl. Mater. Interfaces* **3**, 3078-3083 (2011).

22. Zhou, G., Wang, D. W., Li, F., Zhang, L., Li, N., Wu, Z., S., Wen, L., Lu, Q. G. M. Cheng, H. M. Graphene-Wrapped Fe_3O_4 Anode Material with Improved Reversible Capacity and Cyclic Stability for Lithium Ion Batteries. *Chem. Mater.* **22**, 5306-5313 (2010).

23. Li, Y., Lv, X., Lu, J., Li, J. Preparation of SnO_2-Nanocrystal/Graphene-Nanosheets Composites and Their Lithium Storage Ability. *J. Phys. Chem. C* **114**, 21770-21774 (2010).

24. Ding, S., Luan, D., Boey, F. Y. C., Chen, J. S., Lou, X. W. D. SnO_2 Nanosheets Grown on Graphene Sheets with Enhanced Lithium Storage Properties. *ChemComm* **47**, 7155-7157 (2011).

25. Li, B., Cao, H., Shao, J., Li, G., Qu, M., Yin, G. Co_3O_4@Graphene Composites as Anode Materials for High-Performance Lithium Ion Batteries. *Inorg. Chem.* **50**, 1628-1632 (2011).

26. Yang, X., Fan, K., Zhu, Y., Shen, J., Jaing X., Zhao, P., Li, C. Tailored Graphene-Encapsulated Mesoporous Co_3O_4 Composite Microspheres for High-Performance Lithium ion Batteries. *J. Mater. Chem.* **22**, 17278-17283 (2012).

27. Pavithra, C. L. P., Sarada, B. V, Rajulapati, K. V, Rao, T. N., Sundararajan, G. A New Electrochemical Approach for the Synthesis of Copper-Graphene Nanocomposite Foils with High Hardness. *Sci. Rep.* **4**, 4049 (2014).

28. Yim, T., Park, M. S., Yu, J. S., Kim, K. J., Im, K. Y., Kim, J. H., Jeong, G., Jo, Y. N., Woo, S. G., Kang, K. S., Lee, I, Kim, Y. J. Effect of Chemical Reactivity of Polysulfide Toward Carbonate-Based Electrolyte on the Electrochemical Performance of Li-S Batteries. *Electrochim. Acta* **107**, 454-460 (2013).

29. Shin, B. H., Dong, J., Liu, M. Nanoporous Structures Prepared by an Electrochemical

Deposition Process. *Adv. Mater.* **15**, 1610-1614 (2003).

30. Si, Q., Matsui, M., Horiba, T., Yamamoto, O., Takeda, Y., Seki, N., Imanishi, N. Carbon Paper Substrate for Silicon-Carbon Composite Anodes in Lithium-ion Batteries. *J. Power Sources* **241**, 744-750 (2013).

31. Liu, H., Hu, R., Zeng, M., Liu, J., Zhu, M. Enhancing the Performance of Sn-C Nanocomposite as Lithium ion Anode by Discharge Plasma Assisted Milling. *J. Mater. Chem* **22**, 8022–8028 (2012).

32. Wang, W., Ruiz, I., Guo, S., Favors, Z., Bay, H. H., Ozkan, M., Ozkan, C. S. Hybrid Carbon Nanotube and Graphene Nanostructures for Lithium ion Battery Anodes. *Nano Energy* **3**, 113–118 (2014).

33. Ren, J. G., Wang, C., Wu., Q. H., Liu, X., Yang, Y., He, L., Zhang, W. Silicon Nanowires-Reduced Graphene Oxide Composite as a High-Performance Lithium Ion Battery Anode Material. *Nanoscale* **6**, 3353-3360 (2014).

34. Wang, C., Li, Y., Chui, Y. S., Wu, Q. H., Chen, X., Zhang, W. Three-Dimensional Sn-Graphene Anode for High-Performance Lithium-ion Battery. *Nanoscale* **5**, 10599-10604 (2013).

35. Chen, S., Wang, Y., Ahn, H., Wang, G. Microwave Hydrothermal Synthesis of High Performance Tin-Graphene Nanocomposites for Lithium ion Batteries. *J. Power Sources* **216**, 22-27 (2012).

36. Liu, Y., Wang, W., Gu, L., Wang, Y., Yinh, Y., Mao, Y., Sun, L., Peng, X. Flexible CuO Nanosheets/Reduced-Graphene Oxide Composite Paper: Binder-Free Anode for High-Performance Lithium-ion Batteries. *ACS Appl. Mater. Interfaces* **5**, 9850-9855 (2013).

37. Nara, H., Mukoyama, D., Shimizu, R., Momma, T., Osaka, T. Systematic Analysis of Interfacial Resistance Between the Cathode Layer and the Current Collector in Lithium-ion Batteries by Electrochemical Impedance Spectroscopy. *J. Power Sources* **409**, 139-147 (2019).

38. Li, X., Hu, Y., Liu, J., Lushington, A., Sun, X. Structurally Tailored Graphene Nanosheets as Lithium ion Battery Anodes : an Insight to Yield Exceptionally High Lithium Storage Performance. *Nanoscale* **5**, 12607-12615 (2013).

39. Chen, D., Yi, R., Chen, S., Xu, T., Gordin, M. L., Wang, D. Facile Synthesis of Graphene-Silicon Nanocomposites with an Advanced Binder for High-Performance Lithium-ion Battery Anodes. *Solid State Ionics* **254**, 65-71 (2014).

40. Huang, Q., Loveridge, M. J., Genieser, R., Lain, M. J., Bhagat, R. Electrochemical Evaluation and Phase-related Impedance Studies on Silicon-Few Layer Graphene (FLG) Composite Electrode Systems. *Sci. Rep.* **8**, 1386 (2018).

41. Xiao, Q., Fan, Y., Wang, X., Susantyoko, R. A., Zhang, Q. A multilayer Si/CNT Coaxial Nanofiber LIB Anode with a High Areal Capacity. *Energy Environ. Sci.* **7**, 655-661 (2014).

42. Kim, W. S., Choi, J., Hong, S. H. Meso-Porous Silicon-Coated Carbon Nanotube as an Anode for Lithium-ion Battery. *Nano Res.* **9**, 2174-2181 (2016).

43. Chen, S., Chen, Z., Xu, X., Cao, C., Xia, M., Luo, Y. Scalable 2D Mesoporous Silicon Nanosheets for High-Performance Lithium-Ion Battery Anode. *Small* **14**, 170336 (2018).

44. Zhou, X., Liu, Y., Du, C., Ren, Y., Mu, T., Zuo, P., Yin, G., Ma, Y., Cheng, X., Gao, Y. Polyaniline-Encapsulated Silicon on Three-Dimensional Carbon Nanotubes Foam with Enhanced Electrochemical Performance for Lithium-ion Batteries. *J. Power Sources* **381**, 156-163 (2018).

45. Yao, Y., Liu, N., McDowell, M. T., Pasta, M., Cui, Y. Improving The Cycling Stability of Silicon Nanowire Anodes with Conducting Polymer Coatings. *Energy Environ. Sci.* **5**, 7927-7930 (2012).

46. Ma, B., Lu, B., Luo, X., Deng, X., Wu, Z., Wang, X. The Hollow Mesoporous Silicon Nanobox Dually Encapsulated by SnO_2/C as Anode Material of Lithium ion Battery. *Electrochim. Acta* **288**, 61-70 (2018).

47. Yoon, T., Bok, T., Kim, C., Na, Y., Park, S., Kim, K. S. Mesoporous Silicon Hollow Nanocubes Derived from Metal-Organic Framework Template for Advanced Lithium-Ion Battery Anode. *ACS Nano* **11**, 4808-4815 (2017).

48. Yim, C. H., Courtel, F. M., Abu-Lebdeh, Y. A High Capacity Silicon-Graphite Composite as Anode for Lithium-ion Batteries Using Low Content Amorphous Silicon and Compatible Binders. *J. Mater. Chem. A* **1**, 8234–8243 (2013).

49. Nzabahimana, J., Chang, P., Hu, X. Porous Carbon-Coated Ball-Milled Silicon as High-Performance Anodes for Lithium-ion Batteries. *J. Mater. Sci.* **54**, 4798-4810 (2018).

50. Huang, S., Cheong, L. Z., Wang, D., Shen, C. Nanostructured Phosphorus Doped Silicon/Graphite Composite as Anode for High-Performance Lithium-Ion Batteries. *ACS Appl. Mater. Interfaces* **9**, 23672-23678 (2017).

51. Xiao, C., He, P., Ren, J., Yue, M., Huang, Y., He, X. Walnut-Structure Si-G/C Materials with High Coulombic Efficiency for Long-Life Lithium ion Batteries. *RSC Adv.* **8**, 27580-27586 (2018).

52. Schott, T., Gomez-Camer, J. L., Novak, P., Trabesinger, S. Relationship Between the Properties and Cycle Life of Si/C Composites as Performance-Enhancing Additives to Graphite Electrodes for Li-Ion Batteries. *J. Electrochem. Soc.* **164**, A190-A203 (2017).

53. Li, M., Hou, X., Sha, Y., Wang, J., Hu, S., Liu, X., Shao, Z., Facile Spray-Drying/Pyrolysis Synthesis of Core-Shell Structure Graphite/Silicon-Porous Carbon Composite as a Superior Anode for Li-ion Batteries. *J. Power Sources* **248**, 721-728 (2014).

54. Sun, F., Gao, J., Zhu, Y., Pi, X., Wang, L., Qin, Y., A High Performance Lithium ion Capacitor Achieved by the Integration of a Sn-C Anode and a Biomass-Derived Microporous Activated Carbon Cathode. *Sci. Rep.* **7**, 40990 (2017).

55. Su, M., Wang, Z., Guo, H., Li, X., Huang, S., Xiao, W., Gan, L. Enhancement of the Cyclability of a Si/Graphite@Graphene Composite as Anode for Lithium-ion Batteries. *Electrochim. Acta* **116**, 230-236 (2014).

56. Zhu, S., Zhu, C., Ma, J., Meng, Q., Guo, Z., Yu, Z., Lu, T., Li, Y., Zhang, D., Lau, W. M. Controlled Fabrication of Si Nanoparticles on Graphene Sheets for Li-ion Batteries. *RSC Adv.* **3**, 6141-6146 (2013).

57. Hu, R., Sun, W., Chen, Y., Zeng, M., Zhu, M. Silicon/Graphene Based Nanocomposite Anode: Large-Scale Production and Stable High Capacity for Lithium ion Batteries. *J. Mater. Chem. A* **2**, 9118-9125 (2014).

58. Hassoun, J., Scrosati, B. A High-Performance Polymer Tin Sulfur Lithium Ion Battery. *Angew. Chem. Int. Ed.* **49**, 2371-2374 (2010).

59. Shen, C., Ge, M., Zhang, A., Fang, X., Liu, Y., Rong, J., Zhou, C. Silicon(Lithiated)-Sulfur Full Cells with Porous Silicon Anode Shielded by Nafion Against Polysulfides to Achieve High Capacity and Energy Density. *Nano Energy* **19**, 68-77 (2016).

60. Bruckner, J., Thieme, S., Hiller, F. B., Bauer, I., Grossmann, H. T., Strubel, P., Althues, H., Spange, S., Kaskel, S. Carbon-Based Anodes for Lithium Sulfur Full Cells with High Cycle Stability. *Adv. Funct. Mater.* **24**, 1284-1289 (2014).

61. Pu, X., Yang, G., Yu, C. Safe and Reliable Operation of Sulfur Batteries with Lithiated Silicon. *Nano Energy* **9**, 318-324 (2014).

62. Hassoun, J., Kim, J., Lee, D. J., Jung, H. G., Lee, S. M., Sun, Y. K., Scrosati, B. A

Contribution to the Progress of High Energy Batteries: A Metal-Free, Lithium-ion, Silicon-Sulfur Battery. *J. Power Sources* **202**, 308-313 (2012).

63. Duan, B., Wang, W., Wang, W., Yu, Z., Zhao, H., Yang, Y. A New Lithium Secondary Battery System: The Sulfur/ Lithium-ion Battery. *J. Mater. Chem. A* **2**, 308-314 (2014).

64. Su, Y., Manthiram, A. Lithium-Sulfur Batteries with a Microporous Carbon Paper as a Bifunctional Interlayer. *Nat. Commun.* **3**, 1166 (2012).

65. Agostini, M., Hassoun, J., Liu, J., Jeong, M., Nara, H., Momma, T., Osaka, T., Sun, Y. K., Scrosati, B. A Lithium-Ion Sulfur Battery Based on a Carbon-Coated Lithium-Sulfide Cathode and an Electrodeposited Silicon-Based Anode. *ACS Appl. Mater. Interfaces* **6**, 10924–10928 (2014).

Chapter 5

Synthesis and Electrochemical Studies of Porous Carbon Materials for Application in Supercapacitors
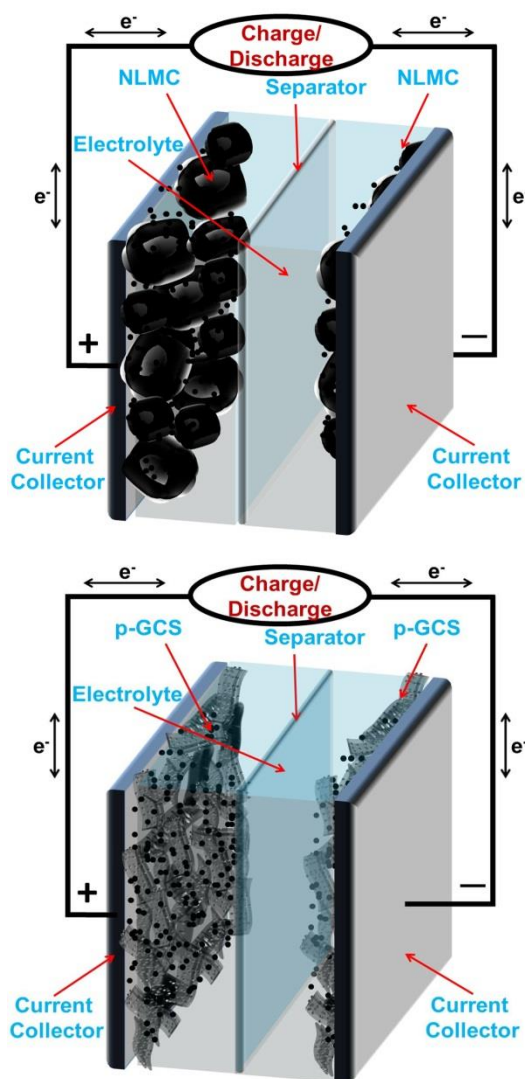
Contents

Introduction

Micro and mesoporous carbon materials find widespread application in supercapacitors due to their unique physicochemical properties such as high specific surface area, excellent electrical conductivity, good chemical and thermal stabilities [1]. Though these porous carbon materials exhibited promising electrochemical performance in terms of improved specific capacitance and good cycle stability, the synthetic process of these porous carbon materials involves complex procedure, toxic chemicals and tedious experimental

157

conditions, which make the process expensive [2,3]. As an alternative to the conventionally prepared carbon materials, the biomass-derived activated carbons (ACs) have drawn attention of researchers owing to their advantages such as environmental friendliness, low cost and easy to synthesize. Further, the high surface area, large pore volume, good electrical conductivity and well developed porous structures of AC have provided promising electrochemical stability during the charge/discharge process. For example, T. Ramesh et al. [4] prepared high surface area carbon with hierarchical porous structure from the tamarind seeds, for application in supercapacitor. The electrode prepared from this porous carbon delivered a high specific capacitance of 157 F g^{-1} in 6M KOH and 76 F g^{-1} in 1-butyl 3-methyl imidazoliumbistrifluorosulfonylimide (ionic liquid) electrolytes at a current density of 0.5 A g^{-1}. Y Han et al. [5] synthesized the AC from fish gills by the method of KOH activation and used it as an electrode for supercapacitor. The prepared carbon sample exhibited a high surface area and large pore volume with the presence of O and N functional groups in them. As a result, the electrode prepared from this activated carbon delivered high specific capacitance of 334 F g^{-1} in 6M KOH electrolyte at a current density of 2 A g^{-1}. The activated carbons derived from various biomass precursors such as rice husk [6], willow catkin [7], corn straw [8] and banana fibers [9] have also been explored for use in supercapacitors and the electrode prepared from these carbons showed an improved electrochemical performance even under fast charge/discharge processes.

In this background, the investigator has extended the studies on the micro and mesoporous carbons developed in the present study for application in supercapacitor. This chapter is divided into three sections. The section 5.1 comprises the results and discussion of the electrochemical studies of micro and mesoporous carbon synthesized from fallen neem leaves and the section 5.2 presents the electrochemical studies of the micro and mesoporous carbon synthesized from tissue paper. The Section 5.3 comprises a comparison of the results of the developed porous carbons with the results of the activated carbons reported in the literature. The mechanism of KOH activation, synthetic process and physico-chemical properties of these porous carbon materials have already been discussed in detail in their respective sections in the chapter 3.

Section 5.1 Neem Leaves-Derived Micro and Mesoporous Carbon as an Electrode for Supercapacitor

The electrochemical performances of the as-prepared NLMC are evaluated in both the three-electrode (3E) and two-electrode (2E) configurations using aqueous 6M KOH solution as the electrolyte. The electrode preparation for 3E and 2E systems and characterization has been given in the chapter 2 and the electrochemical performances of these electrodes are discussed hereunder.

5.1.1 Results and Discussion: Electrochemical Studies (CV, C/D, CY and EIS) of NLMC-1-4 Electrodes

5.1.1.1 Three-Electrode System

The cyclic voltammetric (CV) studies have been carried out in order to evaluate the electrochemical performance of the as-prepared NLMC samples. Figure 5.1.1 shows the CV profiles of the as-prepared NLMC-1-4 in three-electrode system measured at different scan rates ranging from 5 mV s^{-1} to 100 mV s^{-1}. The three electrode assembly consists of the as-prepared NLMC-4 as the working electrode, pt foil as the counter electrode and Ag/AgCl/1M KCl as the reference electrode.

The CV curves of NLMC-2-4 show the quasi-rectangular shape behaviour even at higher scan rates, which is characteristic of the electrical double layer capacitor (EDLC) [8]. This is due to the ease of penetration of ions from the electrolyte into the porous structures of the activated carbons. Whereas, NLMC-1 shows the typical CV curve in the form of a triangular shape at higher scan rate that corresponds to poor capacitive behaviour of EDLC [10]. The poor capacitive behavior of NLMC-1 electrode is due to the non-porous nature of the material. The NLMC-1 is prepared from direct carbonization of neem leaves (without KOH activation). During the low scan rates, the NLMC-1 electrode showed a rectangular shaped behavior due to uniform absorption of ions onto the electrode surface. Thus, the charging and discharging process is in synchronous regime. However, with increase in the scan rate, the shape of the voltammograms deviate from rectangular to triangular shape due to inability of ions to form electric double layer with the applied voltage. Therefore, the charging and discharging of the system is in asynchronous regime [11]. This behavior is mainly attributed to low surface area and negligible pore size in the sample. Among all the electrodes, the CV loop of the NLMC-4 has larger area in comparison to the other NLMC samples, indicating that this electrode has the highest specific capacitance. M. V. Lebedeva et al. [12] also obtained

similar type of CV profile for the activated carbon derived from rice husk. They have observed that the magnitude of the current increases with an increase in the surface area of the electrode material. As a result, the specific capacitance of the device increases. This result infers that the NLMC-4 electrode with high surface area and large pore volume provides more number of active sites for the adsorption of ions onto the surface of electrode and thus the cell exhibits superior electrochemical performance.
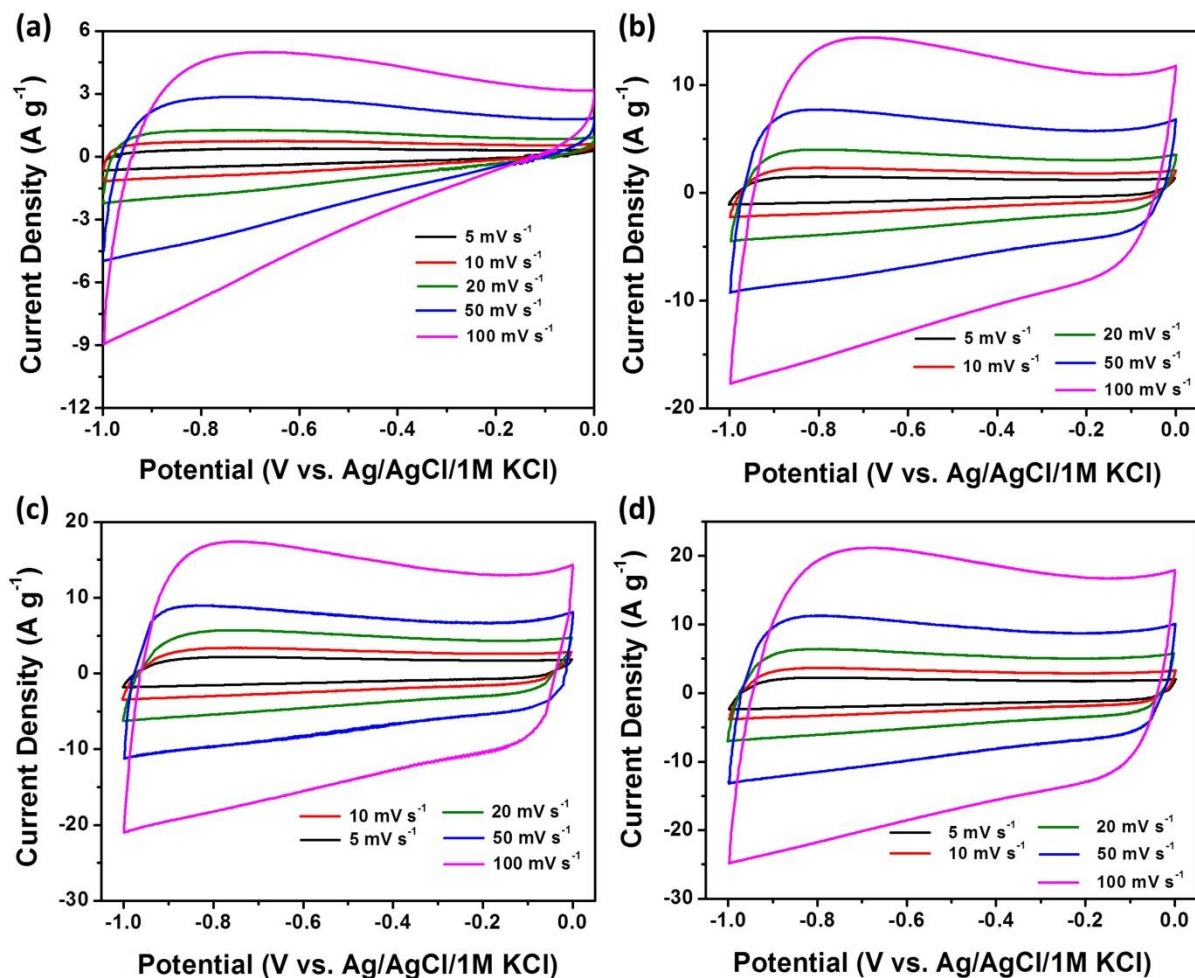
Figure 5.1.1 CV curves of (a) NLMC-1, (b) NLMC-2, (c) NLMC-3 and (d) NLMC-4 obtained at different scan rates in the three-electrode system.

Figure 5.1.2 shows the charge/discharge curves of NLMC-1-4 electrodes measured at different current rates (1 A g^{-1} to 20 A g^{-1}). All the curves are of symmetric triangular shape with negligible iR drop, which indicates less resistance in the electrodes [13]. The specific capacitance values calculated from the CD profiles of NLMC-1, NLMC-2, NLMC-3 and NLMC-4 are 67 F g^{-1}, 161 F g^{-1}, 187 F g^{-1} and 233 F g^{-1} respectively at 1 A g^{-1} current density. The longest discharge time exhibited by NLMC-4 electrode in comparison to the other NLMC1-3 electrodes is because of its higher specific capacitance. The order of the

specific capacitance delivered by the electrodes follows the similar trend observed for the specific surface areas of these carbon materials (figure 3.1.3, chapter 3). These results infer that the NLMC-4 with high surface area and large pore volume has a larger number of active sites for ion adsorption and thus, the resulting electrode exhibited the highest capacitance.
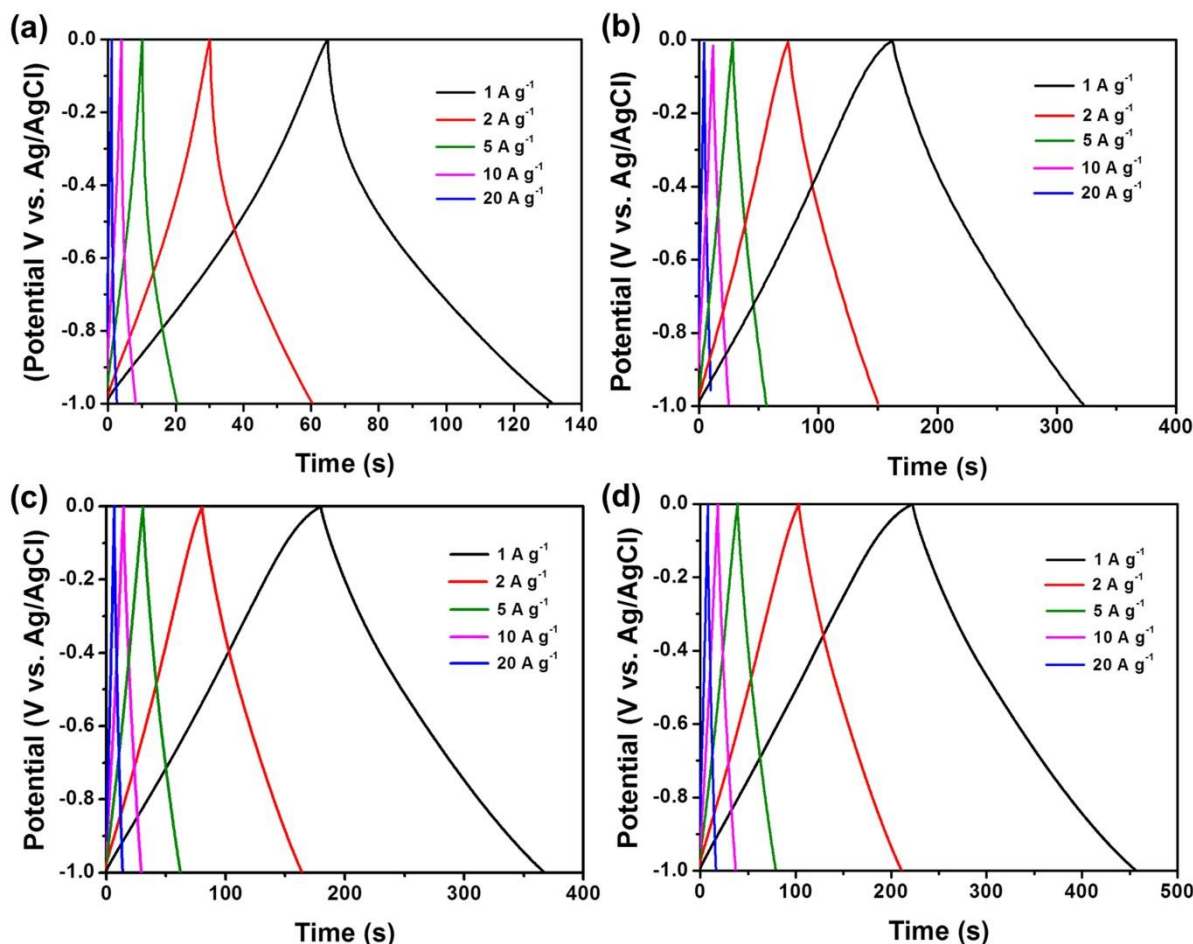
Figure 5.1.2 Charge/discharge profiles of (a) NLMC-1, (b) NLMC-2, (c) NLMC-3 and (d) NLMC-4 measured at different current densities in the three-electrode system.

The rate capability is another important parameter for the application of porous carbon materials in high performing supercapacitors. Therefore, the investigator has studied the electrochemical performance of these electrodes at higher current densities ranging from 1 A g^{-1} to 20 A g^{-1}. Figure 5.1.3 shows the rate capability of the NLMC-1-4 electrodes measured in 6M KOH electrolyte. The NLMC-1, NLMC-2, NLMC-3 and NLMC-4 electrodes showed the capacitance retention of 44%, 67%, 72% and 73%, respectively, even at a current density of 20 A g^{-1}. In general, it is known that the specific capacitance of the electrode material decreases with an increase in the current density, which is ascribed to

diffusion limitation of ions from the electrolyte to the bulk of the electrode [14]. The present result infers that the NLMC-4 electrode with high surface area exhibited good rate capability even at higher current rates in comparison to the other electrodes. Moreover, the presence of more mesoporous structures in the NLMC-4 provides channels for easy penetration of the electrolyte and renders fast ion movement during the fast reaction kinetics.
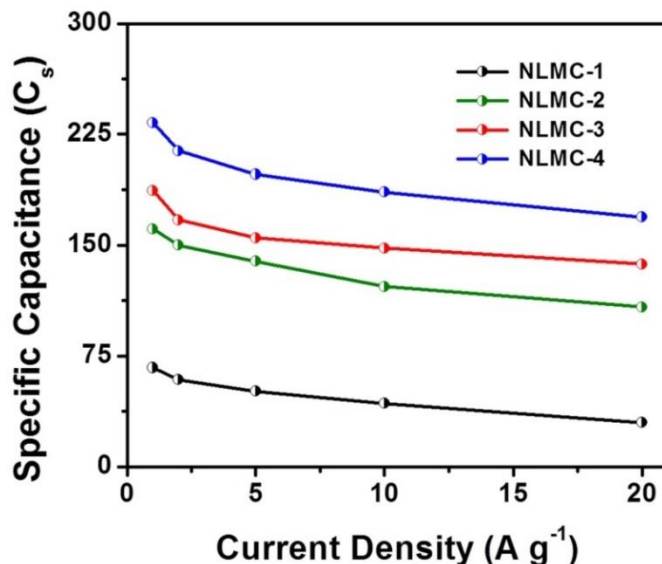
Figure 5.1.3 Rate capability of (a) NLMC-1, (b) NLMC-2, (c) NLMC-3 and (d) NLMC-4 obtained at different current rates in the three-electrode system.

The improved electrochemical performance of the *in-situ* activated samples has been further supported by the electrochemical impedance spectroscopy (EIS). Figure 5.1.4 shows the Nyquist plots of NLMC-1, NLMC-2, NLMC-3 and NLMC-4 electrodes. All the electrodes displayed a depressed semicircle in the high frequency region of the Nyquist plots, which corresponds to the charge transfer region at the interface of the electrode/electrolyte [6]. The Nyquist plots are also characterized by the Warburg impedance in the low frequency region, which is associated with the diffusion of ions from the porous electrode. The experimental results fitted well with the equivalent circuit shown in the in-set of the figure 5.1.4, where R_s is the resistance of the electrolyte, R_{ct} is the charge transfer resistance, CPE is the constant phase element and W_o is the Warburg impedance. The NLMC-2, NLMC-3 and NLMC-4 electrodes showed low R_{ct} values of 1.7 Ω, 0.73 Ω and 0.54 Ω respectively, in comparison to NLMC-1 (2.1 Ω). This result supports the results of rate capability of the electrodes, wherein the NLMC-4 exhibits the highest specific capacitance. M. Zhi et al.[13] also observed the lower R_{ct} value for the activated carbon with high surface area in comparison to

the low surface area carbon associated with higher R_{ct} value. These results suggest that the *in-situ* activated carbon electrodes with high surface area improve the charge transfer process and thus, the resulting electrodes exhibited superior specific capacitance.
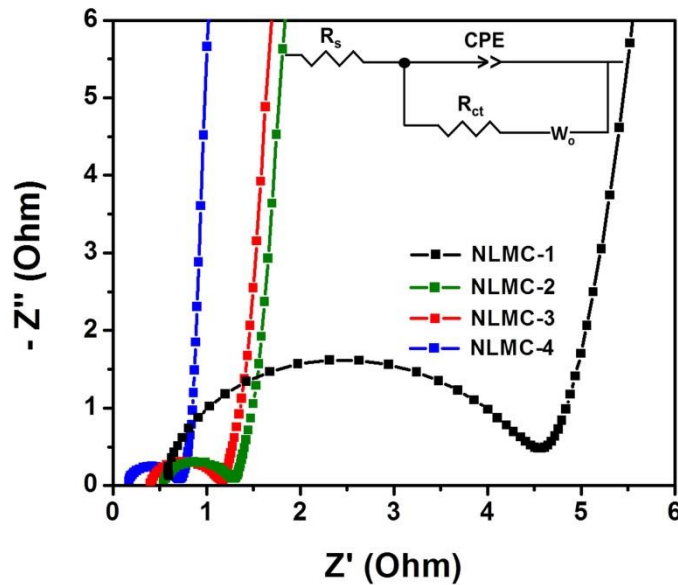
Figure 5.1.4 Nyquist plots of (a) NLMC-1, (b) NLMC-2, (c) NLMC-3 and (d) NLMC-4 electrodes (The equivalent circuit model in the in-set).

5.1.1.2 Two-Electrode System

Since the NLMC-4 electrode has shown superior specific capacitance in the 3E configuration, it is further tested in a 2E symmetric system by using 6M KOH electrolyte in the potential range of 0 to 1 V. Figure 5.1.5 shows the schematic representation of a symmetric supercapacitor, wherein, a the presence of micro and mesoporous structures in NLMC-4 provides more active sites for ion adsorption and also improves the reaction kinetics during the fast charge/discharge process.
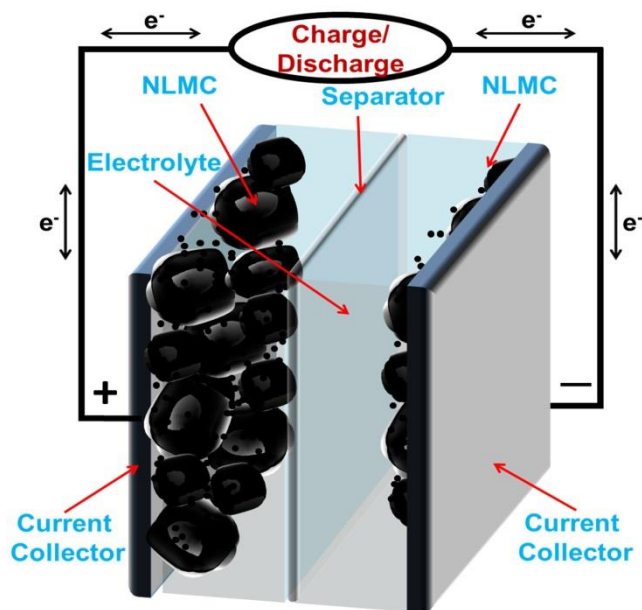
Figure 5.1.5 Schematic representation of NLMC symmetric supercapacitor.

The two-electrode system consists of identical porous carbon electrodes in symmetric configuration. Figure 5.1.6 shows the CV profile of NLMC-4 obtained at different scan rates (5 mV s^{-1} to 100 mV s^{-1}). The NLMC-4 electrode displays a symmetric rectangular voltammogram even at different scan rates, indicating the typical characteristic behaviour of EDLC [14]. Figure 5.1.7 shows the CD curves of the NLMC-4 electrode measured at different current densities (1 A g^{-1} to 20 A g^{-1}). The CD profile shows a perfect linear and symmetric triangular shape even at higher current densities with negligible potential drop. This is due to the low resistance of the electrode. The C_s calculated from the CD profile is 138 F g^{-1} at 1 A g^{-1}, which is comparable with the reported capacitance for porous carbon electrodes in the literature [7,15,16]. The gravimetric capacitance is directly proportional to the specific surface area of the electrode material. Hence, higher BET surface area of the electrode material results in higher capacitance. However, the capacitance also depends on other textural parameters such as appropriate pore size and pore volume. For instance, the material with very high surface area and the total BET surface area of this material result only from ultra micropores, and then it may give less capacitance due to the poor access of the electrolyte ions to the pores for forming effective double layer. Therefore, the effective specific surface area, which is accessible by electrolyte ions (surface area contributed from pores larger than the size of solvated electrolyte ion), will contribute in forming effective electric double layer [17,18]. It has also been demonstrated that the micropores provide active sites for adsorption-desorption of electrolyte ions that are responsible for the enhanced energy storage capability

of carbon materials, while the mesopores provide effective wider transport path for the electrolyte ions to micropores. Thus, the high specific surface area, large pore volume and narrow pore size distribution results in high gravimetric capacitance. For exapmle, L. Yiju et al. [7] prepared the activated porous carbon nanosheets from willow catkin by using one-step KOH activation process. The electrode prepared from this carbon delivered a high specific capacitance of 40 F g^{-1} at 1 A g^{-1}. E. Y. L. P. Hao et al. [19] reported the N-doped graphene aerogel delivered high specific capacitance of 197 F g^{-1} at 0.2 A g^{-1}. Teo et al. [6] reported the higher specific capacitance of 147 F g^{-1} for the activated carbon derived from rice husk.
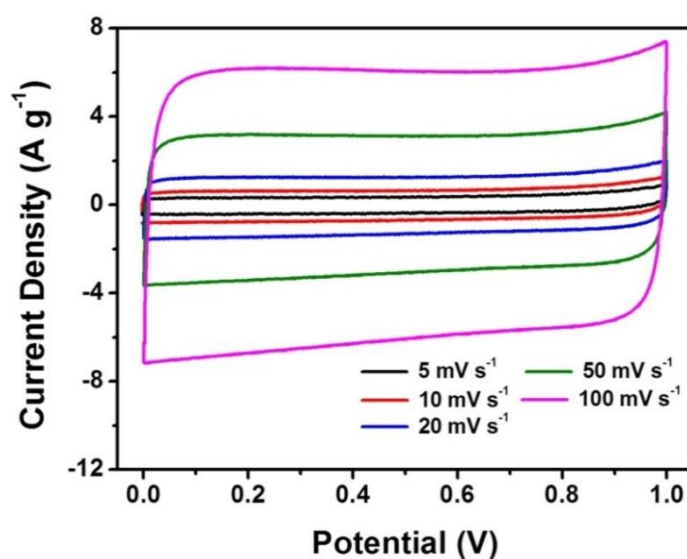
Figure 5.1.6 CV profile of the NLMC-4 electrode obtained at different scan rates in two electrode system.
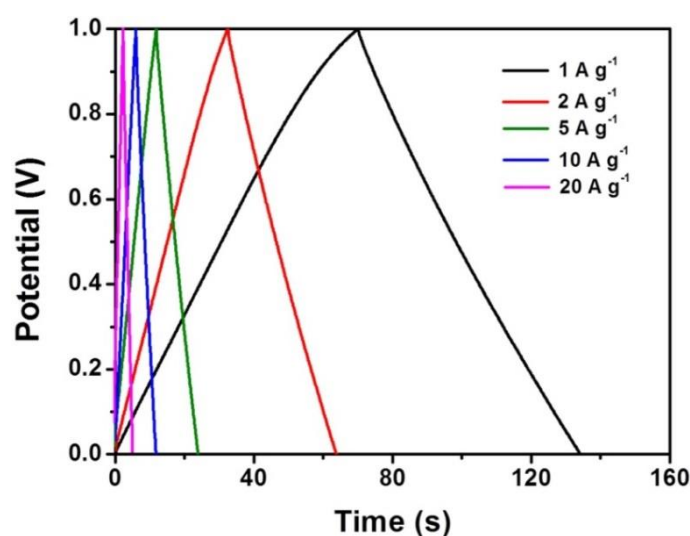
Figure 5.1.7 Charge/discharge profile of the NLMC-4 electrode obtained at different current densities in the two-electrode system.
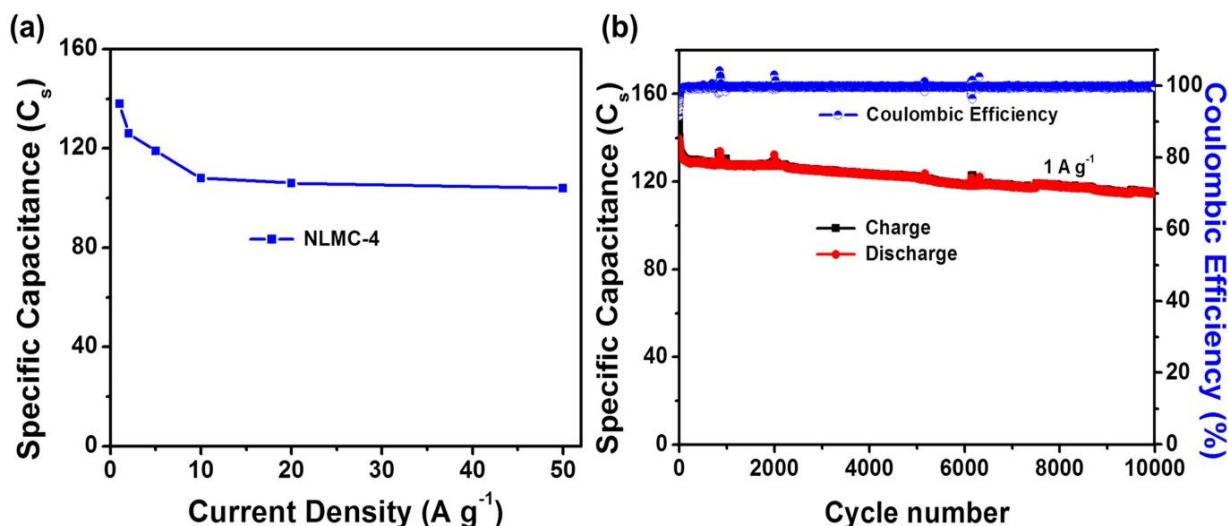
Figure 5.1.8 (a) Rate capability measured at different current densities and (b) long term cycle performance curve of NLMC-4 electrode measured at 1 A g^{-1} in the two-electrode system.

Figure 5.1.8a shows the rate capability of the electrode measured at different current densities in the range of 1 A g^{-1} to 50 A g^{-1}. It can be observed from the figure 5.1.8a that the electrode shows excellent C$_s$ retention of 75% even at high current density of 50 A g^{-1}. This result indicates good charge storage capability of the electrode during the fast reaction kinetics. Further, the NLMC-4 electrode is also tested for the long-term stability at 1 A g^{-1} and the cycle performance curve is shown in the figure 5.1.8b. The electrode retained a capacitance of 83% even after 10,000 cycles, indicating the high electrochemical stability of the electrode. Thus, the NLMC-4 with high surface area, large pore volume and good graphitic carbon structure is considered to be a suitable candidate for high performing supercapacitors.

Figure 5.1.9 shows the Nyquist plot of the NLMC-4 electrode in symmetric configuration measured before the cycling process. The electrode showed a depressed semi-circle in the high frequency region, which corresponds to charge transfer region and an inclined line in the low frequency region, which is associated with the diffusion of ions in the porous electrodes. The experimental results are fitted well with the equivalent circuit shown in the inset of the figure 5.1.9. The electrode showed a low R$_{ct}$ value of 0.51 Ω, which indicates the effective formation of the EDLC at the interface.
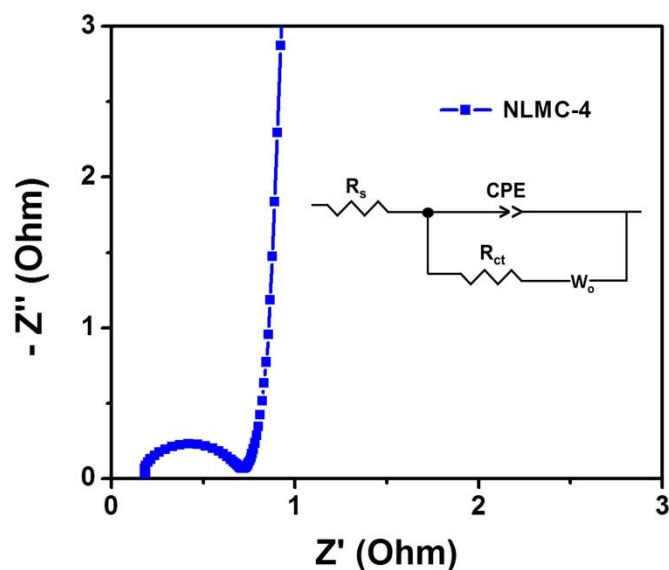
Figure 5.1.9 Nyquist plot of NLMC-4 electrode in the two-electrode system.

5.1.2 Conclusions

A one-step KOH activation process has been employed in the present study to synthesize porous carbon materials from the fallen neem leaves. These activated carbons are characterized with high surface area and large pore volume. Among all the electrodes, the NLMC-4 delivered a high specific capacitance of 233 F g^{-1} at the current density of 1 A g^{-1} in the three-electrode configuration. Further, the NLMC-4 electrode in two-electrode configuration exhibited excellent electrochemical properties in terms of high rate capability with 75% of C_s retention at a current density of 50 A g^{-1}. Moreover, the electrode showed good cycle stability and delivered 85% of C_s retention even after 10,000 cycles. This behaviour is mainly due to the presence of micro and mesoporous structures in the activated carbon with large pore volume.

Section 5.2 Tissue Paper-Derived Micro and Mesoporous Carbon as an Electrode for Supercapacitor

The textural properties and high graphitic nature of the tissue paper-derived micro and mesoporous carbon (p-GCS) are responsible for the p-GCS to be a good matrix for sulfur cathode in a Li-S battery. The results of the electrochemical studies of the p-GCS for sulfur cathode in Li-S battery have already been discussed in the chapter 3. The investigator has also investigated the performance of p-GCS electrode for application in supercapacitors. The electrochemical performance of the as-prepared p-GCS has been measured in both the three-electrode (3E) and the two-electrode (2E) systems by using 6M KOH as the electrolyte. The details of the electrode preparation for both the systems have been given in the chapter 2 and the electrochemical performance of these electrodes is discussed hereunder.

5.2.1 Results and Discussion: Electrochemical Studies (CV, C/D, CY and EIS)

5.2.1.1 Three-Electrode System

The CV studies have been carried out to evaluate the electrochemical performance of the p-GCS electrodes. Figure 5.2.1 shows the CV curves of p-TPC, p-GCS-1 and p-GCS-2 electrodes tested in 3E system at different scan rates ranging from 1 mV s^{-1} to 100 mV s^{-1}. Figure 5.2.1a shows the CV profiles of p-TPC, p-GCS-1 and p-GCS-2 electrodes measured at 100 mV s^{-1} scan rate. Both the *in-situ* activated carbon samples display a quasi-rectangular shape curve, which indicates good rate capability of the electrodes. Whereas, the p-TPC shows a deviation from the rectangular shape, which infers a poor supercapacitive behaviour of the electrode [19]. Further, the CV profiles of the electrodes prepared from p-TPC, p-GCS-1 and p-GCS-2 have also been studied at different scan rates and are as shown in the figure 5.2.1b, c and d. The CV profiles of p-GCS-1 and p-GCS-2 exhibit a symmetric quasi-rectangle shape at different scan rates and the CV profile of the p-TPC displays a triangular shape curve at different scan rates. The former profiles represent the characteristic EDLC behaviour of SC and the later corresponds to a poor EDLC behavior. These results infer that the p-GCS with unique textural properties renders numerous active sites for ion adsorption on its surface and the resulting cell displays good electrochemical performance for supercapacitor application.
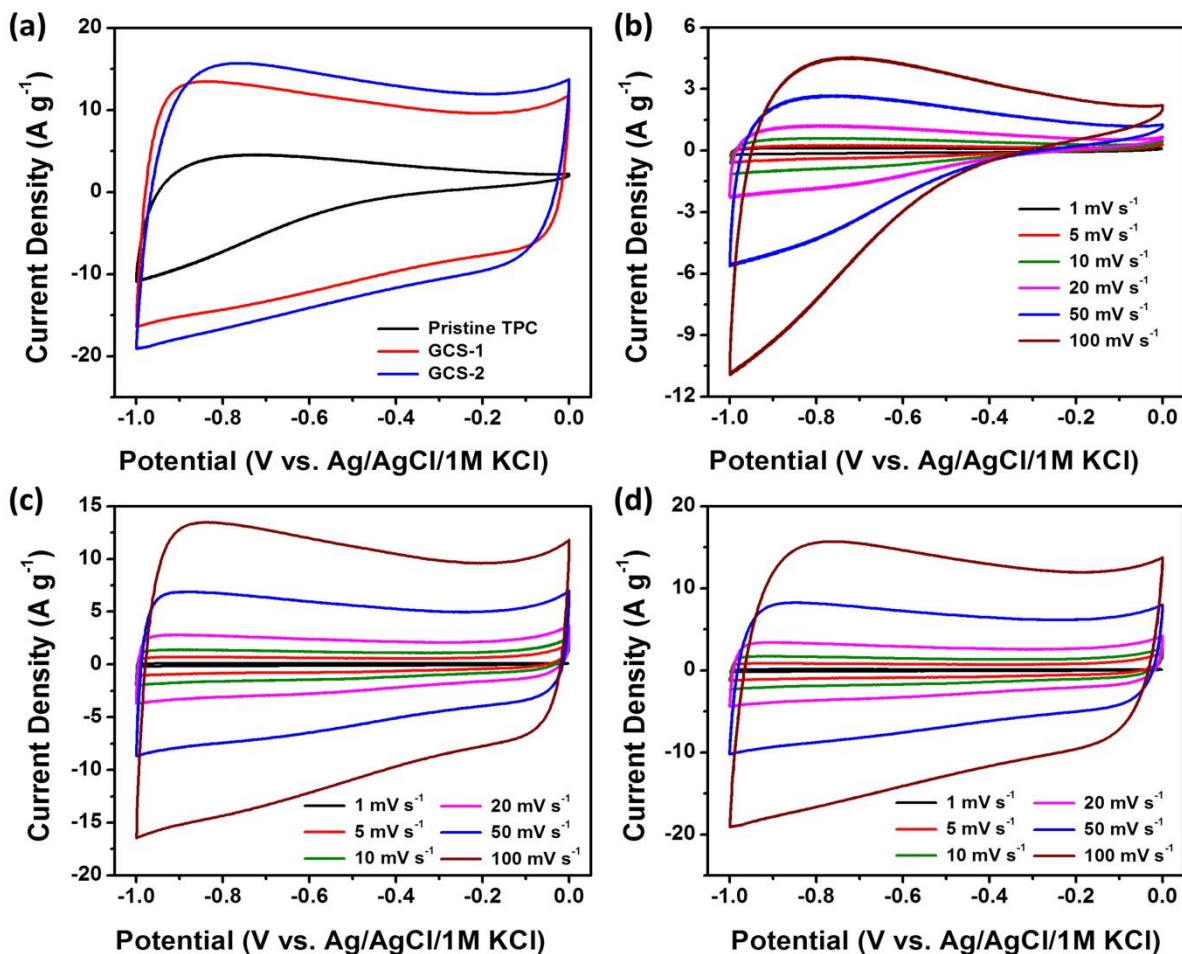
Figure 5.2.1 (a) Comparative cyclic voltammetric profiles measured at 100 mV s^{-1} and (b-d) corresponding CV curves of p-TPC, p-GCS-1 and p-GCS-2 measured at different scan rates in the three-electrode system.

Figure 5.2.2 shows the charge/discharge profiles of p-TPC, p-GCS-1 and p-GCS-2 electrodes measured at different current rates (1 A g^{-1} to 20 A g^{-1}). Initially, all the electrodes were tested at a current density of 1 A g^{-1} and the CD curves are shown in the figure 5.2.2a. The CD profiles of these electrode materials show a symmetric triangle shape with negligible iR drop indicating less resistance in the material. This result indicates the capacitive nature of the electrodes and good electrochemical stability. It has been reported in the literature that the specific capacitance value is higher in carbon with porous structures as well as in carbon with graphitic nature [20,21]. The specific capacitance values calculated from the CD curves of p-TPC, p-GCS-1 and p-GCS-2 at 1 A g^{-1} current density are 63 F g^{-1}, 170 F g^{-1} and 212 F g^{-1}, respectively. Among them, the p-GCS-2 electrode exhibits the best electrochemical performance as supercapacitor in comparison to p-TPC and p-GCS-1 due to its high specific surface area and large pore volume.
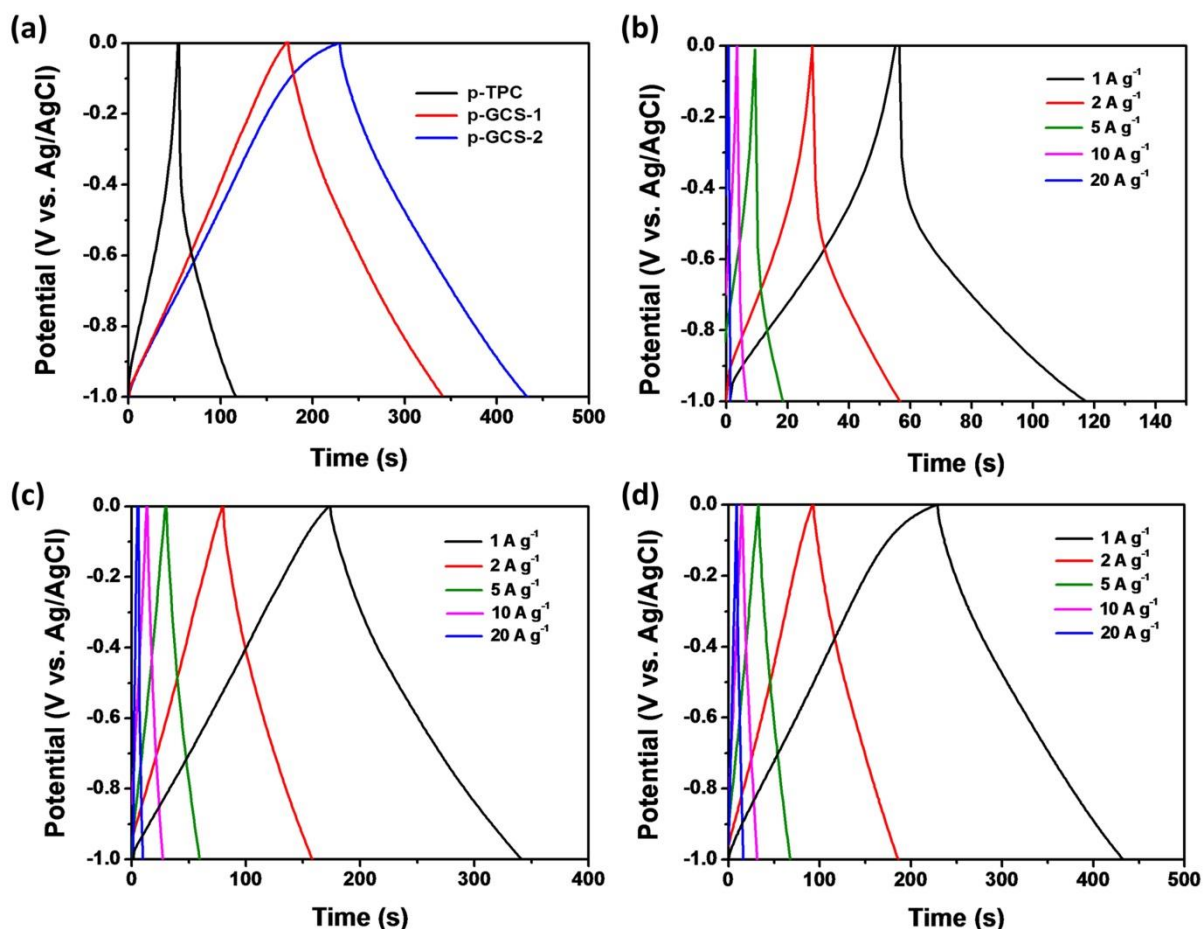
Figure 5.2.2 (a) Comparative charge/discharge curves measured at 1 A g^{-1} and (b-d) Corresponding CD curves of p-TPC, p-GCS-1and p-GCS-2 measured at different current densities in the three-electrode system.

Further, the rate capability of these electrodes has also been measured and compared in the figure 5.2.3. Among all the electrodes, the p-GCS-2 showed the highest specific capacitance retention of 72% at a current density of 50 A g^{-1}. Whereas, the p-GCS-1 and p-TPC exhibit low C$_s$ retention of 50% and 16%, respectively. W. Liu et al. [22] also observed the higher C$_s$ retention values for the activated carbon derived from the wheat straw having high surface area with large pore volume. They reported that superior C$_s$ retention is due to the presence of more number of mesoporous structures in the sample that provide the channels for easy transfer and diffusion of ions from the electrolyte to the bulk of the electrode surface. Moreover, the specific capacitance of the electrode material decreases with an increase in current density, which is ascribed to diffusion limitation [21]. These results infer that the p-GCS-2 with high surface area and large pore volume is considered to be a potent candidate for high performing supercapacitor.
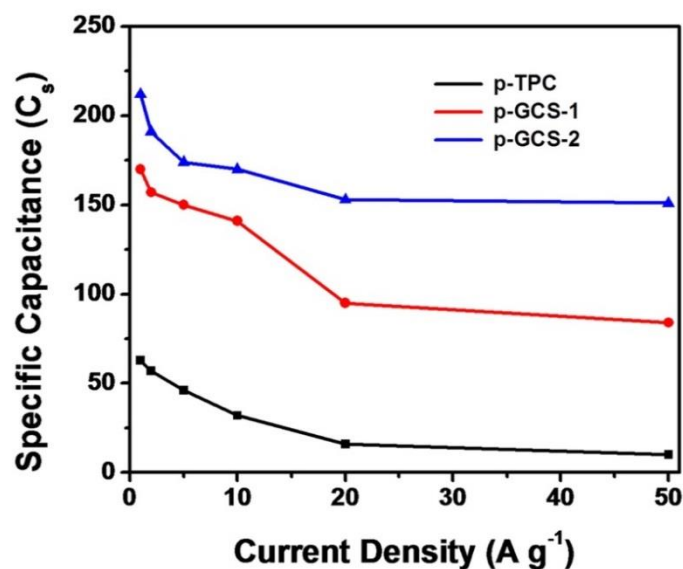
Figure 5.2.3 Rate capability of p-TPC, p-GCS-1 and p-GCS-2 electrode measured in the three-electrode system.

The superior electrochemical performance of the p-GCS electrodes is further supported by EIS. Figure 5.2.4 shows the Nyquist plots of p-TPC, p-GCS-1 and p-GCS-2 electrodes. All the Nyquist plots show depressed semicircles in the charge transfer region, which corresponds to charge transfer resistance (R_{ct}) at the interface between electrode and electrolyte. The polts are also characterized by Warburg impedance in the low frequency region indicating the diffusion of ions [14]. The experimental results are fitted well with those of the equivalent circuit model, shown in the inset of the figure 5.2.4.
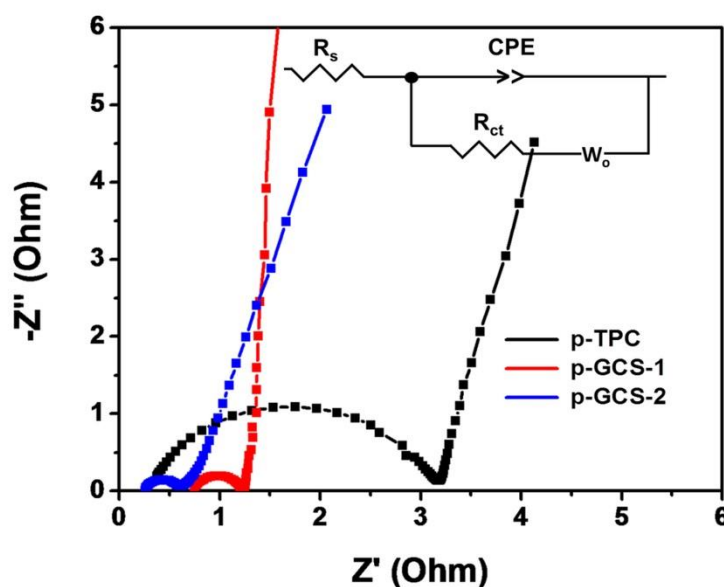
Figure 5.2.4 Nyquist plot curves of p-TPC, p-GCS-1 and p-GCS-2 electrodes measured in the three-electrode system.

The R_{ct} values calculated for p-TPC, p-GCS-1 and p-GCS-2 electrodes are 1.6Ω, 1.1Ω, and 0.9Ω respectively. The less charge transfer resistance exhibited by the *in-situ* activated samples demonstrates good conductivity of the electrodes. A nearly vertical line is observed in the low frequency region indicating a good capacitive behavior of the electrode material [6].

5.2.1.2 Two-Electrode System

Since the p-GCS-2 electrode has shown better electrochemical performance in the 3E configuration, it is further tested in a 2E symmetric system with a cell voltage of 1V. Figure 5.2.5 shows the schematic representation of a symmetric supercapacitor, wherein, a thin sheet-like p-GCS-2 provides more active sites for ion adsorption and also improves the reaction kinetics during the fast charge/discharge process.
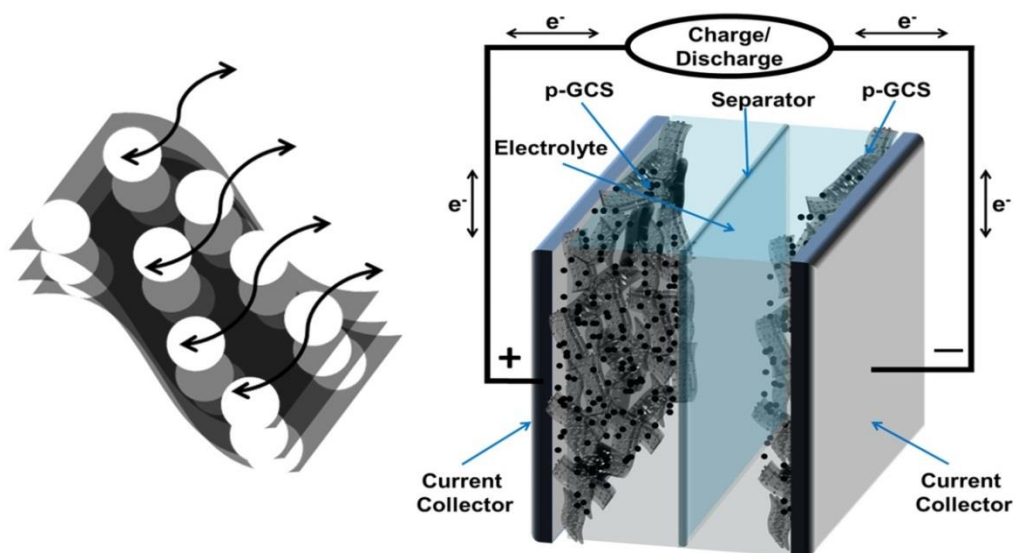
Figure 5.2.5 Schematic representation of symmetric supercapacitor.

Figure 5.2.6 shows the CV profile of the p-GCS-2 electrode obtained at different scan rates. The electrode exhibits a symmetric rectangular shape even at high scan rates, indicating the characteristic EDLC behavior of the GCS-2 electrode. Further, the CD profiles measured at different current densities (figure 5.2.7) are of symmetric triangular-type with negligible voltage drop even at high current rates. This result infers the less resistance in the electrode material. The C_s calculated from the corresponding CD profile is 129 F g^{-1} at 1A g^{-1}, which is comparable with the reported capacitance values for porous carbons in the literature. For example, Yiju Li et al. [7] reported a specific capacitance of 40 F g^{-1} at 1 A g^{-1} for porous carbon nanosheets derived from willow catkin. W. H. Qu et al. [16] synthesized porous carbon from corn cob residue and obtained a specific capacitance of 120 F g^{-1} at 1 A g^{-1}.
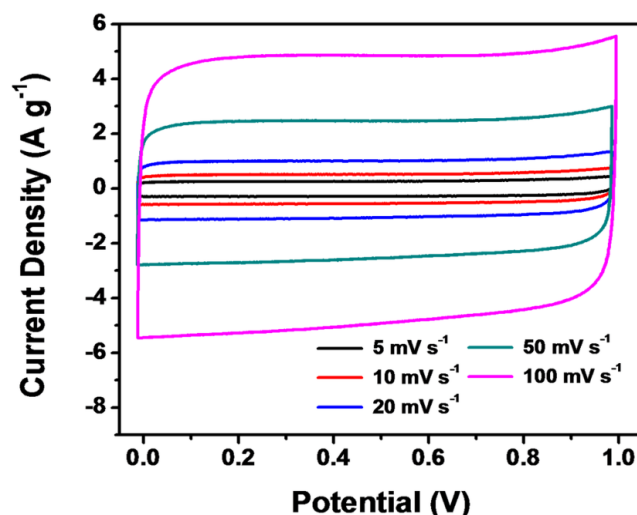
Figure 5.2.6 CV curves of p-GCS-2 electrode measured at different scan rates.
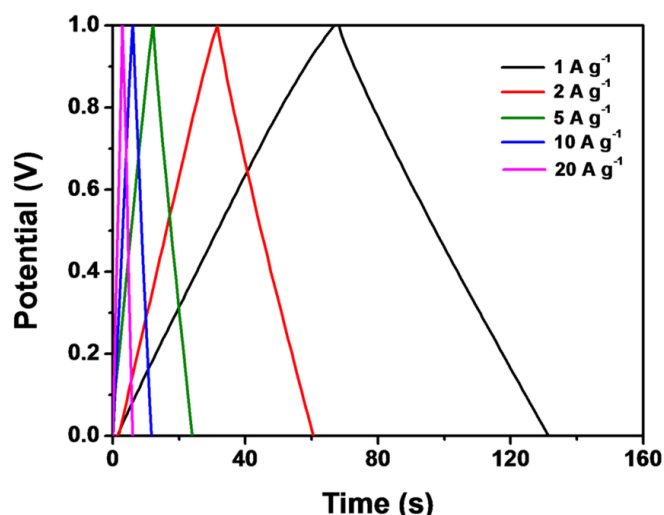
Figure 5.2.7 CD profiles of p-GCS-2 electrode measured at different current densities.

The rate capability of the p-GCS-2 electrode measured in symmetric configuration is shown in the figure 5.2.8a. It is found that the electrode material has shown excellent capacitance retention of 85% at a higher current density of 50 A g^{-1}, which indicates the fast reaction kinetics during the charge/discharge process. The supercapacitor cells (p-GCS-2-symmetric system) fabricated by aqueous 6M KOH were used for demonstrating the lighting of LEDs as shown in the in-set of figure 5.2.8a. The three of such cells are combined in series to attain a maximum output potential of 3 V to light 40 LEDs connected in parallel. Thus, the micro and mesoporous structured p-GCS-2 synthesized in the present study can be considered as suitable electrode for high performing supercapacitors. The p-GCS-2 is also tested for longer cycles at 1 A g^{-1} and the result is shown in figure 5.2.8b. It is observed that the material retains a capacitance of 90% even after 10,000 cycles, indicating the long-term cyclic stability and excellent electrochemical reproducibility.
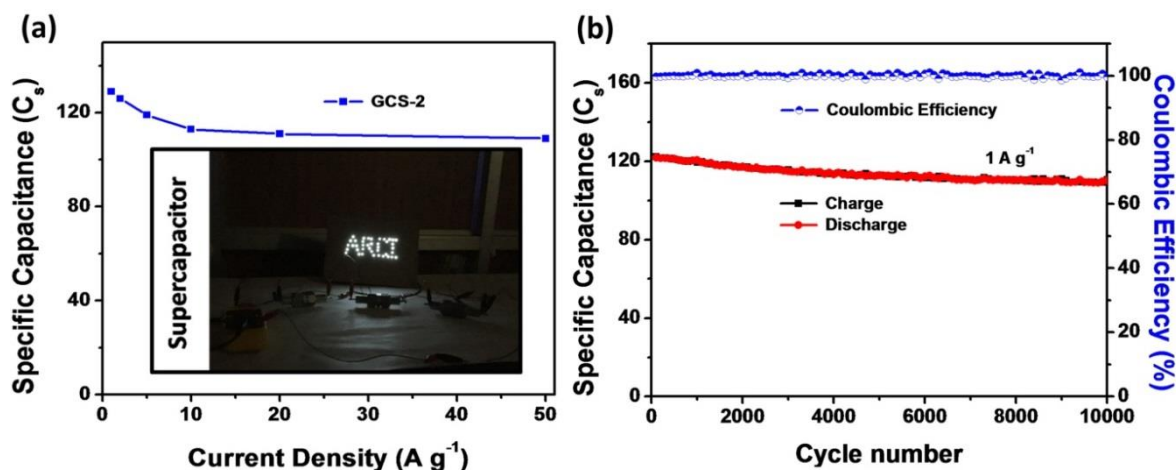
Figure 5.2.8 (a) Rate capability (with in-set of photo image of LED lights with three aqueous KOH based cells connected in series) and (b) cyclic stability profile of p-GCS-2 measured at 1 A g^{-1} current density in two-electrode configuration.

The improved performance of the p-GCS-2 electrode is further supported by impedance studies. The p-GCS-2 electrode showed a depressed semicircle in the high frequency region, which corresponds to the charge transfer region [23]. The inclined line in the relatively low frequency region is due to Warburg impedance, which is associated with the diffusion of ions in the porous structures of electrode. The experimental results are fitted well with the equivalent circuit shown in the inset of the figure 5.2.9. The electrode displayed lower R$_{ct}$ value of 0.4 Ω indicating the improved charge transfer process and effective formation of the electrical double layer at the interface.
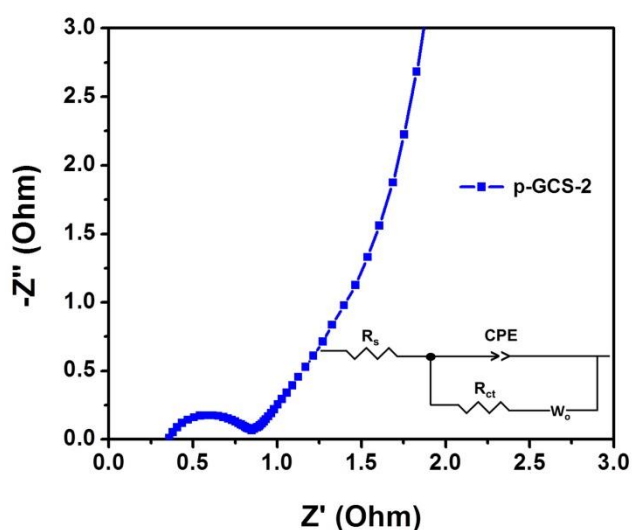
Figure 5.2.9 Nyquist plot of p-GCS-2 electrode measured in two-electrode system.

Furthermore, the investigator has also evaluated the electrochemical performance of the p-GCS-2 electrode at different current densities in the range, 1 A g^{-1} to 20 g^{-1} (figure

5.2.10). Initially, the cell displayed an average specific capacitance of 129 F g^{-1} for 1000 cycles at the current density of 1 A g^{-1}. When the current density is increased to 2 A g^{-1}, 5 A g^{-1}, 10 A g^{-1} and 20 A g^{-1}, the cell still retained good capacitance values of 124 F g^{-1}, 118 F g^{-1}, 113 F g^{-1} and 108 F g^{-1} respectively. After testing the cell at higher current densities, the cell has been again tested at low current density of 1 A g^{-1} and the resulting cell displayed capacitance retention of 119 F g^{-1} even after 6000 cycles. This improved electrochemical performance of the p-GCS-2 at high current densities is attributed to the unique properties of the p-GCS-2 electrode such as high surface area and high electrical conductivity.
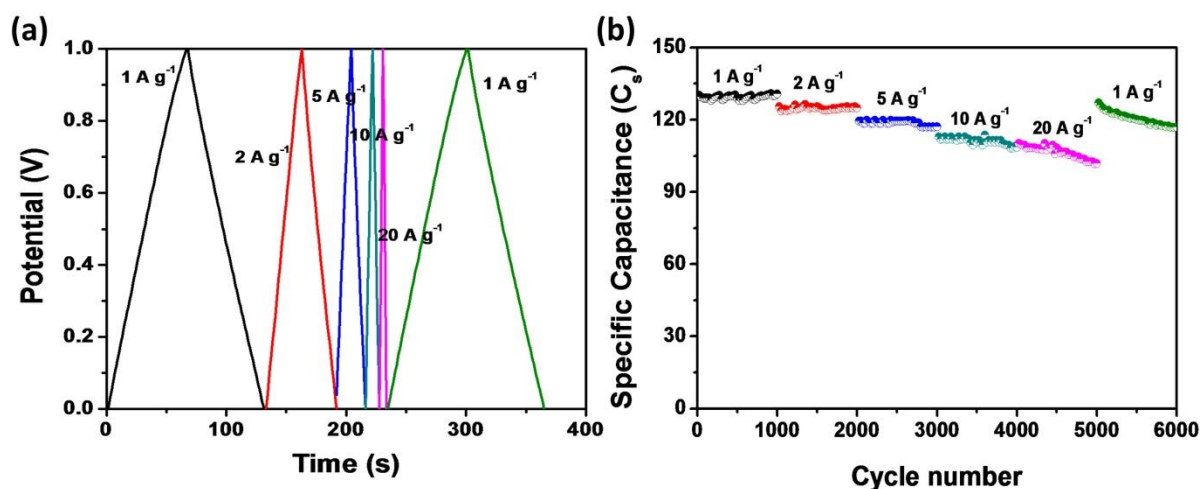
Figure 5.2.10 (a) CD and (b) rate capability of p-GCS-2 electrode measured at different current densities (1 A g^{-1}, 2 A g^{-1}, 5 A g^{-1}, 10 A g^{-1} and 20 A g^{-1}) each for 1000 cycles in symmetric configuration.

5.2.2 Conclusions

The *in-situ* KOH activation process has been adopted to synthesize activated carbon with high surface area (1684 m^2 g^{-1}), large pore volume and highly graphitised carbon structures from commercially available tissue paper. In the three-electrode configuration, the p-GCS electrode delivered a high specific capacitance of 212 F g^{-1} at the current density of 1 A g^{-1}. Further, the p-GCS electrode also showed excellent electrochemical properties in terms of high rate capability of 85% of C$_s$ retention at the current density of 50 A g^{-1} and high cyclic stability of 90% of C$_s$ retention even after 10,000 cycles in the two-electrode system. Good electrochemical properties of the p-GCS-2 electrode can be attributed to the well-developed micro and mesoporous structure, highly ordered graphitic carbon content, high specific surface area and large pore volume. The novel approach reported in the present study is proved to be one of the best methods for the synthesis of the graphitic carbon sheets, which are highly promising for the large scale production of graphitic carbon.

Section 5.3 Comparison of the Micro and Mesoporous Carbon Materials Developed in the Present Study with those reported in the Literature

This section compares the electrochemical performance of the developed micro and mesoporous carbon materials derived from neem leaves and tissue paper with the activated carbons reported in the literature in the form of a table, 5.3.1. Both the electrodes prepared from NLMC-4 and p-GCS-2 has high specific capacitance, high rate capability and excellent electrochemical stability during the charge/discharge process. These results of the present study are compared with those of the bio-derived activated carbons reported in the literature at low and high current densities in two-electrode configuration by using aqueous KOH as the electrolyte (table 5.3.1). For example, N. Guo et al. [24] reported a higher specific capacitance value of 209 F g^{-1} at a current density of 0.2 A g^{-1} for the N-doped hierarchical porous carbon derived from hemp stems. When the electrode was tested at 20 A g^{-1}, the electrode retained a specific capacitance of 130 F g^{-1}. X. Han et al. [23] prepared N-doped porous carbon from pueraria by a two-step activation process. The electrode prepared from this activated carbon delivered higher specific capacitance of 250 F g^{-1} at 0.5 A g^{-1} current density and retained a capacitance retention of 92% even at 10 A g^{-1}. The higher capacitance exhibited by these activated carbons is due to their unique properties such as high surface area, large pore volume and presence of graphitic carbon. Moreover, the presence of heteroatoms on the surface of carbon matrix involved in the redox reaction during charge/discharge process, which provide additional pseudocapacitance value. As a result, the internal resistance of the electrode decreases and the cell exhibits an improved electrochemical performance. E. Y. L. Teo et al. [6] synthesized the activated carbon derived from rice husk by using KOH as activating agent. The electrode delivered a high specific capacitance of 122 F g^{-1} at 1 A g^{-1} current density due to higher surface area and large pore volume.

Thus, the electrodes prepared from NLMC and p-GCS delivered higher specific capacitance with good rate capability, which are comparable with the activated carbons derived from the biomass for application in supercapacitor.

Table 5.3.1 Comparison of specific capacitance values with those of reported in the literature in two-electrode symmetric configuration measured in aqueous electrolyte system.

Carbon source	Activating Agent	Specific capacitance at lower current density		Specific capacitance at higher current density		Capacity retention (%)	Ref
		current density ($A g^{-1}$)	Specific capacitance (C_s)	Current density ($A g^{-1}$)	Specific capacitance (C_s)		
Rice husk	KOH	0.1	147	1	122	83	6
Hemp stems	KOH	0.2	209	20	130	63	24
Willow catkin	KOH	0.1	50	10	30	60	7
Chitosan	KOH	0.2	197	10	108	55	19
Glucose	KOH	0.05	85	2	45	53	15
Pueraria	K_2CO_3	0.5	250	10	231	92	23
Wheat straw	$CaCl_2$	0.1	152	8	80	52	22
Wood sawdust	KOH	0.05	255	8	50	20	25
Neem leaves	KOH	1	138	50	104	75	This work
Tissue paper	KOH	1	129	50	110	85	This work

References

1. Ostafiychuk, B. K., Budzulyak, I. M., Rachiy, B. I., Vashchynsky, V. M., Mandzyuk, V. I., Lisovsky, R. P., Shyyko, L. O., Thermochemically Activated Carbon as an Electrode Material for Supercapacitors. *Nanoscale Res. Lett.* **10**, 1-8 (2015).

2. Nitze, F., Fossum, K., Xiong, S., Matic, A., Palmqvist, A. E. C. Sulfur-Doped Ordered Mesoporous Carbons : A Stability-Improving Sulfur Host for Lithium-Sulfur Battery Cathodes. *J. Power Sources* **317**, 112-119 (2016).

3. Sun, F., Wang, J., Chen, H., Li, W., Qiao, W., Long, D., Ling, L., High Efficiency Immobilization of Sulfur on Nitrogen-Enriched Mesoporous Carbons for Li-S Batteries. *ACS Appl. Mater. Interfaces* **5**, 5630-5638 (2013).

4. Ramesh, T., Rajalakshmi, N., Dhathathreyan, K. S., Reddy, L. R. G. Hierarchical

Porous Carbon Microfibers Derived from Tamarind Seed Coat for High-Energy Supercapacitor Application. *ACS Omega* **3**, 12832-12840 (2018).

5. Han, Y., Shen, N., Zhang, S., Li, D., Li, X. Fish Gill-Derived Activated Carbon for Supercapacitor Application. *J. Alloys Compd.* **694**, 636-642 (2017).

6. Teo, E. Y. L., Muniandy, L., Ng, E. P., Adam, F., Mohamed, A. R., Jose, R., Chong, K. F., High Surface Area Activated Carbon from Rice Husk as a High Performance Supercapacitor Electrode. *Electrochim. Acta* **192**, 110-119 (2016).

7. Li, Y., Wang, G., Wei, T., Fan, Z., Yan, P. Nitrogen and Sulfur Co-doped Porous Carbon Nanosheets Derived from Willow Catkin for Supercapacitors. *Nano Energy* **19**, 165-175 (2016).

8. Xie, Q., Bao, R., Zheng, A., Zhang, Y., Wu, S., Xie, C., Zhao, P. Sustainable Low-Cost Green Electrodes with High Volumetric Capacitance for Aqueous Symmetric Supercapacitors with High Energy Density. *ACS Sustain. Chem. Eng.* **4**, 1422-1430 (2016).

9. Subramanian, V., Luo, C., Stephan, A. M., Nahm, K. S. Thomas, S., Wei, B. Supercapacitors from Activated Carbon Derived from Banana Fibers. *J. Phys. Chem. C* **111**, 7527-7531 (2007).

10. Zhou, M., Pu, F., Wang, Z., Guan, S. Nitrogen-Doped Porous Carbons Through KOH Activation with Superior Performance in Supercapacitors. *Carbon N. Y.* **68**, 185-194 (2013).

11. Fletcher, S., Black, V. J., Kirkpatrick L., A universal equivalent circuit for carbon-based supercapacitors, Journal of Solid State Electrochemistry, 18, 1377-1387 (2014).

12. Lebedeva, M. V., Yeletsky, P.M., Ayupov, A. B., Kuznetsov, A. N., Yakovlev, V. A., Parmon, V. N., Micro-Mesoporous Carbons From Rice Husk as Active Materials for Supercapacitors. *Mater. Renew. Sustain. Energy* **4**, 1-9 (2015).

13. Zhi, M., Yang, F., Meng, F., Li, M., Manivannan, A., Wu, N. Effects of Pore Structure on Performance of An Activated-Carbon Supercapacitor Electrode Recycled from Scrap Waste Tires. *ACS Sustain. Chem. Eng.* **2**, 1592-1598 (2014).

14. Yadav, N., Singh, M. K., Yadav, N., Hashmi, S. A. High Performance Quasi-Solid-State Supercapacitors with Peanut-Shell-Derived Porous Carbon. *J. Power Sources* **402**, 133-146 (2018).

15. Gao, F., Shao, G. Qu, J., Lv, S., Li, Y., Wu, M., Tailoring of Porous and Nitrogen-Rich

Carbons Derived from Hydrochar for High-Performance Supercapacitor Electrodes. *Electrochim. Acta* **155**, 201–208 (2015).

16. Qu, W., Xu, Y., Lu, A., Zhang, X., Li, W. Converting Biowaste Corncob Residue into High Value Added Porous Carbon for Supercapacitor Electrodes. *Bioresour. Technol.* **189**, 285-291 (2015).

17. Sun, L., Tian, C., Li, M., Meng, X., Wang, L., Wang, R., Yin, J., Fu, H., From coconut shell to porous graphene-like nanosheets for high-power supercapacitors, *J. Mater. Chem.* A, **1**, 6462-6470 (2013).

18. Wei, L., Yushin, G., Nanostructured activated carbons from natural precursors for electrical double layer capacitors, *Nano Energy*, **1**, 552-565 (2012).

19. Hao, P., Zhao, Z., Leng, Y., Tian, J., Sang, Y., Boughton, R. I., Wong, C. P., Liu, H., Yang, B. Graphene-Based Nitrogen Self-Doped Hierarchical Porous Carbon Aerogels Derived from Chitosan for High Performance Supercapacitors. *Nano Energy* **15**, 9-23 (2018).

20. Chang, H., Gao, Z., Wang, X., Wu, D., Xu, F., Wang, X., Guo, Y., Kai, J. Activated Porous Carbon Prepared from Paulownia Flower for High Performance Supercapacitor Electrodes. *Electrochim. Acta* **157**, 290-298 (2015).

21. Ba, H., Wang, W., Pronkin, S., Romero, T., Baaziz, W. Biosourced Foam-Like Activated Carbon Materials as High-Performance Supercapacitors. *Adv. Sustain. Syst.* **2**, 1700123 (2018).

22. Liu, W., Mei, J., Liu, G., Kou, Q., Yi, T., Xiao, S. Nitrogen-Doped Hierarchical Porous Carbon from Wheat Straw for Supercapacitors. *ACS Sustain. Chem. Eng.* **6**, 11595–11605 (2018).

23. Han, X., Jiang, H., Zhou, Y., Hong, W., Zhou, Y., Gao, P., Ding, R., Liu, E. A High Performance Nitrogen-Doped Porous Activated Carbon for Supercapacitor Derived from Pueraria. *J. Alloys Compd.* **744**, 544-551 (2018).

24. Guo, N., Li, M., Wang, Y., Sun, X., Wang, F., Yang, R. N-Doped Hierarchical Porous Carbon Prepared by Simultaneous-Activation of KOH and NH$_3$ for High Performance Supercapacitors. *RCS Advnaces* **6**, 101372–101379 (2016).

25. Yu, S., Liu, D., Zhao, S., Bao, B., Jin, C., Huang, W., Chen, H., Shen, Z. Synthesis of Wood Derived Nitrogen-Doped Porous Carbon-Polyaniline Composites for Supercapacitor Electrode Materials. *RCS Advnaces* **5**, 30943-30949 (2018).

Chapter 6
Summary and Conclusions

The next generation energy storage systems such as Li-S batteries and supercapacitors need new electrode materials and design of novel cell configurations that can overcome the scientific and technological issues for commercialization of these systems. In this context, the investigator has developed new porous electrode materials with unique textural properties for application in Li-S batteries and supercapacitors. The nanostructured porous electrodes prepared by using cost effective processes have shown an improved electrochemical performance and excellent cycle stability.

During the course of this research study, the investigator has synthesized the micro and mesoporous structured carbons from neem leaves, tissue paper and jute stalks by the KOH activation process. In Li-S battery, these micro and mesoporous carbon materials act as conducting media, trap the dissolved polysulfide species and also accommodate large volume expansion during the lithiation process. The investigator has also focussed on synthesizing high capacity anodes such as Sn/graphene and Si/graphite composites as alternatives to lithium anode. The results of the electrochemical studies of the electrode materials in half cell configuration have provided enough scope for the fabrication of the lithiated Si-S battery in full cell configuration. For supercapacitor, the micro and mesoporous carbons developed in the present study functioned as high charge storage electrodes due to their high surface to volume ratio and high electrical conductivity.

KOH activation method has been employed in the present study to synthesize the activated carbons (ACs) from neem leaves, tissue paper and jute stalks. The sulfur infused micro and mesoporus carbon/sulfur composites have been prepared by the melt-diffusion method. Electrodeposition and ball milling processes have been employed for the synthesis of Sn/graphene and Si/graphite composites respectively. The morphological studies of the composite materials have been carried out by using field emission scanning electron microscopy (FE-SEM) and transmission electron microscopy (TEM). The distribution of elemental sulfur in the micro and mesoporous carbon/sulfur composites has been obtained using energy dispersive X-ray spectroscopy (EDS) elemental mapping and the amount of elemental sulfur in them has been analysed by thermogravimetry (TG). The surface area and pore size of the ACs have been determined by the BET analysis. The crystal structure and the

type of carbon present in the synthesized composites have been analysed by X-ray diffraction (XRD) technique and Raman spectroscopy.

In Li-S battery, the electrochemical performance of the porous carbon/sulfur, Sn/graphene and Si/graphite electrodes have been evaluated by using lithium metal as anode and 1M LITFSI containing 5 wt% of $LINO_3$ as the electrolyte. The Li-S battery in full cell configuration has also been fabricated by using porous carbon/sulfur cathode and a thin layer of lithium foil placed on the surface of Si/graphite as anode. The cyclic voltammetric studies, charge/discharge and cycle performance studies of the cathodes, anodes and full cells have been carried out in the potential range of 1.5-2.8 V, 0.01-1.5 V and 1.0-2.6 V, respectively. For superapacitor application, both the three-electrode and two-electrode configurations have been adopted for evaluating the electrochemical performance of the porous carbon electrodes by using 6M KOH (aqueous) as the electrolyte. The cyclic voltammetric studies, charge/ discharge and cycle performance curves for the electrodes in both the three-electrode and two-electrode systems have been performed in the potential range of -1.0 to 0.0 V and 0.0 to 1.0 V respectively.

The activated carbon derived from the fallen neem leaves (NLMC-4) exhibited a high surface area of 1872 m^2 g^{-1} and large pore volume of 1.59 cc g^{-1} in comparison to the other NLMC samples. Wherein, NLMC-4 is prepared by mixing the powder of neem leaves to KOH in the weight ratio of 1:0.4 followed by heat treating the dried sample at 1000 ºC under Ar atmosphere. EDS elemental mapping of the porous carbon/sufur composites shows the homogenous distribution of sulfur throughout the carbon matrix. Among all the composites, the sulfur infused NLMC-4/S50 electrode with 50 wt% of sulfur loading delivered the highest discharge capacity of 1396 mAh g^{-1} at 0.1 C rate. Even after 50 cycles, this electrode displayed a high discharge capacity of 896 mAh g^{-1}. This result infers that the presence of abundant micro and mesopores structures in the carbon matrix inhibits the dissolution of polysulfides into the electrolyte. Moreover, when the current is increased from 0.1 to 1 C rate, NLMC-4/S50 electrode exhibited superior electrochemical performance and delivered higher discharge capacity of 506 mAh g^{-1} in comparison to the NLMC-1/S cathode (38 wt% of sulfur loading) with a discharge capacity of 33 mAh g^{-1} at 200th cycle.

Another activated carbon developed in the present study is the porous graphitic carbon sheets (p-GCS) from tissue paper by a facile one-step process, i.e., *in-situ* KOH chemical activation process. The FE-SEM and TEM images of p-GCS materials revealed the presence of graphene-like carbon structures with excellent textural parameters. XRD and Raman

analysis inferred the presence of highly graphitised carbon structures in the sample in comparison to the pristine tissue paper carbon (p-TPC). These results also suggested that the carbon precursor, activating agent and the activation temperature play an important role in the formation of graphitic structures in the carbon. The p-GCS-2/S electrode with p-GCS-2 modified separator delivered a high initial discharge capacity of 1497 mAh g^{-1} and retained a discharge capacity of 992 mAh g^{-1} at 0.2 C rate after 50 cycles. The improved electrochemical performance of the electrode is due to the synergistic effect explained below. The p-GCS-2 acts as a matrix for dissolved polysulfide species, whereas the p-GCS modified separator acts as a barrier film that inhibits the migration of dissolved polysulfides to the anode surface and also increases the reutilization of the active material during the redox process. The modified separator also improves the ionic and electronic conductivities during the redox process. When the p-GCS-2/S electrode is tested at high current rate of 1 C with modified separator, the resulting cell delivered a high discharge capacity of 652 mAh g^{-1} after 200 cycles in comparison to the p-GCS-2/S electrode with pristine polypropylene separator.

The third activated carbon developed by the investigator is the micro and mesoporous carbon (MGC) derived from the jute stalks by two-step KOH chemical activation process. The as-prepared MGC exhibits a high surface area of 2047 m^2 g^{-1} with a large pore volume of 1.69 cc^3 g^{-1}. The TEM and Raman analysis reveal the presence of highly graphitised carbon structures with graphene-like morphological appearance. Studies have been made to optimise the amount of sulfur loading into the carbon matrix. Among the composites, the MGC/S-2 electrode with 64 wt % sulfur loading delivered a stable discharge capacity of 868 mAh g^{-1} at 0.2 C rate for over 40 cycles. In addition, the MGC coated separator has been used in order to further enhance the electrochemical performance of the MGC/S-2 electrode and the resulting half cell delivered a high initial discharge capacity of 1542 mAh g^{-1} at 0.2 C rate. Even after 50 charge/discharge cycles, the electrode retained a discharge capacity of 1016 mAh g^{-1} with good coulombic efficiency. Furthermore, the electrochemical performance of the MGC/S-2 electrode with high active material loading of 5.4 mg cm^{-2} and 9.3 mg cm^{-2} has also been evaluated at 0.2 C rate. The MGC/S-2 electrode with sulfur loading on the electrode of 5.4 mg cm^{-2} and 9.3 mg cm^{-2} delivered discharge capacities of 871 mAh g^{-1} and 632 mAh g^{-1}, respectively even after 50 cycles. The EDS elemental mapping has been done on the modified separator measured after 50 charge/discharge cycles with 9.3 mg cm^{-2} sulfur loading on the electrode. The homogenous distribution of sulfur throughout the carbon infers that the MGC

coated separator acts as a barrier film as well as the upper current collector that improves the reutilization of the active material during the redox process.

Electrodeposition method has been employed in the present study for the synthesis of binder-free Sn/graphene composite material for use as anode in the lithium-sulfur battery. The FE-SEM images reveal that the electrodeposited Sn/graphene shows highly porous 3D dendritic structures. The presence of graphene in the composite has been confirmed by analysing the partially leached Sn/graphene composite by FE-SEM analysis, which was further confirmed by the Raman spectral analysis. In order to further improve the electrochemical performance of Sn/graphene, a protective RGO layer is coated onto the surface of the Sn/graphene composite, which minimizes the progressive SEI layer formation during the redox process. Among all the composites, the Sn-G/RGO electrode delivered a very high discharge capacity of 819 mAh g^{-1} in 1M LITFSI electrolyte at 0.1 C rate at 20th cycle. The presence of graphene in the Sn matrix and RGO coating on the surface plays significant roles in enhancing the electrochemical performance of the composite during the charge/discharge process.

The second anode material developed in the present study is the Si/graphite composite prepared by the ball milling process. The XRD analysis and the Raman spectral analysis of these composites show the crystalline nature of silicon and graphite in them. The investigator has studied the effect of the weight ratio of Si to graphite on the electrochemical performance of the composite by using 1M LITFSI containing 5 wt % LiNO$_3$ as the electrolyte. In this study, the carbon paper has been used as the current collector, which has shown a positive effect in enhancing the electrochemical performance. The 3D porous structure of the carbon paper increases the adhesion of the active material, accommodates huge volume expansion during lithiation and also improves the electrical conductivity. Si5/G5 anode, at the optimised mass ratio (composite containing 1 g of silicon and 1 g of graphite), delivered a high initial discharge capacity of 3574 mAh g^{-1} and retained a discharge capacity of 1443 mAh g^{-1} even after 50 cycles at 0.2 C rate. Furthermore, the electrode exhibited good cycle stability and delivered a high discharge capacity of 816 mAh g^{-1} even at 200th cycle at 1 C rate.

The improved electrochemical performance of the cathode and anode materials in half cell configuration has provided scope for the fabrication of Li-S battery in full cell configuration. In the present study the investigator has selected the best performing and low-cost cathode and anode materials for the fabrication of the full cell. The lithiated Si-S full cells are fabricated by using MGC-2/S cathode and lithiated Si5/G5 as anode. The studies

have been made in order to optimise the weight ratio of the cathode, lithium and anode in the cell in order to achieve high capacity with good cycle stability. Lithiated Si-S cell with a weight ratio of cathode, lithium and anode as 1.0:0.7:0.7 has delivered high initial discharge capacity of 1527 mAh g^{-1} and retained the discharge capacity of 824 mAh g^{-1} after 50 cycles at 0.2 C rate. Moreover, when the current rate is increased to 1 C, the cell exhibited a high discharge capacity of 411 mAh g^{-1} even after 300 cycles. The energy density delivered by the lithiated Si-S cell calculated on the basis of the mass of combined carbon and sulfur on the electrode is about 948 Wh kg^{-1}, which is twice that of the conventional Li-ion battery (LiFePO$_4$/graphite cell: ~544 Wh kg^{-1}). Furthermore, the lithiated Si-S pouch cells fabricated in the present study have been tested for powering small electronic components.

In the present research study, the investigator has also explored the application of the micro and mesoporous NLMC and p-GCS materials for supercapacitors. Among the as-prepared NLMC samples, the NLMC-4 electrode delivered the highest capacitance of 233 F g^{-1} in three electrode system at 1 A g^{-1} current density. This performance is due to the unique textural properties of NLMC-4 such as high surface area, large pore volume and good graphitic nature, which increase the specific capacitance of the electrode. In the two-electrode symmetric configuration, the NLMC-4 electrode exhibited a capacitance of 138 F g^{-1} at 1 A g^{-1} current density with good rate capability. Furthermore, the electrode showed good electrochemical stability with 82% of capacitance retention after 10000 cycles.

The as-prepared p-GCS-2 electrode in the three-electrode configuration, delivered higher specific capacitance of 212 F g^{-1} at 1 A g^{-1} current density in comparison to p-GCS-1 and p-TPC. In the two-electrode system, the p-GCS-2 electrode exhibited a specific capacitance of 129 F g^{-1} at 1 A g^{-1} current density and showed good electrochemical performance in terms of high rate capability with 85% of capacitance (C_s) retention at 50 A g^{-1} current density and good cyclic stability of 90 % of C_s retention after 10,000 cycles. The outstanding electrochemical properties of p-GCS can be attributed to the well-developed micro and mesoporous structures with thin sheet-like morphology, large pore volume and the presence of highly graphitised carbon structures in them.

Table 6.1 New cathode and anode electrode materials developed for Li-S battery and electrodes developed for supercapacitor in the present study.

Li-S battery							
Cathode materials							
S.No	Carbon precursors	Method used for perparation	Electrode material	Electrolyte	Electrochemical performance		
					Initial discharge capacity (mAh g^{-1})	Final discharge capacity (mAh g^{-1})	C rate
1	Neem leaves	KOH activation and melt-diffusion	NLMC-4/S50	1M LITFSI with 5wt% LiNO$_3$	1143	784 (50th cycle)	0.2
2	Tissue paper	KOH activation and melt-diffusion	p-GCS-2/S	1M LITFSI with 5wt% LiNO$_3$	1497	992 (50th cycle)	0.2
3	Jute stalks	KOH activation and melt-diffusion	MGC/S-2	1M LITFSI with 5wt% LiNO$_3$	1542	1016 (50th cycle)	0.2
Anode materials							
4	Tin/ Graphene	Electro-deposition	Sn-G/RGO	1M LITFSI with 5wt% LiNO$_3$	1208	587 (40th cycle)	0.2
5	Silicon/ Graphite	Ball milling	Si5/G5	1M LITFSI with 5wt% LiNO$_3$	3577	1494 (40th cycle)	0.2
Lithiated Si-S full-cell							
1	MGC/S-2 cathode and lithiated Si5/G5 anode			1M LITFSI with 5wt% LiNO$_3$	1547	824 (50th cycle)	0.2
Supercapacitor							
S.No	Carbon precursors	Method used for perparation	Electrode material	Electrolyte	Electrochemical performance		Current Density (A g^{-1})
					Initial specific capacitance (F g^{-1})	Final specific capacitance (F g^{-1})	
1	Neem leaves	KOH activation	NLMC-4	6M KOH	138	114 (10000th cycle)	1
2	Tissue paper	KOH activation	p-GCS-2	6M KOH	122	110 (10000th cycle)	1

From all the studies the following conclusions are drawn.

1. All the porous carbon/sulfur cathodes developed in the present study are proven to be efficient polysulfide inhibitors for the sulfur cathode in a Li-S battery due to efficient trapping of the dissolved polysulfide species in them.

2. The modified separators act as barrier films for polysulfide species as well as upper current collectors that increase the reutilization of the active material during the redox process for longer cycles.

3. The new anode materials developed in the present study exhibit high electrochemical performance and are proven to be the suitable anodes to compensate the charge storage capacity of the sulfur cathode in a Li-S battery.

4. The lithiated Si-S full cell developed in the present study exhibits superior electrochemical performance and delivers higher energy density (calculated on the basis of mass of carbon+sulfur on the positive electrode), which is twice that of the conventional lithium-ion battery (LiFePO$_4$/graphite cell) calculated based on the LiFePO$_4$ cathode. The fabricated, lithiated Si-S pouch cells can be used for functioning of small electronics components.

5. The symmetric supercapacitors fabricated by using the as-prepared NLMC and p-GCS with aqueous 6M KOH electrolyte have also been found to give good electrochemical performance for longer cycles.

List of Publications and Bio-data

List of Publications from the Thesis Work:

[1] **E. Hari Mohan**, S. Anandan, B. V. Appa Rao, Tata. N. Rao, *"Neem Leaves-Derived Micro and Mesoporous Carbon as an Efficient Polysulfide Inhibitor for Sulfur Cathode in a Li-S Battery"*, **Chemistry Letters,** 2019, 48, 62-64.

[2] **E. Hari Mohan,** Katchala Nanaji, Srinivasan Anandan, Sarada V Bulusu, Ramakrishna Mantripragada, A. Jyothirmayi, B.V. Appa Rao, Tata Narasinga Rao, *"One-step Induced Porous Graphitic Carbon Sheets as Supercapacitor Electrode Material with Improved Rate Capability"*, **Materials Letters**, 2019, 236, 205-209.

[3] **E. Hari Mohan**, B.V. Sarada, R. V. R. Naidu, G. Salian, A. K. Haridas, B.V. Appa Rao, T. N. Rao, *"Graphene-Modified Electrodeposited Dendritic Porous Tin Structures as Binder Free Anode for High Performance Lithium-Sulfur Batteries"*, **Electrochimica acta**, 2016, 219, 701-710.

Other Publications by the Investigator:

[1] Katchala Nanaji, **E. Hari Mohan**, Sarada V Bulusu, U. V. Varadaraju, Tata Narasinga Rao, Srinivasan Anandan, *"One Step Synthesized Hierarchical Spherical Porous Carbon as an Efficient Electrode Material for Lithium ion Battery"*, **Materials Letters,** 2019, 237, 156-160.

[2] P. M. Pratheeksha, **E. Hari Mohan**, B. V. Sarada, M. Ramakrishna, K. Hembram, P. V. V. Srinivas, P. J. Daniel, T. N. Rao, S. Anandan, *"Development of a Novel Carbon-Coating Strategy for Producing Core-shell Structured Carbon Coated $LiFePO_4$ for an Improved Li-ion Battery Performance"*, **Phys.Chem.Chem.Phys.**, 2017, 19, 175-188.

[3] **E. Hari Mohan**, V. Siddhartha, R. Gopalan, T. N. Rao, D. Rangappa, *"Urea and Sucrose Assisted Combustion Synthesis of $LiFePO_4/C$ Nano-powder for Lithium-ion Battery Cathode Application"*, **AIMS Materials Science**, 2014, 1, 191-201.

[4] D. Rangappa, **E. Hari Mohan**, V. Siddhartha, R. Gopalan, T. N. Rao, *"Preparation of $LiMn_2O_4$ Graphene Hybrid Nanostructure by Combustion Synthesis and Their Electrochemical Properties"*, **AIMS Materials Science**, 2014, 1, 174-183.

[5] Tejassvi Pakki, **E. Hari Mohan**, Neha Y. Hebalkar, Adduru Jyothirmayi, Sarada V. Bulusu, Srinivasan Anandan, Krishna Mohan Mantravadi, Tata N. Rao, *Flexible and freestanding carbon nanofiber matt derived from electrospun polyimide as an effective*

interlayer for high performance Lithium Sulfur batteries (**Under Revision- Journal of Materials Science**).

List of Papers Presented in the Conferences/Workshops from the Thesis Work:

[1] <u>**E. Hari Mohan**</u>, Katchala Nanaji, Srinivasan Anandan, B. V. Appa Rao, Tata N. Rao, *Development of Sulfur Cathode Comprising of Biomass Derived Activated carbon As Host for Improved Lithium-Sulfur Battery Performance*, **ECS 233rd Meeting**, May 13th-17th 2018, Seattle, WA, **USA**. *(Oral)*

[2] <u>**E. Hari Mohan**</u>, B. V. Appa Rao, Tata. N. Rao, *Silicon/Graphite Composite as High Performance Anode for Lithium-Sulfur Battery Application* **"Frontiers in Chemical Sciences and Technologies"** (FCST) 28th-29th Jan 2016 held at NIT Warangal, **India**. *(Oral)*

[3] <u>**E. Hari Mohan**</u>, B. V. Appa Rao, Tata. N. Rao, *Carbon Based Membrane as an Effective Interlayer for High Performance Lithium-Sulfur Batteries,* **"8th Bangalore INDIA NANO"** Mar 3rd-4th 2016, Banglore, **India**. *(Poster)*

[4] <u>**E. Hari Mohan**</u>, B. V. Appa Rao, Tata. N. Rao, *Activated Carbon Derived from Sodium Carboxymethylcellulose as an Efficient Matrix for Sulfur Cathode in High Performance Lithium-Sulfur Battery*, **"Nanoscience, Nanotechnology and Advanced Materials"** (NANOS 2015), Dec 14th-17th 2015, GITAM university, AP, **India**. *(Oral)*

[5] <u>**E. Hari Mohan**</u>, B. V. Appa Rao, Tata. N. Rao, *A High Performance and Long Life Lithium-Sulfur Battery with Novel Cell Configuration*, **"India International Science Festival"** Dec 4th-8th 2015, IIT Delhi, **India**. *(Oral)*

[6] <u>**E. Hari Mohan**</u>, B. V. Appa Rao, Tata. N. Rao, *Facile Method to Fabricate High Performance Sulfur/Silicon Rechargeable Battery*, **7th Indo-Korean Joint Workshop on "Green Mobility and Energy Materials"**, Nov 26th-27th 2015, Hyderabad, **India**. *(Poster)*

List of Papers Other than the Thesis Work Presented in the Conferences/Workshops by the Investigator:

[1] Tata N. Rao, <u>**E. Hari Mohan**</u>, Tejassvi Pakki, Katchala Nanaji, Srinivasan Anandan *Mesoporous Carbon and Nanofiber Interlayer as Efficient Polysulfide Reservoirs for High Performance Lithium-Sulfur Batteries*, **6th Workshop on Lithium-Sulfur Batteries**, Nov 6th-7th 2017, Fraunhofer IWS Dresden, **Germany**. *(Poster)*

[2] Mahesh Shastri, Vinay Gangaraju, Navya Rani M, **<u>Hari Mohan E</u>**, T N Rao, Dinesh Rangappa, *"Spray Drying Assisted Combustion Synthesis of LiNi$_{0.45}$Mn$_{1.45}$Co$_{0.1}$O$_4$/ Graphene Nanocomposite and its Electrochemical Properties"*, **Materials Today: Proceedings**, 2017, 4, 12223-12228.

Personal Information

E. Hari Mohan

Research Scholar, Department of Chemistry, NIT Warangal, Telangana, India. PIN-506004

&

International Advanced Research Centre for Powder Metallurgy and New Materials (ARCI),
Balapur P.O., Hyderabad-500005, India
+91-9989727396

Email: harimohan_e@yahoo.co.in

Gender: Male, Date of Birth: 21/11/1987, Nationality: Indian

Languages Known: English, Hindi and Telugu, Marital Status: Unmarried

Education

July 2013 - Present	**Ph.D. Thesis submitted**
	NIT Warangal, India
	Research Scholar in **Department of Chemistry**.
	Thesis Title: "*Synthesis and Electrochemical Studies of Nanostructured Electrode Materials for High Energy Density Lithium-Sulfur Battery and High Power Density Supercapacitor***".**
	Course Work : As a part of PhD programme, mandatory Course Work have been completed on the following courses

1. Advanced Analytical Methods
2. Surface Analytical Techniques
3. Advanced Electrochemical Methods
4. Electrochemical Energy Systems
5. English for Scientific Communication

Cumulative Grade Obtained: **A**

June 2008 - July 2010	**Master of Science in Chemistry (Analytical Chemistry)**
	Siddhartha P.G College (Osmania University)
	Percentage of marks : **79 % (First Division with Distinction)**
June 2005 - July 2008	**Bachelor of Science (Biotechnology, Biochemistry and Chemistry)**
	Government City College (Osmania University)
	Percentage of marks : **81 % (First Division with Distinction)**

Awards

- **"Senior Research Fellow"** at **ARCI** Hyderabad in the year 2014
- **"Junior Research Fellow"** at **ARCI** Hyderabad in the year 2012
- **"Holder of Proficiency in M.Sc (Analytical Chemistry) and College Topper"** at Siddhartha P.G College**, Osmania University**, (A.P), India, during 2008-2010
- **Secured Gold Medal** in B.Sc awarded by B. Parthasaradhi Reddy at Govt. City College, **Osmania University,** Hyderabad, (AP), India, during 2005-2008
- **"Holder of Proficiency"** in B.Sc at Govt. City College, **Osmania University,** Hyderabad, (AP), India, during the year 2008